# TYPE 1 AND 2 ISOPENTENYL DIPHOSPHATE:DIMETHYLALLYL DIPHOSPHATE ISOMERASE: SYNTHESIS, ENZYME ENGINEERING AND MECHANISTIC STUDIES

by

Syam Sundar Neti

A dissertation submitted to the faculty of
The University of Utah
in partial fulfillment of the requirements for the degree of

Doctor of Philosophy

Department of Chemistry

The University of Utah

August 2017

**The University of Utah Graduate School**

**STATEMENT OF DISSERTATION APPROVAL**

The dissertation of **Syam Sundar Neti**

has been approved by the following supervisory committee members:

| | | |
|---|---|---|
| **Charles Dale Poulter** | , Chair | **12-14-2016** Date Approved |
| **Jon D. Rainier** | , Member | **12-14-2016** Date Approved |
| **Janis Louie** | , Member | **12-14-2016** Date Approved |
| **Bethany A. Buck-Koehntop** | , Member | **12-14-2016** Date Approved |
| **Eric W. Schmidt** | , Member | **12-14-2016** Date Approved |

and by **Cynthia Burrows** , Chair/Dean of

the Department/College/School of **Chemistry**

and by David B. Kieda, Dean of The Graduate School.

# ABSTRACT

Enzymes are efficient biological catalysts that enormously accelerate the rates of chemical reactions by many orders of magnitude compared to the uncatalyzed reaction. The remarkable catalytic rate enhancement derives from the enzymes three dimensional structure, folding along with the active site geometry and packing. An enzyme active site has selective affinity for the substrates and stabilizes high-energy chemical species and unstable intermediates during the catalysis. To enhance the enzyme's catalytic ability, many enzymes have also evolved coenzymes (or) cofactors for catalysis. These cofactors often provide chemical functionality and reactivity that are not accessible to the twenty canonical amino acids. Thus, cofactors mediate diverse and unique chemical reactions that are catalyzed by enzymes. Isopentenyl diphosphate:dimethylallyl diphosphate isomerase were identified in two isoforms (IDI-1 and IDI-2) that catalyze the IPP/DMAPP isomerization. The work described in this dissertation focuses on attempts towards understanding the role of flavin cofactor in the chemical mechanism of type II isopentenyl diphosphate:dimethylallyl diphosphate (IDI-2) isomerase as well as mechanistic studies of IDI-1 and IDI-2. In the first section of this dissertation, studies will focus on the engineered enzyme variant of type II isopentenyl diphosphate:dimethylallyl diphosphate isomerase (IDI-2) from *Streptococcus pneumoniae*, a crucial enzyme in the isoprenoid biosynthetic pathway that utilizes a flavin mononucleotide (FMN) cofactor for catalysis. In most enzymes, flavin cofactors mediate redox electron transfer reactions.

However, the IDI-2 catalyzed reaction involves no net redox change, raising questions on the role of the flavin in IDI-2 chemical mechanism. The chemical mechanism of IDI-2 will be studied with a combination of spectroscopic studies and biochemical techniques. Others and our studies suggest that the flavin cofactor of IDI-2 may employ an unusual and novel mode of flavin-dependent catalysis involving acid/base chemistry. In the second section, attention will be focused on the site-selective synthesis of $^{15}N$- and $^{13}C$-enriched flavin isotopologues to understand the acid/base functionality of flavin in the chemical mechanism of IDI-2. Finally, mechanistic studies of IDI-1 and IDI-2 in $D_2O$ will address that the IPP/DMAPP isomerization is very likely proceeding through a step-wise mechanism via a tertiary ($3^o$) carbocationic intermediate. Taken together, kinetic, mechanistic, and spectroscopic studies on IDI-2 demonstrate that it catalyzes the reaction utilizing a flavin coenzyme in an atypical manner where the coenzyme performs acid/base chemistry instead of redox chemistry in which the later is the typical function of flavin cofactor.

TABLE OF CONTENTS

LIST OF TABLES

LIST OF FIGURES

LIST OF SCHEMES

# LIST OF ABBREVATIONS

| | |
|---|---|
| BCA | Bicinchoninic acid |
| Bis-TBS | Bis-TRIS buffered saline |
| Bis-TRIS | 2,2-Bis(hydroxymethyl)-2,2',2"-nitriloethanol |
| BSA | Bovine serum albumin |
| C.I. | Confidence interval |
| cIPP | 3-Cyclopropyl-3-buten-1-yl diphosphate |
| *Cp* | *Claviceps purpurea* |
| 5-DeazaFMN | 5-Carba-5-deaza-FMN |
| DMAPP | Dimethylallyl diphosphate |
| 4-DMATS | 4-dimethylallyl tryptophan synthase |
| 4-DMAT | 4-dimethylallyl tryptophan |
| DNA | Deoxyribonucleic acid |
| DPM | Disintegrations per minute |
| DXP | 1-Deoxyxyluluose 5-phosphate |
| DXR | DXP reductoisomerase |
| DXS | DXP synthase |
| EDTA | Ethylenediamine tetraacetic acid |
| eIPP | 3,4-oxido-3-methyl-1-butyl diphosphate |
| ESI-MS | Electron spray ionization-mass spectrometry |
| FMN | Flavin mononucleotide |

| | |
|---|---|
| FAD | Flavin-adenine dinucleotide |
| $FMN_{ox}$ | Oxidized flavin mononucleotide |
| $FMN_{red}$ | Reduced flavin mononucleotide |
| fmIPP | 3-Fluoromethyl-3-buten-1-yl diphosphate |
| FPP | Farnesyl diphosphate |
| FPPase | Farnesyl diphosphate synthase |
| G3P | Glyceraldehyde 3-phosphate |
| GC | Gas chromatography |
| GPP | Geranyl diphosphate |
| GTPase | Guanosine triphosphate isomerase |
| HEPES | 4-(2-Hydroxyethyl)-1-piperazineethanesulfonic acid |
| HMG-CoA | P-Hydroxy-P-methylglutaryl-CoA |
| HMGR | 3-Hydroxy-3-methylglutaryl-CoA reductase |
| HMGS | 3-Hydroxy-3-methylglutaryl-CoA synthase |
| HOMO | Highest occupied molecular orbital |
| HPLC | High performance liquid chromatography |
| IDI | Isopentenyl diphosphate:dimethylallyl diphosphate isomerase |
| IDI-1 | Type 1 isopentenyl diphosphate:dimethylallyl diphosphate isomerase |
| IDI-2 | Type 2 isopentenyl diphosphate:dimethylallyl diphosphate isomerase |
| IspH | 4-hydroxyl-3-methyl-butenyl-1-diphosphate reductase |
| IPTG | Isopropyl P-D-1-thiogalactopyranoside |
| IP | Isopentenyl phosphate |
| IPK | Isopentenyl phosphate kinase |
| IPP | Isopentenyl diphosphate |
| IspG | 2-C-methyl-D-erythritol-2,4-cyclodiphosphate reductase |

| | |
|---|---|
| KIE | Kinetic isotope effect |
| *m*/*z* | Mass over charge ratio |
| MECP | 2C-Methyl-D-erythritol 2,4-cyclodiphosphate |
| MeOH | Methanol |
| MEP | Methylerythritol 4-phosphate |
| MIB | 2-Methylisoborneol |
| MPD | Mevalonate-5-diphosphate decarboxylase |
| MS | Mass spectrometry |
| MVA | Mevalonic acid |
| MVK | Mevalonate kinase |
| MWCO | Molecular weight cut-off |
| NADH | Nicotinamide-adenine dinucleotide, reduced |
| NADPH | Nicotinamide-adenine dinucleotide phosphate, reduced |
| Ni-IDA | Nickel-iminodiacetic acid |
| NIPP | *N,N*-dimethyl-2-amino-1-ethyl diphosphate |
| oIPP | Racemic 3-oxiranyl-3-buten-1-yl diphosphate |
| PDA | Photodiode array |
| PDB | Protein Data Bank |
| PMD | Phosphomevalonate decarboxylase |
| PMK | Phosphomevalonate kinase |
| PPi | Inorganic diphosphate |
| Red. | Reduced |
| RFK | Riboflavin kinase |
| *R*-2fIPP | (*R*)-2-Fluoro-3-methyl-3-buten-1-yl diphosphate |
| RNA | Ribonucleic acid |

| | |
|---|---|
| S.E. | Standard error |
| Semi. | Semiquinone |
| *S*-2fIPP | (*S*)-2-Fluoro-3-methyl-3-buten-1-yl diphosphate |
| *Sp* | *Streptococcus pneumoniae* |
| TFC | Total flavin concentration |
| TIM | Triosephosphate isomerase |
| TOF | Time of flight |
| *Tt* | *Thermus thermophilus* |
| UPLC | Ultra performance liquid chromatography |
| UV-vis | Ultraviolet-visible |
| vIPP | 3-Methylene-4-penten-1-yl diphosphate |
| WT | Wild-type |

# ACKNOWLEDGEMENTS

First and foremost, I am deeply grateful to my advisor, Prof. C. Dale Poulter for providing me an opportunity to perform the cutting-edge chemical and biochemical research work in his laboratory towards my Ph. D. It has been an honor to be his Ph.D. student. His professional and personal support and the freedom to explore and drive my own ideas and research during my time at the University of Utah are invaluable. Dale's continuous support in my potential and abilities created self-confidence in me and motivated me to prepare and face new scientific challenges. His deep insight, brilliance, and analytical thinking capabilities towards research coupled with optimistic, patient, wise, generous, and humble nature continues to inspire me. I could not have imagined a better advisor than Dale at both professional and personal level. I would also like to thank the past and present members of the Poulter group namely, Jian-Jung Pan, Matthew Janczak, Jerome de Ruyck, Gurusankar Ramamoorthy, Jeng-Yeong Chow, and my other friends for their insightful discussions, constructive criticism, technical assistance, and friendly nature over the years.

I would like to specially thank my doctoral committee members Prof. Eric Schmidt, Prof. Gary Keck, Prof. Jon Rainier, Prof. Janis Louie, and Prof. Bethany Buck-Koehntop for their insightful comments, suggestions, and extensive support over the years. I am also grateful to Dr. Debra Eckert, Dr. Jack Skalicky, Dr. James Cox, Dr. Krishna Parsawar, and Dr. Jim Muller who have helped me significantly in my research

and providing me with thoughtful suggestions and assistance. Finally, I would like to thank my beloved parents, wife, and brother for their constant support, love, and confidence when I needed.

The work presented in this dissertation was supported by National Institutes of Health grant GM 25521.

# CHAPTER 1

# INTRODUCTION

## Background and Significance

Isoprenoids (also called terpenoids) are natural products derived from two fundamental and ubiquitous five-carbon precursors, isopentenyl diphosphate (IPP) and dimethylallyl diphosphate (DMAPP), which are found in all the three domains of life (Eukaryota, Bacteria, and Archaea) (Figure 1.1). There are more than 68,000 isoprenoid natural products discovered to date.[1] Isoprenoids serve various biological roles such as electron-transport carriers, vitamins, stabilization of membranes, photosynthetic pigments in plants, and antibiotics to name a few.[2] Isoprenoid compounds have important biological roles in both primary and secondary metabolic pathways (nonessential but important for survival of the organism).

Few representative examples of isoprenoids shown in Figure 1.2 include the monoterpene menthol,[3] the flavor constituent caryophyllene,[4] the antimalarial drugs artemisinin, and quinine,[5,6] the plant hormone abscisic acid,[7] the steroid molecule cholesterol,[6] the electron transport component in the mitochondrial respiratory chain coenzyme Q,[8] the anti-cancer agent taxol,[6] the vitamin A precursor β-carotene,[9] the earthy-oderant produced by *Streptomyces* soil bacteria 2-methylisoborneol,[10] the antiviral and antibacterial compound α-acid humulone,[11] and the indole alkaloid 3α(S)-

strictosidine.[6]

## Isoprenoid Diversity

Carbon skeletons of isoprenoid natural products are constructed from IPP and DMAPP by chain-elongation enzymes[12-14] in a series of reactions that give geranyl diphosphate (GPP, monoterpene), farnesyl diphosphate (FPP, sesquiterpene), geranylgeranyl diphosphate (GGPP, diterpene), sesterpenes ($C_{25}$), and longer chain linear diphosphates with branch points from FPP to produce squalene ($C_{30}$) and from GGPP to give phytoene ($C_{40}$) etc. (Figure 1.3). These five-carbon units and chain-elongated products can undergo a wide variety of reactions such as branching, condensation, and cyclization reactions, and so forth, to generate the structurally diverse array of natural products found in nature.[15-17]

## Biosynthesis of IPP and DMAPP

There are two known biosynthetic pathways for the synthesis of IPP and DMAPP: the mevalonate pathway (MVA) and the nonmevalonate or methylerythritol phosphate (MEP) pathway (Scheme 1.1 and 1.2). The MVA pathway, discovered in the 1960s,[2,18-22] is utilized by eukaryotes, archaea, and some eubacteria is the established pathway. The MEP pathway, which was discovered in 1996,[23-25] found in plant chloroplasts, algae, and most bacteria. Organisms utilizing the MEP pathway include several pathogens such as *Mycobacterium tuberculosis, Plasmodium falciparum, and Listeria monocytogenes*. The MEP pathway is orthogonal to the corresponding the MVA pathway in humans and is an attractive target for drug discovery and development.[26-28]

## MVA Pathway

The MVA pathway (Scheme 1.1) starts with the condensation of two molecules of acetyl-CoA catalyzed by acetyl-CoA acyltransferase to form acetoacetyl-CoA, which is then condensed with another molecule of acetyl-CoA by HMG-CoA synthase to form 3-hydroxy-3-methylglutaryl-CoA (HMG-CoA). In the next step, HMG-CoA reductase catalyzes the reduction of HMG-CoA with two molecules of NADPH to form mevalonate (MVA).[29] HMG-CoA reductase is the target for the highly effective statin class of cholesterol-lowering drugs.[30] The later steps in the pathway include two successive ATP-dependent phosphorylations of mevalonate and mevalonate-5-phosphate by mevalonate kinase (MVK) and phosphomevalonate kinase (PMK) to form mevalonate-5-diphosphate,[31] which is then converted into IPP by an ATP-dependent decarboxylation by mevalonate diphosphate decarboxylase (MPD).[32,33] Interestingly, in archaea there is a hypothetical phosphomevalonate decarboxylase (PMD) that uses mevalonate-5-diphosphate to produce isopentenyl phosphate (IP). IP undergoes phosphorylation by isopentenyl phosphate kinase (IPK) to generate IPP.[34] IPK is a well-characterized enzyme. In the final step of the MVA pathway, IPP and DMAPP are interconverted by the action of isopentenyl diphosphate:dimethylallyl diphosphate isomerase (IDI).[35]

## Non-MVA or MEP Pathway

The MEP pathway for biosynthesis of IPP and DMAPP (Scheme 1.2)[36-38] starts with the condensation of pyruvate and glyceraldehyde-3-phosphate (G3P) to form 1-deoxy-D-xylulose-5-phosphate (DXP), which is also an intermediate in the biosynthesis of thiamin (vitamin $B_1$) and pyridoxine (vitamin $B_6$).[39] In the first committed step in the

MEP pathway, DXP-reductoisomerase (DXR) catalyzes the conversion of DXP to 2-C-methyl-D-erythritol-4-phosphate (MEP), followed by cytidylylation, phosphorylation, and cyclization, catalyzed by the enzymes IspD, IspE, and IspF to generate the cyclic 2,4-diphosphate (MECDP).[40-42]

The two final steps in the MEP pathway are catalyzed by the [4Fe-4S] cluster containing enzymes IspG and IspH, which catalyze two consecutive $2e^-$ reductions of MECDP to give methyl hydroxylbutyl diphosphate, followed by reduction to an 85:15 ratio of IPP and DMAPP.[43,44] Both IspG and IspH are potential antimalarial, anti-tubercular, and antiherbicidal drug targets.

## Isopentenyl Diphosphate:Dimethylallyl Diphosphate Isomerase (IDI)

Isopentenyl diphosphate:dimethylallyl diphosphate isomerase (IDI), which interconverts IPP and DMAPP (Scheme 1.1), is an essential enzyme in organisms utilizing the MVA pathway. In contrast, organisms utilizing the MEP pathway (Scheme 1.2) do not require IDI since both IPP and DMAPP are generated as a mixture.[45] In this case, IDI might exist in these organisms to balance the cellular pools of IPP and DMAPP. Two nonhomologous isoforms of IDI have been identified, type I IDI (IDI-1) and type II IDI (IDI-2). The amino acid sequences of IDI-1 and IDI-2 do not have significant levels of similarity although the enzymes catalyze the same transformation. IDI-1 requires $Zn^{2+}$ and $Mg^{2+}$ for catalysis and utilizes acid/base chemistry to facilitate the 1,3-proton addition/elimination reaction. IDI-2 requires a flavin mononucleotide (FMN) coenzyme and NADPH in addition to divalent metal ion for catalysis. Its mechanism is poorly understood.

## IDI-1

IDI-1 was discovered in 1959 by Lynen and coworkers during their studies of squalene biosynthesis in baker's yeast.[35,46] They demonstrated that IDI-1 catalyzed the reversible interconversion of IPP and DMAPP and subsequently purified the enzyme from yeast, pig liver, rat liver, kidney, and brain tissues.[47,48]

IDI-1 requires two divalent metal ions for catalysis. $Mg^{2+}$ binds the diphosphate moiety in IPP and $Zn^{2+}$ orients the active site residues in a catalytically competent conformation by coordinating to three histidines and two glutamates in an octahedral complex.[49-51] The crystal structures of *E. coli* and Human IDI-1 with 2-(dimethylamino)ethyl pyrophosphate (NIPP) and ethanol amine diphosphate (EAPP) substrate analogs show the structure of the active site, where highly conserved E116, C67 (*E. coli*), and E148 and C86 (Human) (Figure 1.4) residues directly play a role in the catalysis.[52,53] Studies with electrophilic IPP and DMAPP analogues, mechanism-based inhibitors (NIPP, (*Z*)-$CF_3$-DMAPP, eIPP, OPP, etc.) and site-directed mutants indicated that C67, E116, and Y104 (*E. coli* numbering) are important catalytic residues for acid/base catalysis with Y104 performing a structural role in the transfer of a proton from E116 to the double bond in IPP.[54-60] The C67A mutant of *E. coli* IDI-1 formed an irreversible covalent adduct between eIPP and an active site glutamate E116,[61] whereas in wild-type (wt) IDI-1, C67 forms a covalent adduct with eIPP (Figure 1.5).[52] Additionally, the W136 residue near IPP could stabilize formation of the tertiary IPP carbocation or carbocationic transition state through cation-π interactions. These results are consistent with a mechanism where the electrophilic protonated epoxide group in eIPP is opened by nucleophilic attack by E116 or C67. The C67A mutant did not turn

over IPP; whereas, the C67S mutant catalyzes the isomerization ~$10^4$-fold more slowly that wt IDI-1.[55] Thus, E116 protonates C4 of IPP and C67 abstracts the proton on C2 to generate DMAPP. In addition, Cys and Glu are ideally positioned on the opposite faces of the plane of IPP to facilitate the antarafacial stereochemistry observed for protonation-deprotonation.[52,56] Additional support for the carbocationic mechanism was obtained from kinetic studies with (*Z*)-$CF_3$-DMAPP, which has ~$10^6$ fold reduced enzymatic and is similar to the ~$10^7$ decrease of the rate of solvolysis of the corresponding methanesulfonate (Figure 1.6), which presumably proceeds via a carbocation intermediate by an $S_N1$ mechanism.[62,63]

Support for a mechanism involving an IPP $3^o$ carbocation intermediate (Scheme 1.3) was also gained by designing a transition state mimic NIPP that mimics the $3^o$ carbocation. It was found that NIPP is a tight-binding inhibitor of IDI-1 with a 10-100 pM binding affinity which is 4 to 5 orders of magnitude tighter than IPP or DMAPP binding.[58,59] Upon denaturation of IDI-1, NIPP was released into solution, indicating that the inhibition is of a noncovalent in nature. Studies with electrophilic analogs of IPP (Figure 1.7) including fluoro and epoxy substituents led to the formation of irreversible covalent adducts with the enzyme and further supports the $3^o$ carbocationic intermediate or a transition state with substantial carbocationic character. The representative IPP analogs used to probe the mechanism of IDI-1 are shown in Figure 1.7.

Furthermore, previous studies also defined the stereochemical outcome of the IDI-1 catalyzed IPP isomerization. Studies by Cornforth and coworkers with 4-$^3$H-labeled mevalonate showed that the pro-*R* C2 proton in IPP is stereospecifically removed during isomerization and subsequent studies with 2-$^3$H-mevalonate indicated that the

proton is added on to the *re* face of the IPP double bond generating a carbocation or carbocation-like transition state. Utilizing 2-$^{14}$C-mevalonate they also demonstrated that IPP isomerization to DMAPP in which the newly formed methyl group in DMAPP is in *E*-configuration.[48,49,64] Taken together, the IDI-1 catalyzed IPP, DMAPP interconversion was suggested to be highly stereospecific involving 1,3-proton addition/elimination. Poulter and coworkers performed another crucial study with *S. cerevisiae* IDI-1 and demonstrated that all the hydrogens in IPP and DMAPP, except for those at C1, were ultimately exchanged for deuterium when the substrates were incubated with IDI-1 in $D_2O$ (Scheme 1.4).[65] This result suggests that the IDI-1 active site does not rigidly control the stereochemistry of the requisite proton transfers during turnover. Likely, explanations for this lack of stereo- and regioselectivity are the presence of alternative acid/base groups in the enzyme active site and/or the presence of different IPP/DMAPP binding modes.

Based on all the studies with IPP analogs, crystal structures, site-directed mutagenesis, kinetic studies, and identifications of the adducts by both chemical and X-ray structural methods, the generally accepted mechanism of IPP isomerization by IDI-1 is depicted in Scheme 1.5. Although, many groundbreaking mechanistic studies using IPP substrate analogs support the 1,3-proton addition/elimination mechanism of IPP that proceeds *via* a tertiary ($3^o$) carbocation or carbocation-like transition state, there is no direct evidence as to the exact nature of the intermediate or transition state. While literature precedent for $3^o$ carbocationic intermediate were observed for downstream isoprenoid biosynthetic enzymes such as the prenyltransferases and terpene cyclases whose substrates are allylic precursors, these are not directly relevant to $3^o$ carbocation

formed from IDI isomerization.[66,67] Previously, Richard and coworkers provided some clues into the nature of the IDI-1 catalyzed 1,3-proton addition/elimination of IPP with their model studies for the stepwise, acid-catalyzed isomerization of 4-(4-methoxyphenyl)-2-methyl-1-butene in a mixture of trifluoroethanol:$H_2O$ 20:80 (v/v) at pH 7.0.[68,69] Based on the comparisons of rate constants of individual steps of the nonenzymatic reaction of 4-(4-methoxyphenyl)-2-methyl-1-butene (Scheme 1.6A) and the IDI-1 catalyzed reaction of IPP (Scheme 1.6B), a rate enhancement of the enzyme catalyzed reaction $k_{cat}/k_{non}$ was ~ $10^{11}$. The observed rate enhancement is likely derived from the electrostatic and cation-π stabilization of the carbocationic intermediate/transition state by the IDI-1 active site. Based on the model studies and comparisons of the free energy profiles of the deprotonation of a carbocation versus protonation of an enolate, the authors emphasize that the kinetic barrier for the carbocation deprotonation is significantly smaller compared to protonation of the enolate intermediate. From these studies the authors favored a concerted mechanism of IDI-1 catalyzed IPP isomerization that does not go through a carbocationic intermediate. This result is in contrast to the step-wise mechanisms for enzymes that catalyze reversible α-deprotonation of carbonyl compounds via enolate intermediates, where there is a large intrinsic advantage to general base catalysis. For these reasons, the authors of this study favored a concerted protonation/deprotonation mechanism for IDI-1. However, to date, no conclusive experimental evidence to distinguish among these mechanistic possibilities for IDI-1 has been reported.

In 2012, Richard and coworkers reported a study of the hydrogen exchange in IPP catalyzed by IDI-1 in $D_2O$. They identified that IDI-1 catalyzed process produces 66% of

the product DMAPP that has one deuterium on the *E*-methyl group and 34% of the substrate IPP that has also one deuterium at C2 position (Scheme 1.7).[70] Based on the time-course of the enzyme assays, they identified that the product DMAPP formation was accompanied with the concomitant formation of *d*-IPP (1) along with the disappearance of IPP. These observations helped to propose the rates of individual steps in IPP/DMAPP isomerization in which *d*-DMAPP isomerization to *d*-IPP ($k^1_{-1}$) is faster than the product (*d*-DMAPP) release ($k_{dis}$). Since the product release is the slow step they further added that it is the rate-determining step in IDI-1 catalysis.

**IDI-2**

Archaea and eubacteria were known to employ the MVA pathway for the biosynthesis of isoprenoids but apparent lack of orthologs for mammalian IPP isomerase in these organisms fueled the search for IDI.[71] In 2001, Seto and coworkers discovered the gene *orfD* contained an open reading frame (ORF) encoding a protein of unknown function when they cloned a gene cluster containing MVA pathway enzymes from *Streptomyces* sp. strain. They discovered that *orfD* encoded a flavin-dependent enzyme that catalyzes the reversible isomerization of IPP and DMAPP.[72] This protein, named IDI-2, has no sequence similarity with IDI-1. Interestingly, IDI-2 was found in gram-positive bacteria that are known to use the MVA pathway such as *Staphylococcus aureus*, *Streptococcus pneumoniae*, and *Enterococcus faecalis* but are absent in humans. This represents an attractive strategy from the drug design standpoint. IDI-2 prefers flavin mononucleotide (FMN) as a cofactor, with flavin adenine dinucleotide (FAD) approximately half as effective. No activity was detected with riboflavin.[73] The enzyme

also required a reducing agent (for example NADPH) and a divalent metal ion ($Mg^{2+,}$ $Mn^{2+}$ or $Ca^{2+}$) for activity. The authors further demonstrated that the *idi2* complemented an *idi1* deletion in *E. coli*, suggesting that the biological function of IDI-2 is isomerization of IPP to DMAPP.

## Flavins and Flavocoenzymes in Enzyme Catalysis

Flavin coenzymes commonly undergo two electron redox changes in various enzymatic transformations. The structures of oxidized, semiquinone, and reduced flavins are shown in Figure 1.8. Studies indicated that the *pro S* hydrogen of NADPH is transferred to FMN during reduction of the IDI-2•$FMN_{ox}$ complex, suggesting that NADPH is likely to be the physiological reductant.[74] Subsequent studies showed that upon reduction of IDI-2•$FMN_{ox}$ to IDI-2:$FMN_{red}$, the enzyme retained activity for multiple turnovers.[74,75] Thus, there is no net redox change in $FMN_{red}$ after completion of each catalytic cycle, as expected for a reaction where there is no net change in the redox state of the substrates. UV-vis studies of enzyme bound $FMN_{ox}$ (E•$FMN_{ox}$) has characteristic peaks at ~376 nm and ~ 454 nm. (E•$FMN_{ox}$) undergoes reduction with NADPH to give E•$FMN_{red}$ that has a characteristic peak at ~ 352 nm indicating anionic $FMN_{red}$. When IPP/DMAPP binds the anionic $FMN_{red}$ complex (E•$FMN_{red}$), there is a new peak at ~426 nm and a shoulder at ~320 nm indicating protonation of anionic E•$FMN_{red}$ (Scheme 1.8).[76]

Liu and coworkers established that the *pro-R* hydrogen at C2 was removed from IPP during isomerization in incubations with (*S*)- and (*R*)-[2-$^2$H]IPP (Figure 1.9A).[77] Similarly, Barkley et. al. found that the *pro-R* C2 hydrogen and C4 hydrogens of IPP and

*E*-methyl protons in DMAPP are replaced by deuterium when incubations were conducted in $D_2O$ with no detectable exchange of the *pro-S* C2 hydrogen in IPP or the hydrogens in the *Z*-methyl group in DMAPP (Figure 1.9B).[78] These observations indicate that the proton transfer steps catalyzed by IDI-2 catalyzed are more stereoselective than those for IDI-1. Steinbacher and coworkers reported the first X-ray crystal structure of IDI-2 for the protein from *Bacillus subtilis* (*bs*IDI-2) at 2.8 Å resolution.[79] The enzyme adopts a classical TIM-barrel fold, which is structurally distinct from the α/β fold adopted by IDI-1.[56] Crystal structures were obtained both in the presence and absence of FMN because FMN was lost during protein purification and the protein was reconstituted with FMN by soaking with the protein. Shortly afterward, Hemmi and coworkers obtained an X-ray structure of *Sulfolobus shibatae* IDI-2 (*ss*IDI-2) at 2.2 Å (Figure 1.10A)[80] (Figure 1.10B). The *ss*IDI-2 structure contained $FMN_{red}$, IPP and $Mg^{2+}$ in the active site and provided important information about which conserved active-site amino acids are in contact with $FMNH_2$ and IPP (Figure 1.10C).

In the *ss*IDI-2 active site, IPP is located in a "box" with walls formed by His155, Trp225, Lys193, and Gln160 (*S. shibatae* numbering), and a floor formed by the isoalloxazine ring in FMN. Distances between C2 and C4 of IPP (where IPP/DMAPP undergoes the 1,3-proton addition/elimination) to the N1 and N5 of flavin is shown on Figure 1.10D. The next question was the mechanism of IPP/DMAPP isomerization. IPP and DMAPP can undergo isomerization either by hydrogen atom addition-abstraction or protonation-deprotonation mechanism as depicted in Figure 1.11. When IDI-2•FMN•IPP complex was reduced irrespective of the reducing agent, a flavin semiquinone radical was detected by EPR.[76] However, flavin semiquinone radical species was not detected when

the IPP was added to the prereduced complex IDI-2.FMNH$^-$. Attempts to detect the substrate IPP, flavin semiquinone radical pair were unsuccessful although the redox potentials are different for free flavin and the flavin bound to the enzyme.[74,81] Although observed by UV-vis, the detection of flavin semiquinone radical by stopped-flow failed.[82] Furthermore, studies with radical clock analogs of IPP, cyclopropyl (cIPP), and epoxy IPP (eIPP) analogs, which should operate through radical mechanism via ring opening and a "radical clock rearrangement"[83,84] indicated that cIPP isomerized to the cDMAPP product (Figure 1.12A) and eIPP formed a covalent adduct with flavin which could happen only by protonation of epoxide followed by ring opening (Figure 1.12B).[85] These studies support the protonation-deprotonation mechanism rather than radical mechanism of IPP/DMAPP isomerization and provide insights about the close contacts between flavin and the substrate in the active site.

Additional support for the protonation-deprotonation mechanism of IDI-2 came from studies with substrate analogs eIPP, vIPP, and fmIPP, which were potent electrophilic mechanism-based inhibitors of IDI-1 upon activation by protonation.[86-88] Incubation of these substrates led to the formation of flavin inhibitor adducts rather than the corresponding isomerized products. UV-vis spectral features first indicated the inhibitors attached to N5 of flavin but more thorough investigation showed that inhibitor analogs modified C4a of flavin through alkylation.[79] FmIPP and vIPP are also alternate substrates in addition to functioning as inhibitors. *Z*-fmDMAPP, *Z*-dfmDMAPP analogs were found to be alternate substrates of the enzyme. Although NIPP strongly inhibits IDI-1 at a much greater affinity, it weakly inhibits IDI-2.[80] The structures of representative IPP analogs used to probe the IDI-2 catalysis are shown in Figure 1.13.

1-OPP and 2-OPP were good alternate substrates for the radical mechanism since they are substantially less reactive to form a carbocation but can react to generate a radical. For both 1-OPP and 2-OPP, it is 15 kcal/mol more endothermic to form a carbocation than IPP/DMAPP calculated gas-phase heats of reaction. On the other hand, to generate a radical species it is only 2 kcal/mol more endothermic than IPP/DMAPP. Incubation of 1-OPP and 2-OPP with IDI-2 resulted in covalent inhibition in a time-dependent manner.[88] Studies with vinyl thioether IPP analog showed that C4 protons were exchanged with solvent deuterium without isomerization.[89] Taken together, these studies support the protonation-deprotonation mechanism of IDI-2 (Figure 1.14).

As described, flavin does not undergo a net redox change during IDI-2 catalysis, and has attracted great attention to understand the role of flavin in acid-base catalysis. Liu and coworkers performed linear free energy studies with FMN analogs modified at 7,8 positions with electron-donating and withdrawing groups and found negative Hammett plots ($\rho$ = -2.0) and Brϕnsted plots with positive slopes ($\beta$ = 0.7). The data suggested that flavin loses electron density and that the proton is donated to N5 of $FMN_{red}$. The source of the proton added to the C4 of IPP still remains unclear although the authors propose that the proton could be derived from an H10-E22-Q154 relay (*S. aureus* numbering).[90] This study confirmed the general base catalysis of reduced FMN. The active site amino acid residues surrounding IPP (W225, H155, Q160) that are close to the C4 and C2 carbons in IPP/DMAPP are not suitably acidic or basic to perform acid-base catalysis. Site-directed mutagenesis of these residues resulted in catalytically active mutant enzymes although their activities were substantially decreased indicating a possible acid-base role of $FMN_{red}$.[92] Subsequently, Liu and coworkers determined the stereochemistry

for protonation of IPP at C4 in an effort to identify the role of active site amino acids and $FMN_{red}$ in the substrate protonation step.[91] The active site amino acid residue (Q154) and $FMN_{red}$ are located on the opposite side of the plane of IPP, their corresponding stereochemistry of protonation (*E*-methyl group in DMAPP) should differ. Incubation of *E*- and *Z*-[4-$^3$H]-IPP with IDI-2 in $D_2O$ resulted in deuterated chiral *R* and *S* methyl isomers of [4-$^2$H,$^3$H]-DMAPP (Figure 1.15A and B) of DMAPP which can only be generated if the protonation occurs from the side of the flavin isoalloxazine ring. Based on these results, they suggest that flavin plays a central role in IPP protonation.

Studies with the incorporation of 1-deazaFMN and 5-deazaFMN analogs into IDI-2 revealed that IDI-2•1-deaza$FMN_{red}$ catalyzed IPP/DMAPP isomerization, while the IDI-2•5-deaza$FMN_{red}$ was catalytically inactive.[74,93] This study indicates that N5 plays an important role in acid-base catalysis of IDI-2. Furthermore, in the X-ray structure of IDI-2•$FMN_{red}$•IPP, the distance between N5 to C4 and C2 of IPP (3.6 and 3.3 Å respectively) is less compared to N1 (3.9 and 4.8 Å, respectively). Taken together, these studies indicate that flavin plays a direct role in acid-base catalysis of IDI-2 and N5 is better positioned compared to N1 in the active site.

As described above, N5 of $FMN_{red}$ plays a key role in acid/base chemistry, the pKa of N5 in neutral and anionic $FMN_{red}$ in solution was estimated to be ~20 which is only suitable to act as a base (Figure 1.16A and B).[94] N1 hydrogen (pKa ~ 7) is deprotonated and exists in anionic form when $FMN_{red}$ binds IDI-2 which is stabilized by the nearby Lys residue. As mentioned, there is no suitable acidic amino acid residue (proton donor) in the active site of IDI-2 close to C4/C2 carbons of IPP. The possibility that $FMN_{red}$ could exists in N1/N5 $FMN_{red}$ zwitter-ionic tautomer and the pKa of N5 in

the zwitter-ionic $FMN_{red}$ has been estimated to be ~4 (Figure 1.16C) could serve as a proton donor.[94]

We and other groups have proposed the mechanism of IDI-2 catalysis consistent with the zwitter-ionic $FMNH_2$ acting as a both acid and base in the IPP and DMAPP isomerization (Figure 1.17). In this mechanism the N5 of $FMN_{red}$ zwitterion donates the proton to the C4/C2 of IPP/DMAPP generating a positively charged $3^o$ carbocation in the active site stabilized by the negative charge on the $FMN_{red}$ isoalloxazine ring by HOMO-LUMO interactions,[95] and also through cation-π interactions from the near by amino acid residues W225 and H155 (*S. shibatae* numbering). In the next step, N5 in the conjugated base form (pKa of ~ 20) is suitable to abstract the proton from C2/C4 of the $3^o$ carbocation generating DMAPP and IPP and regenerating (5,5)-$FMN_{red}$ zwitter-ion for multiple turnovers in the IDI-2 active site. The proposed mechanism also highlights that IDI-2 catalysis is a suprafacial 1,3-proton addition/elimination of IPP and DMAPP unlike IDI-1, which is an antarafacial mechanism.

Acid/base catalysis by reduced flavins in reactions with no net redox change have been observed for CRTISO,[96] which catalyzes the FAD-dependent cis-to-trans isomerization of prolycopene to all-trans-lycopene, and CRTY,[97] which requires reduced FAD to catalyze cyclization of lycopene to β–carotene (Figure 1.18). In CRTY, the negative charge on the pyrimidine nucleus of $FAD_{red}$ is proposed to stabilize the positive charged intermediate/transition state of lycopene similar to proposals for stabilization of the charged intermediate/transition state by IDI-2. CRTISO, CRTY, and IDI-2 are the enzymes in isoprenoid biosynthesis reported to catalyze employing neutral no redox flavin chemistry.

In 2011, Poulter and coworkers obtained evidence for the step-wise mechanism of IDI-2 that goes through $3^o$ carbocationic intermediate (Figure 1.19).[89] This study supported the step-wise mechanism in addition to the large body of evidence accumulated based on the studies with electrophilic mechanism-based inactivators of IDI-2 which suggested an existence of carbocationic intermediate or a transition state with substantial carbocationic character. Upon proton addition, the thiomethyl substituent at C3 of IPP stabilizes the tertiary carbocationic intermediate more effectively than a methyl group in the natural substrate IPP. This analog did not undergo isomerization and bound in an orientation that C4 hydrogens were exchanged with solvent deuterium. This study confirms the existence of a $3^o$ carbocationic intermediate that can only be formed by a stepwise process.

More recently, Poulter and coworkers determined the crystal structure of IDI-2 from *Streptococcus pneumoniae* at 1.4 Å, which is the highest resolution among the crystal structures of IDI-2 obtained to date (Figure 1.20).[98] During purification of the enzyme, the enzyme bound FMN cofactor was lost when protein binds Ni-NTA column similar to *bacillus subtilis* IDI-2, thereby generating apoenzyme. The apoenzyme was reconstituted with FMN to characterize and to study the catalysis. The substrate binding and catalytic constants of *sp*IDI-2 were similar to other IDI-2 homologs. Subsequent kinetic characterization of the enzyme revealed that $FMNH_2$ binds first to the enzyme followed by the substrate (IPP) binding and followed a sequential ordered binding mechanism.

Janczak et. al. obtained further support about the ordered mechanism of *sp*IDI-2 where FMN binds the enzyme before IPP by undertaking detailed bisubstrate kinetic

studies. Inhibition studies with 5-deazaFMN and NIPP, which are the competitive inhibitors for FMN and IPP, supported the modified sequential ordered mechanism of IDI-2. Kinetic assays performed under aerobic conditions and the plots of initial velocities versus FMN at fixed IPP concentration have shown a sigmoidal behavior for FMN with a hill-coefficient of $n$=2. Sigmoidal behavior was not observed under strict anaerobic conditions when the FMN was prereduced with sodium dithionite to $FMNH_2$.[99] Interestingly, FMN reduction by NADH in the IDI-2 active site ($k$ = 2.8 x $10^{-3}$ $s^{-1}$) was faster in the presence of IPP ($k$ = 8.9 $s^{-1}$). Similar experiments with sodium dithionite as a reductant followed a biphasic pattern of reduction, which is categorized into fast ($k$ = 326 $s^{-1}$) and slow rates ($k$ = 6.87 $s^{-1}$) of reduction. The effect of IPP on the rate enhancements of IDI-2•FMN reduction was proposed to be IPP induced conformational change in the homotetrameric IDI-2 by binding of IPP to a sub-unit other than the active site of the tetramer where the FMN undergoes reduction by NADH. We thought to investigate this problem by making a monomeric IDI-2. Creation of monomeric IDI-2 eliminates inter subunit-dependent mechanisms for the enhanced rate of FMN reduction. This work will be presented in more detail in Chapter 2 of this dissertation.

In 2012, Hemmi and coworkers performed a more detailed study of *ss*IDI-2 to obtain insights into the changes in solution structure caused by substrate binding. They observed that *ss*IDI-2 without a N-terminal $His_6$-tag exists as a mixture octamers and tetramers with a $K_d$ of 3.5 μM; whereas, the same enzyme with an *N*-terminal $His_6$-tag is a tetramer.[100] The tetramer-tetramer interface in the octameric protein was disrupted by E13R/R235E double mutation to give an active tetramer. By using SAXS, tryptophan fluorescence, and DLS analysis they showed that substrate (IPP) binding disrupts

tetramer-tetramer interface in *ss*IDI-2 octamer and generates a tetramer since this interface is required for IPP binding. Similar effect was observed for *bacillus subtilis* IDI-2 (*bs*IDI-2) where IPP binding disrupts octamer formation.[101] Few earlier studies by Poulter and coworkers showed that *M. thermautotrophicus* IDI-2[102] and *Synechocystis* IDI-2[103] also exists octamer-tetramer equilibrium in a concentration dependent manner with a $K_d$ of 17 and 0.2 μM. There was no evidence for the formation of octamer or tetramer-octamer equilibrium for *sp*IDI-2 at the concentrations tested based on both the gel-filtration chromatography and sedimentation equilibrium experiments. The solution and crystal structure of all the available IDI-2 homologs is presented in Table 1.1.

## Implications in Drug Design

The enzymes in the MEP pathway for the production of five carbon isoprenoid precursors IPP and DMAPP are novel drug targets since the human pathogens like *Mycobacterium tuberculosis* and *plasmodium falciparum,* the causative agents for tuberculosis and malaria, rely on this pathway. Other pathogenic organisms such as *Staphylococci, streptococci,* and *enterococci* completely rely on MVA pathway for the production of IPP and DMAPP. As mentioned, IDI-2 is an essential enzyme in the MVA pathway for the interconversion of IPP and DMAPP. Although both humans and these pathogenic bacteria uses the MVA pathway, humans use IDI-1 and these pathogenic bacteria use IDI-2 making it an attractive target for drug discovery. IDI-1 and IDI-2 are nonhomologous, structurally and mechanistically divergent, so development of inhibitors that selectively blocks IDI-2 in bacteria is a growing need for the development of antibacterial agents. In addition, drug resistance has been commonly observed with the

hospital acquired infections with the currently available antibiotics such as methicillin and vancomycin. Therefore, there is a growing need to develop antibacterial agents for drug-resistant bacterium such as methicillin- and vancomycin-resistant *Staphylococcus aureus* and *Enterococci* (MRSA, VRSA, and VRE). Some of the mechanism-based inhibitors described above commonly inhibit both IDI-1 and IDI-2 such as eIPP, oIPP, and so forth. Development of novel chemotherapeutic agents selective towards IDI-2 can be rationally designed utilizing the crystal structure of IDI-2 from pathogenic organisms. The crystal structure of *sp*IDI-2 is available although it did contain the substrate IPP in the active site. Scaffolds that bind to the flavin in the active site is one strategy and also as De ruyck et. al. suggested three potential target sites near the active site of *sp*IDI-2 to target with negatively charged scaffolds that bind to the arginine and lysine residues or sulfur binding agents that bind to the methionine. For other IDI-2 homologs from *Staphylococci* and *Enterococci,* the X-ray structures are yet to be solved. Nevertheless, homology modeling and docking studies could be a starting point to design novel inhibitors for these enzymes.

## Dissertation Overview

Isopentenyl diphosphate:dimethylallyl diphosphate isomerase (IDI) catalyzes an essential reaction in the isoprenoid biosynthetic pathway generating the allylic diphosphate substrate (DMAPP) from the homoallylic diphosphate (IPP), which is a required step in isoprenoid biosynthesis. Two convergently evolved, structurally and mechanistically distinct IDI enzymes have been identified. The type 1 enzyme (IDI-1) requires only divalent metal ions for catalysis and uses acid/base chemistry supplied by

active site amino acid residues to catalyze the 1,3-proton addition/elimination of IPP to DMAPP. The more recently discovered IDI-2 catalyzes an identical chemical transformation, and requires a reduced flavin mononucleotide ($FMNH_2$) coenzyme in addition to divalent metal ion for catalysis. The reaction catalyzed by IDI-2 does not involve a net change in the oxidation/reduction states of the substrates or the flavin coenzyme. The overall goal of our studies is to 1) define the general mechanistic features of IDI-1 and IDI-2 catalysis and to identify the role of $FMNH_2$ in this unusual flavin-dependent reaction, and 2) to understand the kinetics and mechanism of substrate binding, catalysis, and product release. This information could potentially assist in the development of novel inhibitors of IDI-2, as this enzyme in absent in humans, but is essential for the survival of several human pathogens including *S. pneumoniae, S. aureus,* and so forth.

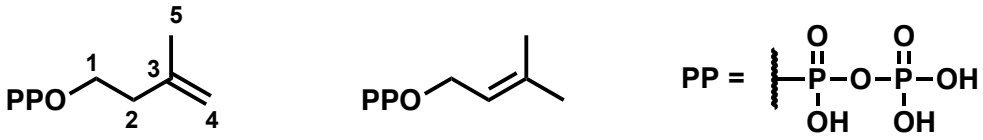


Isopentenyl Diphosphate (IPP)

Dimethylallyl Diphosphate (DMAPP)

**Figure 1.1.** Five-carbon precursors of Isoprenoid natural products. Carbon numbering is shown for IPP.

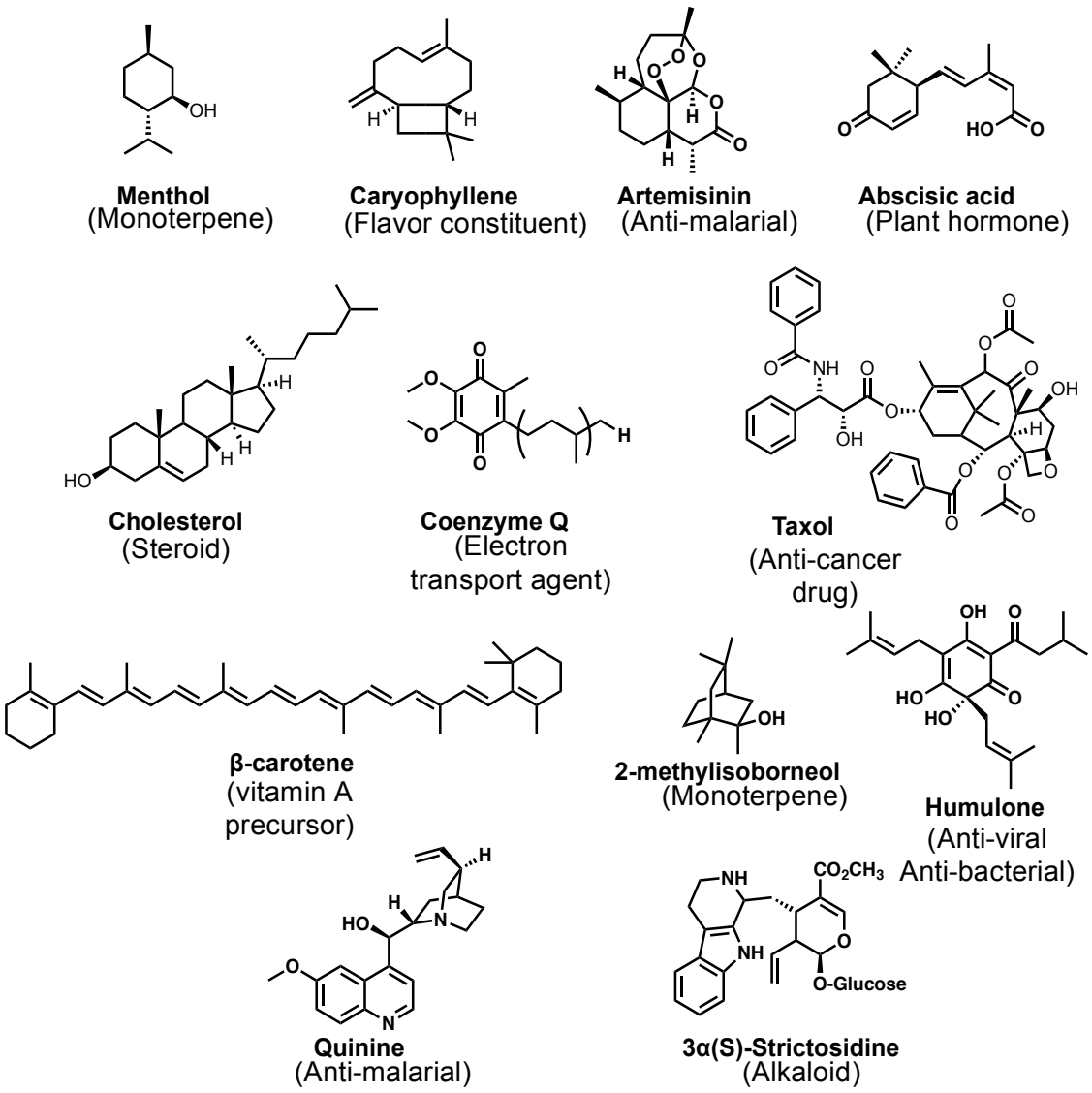


**Figure 1.2.** A few representative isoprenoid natural products.

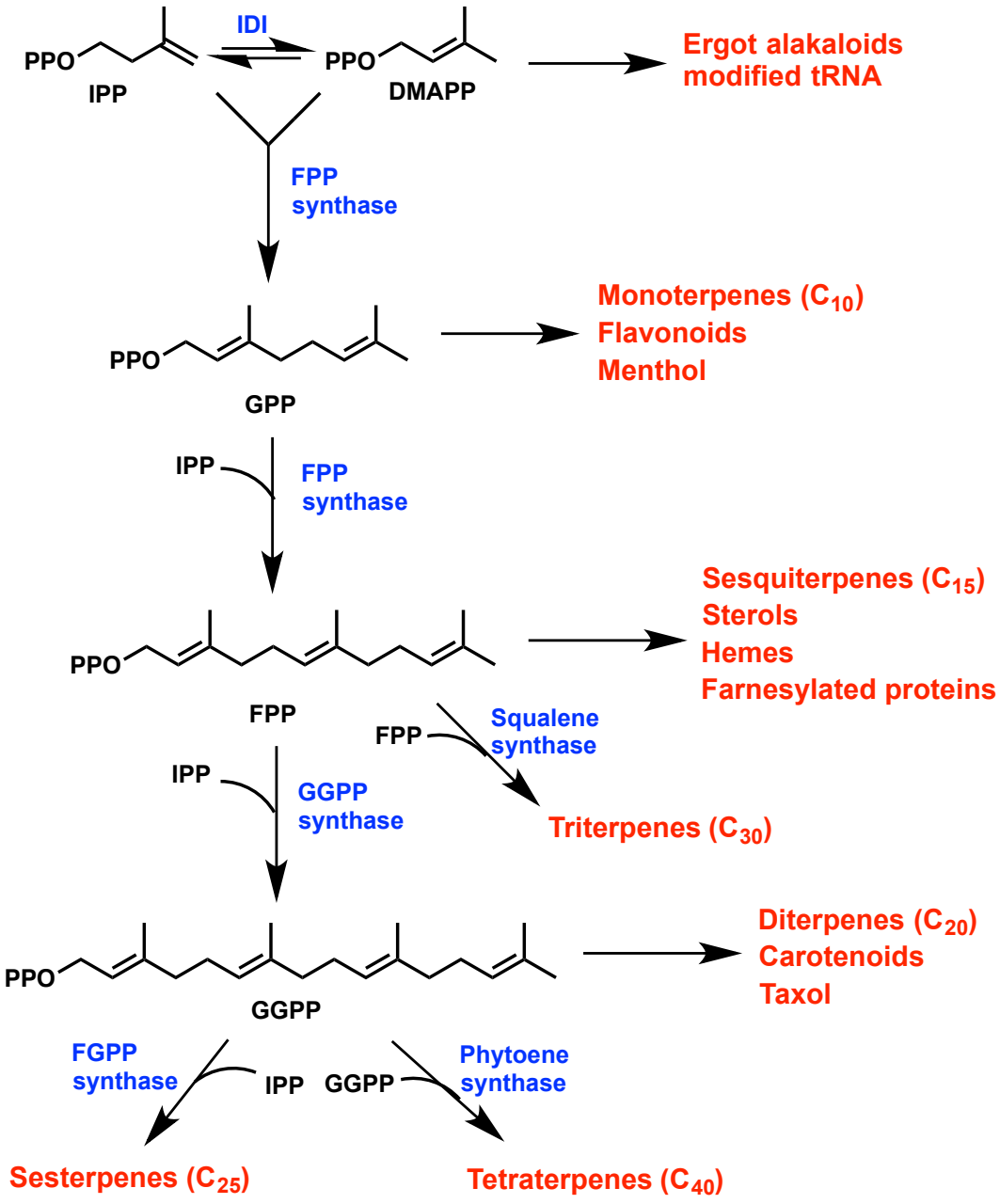


**Figure 1.3.** Structural diversity of isoprenoid compounds generated through chain-elongation.

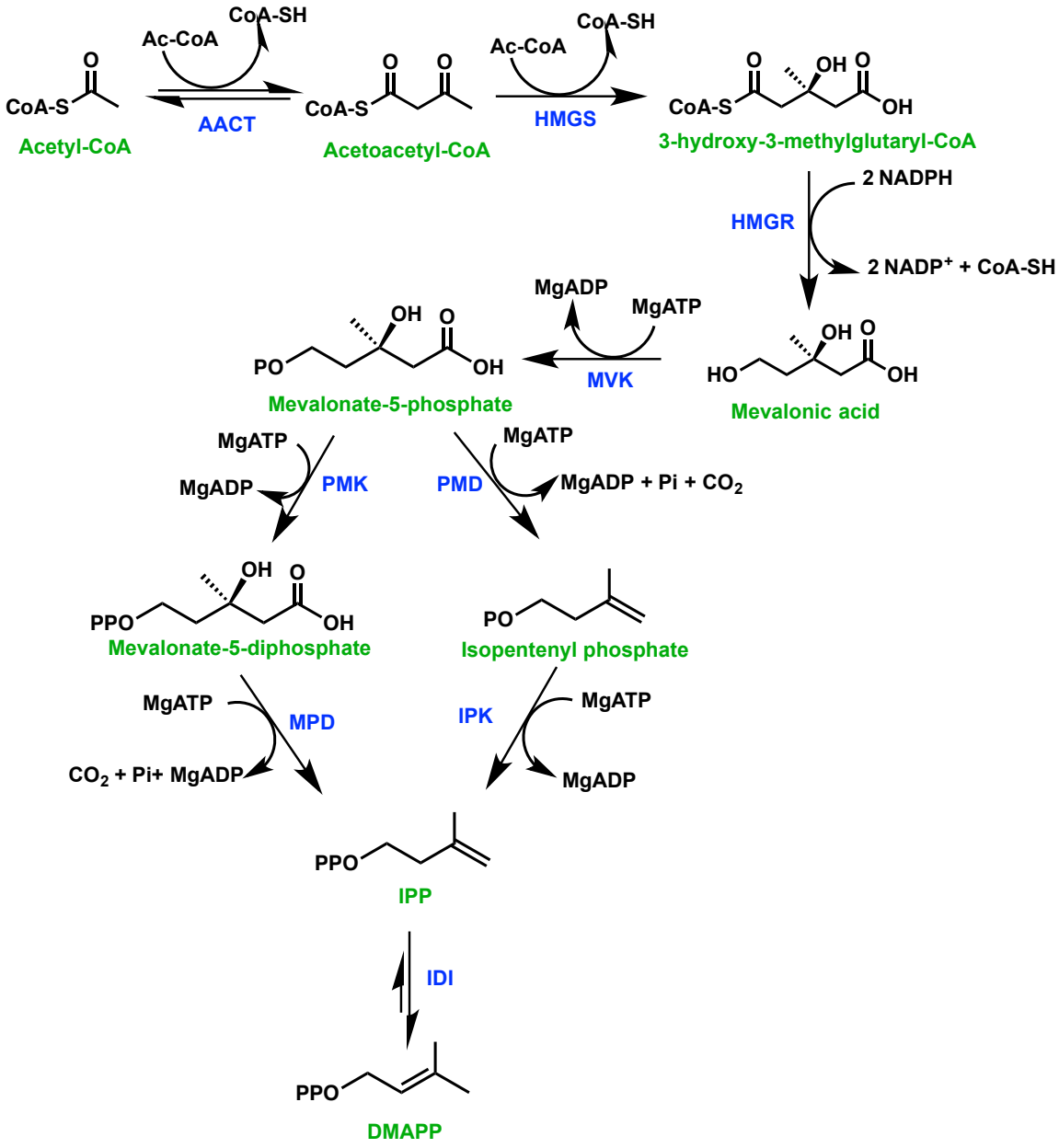


**Scheme 1.1.** Biosynthesis of IPP and DMAPP by the MVA pathway.

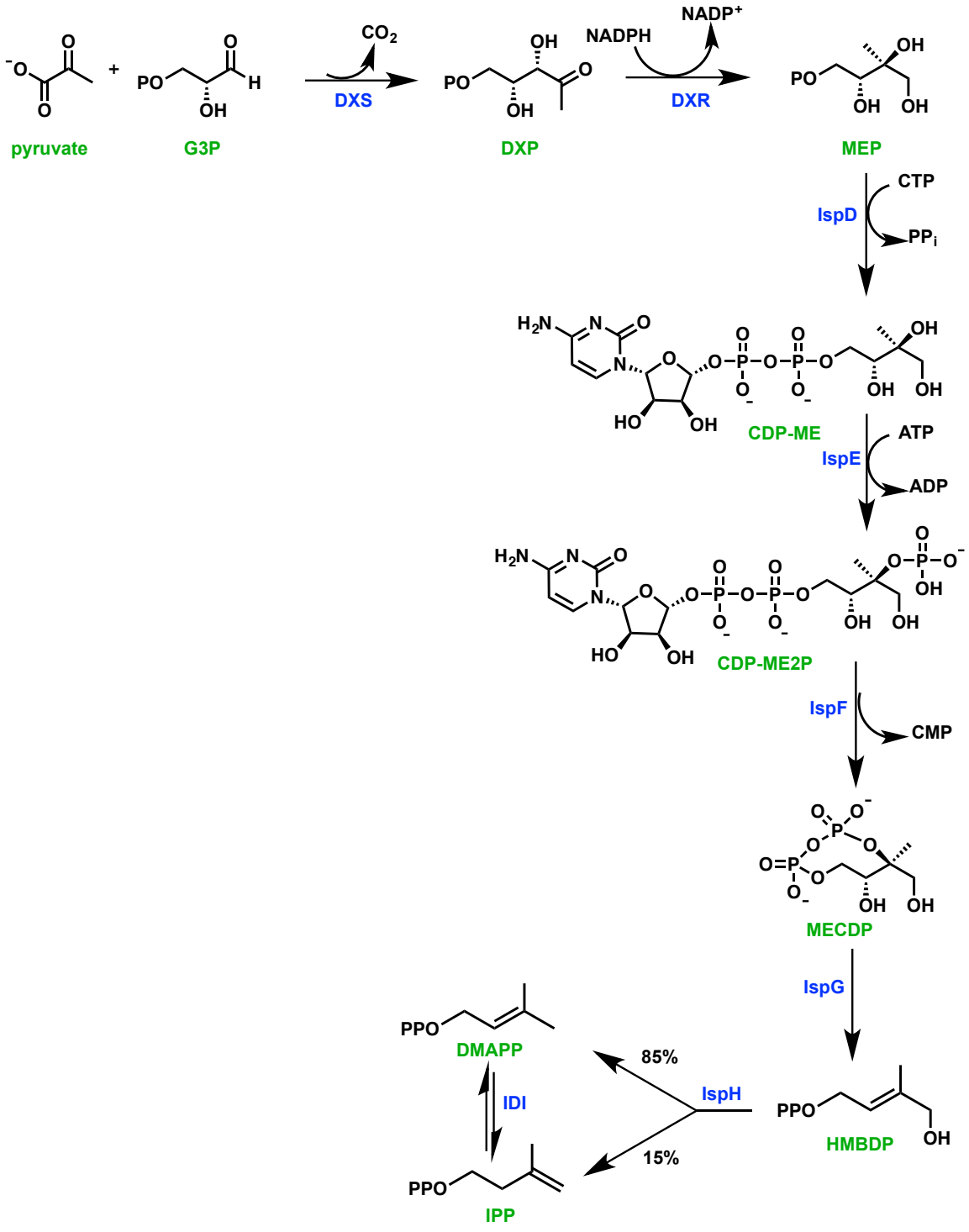


**Scheme 1.2.** Biosynthesis of IPP and DMAPP by the MEP pathway.

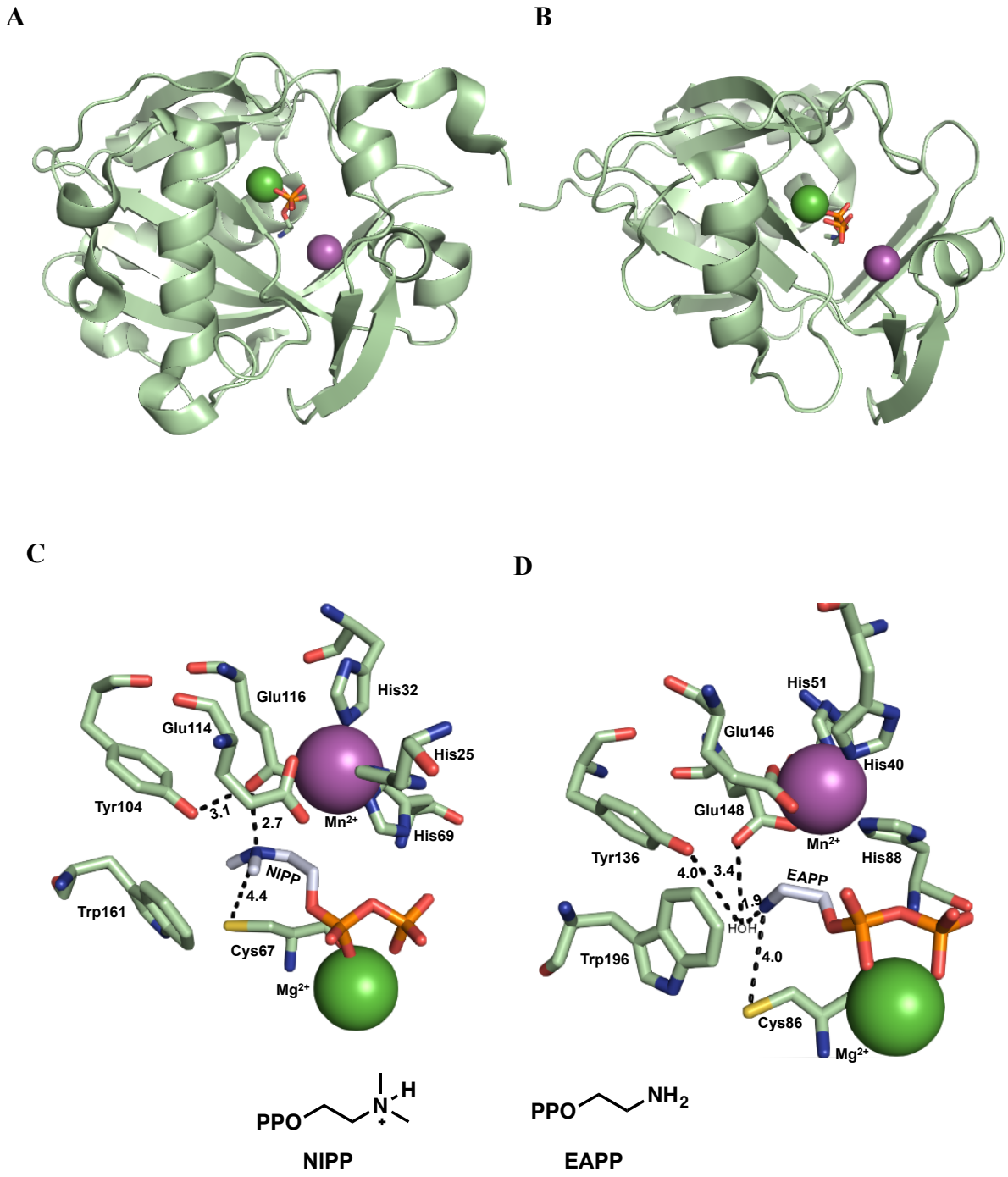


**Figure 1.4.** Crystal structures of A) *E. coli* IDI-1 and B) *H. sapiens* IDI-1. Active site of C) *E. coli* IDI-1 and D) Human IDI-1. Representative structures of NIPP and EAPP.[52,53]

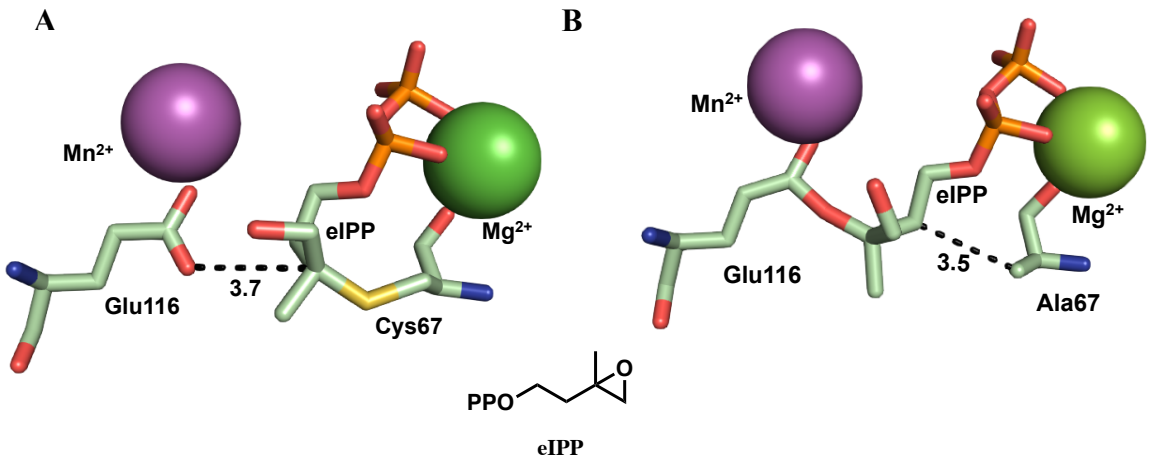


**Figure 1.5.** *E. coli* IDI-1 A) the C67A mutant showing the E116-eIPP adduct B) wt enzyme showing the C67-eIPP adduct.[52,61]

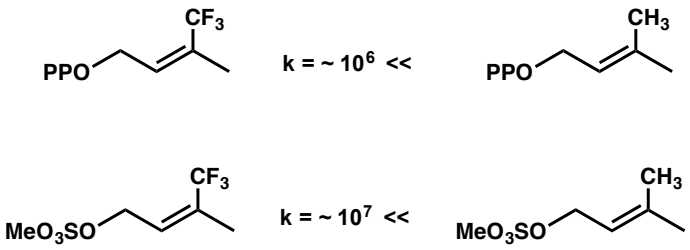


**Figure 1.6.** Relative rates of $CF_3$ analogs of IPP isomerization and methane sulfonate solvolysis

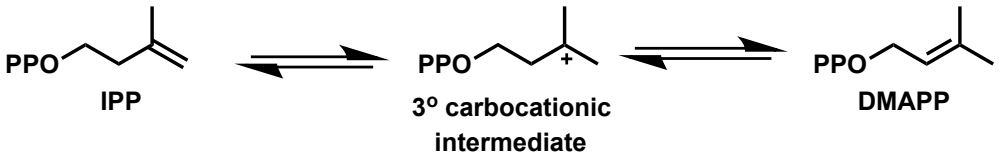


**Scheme 1.3.** IPP and DMAPP interconversion by IDI-1

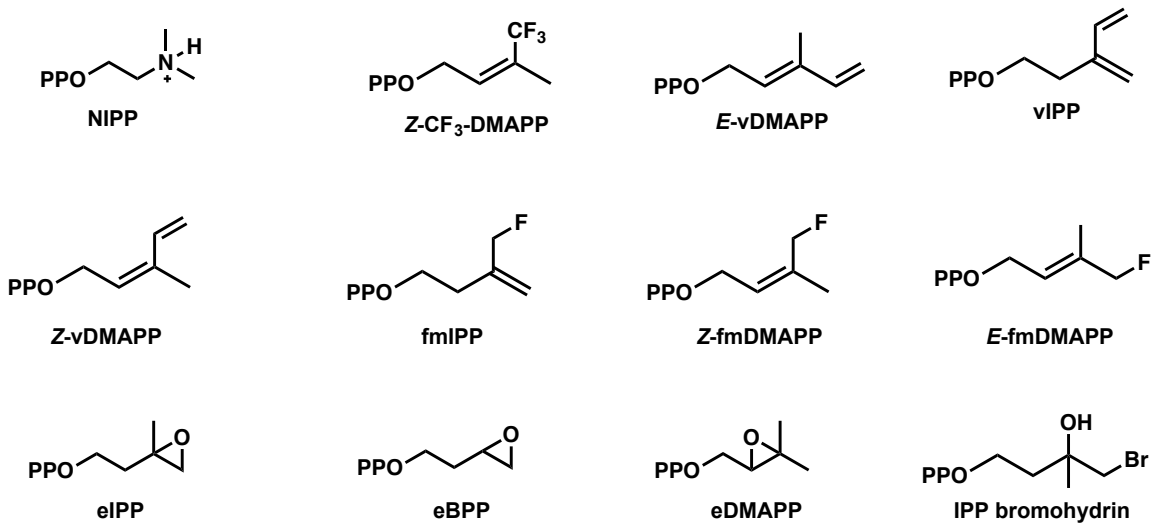


**Figure 1.7.** Representative structures of IPP analogs, mechanism-based inhibitors, transition state mimics used to probe the mechanism of IPP isomerization.

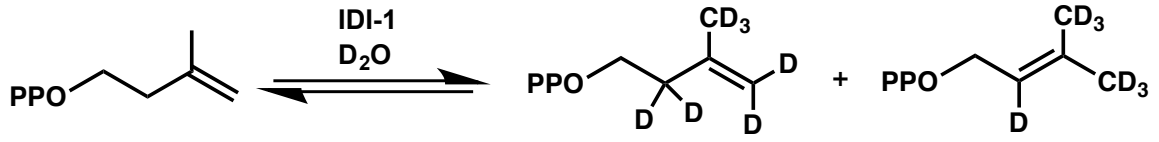


**Scheme 1.4.** IDI-1 catalyzed IPP isomerization in $D_2O$.

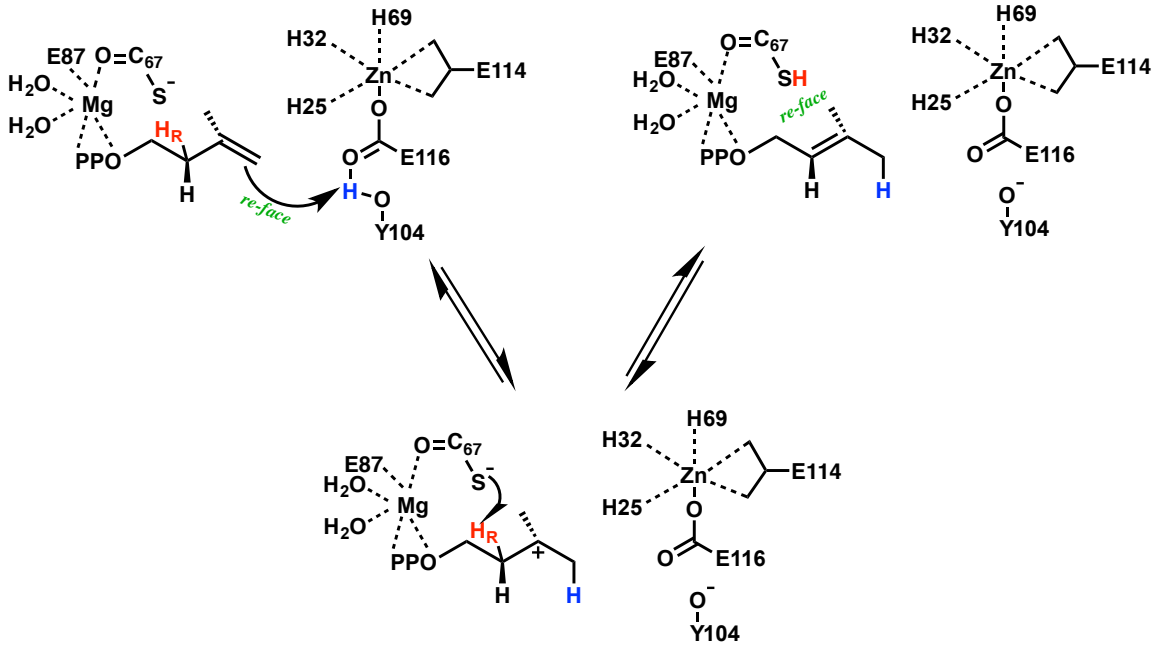


**Scheme 1.5.** IPP and DMAPP isomerization by IDI-1. Numbering of the residues was based on the *E. Coli* enzyme.

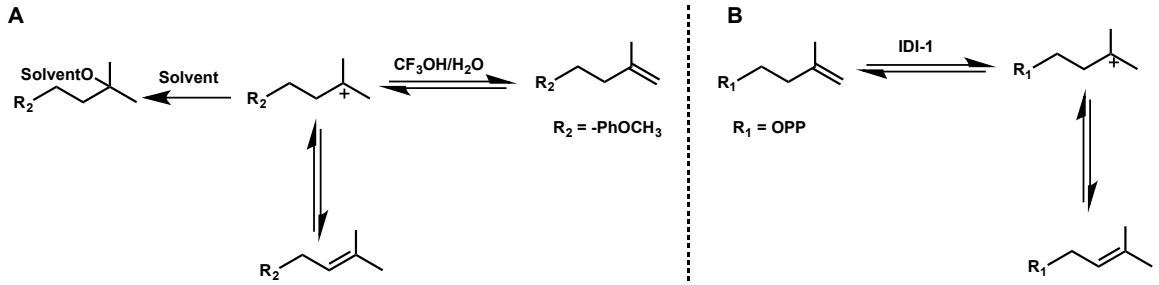


**Scheme 1.6.** A) $CF_3OH/H_2O$ and B) IDI-1 catalyzed 1,3-proton addition/elimination steps.

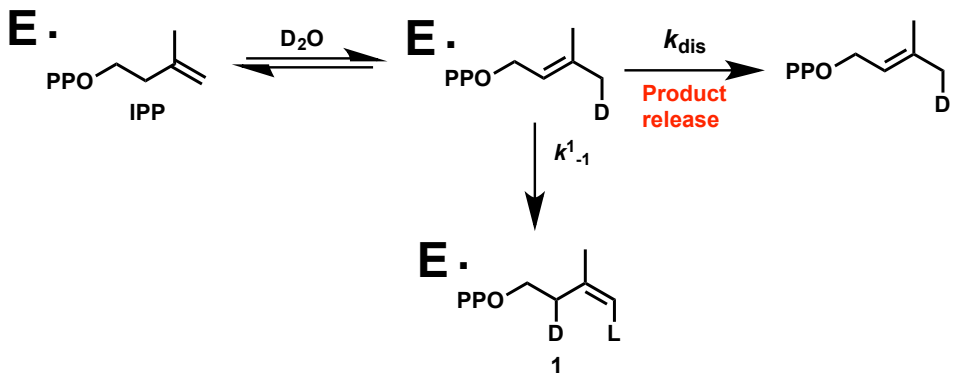


**Scheme 1.7.** Partitioning of the enzyme bound DMAPP in the IDI-1 active site.

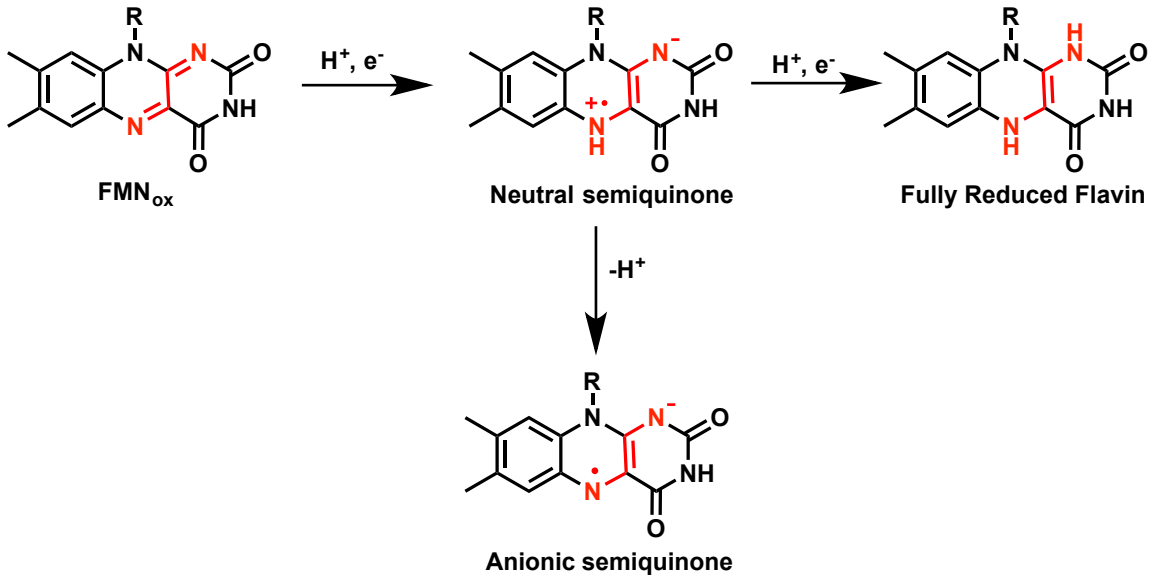


**Figure 1.8.** Two-electron reduction of oxidized flavin.

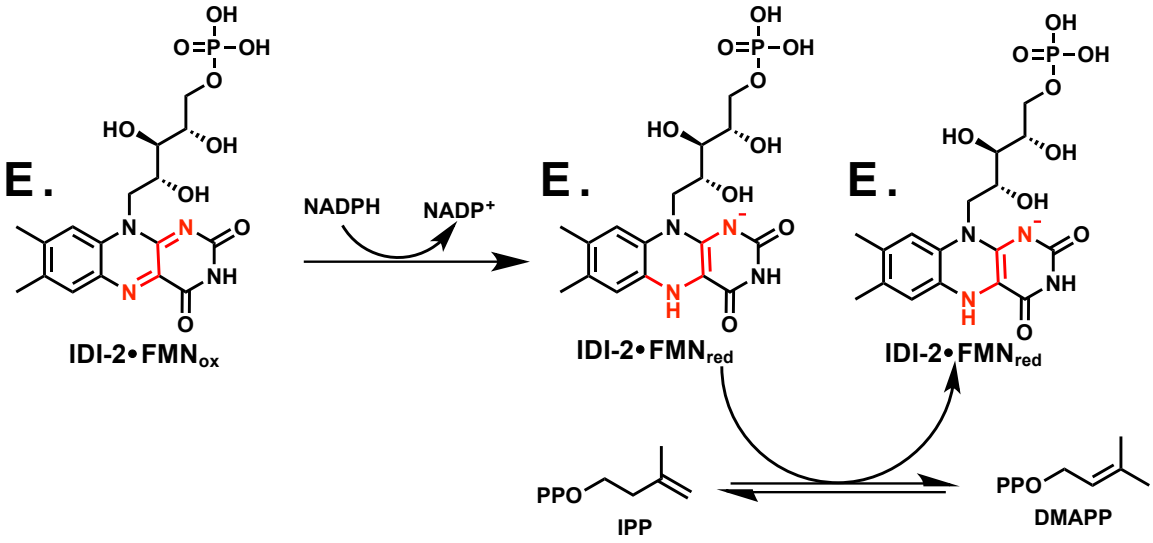


**Scheme 1.8.** IPP and DMAPP isomerization by IDI-2.

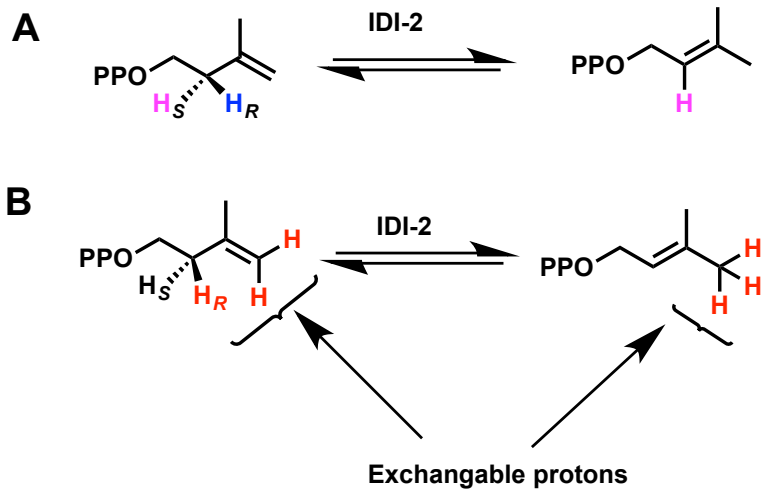


**Figure 1.9.** A) Stereospecific *pro R* hydrogen abstraction and B) Exchangeable protons (red) in IDI-2 catalyzed reactions.

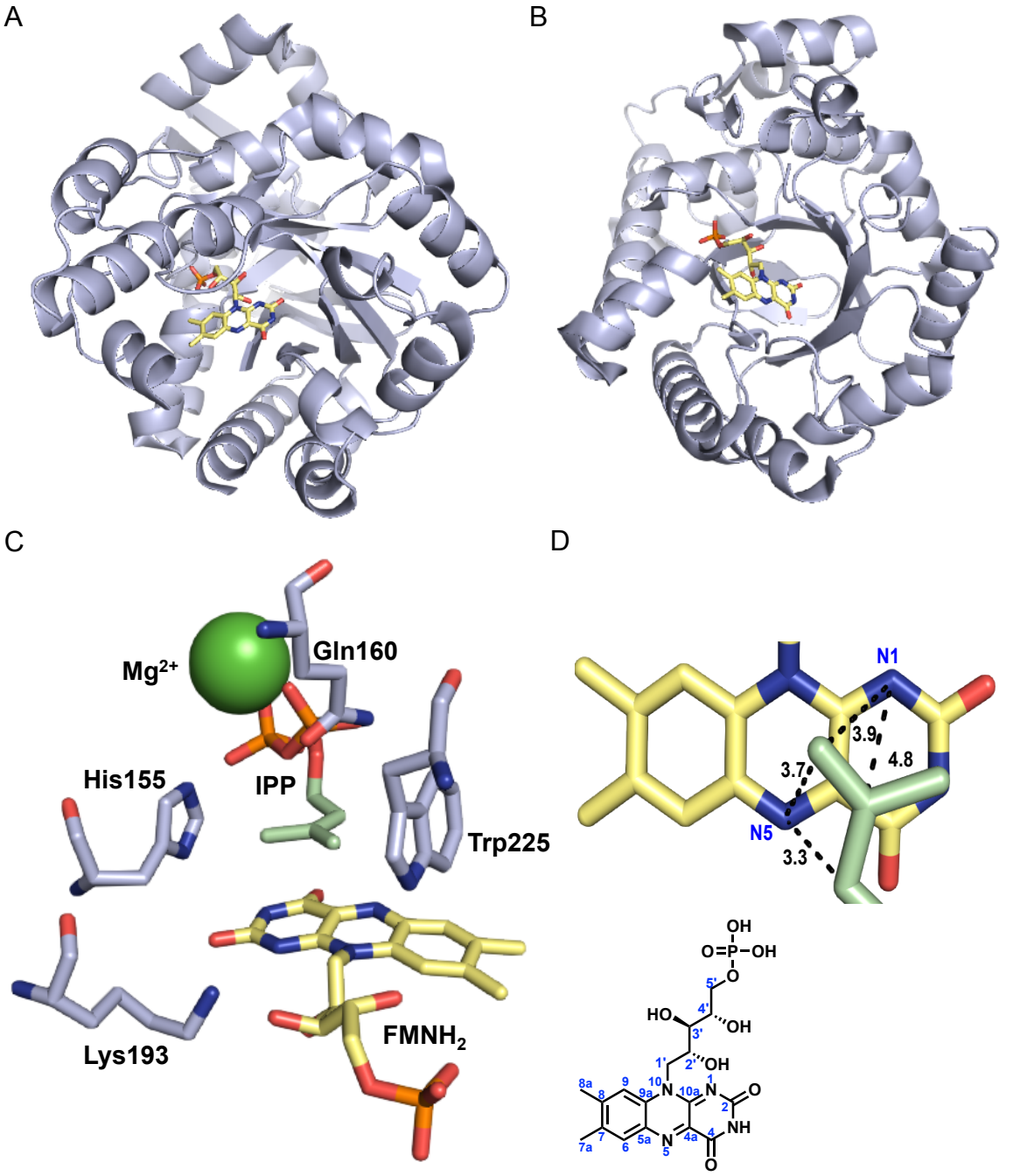


**Figure 1.10.** Monomers from the crystal structures of A) tetrameric *Sulfolobus shibatae* (*ss*) IDI-2 and B) octameric *Bacillus subtilis* (*bs*) IDI-2. C) The active site of *ss*IDI-2 and D) an enlargement showing distances between N1 and N5 of $FMNH_2$ and C2 and C4 of IPP.[80] Numbering on FMN also shown.

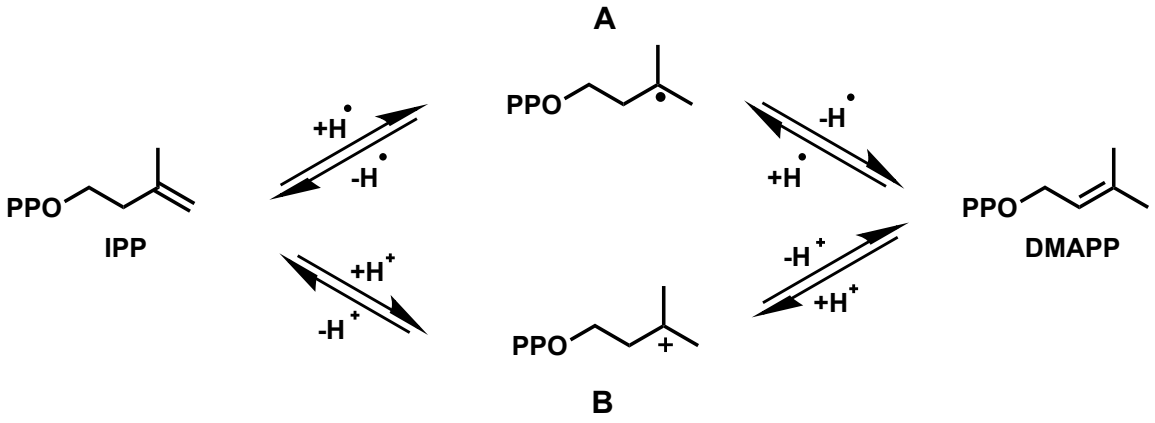


**Figure 1.11.** A) Hydrogen atom addition-abstraction and B) Protonation-deprotonation mechanism of IDI-2.

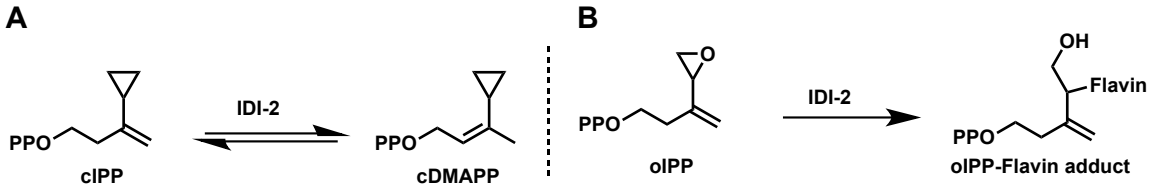


**Figure 1.12.** A) cIPP-IDI-2 reaction B) oIPP-IDI-2 reaction

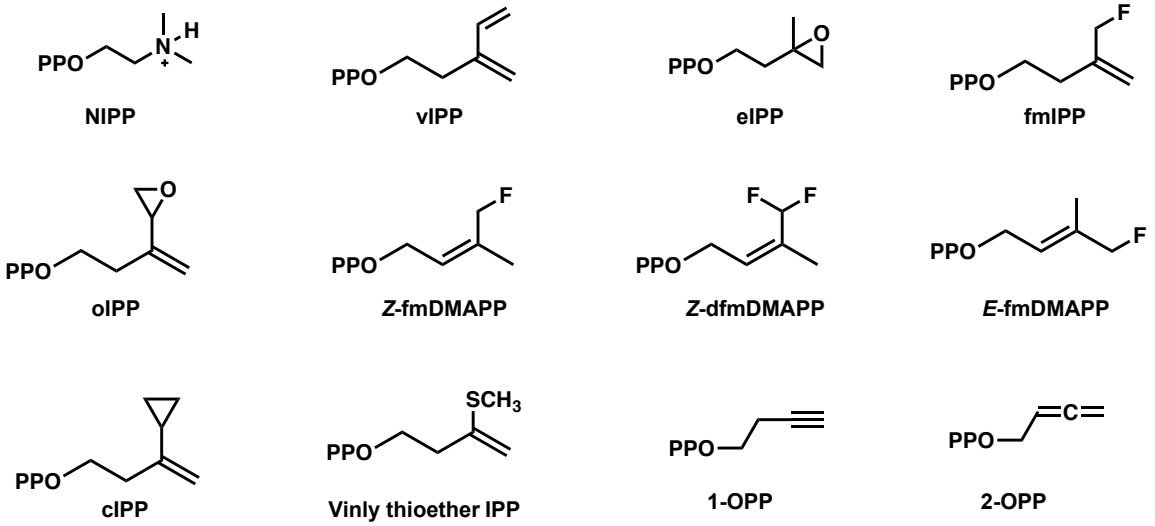


**Figure 1.13.** Representative IPP analogs used to probe the mechanism of IDI-2.

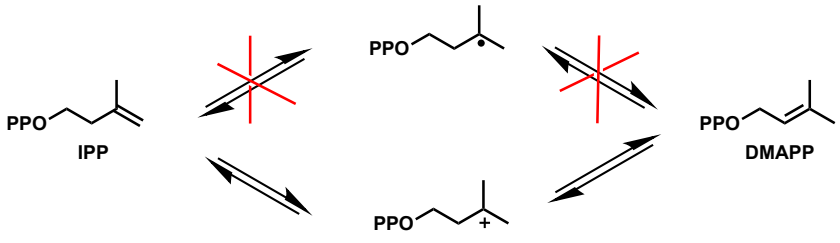


**Figure 1.14.** Protonation-deprotonation mechanism of IDI-2.

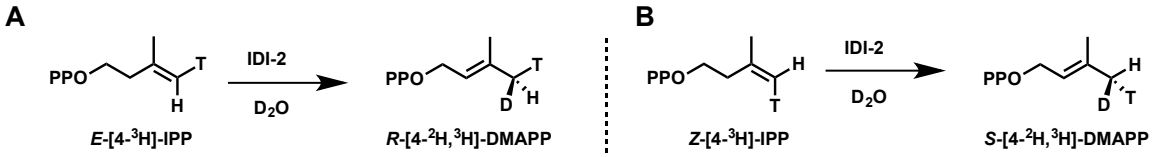


**Figure 1.15.** Chiral methyl analysis of IDI-2 reaction.

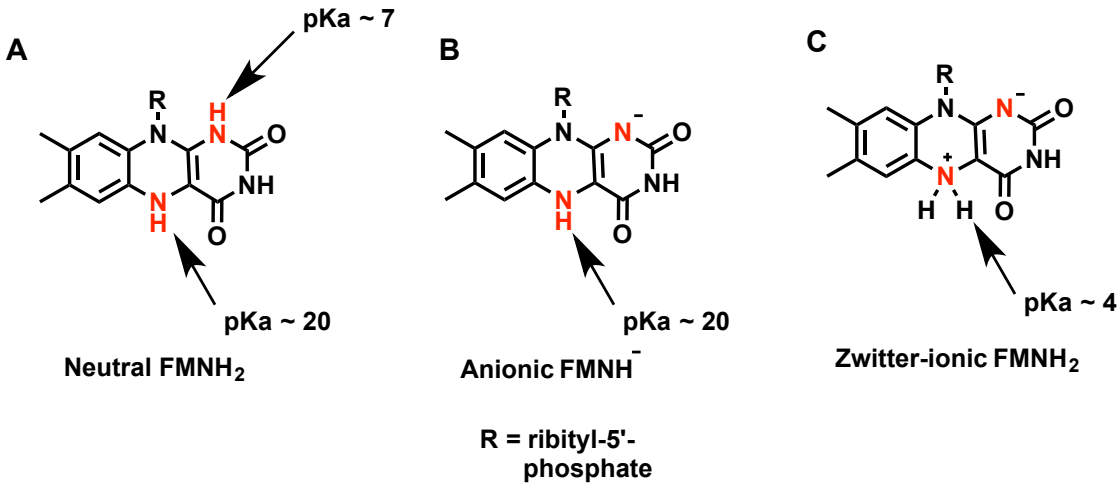


**Figure 1.16.** FMN in neutral reduced (A), anionic reduced (B), and zwitter-ionic reduced (C) forms.

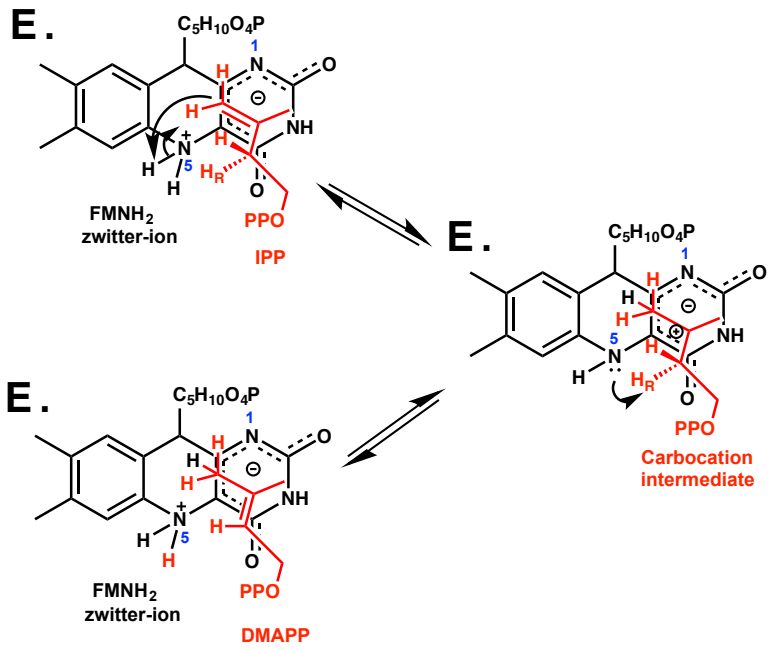


**Figure 1.17.** Mechanism of IDI-2 catalysis. E represents enzyme.

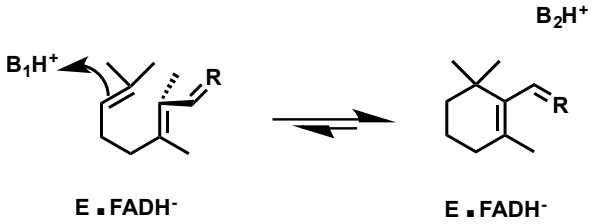


**Figure 1.18.** FAD-dependent cyclization of lycopene to β-carotene by CRTY with no $FAD_{red}$ net redox change.

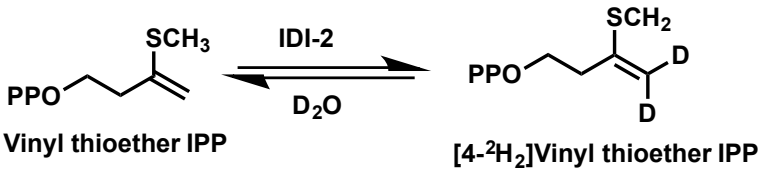


**Figure 1.19.** IDI-2 catalyzed vinyl thioether IPP reaction in $D_2O$.

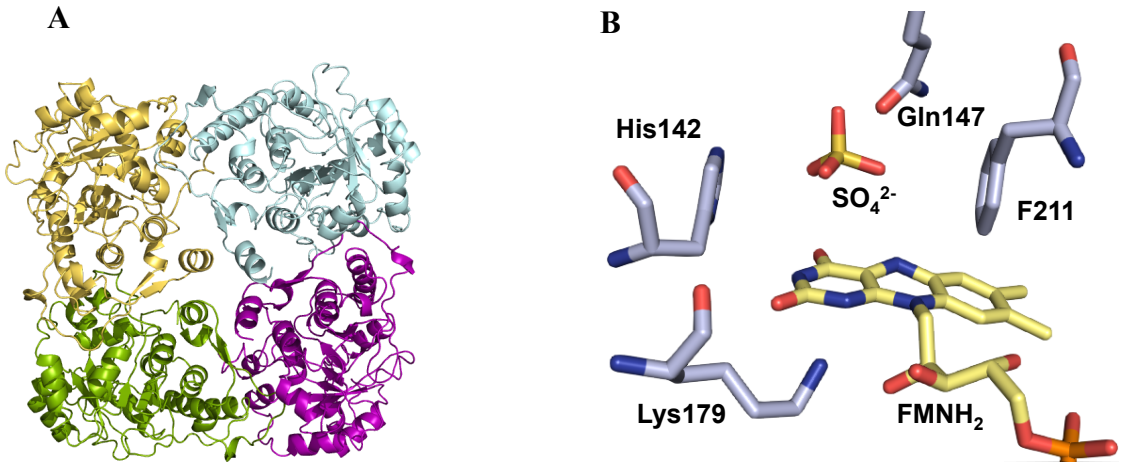


**Figure 1.20.** A) Wild type homotetrameric *sp*IDI-2 B) Active site of *sp*IDI-2.[98]

**Table 1.1.** Solution and crystal structures of IDI-2

| Enzyme | Solution Structure | X-ray structure |
|---|---|---|
| *Streptococcus pneumoniae* IDI-2 (*sp*IDI-2)[98] | Tetramer | Tetramer per asymmetric unit |
| *Thermus thermophilus* IDI-2 (*Tt*IDI-2)[104,105] | Tetramer | Octamer |
| *Sulfolobus Shibatae* IDI-2 (*ss*IDI-2)[75] | Octamer-Tetramer (without $His_6$)/Tetramer (with $His_6$) | Octamer |
| *Staphylococcus aureus* IDI-2 (*sa*IDI-2)[74] | Tetramer | N.D |
| *Streptomyces* sp CL. 190[72] | Tetramer | N.D |
| *M. Thermaautotrophicus* IDI-2 (*Mt*IDI-2)[102] | Tetramer | N.D |
| *Methanocaldococcus jannaschii* IDI-2 (*Mj*IDI-2)[106] | N.D | Monomer per asymmetric unit |
| *P. furiosis* IDI-2 (*Pf*IDI-2)[107] | Tetramer | N.D |
| *Synechocysis* sp strain 6803[103] | Tetramer | N.D |
| *T. kodakaraensis* IDI-2 (*Tk*IDI-2)[108] | Octamer | N.D |
| *B. Subtilis* IDI-2 (*bs*IDI-2)[78,101] | Probably Tetramer | Octamer |

CHAPTER 2

# CONSTRUCTION OF CATALYTICALLY ACTIVE MONOMERIC TYPE 2 ISOPENTENYL DIPHOSPHATE:DIMETHYLALLYL DIPHOSPHATE ISOMERASE

## Introduction

Protein oligomerization is a fundamental chemical process governed by the formation of stable noncovalent interactions across the protein subunit interfaces.[109] An oligomer is a stable complex formed from monomeric units held together by these non-covalent interactions. Approximately 35% of proteins in a cell exist in an oligomeric state.[110] In some instances, active sites are located at the interface between subunits,[111] while in others cooperative motion among subunits is important for substrate binding.[112] Identifying and utilizing these interactions to manipulate protein structure and function can provide important insights about structure-function relationships or can provide proteins for structural studies by NMR spectroscopy and X-ray crystallography.[113,114] Wild-type (wt) Streptococcus pneumoniae IDI-2 is a homotetramer in solution where the monomers are related by a 4-fold axis of symmetry perpendicular to the plane of the sub-units (Figure 2.1).[98] In the X-ray structure of homotetrameric wt *sp*IDI-2, the four sub-units make identical contacts at the intersubunit interfaces. We have identified noncovalent interactions between monomeric subunits in the X-ray crystal structure of

homotetrameric *sp*IDI-2[98] involving amino acids at three distinct locations at the interface as mentioned below:

(i) near the amino terminus

(ii) in the middle of the polypeptide chain

(iii) near the carboxy terminus of the monomers

We aimed to disrupt the inter-subunit interactions to create a catalytically active soluble form of monomeric *sp*IDI-2 with goals of understanding the kinetic mechanism of the enzyme and reducing the size of the system to improve the sensitivity of $^{1}H$, $^{13}C$, and $^{15}N$ for NMR experiments. Mutagenesis experiments to disrupt the inter-subunit interactions resulted in formation of a soluble, catalytically active form of monomeric *sp*IDI-2.

## Experimental Procedures

*Materials*. HEPES and NADH were purchased from Research Products International (RPI). Cell culture growth media, chemicals, and salts were purchased from Fisher Scientific, Sigma-Aldrich, and B & D. $^{14}C$-labelled IPP (50.8 μCi/μmol) was purchased from Perkin-Elmer. The oligonucleotide primers used for mutagenic studies were synthesized by the DNA/peptide synthesis HSC core facility at the University of Utah.

*Site-directed mutagenesis*. The gene encoding *sp*IDI-2 contained in the plasmid pQE-30Xa (p-*sp*IDI-2). The *sp*IDI-2 gene has a hexahistidine ($His_6$)-tag at the N-terminus of the protein. Construction of this plasmid was previously reported.[98] p-*sp*IDI-2 was the template for the site directed mutagenesis experiments using mutagenic primers for polymerase chain reaction (PCR) followed as per the QuikChange Lightning

mutagenesis kit (Agilent).

*Protein expression and purification.* *sp*IDI-2 mutants containing the desired changes were transformed into E. coli M15pREP4 cells. The cell cultures were grown in MDG [LB+1% glucose] media containing 100 μg/mL ampicillin and 50 μg/mL kanamycin at 37 °C, 250 rpm to $OD_{600}$ ~ 0.6. Protein overexpression was induced by the addition of isopropyl-β-D-thiogalactoside (IPTG, final concentration of 0.4 mM) that contained flavin mononucleotide (FMN, final concentration 40 mg/L). The cell culture medium was incubated for 12 h at 30 °C. The cells were then harvested by centrifugation (6000g, 25 min, 4 °C) and stored at -80 °C until use. The frozen cell pellet was suspended in lysis buffer (50 mM sodium phosphate, pH 8.0, containing 300 mM NaCl and 10 mM imidazole) and the cells were lysed by incubation with 10 mg lysozyme, one protease inhibitor tablet (Roche), and 2 mg of DNase I on ice for 30 min followed by sonication (6 X 30 s with 1 min cooling intervals on ice). The cell lysate was centrifuged (12000 rpm, 25 min, 4 °C) and the resulting supernatant was mixed with 10 mL of Ni-NTA Agarose resin (Qiagen) and loaded on to the column. Flow-through was collected, and the protein bound Ni-NTA agarose resin was washed with 50 mM sodium phosphate, pH 8.0, containing 300 mM NaCl and 20 mM imidazole containing 2M KBr until all the yellow color disappears. Protein was eluted with elution buffer (50 mM sodium phosphate, pH 8.0, containing 300 mM NaCl and 250 mM imidazole) and fractions containing *sp*IDI-2 were pooled, concentrated with a 10 kDa MWCO filter (Centriprep, Millipore) and dialyzed against 10 mM Tris-HCl buffer, pH 8, containing 15% glycerol and 150 mM NaCl. The purity of the protein was determined by sodium dodecyl sulphate-polyacrylamide gel (SDS-PAGE) electrophoresis. Protein concentration was determined

by the BCA assay (Pierce).[115]

*Gel-filtration chromatography.* The quaternary structures of the *sp*IDI-2 mutants were estimated by gel filtration chromatography using an AKTA FPLC system with a Superdex 200 (Tricorn, 10/30 GL, GE) column. The column was pre-equilibrated and eluted at 4 $^{o}$C with 50 mM potassium phosphate buffer, pH 8.0, containing 150 mM NaCl. Thyroglobulin (669 kDa), ferritin (440 kDa), BSA (67 kDa), ovalbumin (43 kDa), and ribonuclease A (14 kDa) were used as standards to calibrate the column, and the oligomeric state of proteins was determined based on the calibration data generated from the known standards mentioned above. Prior to the kinetic, CD, sedimentation, NMR, UV-Vis, and fluorescence thermal shift assays, the *sp*IDI-2 proteins were purified by Ni-NTA chromatography followed by gel-filtration chromatography purification on a Superdex 75 16/60 HiPrep column.

*Analytical equilibrium sedimentation.* Purified monomeric-*sp*-IDI-2 (m-*sp*IDI-2) was dialyzed against 10 mM Tris buffer, pH 8.0, containing 150 mM NaCl and 8 mM TCEP to remove glycerol present in the protein storage buffer and the resulting protein centrifuged at 18,000 g to clarify the sample. The protein was then spun at three concentrations (11 μM, 5.5 μM, 2.75 μM) and three speeds (9000, 12,000, and 15,000 rpm) using a An-50-Ti rotor (Beckman Coulter) at 4 °C until equilibrium was established. Data were fit globally to an ideal single species model with a floating molecular weight using nonlinear least squares analysis as implemented in HeteroAnalysis.[116] Buffer densities and protein partial specific volumes were calculated with SEDNTERP (version 1.09).[117]

*Circular dichroism (CD) spectroscopy.* The CD spectroscopy experiments were performed on a Jasco J-815 spectropolarimeter. The spectrum for wt *sp*IDI-2 was

measured in 10 mM Tris buffer, pH 8.0, containing 10 % glycerol; whereas the spectrum for m-sp-IDI-2 was measured in 10 mM Tris buffer, pH 8.0, containing 150 mM NaCl and 15 % glycerol. CD spectra were recorded for 4 μM samples in a 1 cm path length cuvette at 25 $^{o}$C as the average of three scans (0.1 nm steps) from 200 to 260 nm in with a signal averaging time of 1 s and a bandwidth of 1 nm.

*UV-visible assays.* UV-visible spectra for m-*sp*-IDI-2 were performed under anaerobic conditions as described.[98] Apo-m-*sp*IDI-2 was reconstituted with FMN using the procedure described previously, except that all washes were performed under ambient $O_2$ conditions.[99] The resulting m-*sp*IDI-2•FMN solution, and the substrates IPP and DMAPP were degassed and transferred in to anaerobic chamber. m-*sp*IDI-2•FMN was reduced with 8 mM $Na_2S_2O_4$ and excess $Na_2S_2O_4$ was removed by centrifugation using a 10 kDa MWCO filter (Amicon Ultra) with 100 mM HEPES buffer, pH 7.0 containing 150 mM NaCl as the wash solution. Assays were conducted in 100 mM HEPES buffer, pH 7.0 containing 80 μM m-*sp*IDI-2•FMN, 150 mM NaCl, 25 mM $MgCl_2$, 2.5 mM DTT, and 2 mM IPP and DMAPP. Measurements were recorded on Agilent 8453 diode array spectrophotometer.

*Fluorescence thermal shift assays*. $T_m$s for wt and monomeric *sp*IDI-2 were measured from pH 5-10 in 50 mM buffer (pH 5.0, citric acid; pH 6–8, phosphate; pH 9.0, CAPSO; pH 10–11, CAPS) containing 150 mM NaCl. Assays were carried out in a 96-well plate. Each well contained 20 μL total volume consisting of 40 x SyproOrange dye and 2 μM of wt or m-*sp*-IDI-2. The plate temperature was ramped from 27 $^{o}$C to 95 $^{o}$C and the assays were run in duplicate.

*$^{15}$N-$^{1}$H HSQC protein NMR studies*. Bacterial cultures for the overproduction of

$^{15}$N-labeled wt and m-*sp*IDI-2 were grown in 1L scale using the same IDI-2 expression plasmid, *E. Coli* strain and antibiotics described above. Wt and monomeric *sp*IDI-2 were uniformly labeled with $^{15}$N by expression in minimal (M9) media using $^{15}$N-enriched $(NH_4)_2SO_4$ (500 mg) and $NH_4Cl$ (500 mg) as a $^{15}$N-nitrogen source in 1L culture.[118] Ten milliters of overnight LB cultures were used to inoculate 1L M9 medium for protein overexpression. Procedure for protein overexpression and purification was the same as described in protein expression and purification section. NMR spectra obtained at 25 $^{o}$C on a 600 MHz spectrometer equipped with a cold probe. $^{15}$N-$^{1}$H HSQC NMR[119] spectra were collected for samples containing 150 μM $^{15}$N-labeled protein in 50 mM phosphate buffer pH 7.0 containing 10% $D_2O$ in 700 μL volume. Monomeric *sp*IDI-2 NMR sample additionally contained 150 mM NaCl and 2 mM DTT.

*Enzyme activity and kinetic assays*. Isomerase activity of the *sp*IDI-2 mutants was measured using the acid lability protocol.[72,120] Assays under aerobic conditions with varied IPP and FMN were initiated by the addition of 100 nM enzyme to 100 mM HEPES buffer, pH 7.2, containing 150 mM NaCl, 10 mM $MgCl_2$, and 60 – 2500 μM [$^{14}$C]IPP (2.83 – 0.67 μCi/μmol) at 465 μM FMN and 17 – 441 μM FMN at 2 mM [$^{14}$C]IPP (3.2 μCi/μmol) in a total volume of 50 μL. Anaerobic assays were performed in anaerobic chamber with 2 mM [$^{14}$C]IPP (3.2 μCi/μmol), 8 mM $Na_2S_2O_4$, and 0.2-238.5 μM FMN. After 10 min at 37 °C, the reactions were stopped by addition of 200 μL of 4:1 MeOH/HCl, followed by a incubation 10 min at 37 °C. Soluble organic products were extracted with 0.8 mL of ligroine and 0.4 mL of the extract was mixed with scintillation cocktail (Ultima Gold Cocktail, Perkin-Elmer). Radioactivity (Disintegrations per minute (DPM)) was counted by liquid scintillation spectrometry (TriCarb 2910TR, Perkin

Elmer). Kinetic assays were replicated three times under initial velocity conditions (<10% completion) and the data were fit with Michealis-Menten and Hill-equations (Table 2.3) using nonlinear regression protocols (Grafit 5.0, Erithacus Software). Blank samples contained $H_2O$ instead of enzyme. FMN stock concentration was determined using UV-vis spectroscopy with FMN extinction coefficient ($\lambda_{450}$) of 12, 200 $M^{-1}cm^{-1}$.

*Stopped-flow kinetic assays.* FMN reduction rates were measured with a KinTek SF-2004 stopped-flow spectrometer equipped with a xenon arc lamp monochromater. The reaction buffer consisted of 100 mM HEPES, pH 7.0 containing 25 mM $MgCl_2$ and 150 mM NaCl at 20 °C. Measurements were performed with substrates (10 μM FMN, 2 mM IPP), reductants (20 mM NADH or 5 mM $Na_2S_2O_4$), and enzyme (10 μM IDI-2•FMN). IDI-2•FMN complex was prepared as described in the "UV-vis assays" section. Changes in FMN redox state was monitored by fluorescence emission with a 530 nm wavelength bandpass filter (Newport Corporation) with an excitation wavelength of 420 (IDI-2•FMN) or 450 nm (free FMN). Data were fit to a single- or double-exponential equation to determine pseudo-first order rate constants. Analysis was performed using Prism version 6.0.[121]

## Results and Discussion

*Analysis of the interface between subunits in homotetrameric spIDI-2.* In the crystal structure of wt *sp*IDI-2, the subunits in the homotetramer are linked non-covalently by hydrogen bonding and ionic interactions between amino acid side chains in one subunit with side-chains and backbone peptides in the adjacent subunit. The contact surfaces at the four interfaces between subunits in the homotetramer are identical,

forming a quaternary structure with a 4-fold axis of symmetry perpendicular to the plane of the subunits. Each contact surface consists of two distinct regions (Figure 2.2).

In the first region (site 1), a loop in the subunit A (cyan), which includes amino acids H30 to N37, binds into a cleft between two α-helices in subunit B (gold) as shown in Figures 2.2 and 2.3A. Specific polar interactions at the site 1 surface involve contacts between the side chains of amino acids $R_B159$, $D_B186$, and $T_B189$ with the backbone amide moieties of amino acids $L_A35$, $S_A32$, and $S_A32/L_A33$, respectively, while the backbone amide moieties of amino acids $F_B183/G_B184$, $D_B186$, and $F_B158/R_B159$ interact with side chains of amino acids $H_A30$, $S_A32$, and $N_A37$, respectively (Figure 2.3B).

In the second region (site 2), the C-terminal α-helix of one subunit in the homotetramer interacts with the same α-helix in the neighboring subunit. The non-covalent attachments between the two helices consist of a combination of interactions between the amine group of $G_A324$ and the side chain of $E_B328$ (H-bonding), the side chains of $K_A327$ and $D_B331$ (ionic), and the side chains of $K_A330$ and $Q_B332$ (H-bonding). These interactions are shown in Figure 2.4. All of the interactions identified in sites 1 and 2 are listed in Table 2.1. The amino acids at the subunit interface surfaces are distant from the active site.

*Disruption of noncovalent interactions at the monomer-monomer interface.* The initial set of disruptions between non-covalent interactions at the interface between wt sp-IDI-2 monomers was at site 1. The first set of mutations, H30A, S32A, N37A, and T189A, disrupted hydrogen bonds in $H_A30$-$F_B183/G_B184$, $S_A32$-$D_B186$, $N_A37$-$F_B158/R_B159$, and $S_A32/L_A33$-$T_B189$ units. The elution volume of soluble (H30A:S32A:N37A:T189A)-spIDI-2 on a gel filtration column was similar to that of

homotetrameric wt-sp-IDI-2 (Figure 2.5A and 2.5B), indicating that the removing the side chain-backbone hydrogen bonding interactions in site 1 did not change the quaternary structure of the enzyme. Two additional mutations in the site 1 region were studied. The R159S, D186S double mutant was a soluble homotetramer, as was the protein with six additional mutations (H30A, S32A N37A, R159S, D186S, T189A), where all of the original side chain-backbone interactions at site 1 had been altered (Figure 2.6).

Next, we investigated mutations at site 2, with and without additional mutations at site 1. Deletion of the C-terminal α-helix ($^{324}$GKLKEAKDQ$^{333}$M) at site 2 in wt *sp*IDI-2, as well the same deletion in a R159S:D186S site 1 double mutant background, gave insoluble proteins (data not shown). Furthermore, replacement of lysines K325, K327, and K330 in the C-terminal α-helix of (H30A:S32A: N37A:R159S:D186S:T189A)-*sp*IDI-2 also gave insoluble protein. These observations indicate that deletion of, or substantial alterations in, the C-terminal α-helix results in a loss of solubility. We then deleted amino acids $^{328}$EAKDQ$^{333}$M in the C-terminal α-helix in (H30A:S32A:N37A:T189A)-*sp*IDI-2. The resulting protein was both soluble and monomeric in solution (Figure 2.7), but was not active.

In further attempts to identify a catalytically active monomer, we constructed single point alanine mutants and a few combinations of double point alanine mutants of amino acids H30, N37, and T189 in the $^{328}$EAKDQ$^{333}$M-deletion background (Table 2.2). Among these, the individual single point alanine mutations gave catalytic active enzymes; whereas, the proteins with two point mutations were inactive (Table 2.2). Gel-filtration chromatography of the H30A and T189A single mutants indicated that the

proteins were a mixture of monomers and tetramers in solution with the tetrameric form predominating (Figures 2.8A and 2.8B). In contrast, gel-filtration chromatography of the N37A point mutant in the $^{328}$EAKDQ$^{333}$M-deletion background showed that the active protein was monomeric in solution with an estimated mass of 44.5 kDa (Figure 2.9). The monomeric state for (N37A:$^{328}$EAKDQ$^{333}$M-deletion)-*sp*IDI-2 was confirmed by equilibrium sedimentation experiments, which gave an estimated mass of 40.5 kDa (Figure 2.10). The calculated mass of the protein (~39.1 kDa) corresponded to the mass of (N37A:$^{328}$EAKDQ$^{333}$M-deletion)-*sp*IDI-2 determined by electrospray mass spectrometry (observed 39133.6 Da, calculated 39122.6 Da). In contrast, the N37A mutant without the C-terminal truncation was a catalytically active tetramer in solution (Figure 2.11). An overlay of chromatograms of wt and monomeric *sp*IDI-2 clearly shows the difference between homotetrameric and monomeric forms of the proteins (Figure 2.12). Both wild type and monomeric enzymes have N-terminal $His_6$-tag, and at the concentrations tested these two enzymes are tetramer and monomers based on both the gel-filtration chromatography and sedimentation equilibrium experiments (Figure 2.13).

*Characterization of (N37A:$^{328}$EAKDQ$^{333}$M-deletion)-spIDI2*. Steady-state kinetic constants were determined for monomeric (N37A:$^{328}$EAKDQ$^{333}$M-deletion)-*sp*IDI2 and wt-*sp*IDI-2[99] (Figures 2.14A, 2.14B, and 2.15) under aerobic conditions with NADH as a reductant and are summarized in Table 2.3. Interestingly, the $k_{cat}$ for monomeric *sp*IDI-2 is nearly same as the homotetramer; however, $K_m^{IPP}$ was 14-fold larger, and $K_m^{FMN}$ was 54-fold higher for the monomer than the homotetramer! While turnover under saturating conditions is faster in the monomer, the homotetramer is a more efficient catalyst. The plot of initial velocity for different [FMN] at constant IPP was sigmoidal. A fit of the data

to the Hill-equation (Figure 2.14B) gave a value of n = 1.43. Sigmoidal behavior was seen earlier for kinetic measurements of the wild type enzyme in the presence of oxygen when NADH was used to reduce FMN.[99] In contrast, when the kinetic studies were conducted in an anaerobic chamber using sodium dithionite ($Na_2S_2O_4$) as the reductant, no sigmoidal behavior was seen (n =1, Figure 2.15). The $k_{cat}$ was slightly higher than measured in the presence of oxygen, but $K_m^{FMNH_2}$ was 16-fold smaller. The circular dichroism spectrum of (N37A:$^{328}$EAKDQ$^{333}$M-deletion)-*sp*IDI-2 was similar to that for the wt homotetramer (Figure 2.16). Both spectra had broad minima at ~208 and ~220 nm, suggesting that the secondary structure of the monomer is similar to the four subunits in the homotetramer.

UV-visible spectra of wt-IDI-2 from *S. pneumoniae* and a variety of other organisms are similarly distinctively different for the IDI-2•$FMN_{ox}$, IDI-2•$FMN_{red}$, and IDI-2•$FMN_{red}$•IPP or IDI-2•$FMN_{red}$•DMAPP forms of the enzyme.[80,82,99] The spectra for wt homotetrameric *sp*IDI-2 (Figure 2.17B)[99] and (N37A:$^{328}$EAKDQ$^{333}$M-deletion)-*sp*IDI-2 were virtually identical for the respective IDI-2-FMN (Figure 2.17A, 2.17B; orange), IDI-2•$FMN_{red}$ (Figure 2.17A, 2.17B; red), and IDI-2•$FMN_{red}$•IPP (Figure 2.17A, 2.17B; cyan), and IDI-2•$FMN_{red}$•DMAPP (Figure 2.17A, 2.17B; black) forms of the proteins.

Wt *sp*IDI-2 is more stable than the (N37A:$^{328}$EAKDQ$^{333}$M-deletion) mutant. Fluorescence thermal shift assays gave a substantially higher melting temperature for wt-*sp*IDI-2 ($T_m$ ~ 69 $^oC$) than (N37A:$^{328}$EAKDQ$^{333}$M-deletion)-*sp*IDI-2 ($T_m$ ~ 49 $^oC$; Figure 2.18A-C) between pH 5 – 10 (Figure 2.18D-E). Moreover, changes in pH did not

contribute to significant changes in $T_m$ for both the wild type and monomeric enzymes (Figure 2.18D-E).

$^{15}N$-$^{1}H$ HSQC spectra for uniformly $^{15}N$-labeled wt and monomeric *sp*IDI-2 are shown in Figure 2.19. The spectrum for the homotetramer has a limited number of cross peaks for the amide groups in the protein, and the dispersion is poor. While the number and intensity of the cross peaks are higher in the monomer, the dispersion remains poor. Thus, while (N37A:$^{328}$EAKDQ$^{333}$M-deletion)-*sp*IDI-2 behaves as a monomer during gel filtration or sedimentation equilibrium experiments, its NMR spectrum suggests that the protein is loosely associated in solution.

Kinetic comparisons between *sp*IDI-2 and (N37A:$^{328}$EAKDQ$^{333}$M-deletion)-*sp*IDI-2. We performed stopped-flow kinetic studies of the reduction of FMN by monomeric *sp*IDI-2 to compare the effect of IPP on the reduction of FMN by NADH in the monomeric and homotetrameric forms of the enzyme. Fluorescence emission with a 530 nm bandpass filter was used to minimize interference by NADH or dithionite. In our previous report,[99] we suggested that substrate (IPP) binding to one of the subunits in native *sp*IDI-2•FMN homotetramer induced a conformational change in the other subunits of the homotetramer leading to faster FMN reduction rates both by NADH and dithionite. We also observed a time-dependent change in the fluorescence intensity of wt *sp*IDI-2•FMN upon addition of IPP that we attributed to a conformational change in the chromophore. Interestingly, stopped flow measurements for monomeric *sp*IDI-2 revealed an enhancement in the rates of reduction of FMN similar to that seen for homotetrameric wt *sp*IDI-2, in which the reduction by NADH ($k = 1.64 \times 10^{-3}\ s^{-1}$) is substantially faster when IPP is added to the enzyme ($k = 0.57\ s^{-1}$) (Table 2.4), and reduction by dithionite is

faster than by NADH. In addition, reduction of enzyme bound FMN by dithionite follows a biphasic double exponential pattern (Figure 2.20E) similar to that seen for the wt homotetramer. Unexpectedly, we also saw a time-dependent change in the fluorescence spectrum of monomeric *sp*IDI-2•FMN similar to that observed for the wt homotetramer with a rate constant slightly faster than for the reduction by NADH, which presents a conundrum. We previously suggested that increases in the rates of reduction might result from a global conformational change in the homotetramer induced upon IPP binding to one of the *sp*IDI-2•FMN subunits. However, this explanation is not valid for similar rate enhancements in the monomer. Moreover, an X-ray structure of wt *ss*IDI-2•$FMNH_2$•IPP indicates that both faces of the isoalloxazine ring are shielded, by the protein on one side and IPP on the other, with no apparent access of NADH to FMN for a two-electron reduction in the ternary IDI-2•$FMNH_2$•IPP complex.[92] Perhaps a conformational change is induced by IPP binding to an allosteric site, although there is no evidence for this type on interaction in IDI-2. Alternatively, IPP might bind in the active site, induce a conformational change, and dissociate to leave IDI-2•$FMNH_2$ imprinted in an activated state.

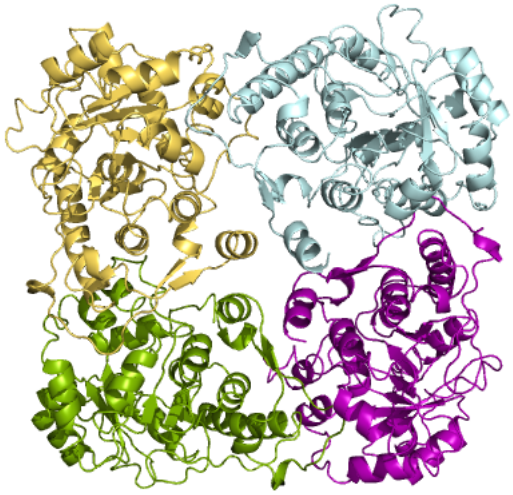

**Figure 2.1.** Wild type *sp*IDI-2 crystal structure

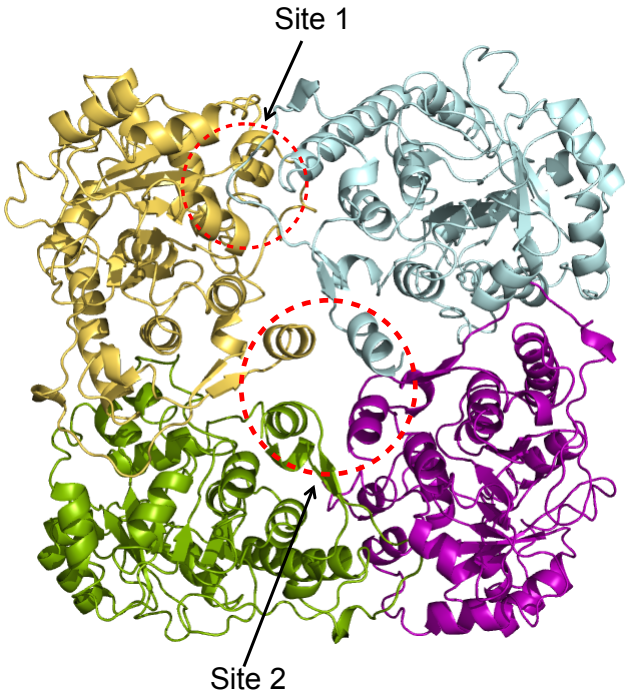


**Figure 2.2.** The *sp*IDI-2 homotetramer showing the two regions of contact at the monomer-monomer interface.[98]

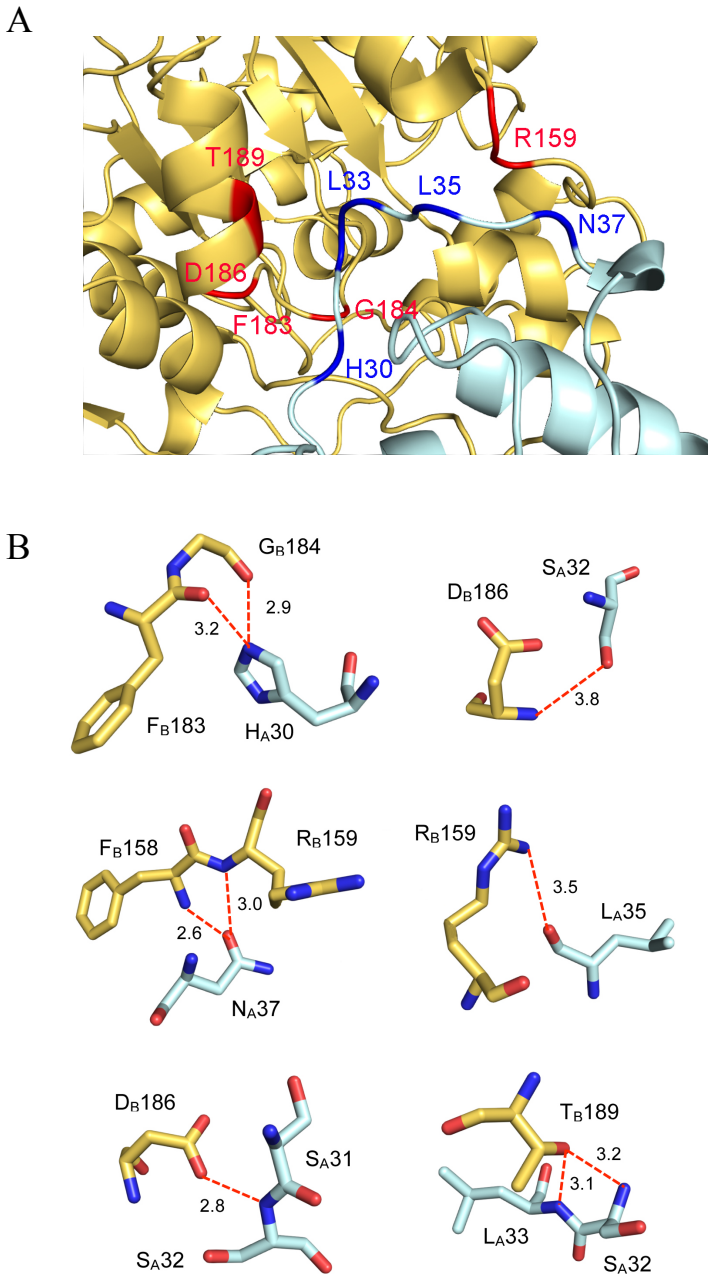


**Figure 2.3.** Region 1. Side chains in $H_A30$, $S_A32$, $N_A37$ in subunit A (cyan) interact with backbone amides in subunit B (gold) at residues $F_B183/G_B184$, $D_B186$, $F_B158/R_B159$, respectively, while side-chains in $R_B159$, $D_B186$ and $T_B189$ in subunit B (gold) interact with backbone amides in subunit A (cyan) at residues $L_A35$, $S_A32$, and $S_A32/L_A33$, respectively.[98] A) Ribbon diagram showing helix/loop interactions. B) Interactions between side-chains and backbones.

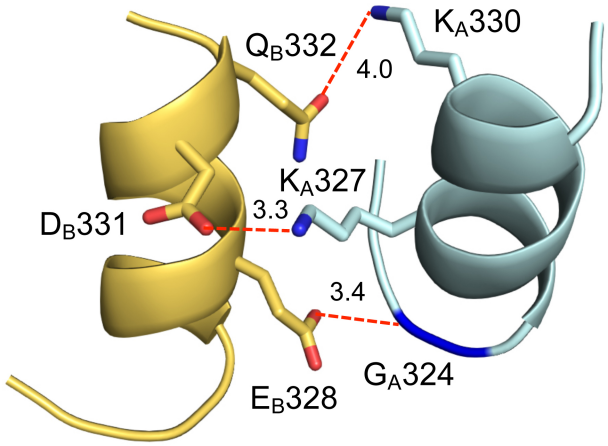


**Figure 2.4.** Noncovalent interactions between the C-terminal α-helices in adjacent subunits. $G_A324$ (cyan) with $E_B328$ (gold), $K_A327$ (cyan) with $D_B331$ (gold), and $K_A330$ with $Q_B332$ (gold).

**Table 2.1.** Noncovalent interactions identified at the subunits interface of wt-*sp*IDI-2.

| S. No | Amino acid Residue | Interacting Partner Residue(s) | H-bonding distance (Å) | Interaction site |
|---|---|---|---|---|
| 1 | $H_A30$ (side-chain) | $F_B183$, $G_B184$ (peptide back-bone) | 3.2, 2.9 | Site 1 |
| 2 | $S_A32$ (side-chain) | $D_B186$ (peptide back-bone) | 3.8 | Site 1 |
| 3 | $N_A37$ (side-chain) | $F_B158$, $R_B159$ (peptide back-bone) | 2.6, 3.0 | Site 1 |
| 4 | $R_A159$ (side-chain) | $L_B35$ (peptide back-bone) | 3.5 | Site 1 |
| 5 | $D_A186$ (side-chain) | $S_B32$ (peptide back-bone) | 2.8 | Site 1 |
| 6 | $T_A189$ (side-chain) | $S_B32$, $L_B33$ (peptide back-bone) | 3.2, 3.1 | Site 1 |
| 7 | $G_A324$ (amine) | $E_B328$ (side-chain) | 3.4 | Site 2 |
| 8 | $K_A327$ (side-chain) | $D_B331$ (side-chain) | 3.3 | Site 2 |
| 9 | $K_A330$ (side-chain) | $Q_B332$ (side-chain) | 4.0 | Site 2 |

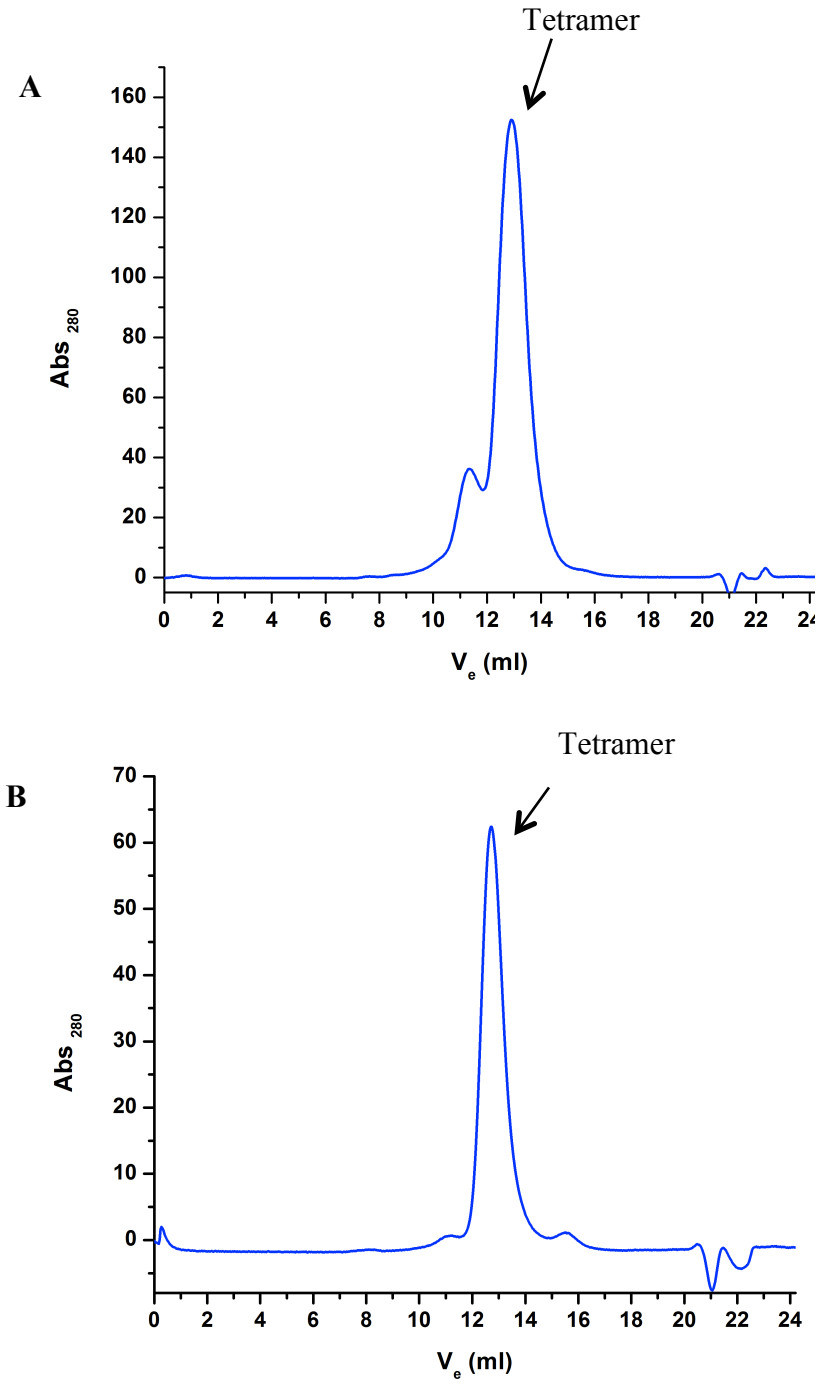


**Figure 2.5.** Gel-filtration trace of A) wt-*sp*-IDI2, estimated molecular weight of the tetramer peak – 169707 Da B) H30A S32A N37A T189A-*sp*IDI-2, estimated molecular weight of the tetramer peak – 164431 Da on a Superdex 200 10/300 GL column. (Calculated molecular weight of the tetramer from protein sequence – 159472 Da)

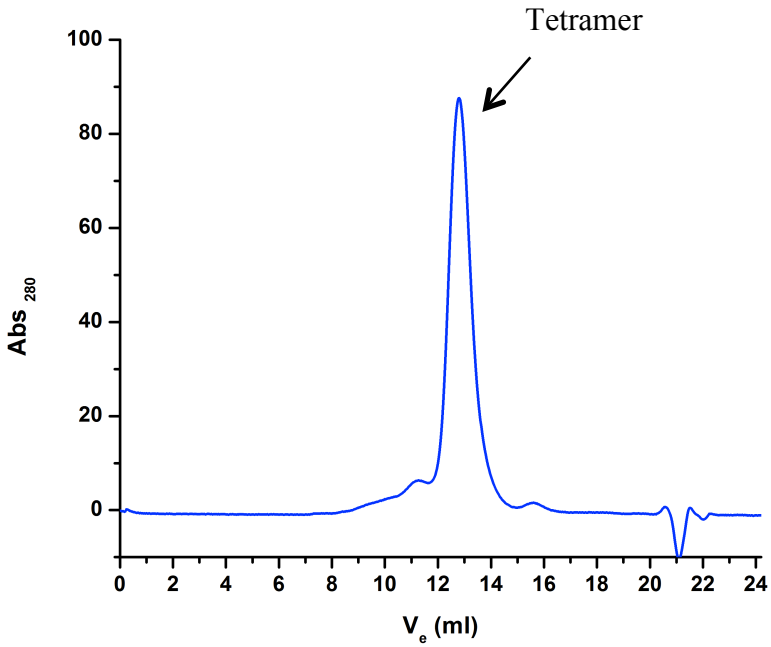


**Figure 2.6.** Gel-filtration trace of H30A S32A N37A R159S D186S T189A-*sp*IDI-2 on a Superdex 200 10/300 GL column, estimated molecular weight of the tetramer peak – 159318 Da (Calculated molecular weight of the tetramer from protein sequence – 159472 Da).

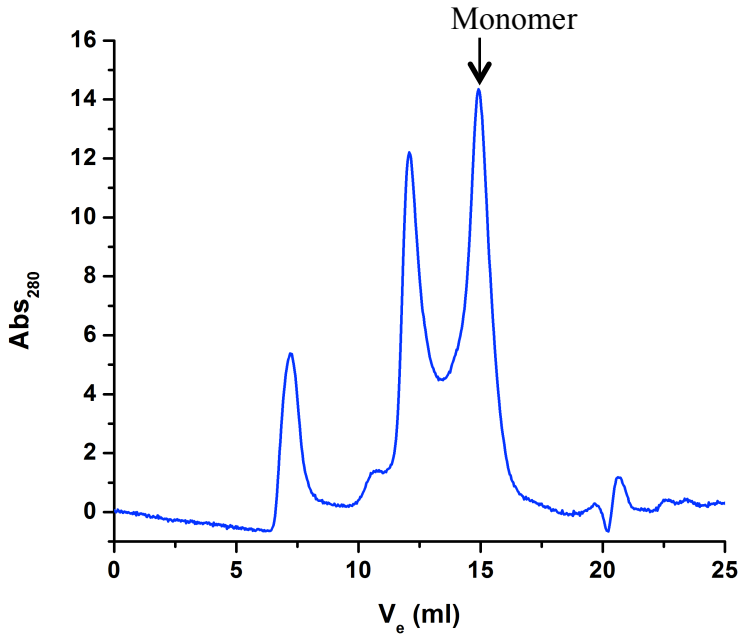


**Figure 2.7.** Gel-filtration trace of H30A S32A N37A T189A 328EAKDQM333-deleted-*sp*IDI-2 on a Superdex 200 10/300 GL column, estimated molecular weight of the tetramer peak – 168493 Da, monomer peak – 47116 Da (Calculated molecular weight of the tetramer from protein sequence – 159472 Da, monomer – 39868 Da).

**Table 2.2.** *sp*IDI-2 mutagenesis for monomer formation.

| S.No | ***sp*IDI-2 mutant** | **Solubility** | **Structure** | **Activity** |
|---|---|---|---|---|
| 1 | 328EAKDQM333-deleted | Soluble | Tetramer | Active |
| 2 | 328EAKDQM333-deleted $328His_6333$ | Soluble | Tetramer | Active |
| 3 | 328EAKDQMKKA336-deleted $328His_6333$ | Soluble | Tetramer | Active |
| 4 | N-term-$His_6$ 328EAKDQM333-deleted $328His_6333$ | Soluble | Tetramer | Active |
| 5 | N37A-328EAKDQM333-deleted | Soluble | Monomer | Active |
| 6 | N37A | Soluble | Tetramer | Active |
| 7 | H30A-328EAKDQM333-deleted | Soluble | Tetramer (major)/ Monomer (minor) | Active |
| 8 | T189A-328EAKDQM333-deleted | Soluble | Tetramer (major)/ Monomer (minor) | Active |
| 9 | H30A N37A-328EAKDQM333-deleted | Soluble | Monomer (major) | Inactive |
| 10 | N37A T189A-328EAKDQM333-deleted | Soluble | Monomer (major) | Inactive |
| 11 | H30A N37A T189A-328EAKDQM333-deleted | Soluble | Monomer (major) | Inactive |
| 12 | H30A S32A N37A T189A | Soluble | Tetramer | Active |
| 13 | H30A S32A N37A T189A-328EAKDQM333-deleted | Soluble | Monomer (major)/ Tetramer (minor) | Inactive |
| 14 | H30A S32A N37A T189A-328EAKDQM333-deleted $328His_6333$ | Soluble | Monomer (major – less % to 13) | Inactive |
| 15 | H30A S32A N37A T189A-328EAKDQM333-deleted 328KKKK331 | Less soluble | - | - |
| 16 | H30A S32A N37A R159S D186S T189A | Soluble | Tetramer | Inactive |
| 17 | H30A S32A N37A R159S D186S T189A-328EAKDQM333-deleted | Soluble | Monomer | Inactive |
| 18 | 324GKLKEAKDQM333-deleted | Insoluble | - | - |
| 19 | R159S D186S 324GKLKEAKDQM333-deleted | Insoluble | - | - |
| 20 | H30A S32A N37A R159S D186S T189A K325D K327D K330D | Insoluble | - | - |
| 21 | C-term-$His_6$-wt-*sp*-IDI2 | Soluble | Tetramer | Active |

**Table 2.2. continued**

| | | | | |
|---|---|---|---|---|
| 22 | H30D S32D N37D T189D | Less soluble | Tetramer/Monomer | Less Active |
| 23 | H30D S32D N37D T189D-328EAKDQM333-deleted | Insoluble | - | - |
| 24 | N37A D186A | Soluble | Trimer/Tetramer | Active |
| 25 | N37A D186A 328EAKDQM333-deleted | Soluble | Monomer | Active |

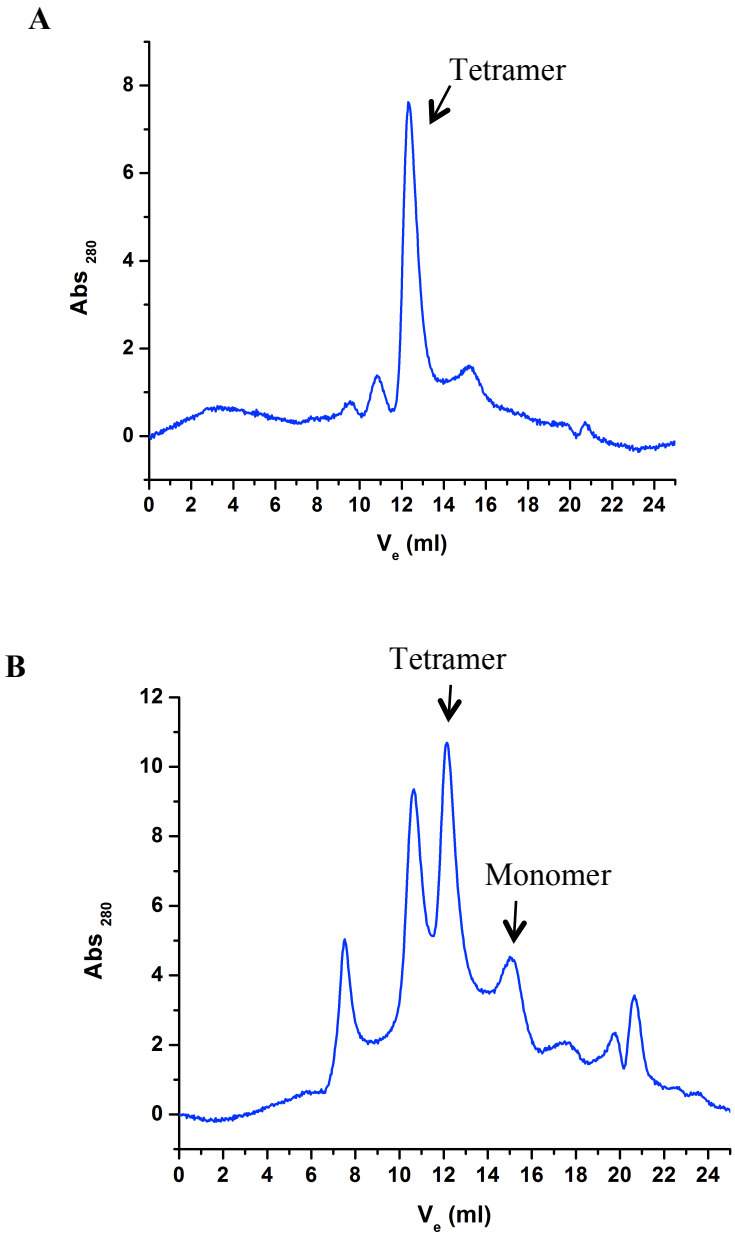


**Figure 2.8.** A) Gel-filtration trace of H30A 328EAKDQM333-deleted-*sp*IDI-2, Estimated molecular weight of the tetramer peak – 152289 Da, monomer peak – 41151 Da B) T189A 328EAKDQM333-deleted-*sp*IDI-2, estimated molecular weight of the tetramer peak - 163690 Da, monomer peak – 43245 Da on a Superdex 200 10/300 GL column.

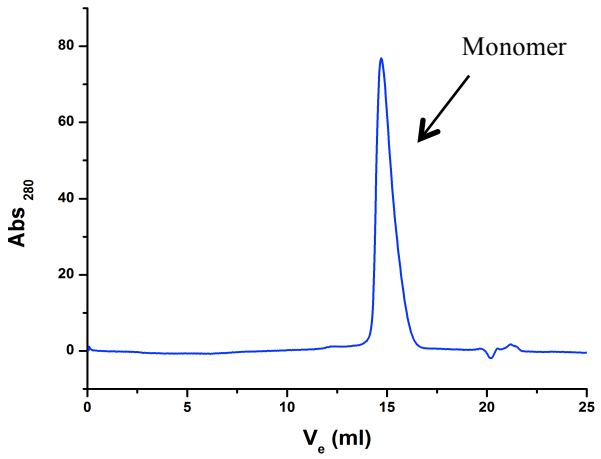


**Figure 2.9.** Chromatography of (N37A:$^{328}$EAKDQ$^{333}$M-deletion)-*sp*IDI-2 on a Superdex 200 analytical 10/300 GL column. The estimated mass of the protein (44505 Da) is similar to the calculated mass of the protein (39122.6 Da).

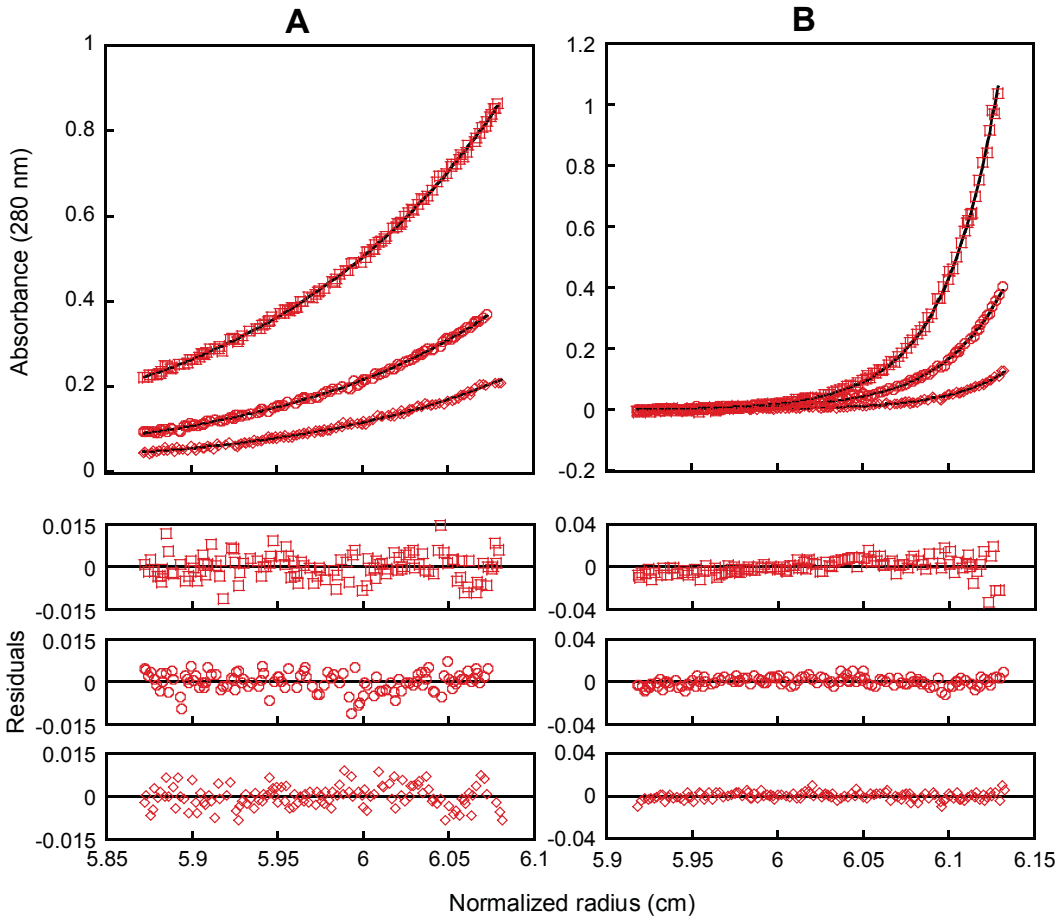


**Figure 2.10.** Analytical equilibrium sedimentation analyses of the A) monomeric (N37A:$^{328}$EAKDQ$^{333}$M-deletion)-*sp*IDI-2 B) tetrameric wild type *sp*IDI-2 and the corresponding ideal single species global fits. Bottom, residual differences between the data and fits. Representative data are shown for 15,000 rpm and three concentrations. The observed molecular weight of the monomer was 40,529 Da (MWobs/MWcalc = 1.04) and the tetramer was 156,244 Da (MWobs/MWcalc = 3.92).

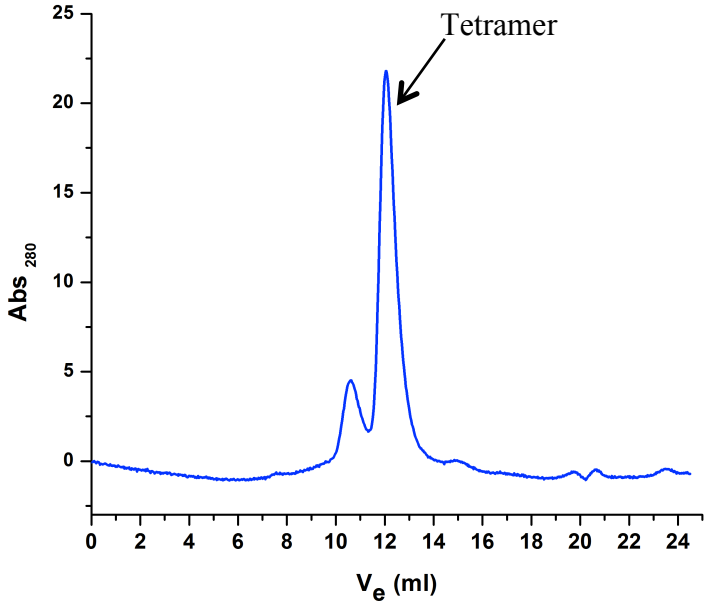


**Figure 2.11.** Gel-filtration trace of N37A *sp*IDI-2 on a Superdex 200 10/300 GL column, Estimated molecular weight of the tetramer peak – 161323 Da (Calculated molecular weight of the tetramer from protein sequence– 159472 Da).

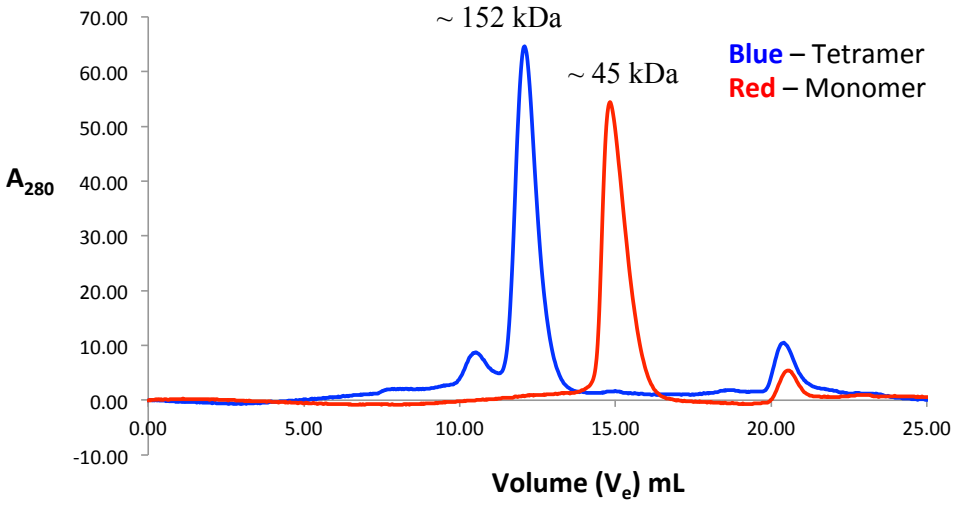


**Figure 2.12.** Overlay gel-filtration traces of wt homotetrameric and monomeric *sp*IDI-2 on a Superdex 200 10/300 GL column.

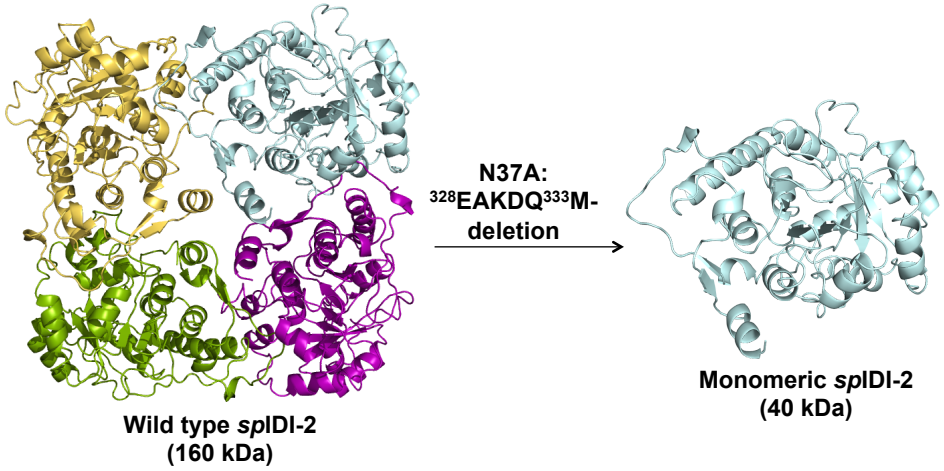


**Figure 2.13.** Monomer formation from the wild type homotetrameric *sp*IDI-2.

**A**

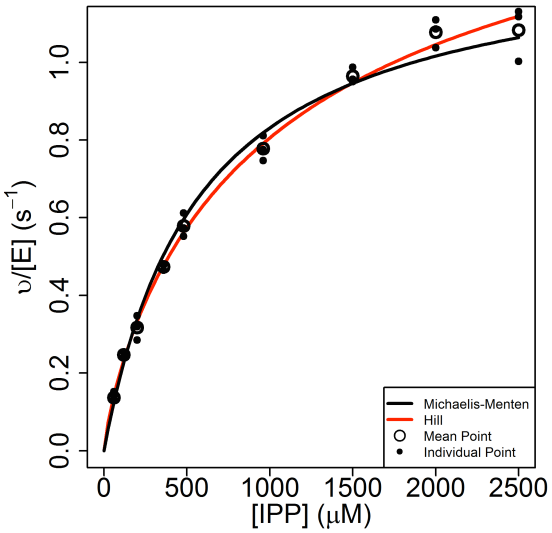


$K_m$ $^{IPP}$ = 572 ± 34 μM
$k_{cat}$ = 1.31 ± 0.04 s$^{-1}$
at [FMN] = 464.67 μM

**B**

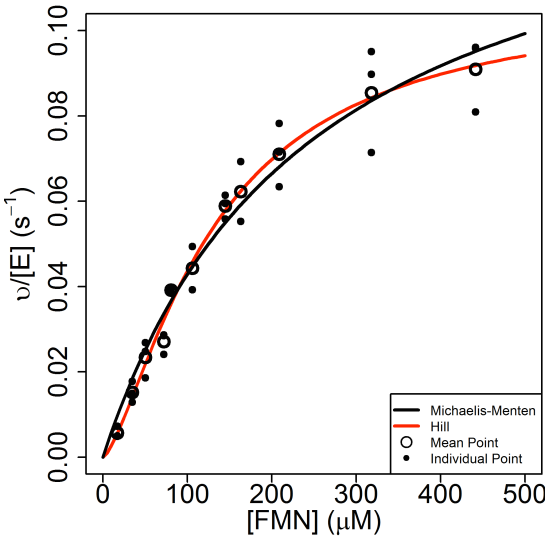


Hill equation

$$\upsilon = \frac{k_{cat}\,[S]^n}{{K_m}^n + [S]^n}$$

$k_{cat}$ = 1.08 ± 0.09 s$^{-1}$
$K_m$ $^{FMN}$ = 131 ± 19 μM
$n$ = 1.43 ± 0.17
at [IPP] = 2 mM

**Figure 2.14.** a) Michaelis-Menten plot of N37A 328EAKDQM333-deleted-*sp*IDI-2 Monomer (Varied IPP and constant FMN) b) Hill-Equation plot (Varied FMN and constant IPP) under aerobic conditions.

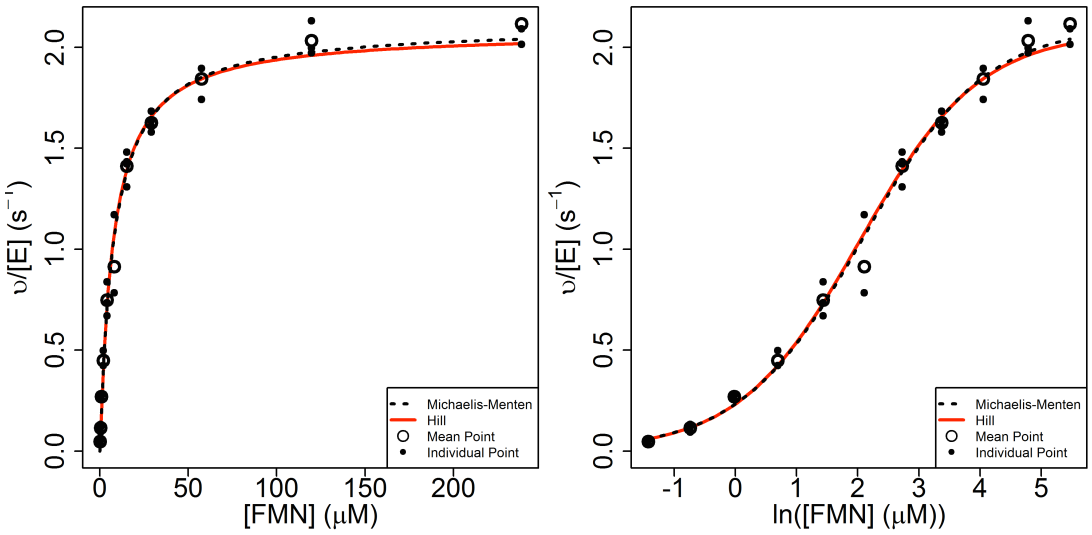


$K_m^{IPP} = 8.01 \pm 0.54$ μM
$k_{cat} = 2.11 \pm 0.08$ $s^{-1}$
at [IPP] = 2 mM
$n = 1.02 \pm 0.04$

**Figure 2.15.** Varying FMN at saturating IPP of N37A 328EAKDQM333-deleted-*sp*IDI-2 Monomer under anaerobic conditions.

**Table 2.3.** Steady-state kinetic constants

| Conditions | Enzyme (Solution structure) | Substrate | $K_m$ (μM) | $k_{cat}$ ($s^{-1}$) | $K_i$ (μM) |
|---|---|---|---|---|---|
| Aerobic | (N37A:$^{328}$EAKDQ$^{333}$M-deletion)-*sp*IDI2[a] (monomer) | IPP[b] | 572 ± 34[d] | 1.31 ± 0.04[d] | - |
| | | FMN[c] | 131 ± 19[d] | 1.08 ± 0.09[d] | - |
| Anaerobic | (N37A:$^{328}$EAKDQ$^{333}$M-deletion)-*sp*IDI2 (monomer) | FMN[e] | 8.01 ± 0.54[d] | 2.11 ± 0.08[d] | - |
| Aerobic | wt-*sp*IDI2 (homotetramer)[f] | IPP | 40.8 ± 5.6 | 0.983 ± 0.078 | 292 ± 39[g] |
| | | FMN | 2.39 ± 0.26 | | 6.40 ± 1.01[g] |
| Anaerobic | wt-*sp*IDI2 (homotetramer)[f] | IPP | 5.95 ± 0.68 | 0.875 ± 0.048 | - |
| | | FMN | 5.12 ± 0.73 x $10^{-2}$ | | |

[a]Assay conditions: 100 mM HEPES, pH 7.0, containing 150 mM NaCl, 10 mM $MgCl_2$, 20 mM NADH, 2 mM DTT, 0.14 mg/mL BSA, and 100 nM (N37A:$^{328}$EAKDQ$^{333}$M-deletion)-*sp*IDI-2 at 37 ºC. [b]60-2500 μM IPP, 0.46 mM FMN. [c]17–441 μM FMN, 2 mM IPP. [d]Apparent values determined at saturating levels of the second substrate. [e]8 mM $Na_2S_2O_4$, 0.2 – 238.5 μM FMN, 2 mM IPP. [f]Ref. 99. [g]Ref. 98.

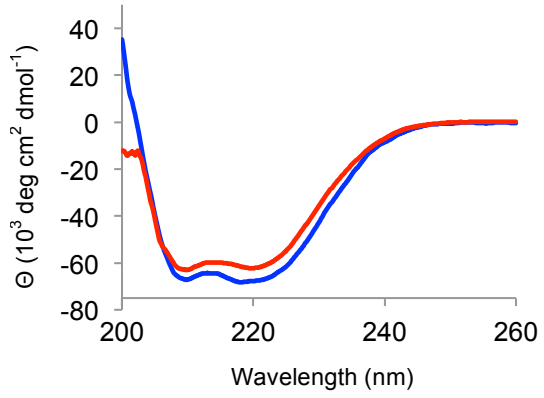


**Figure 2.16.** Circular dichroism spectra of wt *sp*IDI-2 (blue) and (N37A:$^{328}$EAKDQ$^{333}$M-deletion)-*sp*IDI-2 (red).

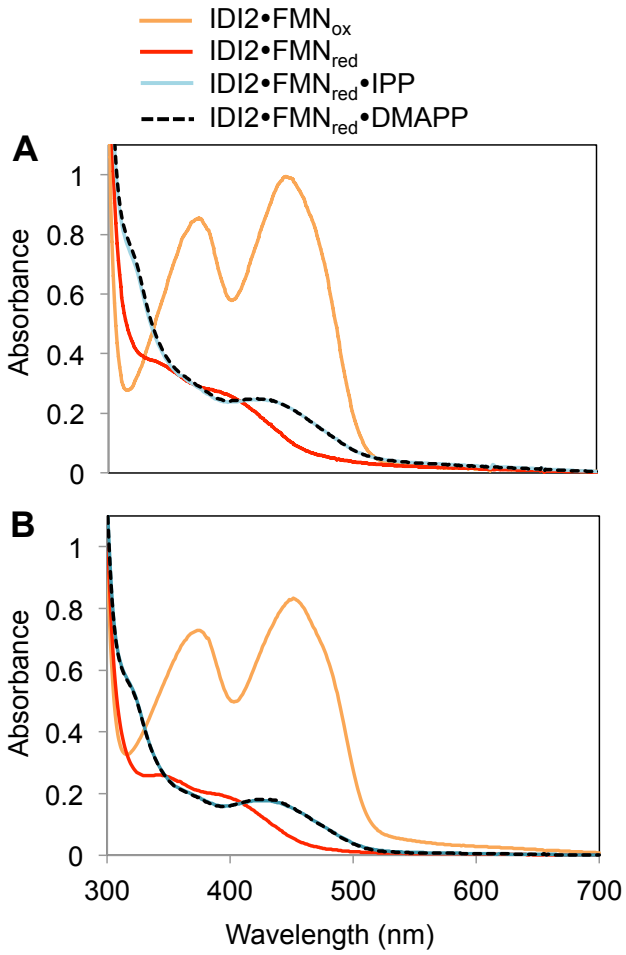


**Figure 2.17.** UV-vis spectra of various forms of the IDI2-bound FMN. Reaction conditions are given in the Methods section. (A) Monomeric *sp*IDI-2 (B) wt-*sp*IDI-2.[99] Orange, red, cyan, black dotted curves represent IDI2•$FMN_{ox}$, IDI2•$FMN_{red}$, IDI2•$FMN_{red}$•IPP, IDI2•$FMN_{red}$•DMAPP, respectively.

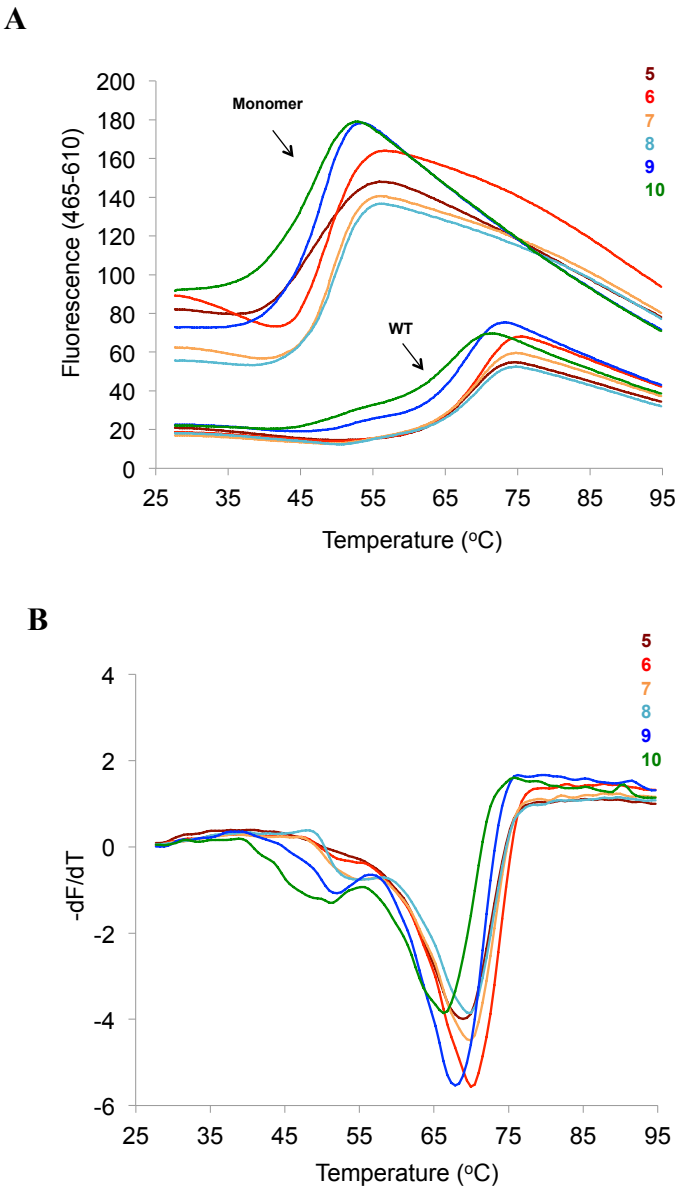


**Figure 2.18.** Fluorescence thermal shifts assays for wt and monomeric *sp*IDI-2. (A) Thermograms for the proteins in 50 mM buffer (pH 5.0 citric acid; pH 6–8 phosphate; pH 9.0 CAPSO; pH 10–11 CAPS); pH 5 (brown), pH 6 (red), pH 7 (orange), pH 8 (cyan), pH 9 (blue), pH 10 (green). (B and C) Negative derivatives of the thermograms (-dF/dT) of wt and monomer. $T_m$s as a function of pH for wt (D) and monomeric (E) *sp*IDI-2, respectively.

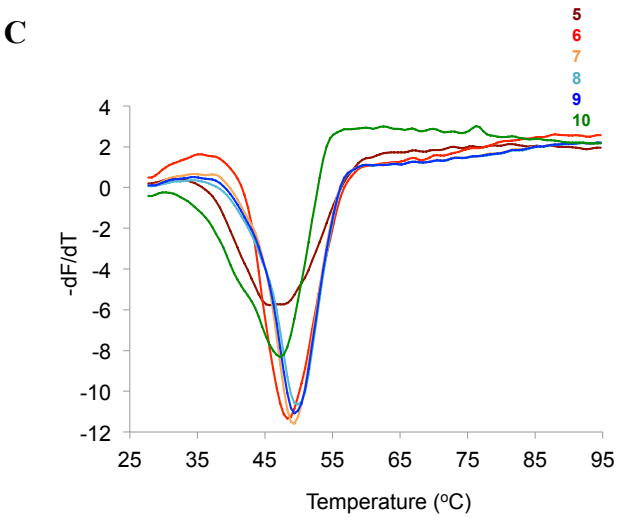


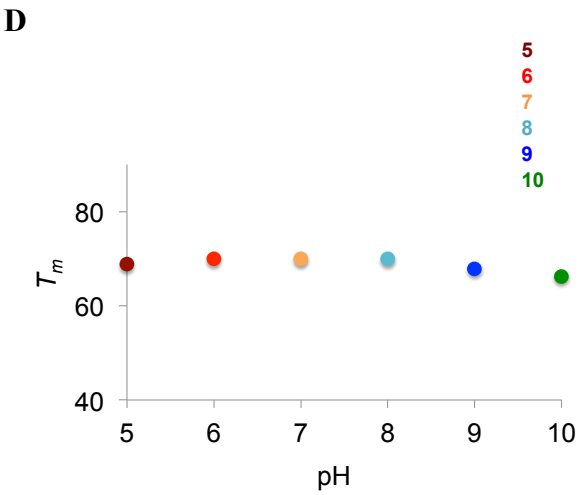


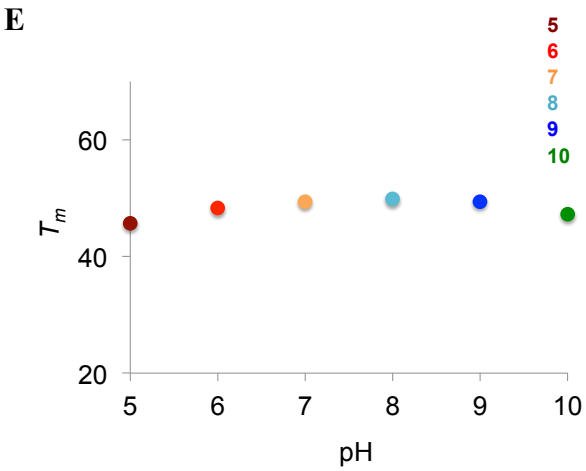


**Figure 2.18 continued.**

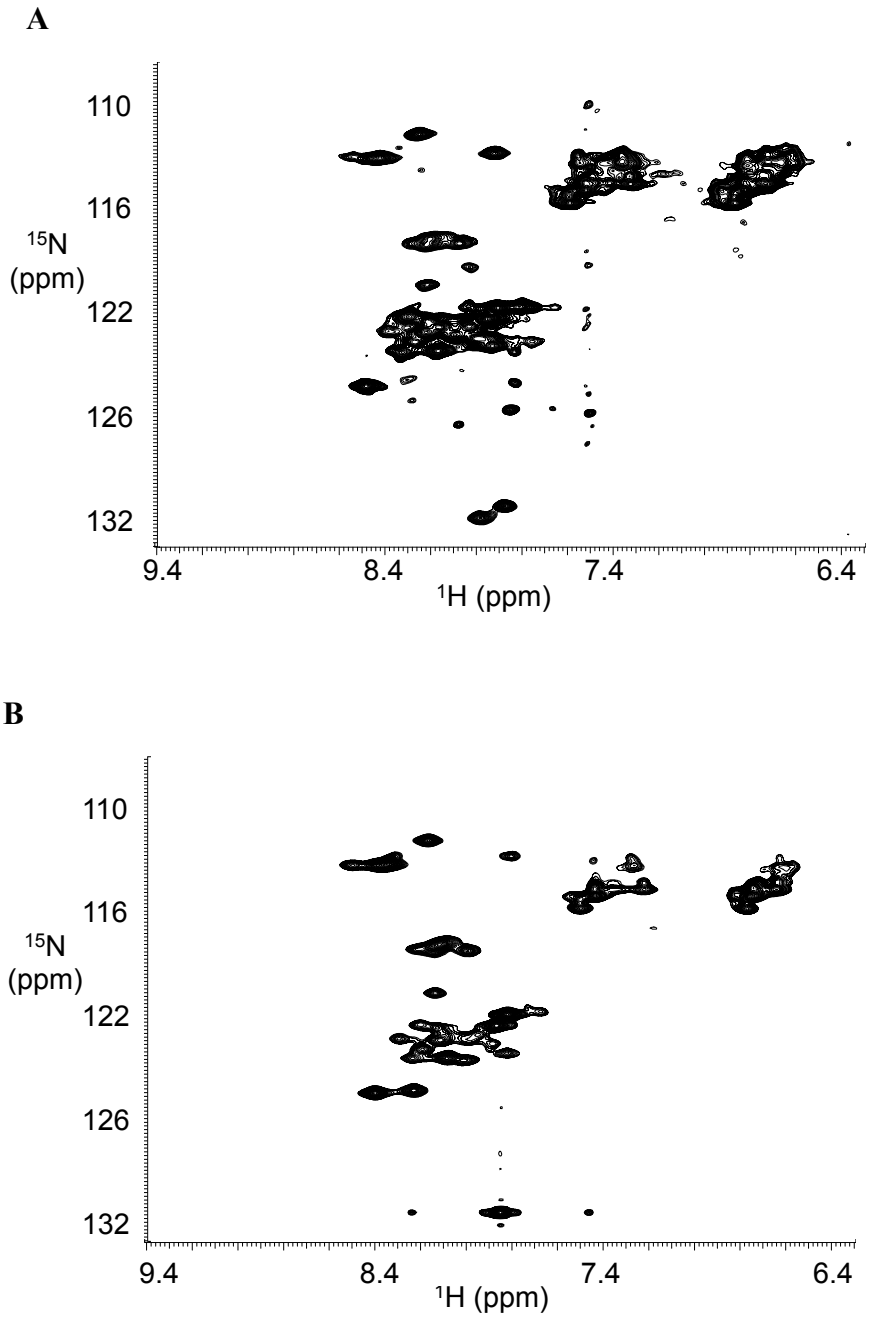


**Figure 2.19.** $^{15}$N-$^{1}$H HSQC comparison of (A)$^{15}$N-labeled monomeric and (B) $^{15}$N-labeled wild-type *sp*IDI-2 enzymes.

**Table 2.4**. Rates of reduction for FMN, monomeric *sp*IDI-2•FMN, and monomeric *sp*IDI-2•FMN•IPP at 20 $^{o}$C.

| Reaction | Reductant | $k$ ($s^{-1}$) |
|---|---|---|
| FMN → $FMNH_2$ | Dithionite | 62.4 ± 0.4 |
| | NADH | $3.4 \times 10^{-3} \pm 3.0 \times 10^{-5}$ |
| *sp*IDI-2•FMN → *sp*IDI-2•$FMNH_2$ | Dithionite | 50.2 ± 0.9 |
| | NADH | $1.6 \times 10^{-3} \pm 1.2 \times 10^{-5}$ |
| *sp*IDI-2•FMN•IPP → *sp*IDI-2•$FMNH_2$•IPP | Dithionite | 32.4 ± 2.3 ($k_1$) |
| | | $0.67 \pm 4.7 \times 10^{-3}$ ($k_2$) |
| | NADH | 0.57 ± 0.018 |
| IPP + *sp*IDI-2•$FMN_{ox}$ → *sp*IDI-2•$FMN_{ox}$•IPP | None | 1.11 ± 0.005 |

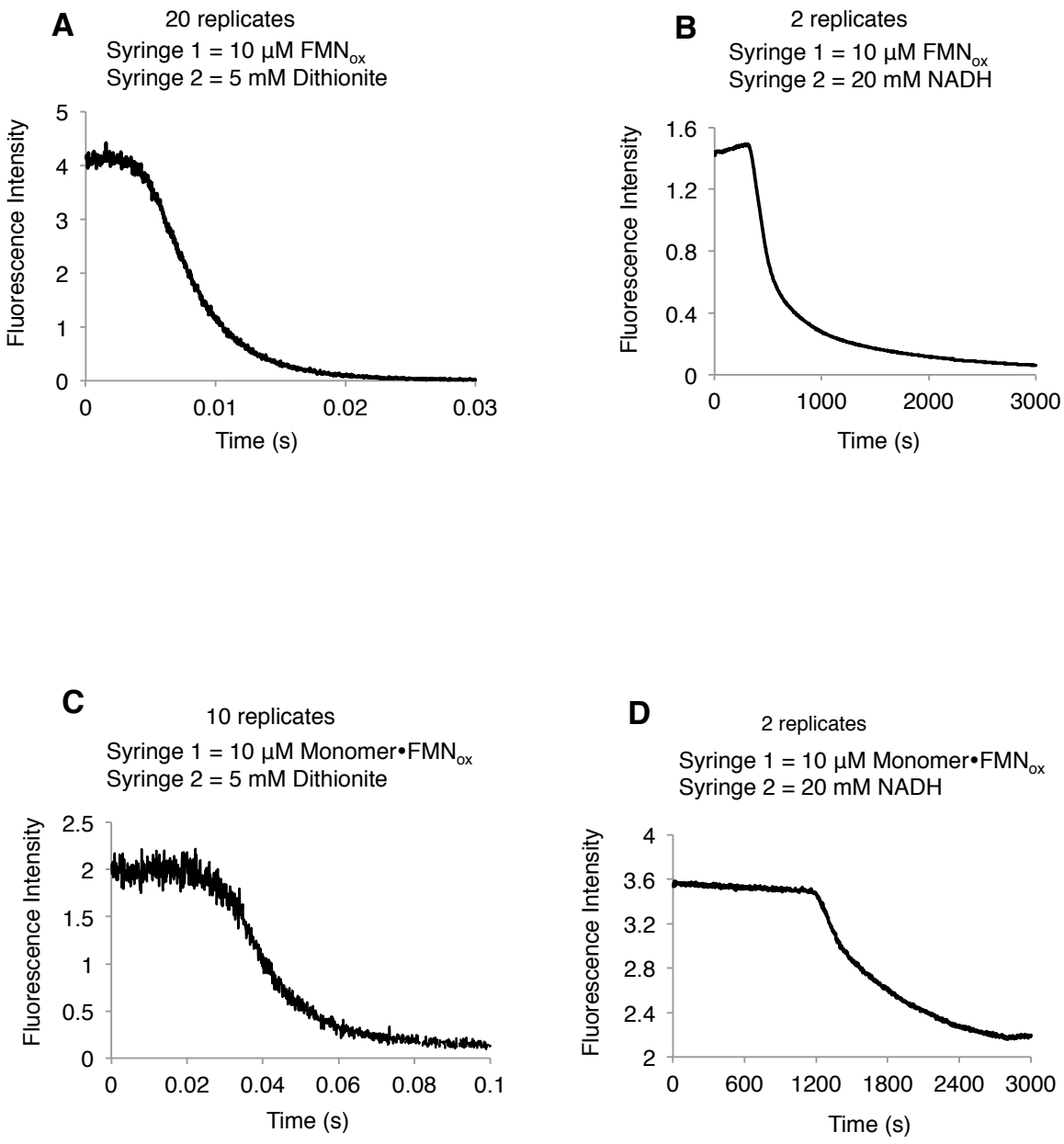


**Figure 2.20.** Stopped-flow kinetic figures. Black lines represent the average of replicates. Excitation wavelength 420 nm for Monomer•FMN and 450 for free FMN. Fluorescence emission was detected with >530 nm wavelength bandpass filter.

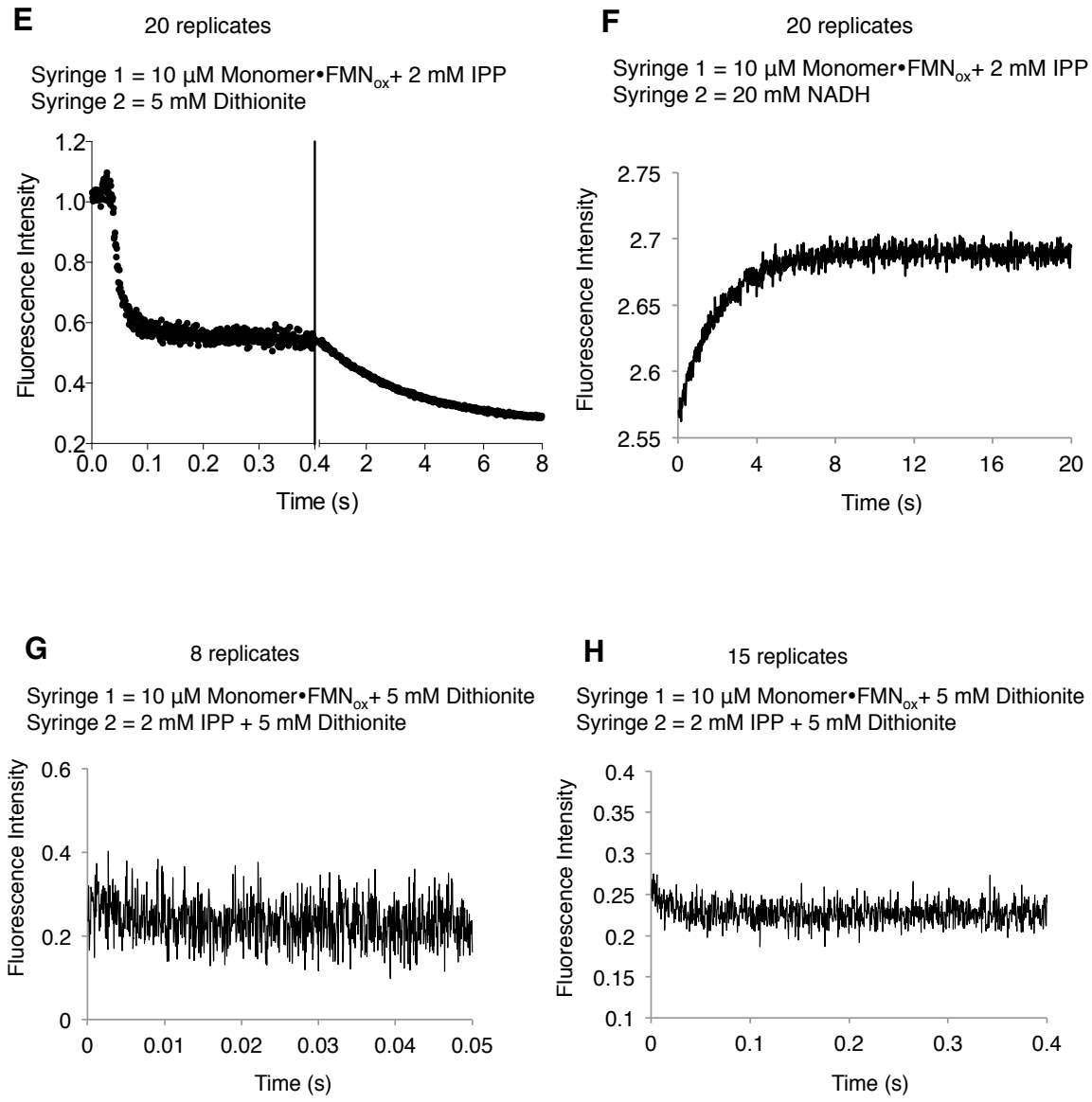


**Figure 2.20 continued.**

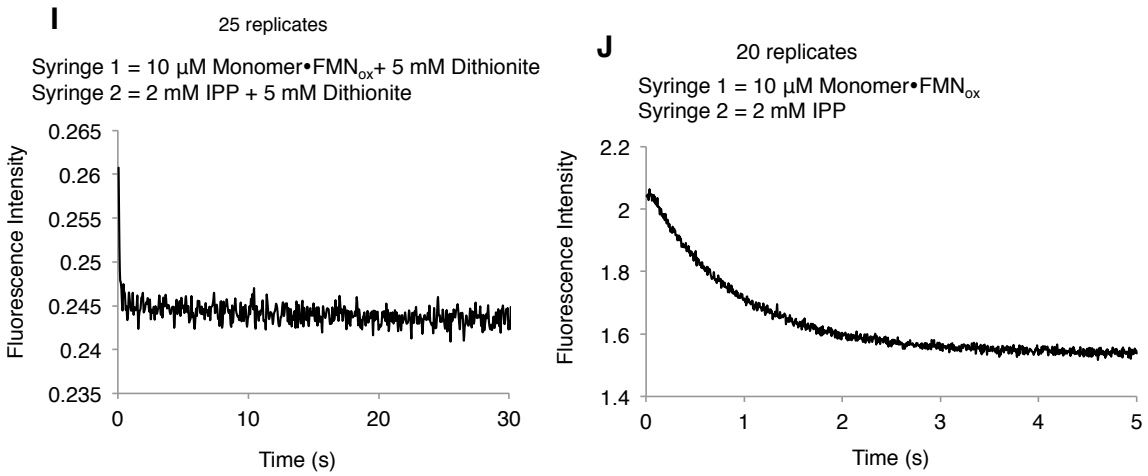


**Figure 2.20 continued.**

# CHAPTER 3

# SITE-SELECTIVE SYNTHESIS OF $^{15}$N- AND $^{13}$C-ENRICHED FLAVIN MONONUCLEOTIDE COENZYME ISOTOPOLOGUES AND NMR STUDIES

## Introduction

Flavins, derived from the Latin word flavus (yellow), are widely spread in nature, where they serve as coenzymes in a wide variety of biological processes. Three different types of flavins are found in nature (Figure 3.1). Riboflavin (vitamin $B_2$) is the biosynthetic precursor for flavin mononucleotide (FMN) and flavin adenine dinucleotide (FAD), which are the biologically active coenzymes. Typically, flavin coenzymes mediate one and two-electron redox reactions,[122,123] but they serve in other roles such as electrophilic and nucleophilic substitution,[124,125] flavin-based (BLUF) blue light photoreceptors,[126] DNA repair,[127-129] signal transduction, and light sensing.[130] Additionally, many flavoenzymes are targets for drug development,[98,131] where a thorough understanding of structure and mechanism could facilitate the design of novel lead compounds as therapeutic agents. There are more than 100,000 entries in the National Center for Biotechnology Information database related to flavoproteins, which constitute a large family with novel functions.[122,132] Isotopically enriched flavins and flavin analogs are useful probes for studying the structure and function of the coenzyme

in flavin-dependent processes. A few notable applications include investigations of flavin transport and metabolism[133], elucidation of the mechanisms of flavoenzyme-catalyzed reactions where the cofactor is involved in the chemistry of enzyme catalysis,[134-137] and studies of the dynamics of light receptors.[138] Flavins uniformly enriched with $^{15}N$ and $^{13}C$ are employed to improve the NMR signal sensitivity, particularly when the cofactors are bound to proteins. Selective $^{15}N$ and $^{13}C$ enrichment is used to enhance signals for specific atoms of interest in an unlabeled background and for individual peak assignments.[139] Site-specifically $^{15}N$ and $^{13}C$ enriched flavins are highly useful for unequivocal band assignments in NMR, IR, and Raman spectroscopy.[140] $^{13}C$-FAD isotopologues were used to study the BLUF-domain protein photoreceptor[141] and both $^{13}C$ and $^{15}N$-FMN were used to investigate flavin-protein interactions in flavocytochrome $b_2$.[142]

Several flavin analogues have been used as mechanistic probes for the active sites of flavoenzymes (Figure 3.2). Flavins are typically bound noncovalently in the active site, and methods have been developed to remove the enzyme bound flavin in order to reconstitute the proteins with flavin analogs. In the fully oxidized state, flavins exhibit strong UV-vis signatures with maxima at ~370 nm and ~ 450 nm. The UV-vis spectra of flavin probes often change for free and protein bound forms. For example, the reactivity of 8-chloroflavin towards sulfur nucleophiles has been used to identify cysteine thiol residues in the active site near 8-position of the bound analog.[143] The spectral changes upon conversion of 8-chloro to 8-mercaptoflavin are dramatic as they have absorption maxima at ~ 470 nm and 8-mercaptoflavins have been used to study the redox processes of flavin in various flavin-dependent enzymes.[144] Similarly, 4-thioflavins have been used

to study the environment around the C4 carbonyl of flavin. It was found that 4-thioflavins are reactive towards both nucleophiles and electrophiles.[145] 1-carba-1-deaza- and 5-carba-5-deazaflavins (1-deaza and 5-deaza flavins) are commonly used mechanistic probes.[143] $^{3}$H-, $^{17}$O-, $^{18}$O-, $^{15}$N- and $^{13}$C-flavin isotopologues are used to study the mechanism and structure of flavins in flavoenzyme-catalyzed reactions by standard spectroscopic techniques.[146-148] 5-Deazaflavins have been used to determine the existence of covalent intermediates and radical flavin intermediates in a variety of reactions. The covalent adducts can be isolated and detected by conventional spectroscopic techniques.[149]

Synthetic methods, biosynthetic methods, and a combination of the two have been used to insert $^{15}$N and $^{13}$C-labels into riboflavin.[150] The Tishler condensation of *o*-aminoazo compounds with barbituric acid is a classic chemical approach for synthesis or riboflavin.[151] GTP and ribulose 5-phosphate are precursors for biosynthesis of riboflavin through the sequence of steps catalyzed by GTP cyclohydrolase II, lumazine synthase, and riboflavin synthase.[152] Recently, Fischer and coworkers reported an in vivo biotransformation method using an engineered bacterial strain to synthesize $^{15}$N, $^{13}$C, $^{17}$O, and $^{18}$O-labeled flavins from isotopically labeled precursors.[153] In another report, Kohen and coworkers reported an enzymatic synthesis of $^{3}$H-, $^{15}$N-, and $^{13}$C-labeled flavins from commercially available isotope-labeled riboflavin precursors.[154] In this chapter, I describe a combination of chemical and biotransformation steps for labeling nitrogen and carbon sites in the pyrazine and pyrimidine rings of the isoalloxazine core in FMN.

## Experimental Procedures

*Materials.* Cell culture growth media, salts, and chemicals were purchased from Fisher Scientific, B&D, and Sigma-Aldrich. $Na^{15}NO_2$ (98% $^{15}N$) was purchased from Sigma-Aldrich, $^{15}N_2$-Urea (98%+ $^{15}N_2$), and $^{13}C$(2)-diethyl malonate (99% $^{13}C$) were purchased from Cambridge Isotope Laboratories (CIL), $^{14}C$-labelled IPP was purchased from Perkin-Elmer, *Homo sapiens* (*hs*) riboflavin kinase plasmid (HS_RFK_EC_1_pQE-T7) was purchased from Qiagen.

Anhydrous reaction conditions were employed using anhydrous solvents under a nitrogen atmosphere in oven-dried glassware (100 °C). Anhydrous methanol (MeOH), ethyl alcohol (ethanol) was obtained by passing through a column of activated alumina. Purification of the **5**, **6**, [$^{15}N$]**6** was carried out using the silica gel flash column chromatography with silica gel (230−400 mesh, 60 Å). EMD Silica Gel 60 Å F254 TLC aluminum plates were for the thin-layer chromatographic analysis, and the spots were visualized under UV light. All the $^{1}H$, $^{13}C$, and $^{31}P$ NMR spectra were recorded at 25 °C, and chemical shifts were reported in δ ppm (parts per million) values. $^{1}H$ NMR spectra were recorded at 300 and 500 MHz and were referenced using $CD_3OD$, $d_6$-DMSO, and $D_2O$ NMR solvents. $^{13}C$ NMR spectra were recorded at 75 and 125 MHz, and $^{31}P$ NMR was recorded at 121 MHz. $^{13}C$ and $^{31}P$ NMR spectra recorded in $D_2O$ were unreferenced. HRMS-ESI data were recorded on LC-TOF and LTQ-FTMS mass spectrometers. HPLC purification of crude isotopically labeled FMN mixture was applied to a reverse phase column (XBridge C18, Waters, 19 × 100 mm) that had been equilibrated with 100% ammonium bicarbonate ($NH_4HCO_3$). $NH_4HCO_3$ – acetonitrile (ACN) gradient run was performed for a total run time of 45 min at a flow rate of 2 mL/min (rt). The retention

time for FMN was 28.5 min. Fractions were combined, lyophilized and stored at −80 °C.

*Barbituric acid (3).* In a 50 mL round bottomed flask**,** sodium (250 mg, 10.8 mmol) was carefully added to 15 mL of ethanol. After the sodium metal had been consumed, diethyl malonate (**2**, 1.65 mL, 10.8 mmol) was added followed by urea (**1**, 0.65 g, 10.8 mmol). The stirred mixture was heated at reflux for 7 h in an oil bath, during which time a white solid precipitated. The reaction was acidified with 13 mL of $H_2O$ and 1.2 mL of 12 N HCl to a pH ~ 4. The clear solution was then filtered and cooled in an ice bath. The precipitate was removed by filtration and washed with 1 mL of cold $H_2O$ to give 0.99 g (72%) of a white solid[155]; $^1$H NMR (300 MHz, $d_6$-DMSO) $\delta$ ppm 11.13 (s, 2H), 3.46 (s, 2 H); $^{13}$C NMR (300 MHz, $d_6$-DMSO) $\delta$ ppm 168, 151.8; GC-MS $[M]^+$ calculated for $C_4H_4N_2O_3$ 128.09, observed 128.1.

*[5-$^{13}$C]Barbituric acid ([5-$^{13}$C]3).* Following the procedure described for **3**; sodium (200 mg, 8.699 mmol) in 5 mL ethanol, diethyl [2-$^{13}$C]malonate (**[2-$^{13}$C]2**) **(**0.5 mL, 6.204 mmol), and **1** (0.372 g, 6.204 mmol) were combined to give 0.54 g (68%) of a white solid; $^1$H NMR (500 MHz, $d_6$-DMSO) $\delta$ ppm 11.09 (s, 2H), 3.47 (d, 2H, $^1J_{C\text{-}H}$ = 130 Hz) ppm; $^{13}$C NMR (500 MHz, $d_6$-DMSO) $\delta$ ppm 167.3 (d, $^1J_{C\text{-}C}$ = 39.18 Hz), 151.31. HRMS (ESI$^-$) calculated for $^{13}C_1C_3H_3N_2O_3$ $[M\text{-}H]^-$ (*m/z*) = 128.0183, found 128.0182.

*[1,3-$^{15}N_2$]Barbituric acid ([1,3-$^{15}N_2$]3).* Following the procedure described for **3**; sodium (90 mg, 3.91 mmol) in 5 mL ethanol, **2 (**0.5 mL, 3.223 mmol), and **[1,3-$^{15}$N$_2$]1** (0.20 g, 3.22 mmol) were combined to give 0.275 g (66%) of a white solid; $^1$H NMR (400 MHz, $d_6$-DMSO) $\delta$ ppm 11.12 (d, 2H, $^1J_{N\text{-}H}$ = 92 Hz), 3.46 (s, 2H); $^{13}$C NMR (400 MHz, $d_6$-DMSO) $\delta$ ppm 167.4 (d, $^1J_{C\text{-}N}$ = 11 Hz), 151.3 (t, $^1J_{C\text{-}N}$ = 18.1 Hz). HRMS (ESI$^-$)

calculated for $C_4H_3{}^{15}N_2O_3$ $[M-H]^-$ (*m/z*) =129.0090, observed 129.0090.

*N-Ribityl 3,4-dimethyl aniline (5).* In a 250 mL round bottomed flask**,** 3,4-dimethyl aniline (**4**) (2.06 g, 17 mmol), D-ribose (7.9 g, 53.0 mmol), and sodium cyanoborohydride (2.07 g, 33.0 mmol) were dissolved in 100 mL of methanol. The mixture was heated at reflux for 48 h with stirring. Solvent was removed under reduced pressure, and the residue was dissolved in 1 M HCl (40 mL) and swirled. A saturated solution of $NaHCO_3$ was added and the mixture was extracted with ethyl acetate (6 x 35 mL). The combined organic layers were washed with brine and dried over $MgSO_4$. Solvent was removed under reduced pressure to give 3.81 g (88%) of a white solid[156]; $^1$H NMR (300 MHz, $d_3$-MeOD*)* $\delta$ ppm 6.88 (d, 1H, *J*= 9 Hz), 6.55 (d, 1H, *J*= 2.3 Hz), 6.47 (dd, 1H, *J*= 2.4, 8 Hz), 3.91 (ddd, 1H, *J*= 8, 6.1, 3.5 Hz), 3.81-3.6 (m, 4H), 3.43 (dd, 1H, *J*= 12.8, 3.5 Hz), 3.08 (dd, 1H, *J*=12.8, 8 Hz), 2.17 (s, 3H), 2.12 (s, 3H); $^{13}$C NMR (300 MHz, $d_3$-MeOD*)* $\delta$ ppm 148.2, 138.1, 131.2, 126.9, 116.9, 112.7, 75, 74.5, 72.2, 64.8, 48.2, 20.2, 19.

*N-Ribityl-2-phenylazo-4,5-dimethyl aniline (6).* Aniline (0.22 g, 2.36 mmol), 12 N HCl (0.66 mL) and $H_2O$ (1.55 mL) were mixed in a 50 mL round bottom flask and allowed to stir at 0 $^o$C for 10 min, followed by slow addition of solid $NaNO_2$ (0.163 g, 2.36 mmol) in small portions. The solution was maintained at 0 $^o$C for 30 min. In a second 50 mL round bottomed flask, *N*-ribityl 3,4-dimethyl aniline **5** (0.5 g, 1.95 mmol) was dissolved in 4 mL of $H_2O$ followed by the addition of 0.7 mL of 12 N HCl and 0.66 g (8.04 mmol) of sodium acetate. The mixture was cooled to -5 $^o$C, the solution of diazotized aniline was added, and the resulting solution was stirred at -9 to -5 $^o$C for 1 h and at 0 $^o$C for 2 h. After warming to 20 $^o$C, a solution of 0.33 g (4.02 mmol) of sodium

acetate in 2.5 mL $H_2O$ was slowly added to maintain pH ~ 3 and the temperature at 17-20 $^oC$. The resulting mixture was allowed to stir at 22-25 $^oC$ for 17 h to give a dark orange suspension. The solid was removed by filtration and purified by flash chromatography (1:10 v/v MeOH/DCM) to give 0.67 g (95%) of a orange solid[157]; $R_f$ 0.35 (1:10 v/v MeOH/DCM); $^1H$ NMR (300 MHz, $d_3$-MeOD*)* $\delta$ ppm 7.82-7.79 (m, 2H), 7.52 (s, 1H), 7.47-7.42 (m, 2H), 7.36-7.32 (m, 1H), 6.72 (s, 1H), 4.05-3.97 (m, 1H), 3.82-3.61 (m, 5H), 3.39 (dd, 1H, $J$ = 13.1, 7.7 Hz), 2.28 (s, 3 H), 2.22 (s, 3 H); LC-MS $[M+Na]^+$ calculated for $C_{19}H_{25}N_3O_4Na$ 382.92, observed 382.2.

*[$^{15}$N]-N-ribityl-2-phenylazo-4,5-dimethyl aniline ([$^{15}$N]6).* Following the procedure described for **6**; aniline (0.109 g, 1.18 mmol), 0.33 mL of 12 N HCl, 0.77 mL of $H_2O$ and $Na^{15}NO_2$ (0.0825 g, 1.18 mmol) were combined to prepare the corresponding diazonium salt. The diazonium salt was added to **5** (0.25 g, 0.979 mmol) to give 0.34 g (97%) of an orange solid; $R_f$ 0.35 (1:10 v/v MeOH/DCM); $^1H$ NMR (300 MHz, $d_3$-MeOD*)* $\delta$ ppm 7.85-7.81 (m, 2H), 7.53 (s, 1H), 7.49-7.44 (m, 2H), 7.39-7.34 (m, 1H), 6.75 (s, 1H), 4.05-3.99 (m, 1H), 3.84-3.61 (m, 5H), 3.39 (dd, 1H, $J$ = 13.2 Hz, 7.7 Hz), 2.29 (s, 3H), 2.23 (s, 3H); $^{13}C$ NMR (300 MHz, $d_3$-MeOD*)* $\delta$ ppm 154.5 (d, $J_{C\text{-}N}$ = 5.1 Hz), 144.1, 143.8, 136.7, 131.2 (d, $J_{C\text{-}N}$ = 6.75 Hz), 130.4, 130.2, 125.2 (d, $J_{C\text{-}N}$ = 2.92 Hz), 123 (d, $J_{C\text{-}N}$ = 3.75 Hz), 114.3, 74.7, 72.5, 64.8, 46, 20.8, 18.9; HRMS ($ESI^+$) calculated for $C_{19}H_{25}N_2{}^{15}N_1O_4Na$ $[M+Na]^+$ (*m/z*) = 383.1713, found 383.1726.

*Riboflavin (7).* To *N*-ribityl-2-phenylazo-4,5-dimethyl aniline **6** (100 mg, 0.278 mmol) in a 10 mL round bottomed flask, 2 mL of *n*-butanol, barbituric acid **3** (56.5 mg, 0.44 mmol) and 0.5 mL of AcOH was added. The mixture was stirred and heated to reflux for 5 h, stirred for additional 1 h in an ice-bath, and then filtered. The solid on the

filter was washed with hot $H_2O$ and methanol to give 62.5 mg of a crude yellow solid; HRMS ($ESI^+$) calculated for $C_{17}H_{21}N_4O_6$ $[M+H]^+$ (*m/z*) 377.1461, observed 377.1463.

*[5-$^{15}$N]Riboflavin ([5-$^{15}$N]7).* Following the procedure described for **7**; **[5-$^{15}$N]6** (100 mg, 0.278 mmol), 2 mL of *n*-butanol, **3** (56 mg, 0.44 mmol) and 0.5 mL of AcOH were combined to give 85.5 mg of a crude yellow solid (75% pure as determined by HPLC); HRMS ($ESI^+$) calculated for $C_{17}H_{20}N_3{}^{15}NO_6Na$ $[M+Na]^+$ (*m/z*) 400.1251, observed 400.1255.

*[5-$^{15}$N, C4a-$^{13}$C]Riboflavin ([5-$^{15}$N, 4a-$^{13}$C]7).* Following the procedure described for **7**; **[$^{15}$N]6** (54.6 mg, 0.1515 mmol), 1.5 mL of *n*-butanol, **[5-$^{13}$C]3** (40 mg, 0.3121 mmol) and 0.3 mL of AcOH were combined to give 42 mg of a crude yellow solid (59% pure as determined by HPLC); HRMS ($ESI^+$) $[M+H]^+$ calculated for $C_{16}{}^{13}CH_{21}N_3{}^{15}NO_6$ 379.1460, observed 379.1459.

*[4a-$^{13}$C]Riboflavin ([4a-$^{13}$C]7).* Following the procedure described for **7**; **6** (60 mg, 0.166 mmol), 1.5 mL of *n*-butanol, **[5-$^{13}$C]3** (40 mg, 0.3121 mmol) and 0.3 mL of AcOH were combined to give 50 mg of a crude yellow solid (80% pure as determined by HPLC); HRMS ($ESI^+$) $[M+Na]^+$ calculated for $C_{16}{}^{13}CH_{20}N_4O_6Na$ 400.1309, observed 400.1286.

*[1,3-$^{15}N_2$]Riboflavin ([1,3-$^{15}N_2$]7).* Following the procedure described for **7**; **6** (100 mg, 0.2766 mmol), 1.5 mL of *n*-butanol, **[1,3-$^{15}$N$_2$]3** (56 mg, 0.43 mmol) and 0.3 mL of AcOH were combined to give 76.8 mg of a crude yellow solid (86% pure as determined by HPLC); HRMS ($ESI^+$) $[M+H]^+$ calculated for $C_{17}H_{21}N_2{}^{15}N_2O_6$ 379.1396, observed 379.1401.

*5-Deazariboflavin (8).* 5-Deazariboflavin (88% pure as determined by HPLC)

was synthesized as previously described[156] and was a generous gift from Dr. Seoung Ryoung-Choi. HRMS ($ESI^+$) $[M+H]^+$ calculated for $C_{18}H_{22}N_3O_6$ 376.1503, observed 376.1505.

*Expression and purification of homo sapiens (hs) riboflavin kinase (RFK).* *E. coli* BL21 (DE3) cells were transformed with *homo sapiens* (*hs*) riboflavin kinase plasmid (HS_RFK_EC_1_pQE-T7) containing the gene for RFK with a N-terminal $His_6$ affinity tag (Qiagen). Starting from a single colony, the cells were grown in 1L of MDG [Luria Broth[158] +1% glucose] containing 34 μg/mL kanamycin at 37 °C, 250 rpm to $OD_{600}$ ~ 0.6. Expression of the protein was induced by addition of isopropyl-β-D-thiogalactoside (IPTG, final concentration of 1 mM). Incubation was continued for 4 h at 37 °C. The cells were harvested by centrifugation (6000*g*, 25 min, 4 °C) and stored at -80 °C until used. A frozen cell pellet was suspended in lysis buffer (50 mM sodium phosphate, pH 8.0, containing 300 mM NaCl and 10 mM imidazole) and the cells were lysed by incubation with lysozyme, one protease inhibitor tablet (Roche), and DNase I (2 mg) on ice for 30 min followed by sonication (6 cycles of 30 s, 1 min cooling on ice). The cell lysate was centrifuged (12000 rpm, 25 min, 4 °C) and the resulting supernatant was mixed with 10 mL of Ni-NTA Agarose resin (Qiagen) and loaded on to a column. The resin was washed with 80 mL of 50 mM sodium phosphate buffer, pH 8.0, containing 300 mM NaCl and 20 mM imidazole and then eluted 50 mM sodium phosphate buffer, pH 8.0, containing 300 mM NaCl and 500 mM imidazole. Fractions were analyzed by SDS gel electrophoresis and those containing RFK were pooled, concentrated by centrifugation with a 10 KDa MWCO filter (Centriprep, Millipore), and dialyzed against 10 mM Tris-HCl buffer, pH 8, containing 10% glycerol. Protein concentration was

determined by the BCA assay (Pierce).

*FMN.* In a 100 mL round bottomed flask, crude riboflavin **7** (25 mg, 0.066 mmol, 0.66 mM), ATP (275.57 mg, 0.5 mmol, 5 mM) were incubated with riboflavin kinase (18.84 mg, 1 μmol, 10 μM) in 100 mL of buffer (100 mM 3-(*N*-morpholino)propanesulfonic acid (MOPS), pH 7.9) containing 5 mM $MgCl_2$ for 12 h at 30 $^{o}$C. After incubation, the enzyme was removed by filtration (Millipore Centricon, 10000 molecular weight cutoff (MWCO)). The solvent was then removed under lyophilization and the solid was purified on high performance liquid chromatography equipped with RP-C18 column to give 19.2 mg of a yellow solid; $^{1}$H NMR (300 MHz, $D_2O$) $\delta$ ppm 7.69 (s, 1H), 7.48 (s, 1H), 4.97 (t, $J$=11.7 Hz, 1H), 4.6 (d, $J$= 13.8 Hz, 1H), 4.34-4.31 (m, 1H), 4.11-3.97 (m, 4H), 2.45 (s, 3H), 2.31 (s, 3H); $^{13}$C NMR (75 MHz, $D_2O$) $\delta$ ppm 160.8, 157.8, 150.8, 149.8, 139.6, 134.2, 133.7, 131.6, 130.3, 117.1, 72.6, 71.4 (d, $J_{C\text{-}P}$ = 7.95 Hz), 69.3, 66, 47.6, 20.9, 18.7; $^{31}$P NMR (121 MHz, $D_2O$) $\delta$ ppm 2.72; HRMS (ESI$^-$) calculated for $C_{17}H_{20}N_4O_9P$ $(M - H)^-$ *m/z* = 455.0973, found 455.0971.

*[5-$^{15}$N]FMN.* Following the procedure described for **FMN**; Crude **[5-$^{15}$N]7** (10 mg, 0.0265 mmol, 0.53 mM) and ATP (137.785 mg, 0.25 mmol, 5 mM) were incubated with riboflavin kinase (9.423 mg, 0.5 μmol, 10 μM) in 50 mL of buffer containing 5 mM $MgCl_2$ and purified by HPLC to give 8.94 mg (98 %) of a yellow solid; $^{1}$H NMR (500 MHz, $D_2O$) $\delta$ ppm 7.77 (s, 1H), 7.61 (s, 1H), 5.04 (t, $J$=10 Hz, 1H), 4.69 (d, $J$= 15 Hz, 1H), 4.39-4.36 (m, 1H), 4.16-3.99 (m, 4H), 2.51 (s, 3H), 2.38 (s, 3H); $^{13}$C NMR (125 MHz, $D_2O$) $\delta$ ppm 163.5 (d, $^{2}J_{C\text{-}N}$ = 6.3 Hz), 160.3, 153.3, 152.4, 142, 136.8, 136.4 (d, $J_{C\text{-}N}$ = 4.28 Hz), 134.2, 132.9 (d, $^{2}J_{C\text{-}N}$ = 7.56 Hz), 119.5, 75, 73.8 (d, $J_{C\text{-}P}$ = 7.56 Hz), 71.8,

50.1, 23.4, 21.2; $^{31}$P NMR (121 MHz, $D_2O$) $\delta$ ppm 1.92; HRMS ($ESI^-$) calculated for $C_{17}H_{20}{}^{14}N_3{}^{15}NO_9P$ $(M-H)^-$ *m/z* = 456.0938, found 456.0950.

*[5-$^{15}$N, 4a-$^{13}$C]FMN.* Following the procedure described for **FMN**; Crude **[5-$^{15}$N, 4a-$^{13}$C]7** (10 mg, 0.0264 mmol, 0.53 mM) and ATP (137.785 mg, 0.25 mmol, 5 mM) were incubated riboflavin kinase (9.423 mg, 0.5 μmol, 10 μM) in 50 mL of MOPS buffer containing 5 mM $MgCl_2$ and purified by HPLC to give 7.19 mg (98 % yield) of a yellow solid; $^1$H NMR (500 MHz, $D_2O$) $\delta$ ppm 7.76 (s, 1H), 7.60 (s, 1H), 5.03 (t, $J$ = 10 Hz, 1H), 4.68 (d, $J$ = 15 Hz, 1H), 4.38-4.35 (m, 1H), 4.15-3.97 (m, 4H), 2.49 (s, 3H), 2.37 (s, 3H); $^{13}$C NMR (125 MHz, $D_2O$) $\delta$ ppm 163.6 (dd, $^1J_{C\text{-}C}$ = 76.1 Hz, $^2J_{C\text{-}N}$ = 7.56 Hz), 160.3, 153.2, 152.4 (d, $^1J_{C\text{-}C}$ = 55.44 Hz), 142, 136.8, 136.4 (d, $J_{C\text{-}N}$ = 3.78 Hz), 134.2 (d, $^3J_{C\text{-}C}$ = 6.17 Hz), 132.9 (t, $^3J_{C\text{-}C}$ = 6.3 Hz), 129, 119.5, 75, 73.8 (d, $J_{C\text{-}P}$ = 7.56 Hz), 71.8, 68.8, 50, 23.3, 21.2; $^{31}$P NMR (121 MHz, $D_2O$) $\delta$ ppm 1.95; HRMS ($ESI^-$) calculated for $C_{16}{}^{13}CH_{20}{}^{14}N_3{}^{15}NO_9P$ $(M - H)^-$ *m/z* = 457.0972, found 457.0971.

*[4a-$^{13}$C]FMN.* Following the procedure described for **FMN**; Crude **[4a-$^{13}$C]7** (10 mg, 0.0265 mmol, 0.53 mM) and ATP (137.785 mg, 0.25 mmol, 5 mM) were incubated with riboflavin kinase (9.423 mg, 0.5 μmol, 10 μM) in 50 mL of buffer containing 5 mM $MgCl_2$ and purified by HPLC to give 9.38 mg (97 % yield) of a yellow solid; $^1$H NMR (500 MHz, $D_2O$) $\delta$ ppm 7.74 (s, 1H), 7.56 (s, 1H), 5.01 (t, $J$ = 10 Hz, 1H), 4.65 (d, $J$ = 15 Hz, 1H), 4.38-4.34 (m, 1H), 4.13-3.98 (m, 4H), 2.48 (s, 3H), 2.35 (s, 3H); $^{13}$C NMR (125 MHz, $D_2O$) $\delta$ ppm 163.4 (d, $^1J_{C\text{-}C}$ = 76.86 Hz), 160.3, 153.2, 152.3 (d, $^1J_{C\text{-}C}$ = 55.44 Hz), 142, 136.7, 136.3, 134.1 (d, $^3J_{C\text{-}C}$ = 6.04 Hz), 132.8 (d, $^3J_{C\text{-}C}$ = 6.1 Hz), 128.8, 119.5, 75, 73.8 (d, $J_{C\text{-}P}$ = 7.2 Hz), 71.8, 68.6, 50, 23.3, 21.2; $^{31}$P NMR (121 MHz, $D_2O$) $\delta$ ppm 1.85; HRMS ($ESI^-$) calculated for $C_{16}{}^{13}CH_{20}N_4O_9P$ $(M - H)^-$ *m/z* = 456.1001, found 456.0995.

*[1,3-$^{15}N_2$]FMN.* Following the procedure described for **FMN**; Crude **[1,3-$^{15}N_2$]7** (10 mg, 0.0265 mmol, 0.53 mM) and ATP (137.785 mg, 0.25 mmol, 5 mM) were incubated with riboflavin kinase (9.423 mg, 0.5 μmol, 10 μM) in 50 mL of buffer containing 5 mM $MgCl_2$ and purified by HPLC to give 10.66 mg (> 98 % yield) of a yellow solid; $^1$H NMR (500 MHz, $D_2O$) $\delta$ ppm 7.75 (s, 1H), 7.57 (s, 1H), 5.02 (t, $J$ = 10 Hz, 1H), 4.67 (d, $J$= 15 Hz, 1H), 4.39-4.36 (m, 1H), 4.17-3.99 (m, 4H), 2.50 (s, 3H), 2.36 (s, 3H); $^{13}$C NMR (125 MHz, $D_2O$) $\delta$ ppm 163.4 (d, $J_{C\text{-}N}$ = 13.86 Hz), 160.3 (t, $J_{C\text{-}N}$ = 11.0 Hz), 153.3, 152.3 (d, $J_{C\text{-}N}$ = 7.93 Hz), 142, 136.8, 136.3, 134.1, 132.9, 119.5, 75, 73.8 (d, $J_{C\text{-}P}$ = 7.56 Hz), 71.8, 68.8, 50.1, 23.5, 21.2; $^{31}$P NMR (121 MHz, $D_2O$) $\delta$ ppm 1.9; HRMS (ESI$^-$) calculated for $C_{17}H_{20}{}^{14}N_2{}^{15}N_2O_9P$ $(M - H)^-$ *m/z* = 457.0909, found 455.0913.

*5-deazaFMN (9).* Following the procedure described for **FMN**; crude **8** (12 mg, 0.032 mmol, 0.53 mM) and ATP (137.785 mg, 0.25 mmol, 5 mM) were incubated with riboflavin kinase (9.423 mg, 0.5 μmol, 10 μM) in 50 mL of buffer containing 5 mM $MgCl_2$ and purified by HPLC to give 13 mg (> 98% yield) of a yellow solid;[159] $^1$H NMR (500 MHz, $D_2O$) $\delta$ ppm 7.78 (s, 1H), 7.45 (s, 1H), 7.03 (s, 1H), 4.27-3.97 (m, 7H), 2.3 (s, 3H), 2.12 (s, 3H); $^{13}$C NMR (125 MHz, $D_2O$) $\delta$ ppm 164.7, 161, 158.7, 152.1, 143.6, 141.2, 138.9, 132.6, 121.6, 119.5, 113.3, 74.9, 74 (d, $J_{C\text{-}P}$ = 7.3 Hz), 72.3, 68.8, 49.3, 23.2, 20.8; $^{31}$P NMR (121 MHz, $D_2O$) $\delta$ ppm 2.5; HRMS (ESI$^-$) calculated for $C_{18}H_{21}N_3O_9P$ $(M-H)^-$ *m/z* = 454.1015, found 454.1016.

*FMN binding assays.* Binding assay solutions contained apo wild type and monomeric *sp*IDI-2, 1 % glycerol and substrate in 100 mM HEPES, pH 7.0. Mixtures were incubated for 10 min at 37 °C, then transferred to a 30 kDa MWCO centrifugal

filter and incubated an additional 5 min at 37 °C. The samples were centrifuged at different speeds to allow < 10 % of the assay volume to pass through the membrane. UV-vis absorption spectra were collected for the filtrates. Spectra were collected until there was no increase in absorption at 450 nm for 3 consecutive measurements, and then averaged. All binding assay experiments were replicated 3 times.

*$^{15}$N-$^{1}$H HMBC protein-FMN NMR studies*. NMR spectra obtained at 25 $^{o}$C on a 600 MHz spectrometer equipped with a cold probe. $^{15}$N-$^{1}$H HMBC NMR spectra were collected for samples containing 300 μM wild type protein in 50 mM phosphate buffer pH 7.0 containing 240 μM FMN, 10% $D_2O$ in 700 μL volume. For the monomer, 300 μM protein in 50 mM phosphate buffer pH 7.0 containing 300 and 600 μM FMN, 10% $D_2O$ in 700 μL volume. Monomeric *sp*IDI-2 NMR sample additionally contained 150 mM NaCl and 2 mM DTT. For the free FMN NMR, 240 μM FMN in 50 mM phosphate buffer pH 7.0 containing 10% $D_2O$ in 700 μL volume.

## Results and Discussion

Our synthetic approach consists of the five step chemo-enzymatic route shown in Scheme 3.1, where four chemical steps are followed by a final enzyme-catalyzed phosphorylation of riboflavin **7**. The overall sequence is based on literature precedents for each chemical step through the Tishler condensation to give **7**, although the reaction conditions, work-up procedures and purification steps were substantially modified. We then used riboflavin kinase (RFK), which is regiospecific for the 5'-OH**,** to convert **7** to 5'-FMN.[160] In contrast, chemical phosphorylation of **7** is not regiospecific, giving a mixture of monophosphates, bisphosphates, and cyclic phosphates that is difficult to

separate.[161] This approach not practical when using expensive $^{15}N$ and $^{13}C$-enriched substrates.

The substrates for the Tishler condensation, barbituric acid **3** and amino *o*-azoribitol derivative **6**, were synthesized from materials that permit us to introduce labels at N1/N3, N5, N10, C4a, and C2/C4 of **7** by the route outlined in Scheme 3.11. We reproduced the reported good yields for synthesis of **3** from urea **1** and diethyl malonate **2**[155] and the reductive amination of 3,4-dimethyl aniline **4** with D-ribose and sodium cyanoborohydride ($NaCNBH_3$) to give *N*-ribityl 3,4-dimethyl aniline **5**.[156] The low yield (~20%) for conversion of **5** to **6** with $NaNO_2$/HOAc/NaOH was improved considerably (95%) by adapting the procedure reported by Folkers and coworkers for synthesis of L-lyxoflavin where HOAc/NaOH was replaced by NaOAc.[157]

Purification of **7** following condensation of **6** with barbituric acid **3** proved to be difficult. We were not able to obtain good yields following the lengthy purification protocol, which includes several washes with water and MeOH, extractions with ether, and recrystallization with superoxol,[157] which are necessary to provide pure **7** for a chemical phosphorylation. We verified that phosphorylation of **7** with $POCl_3$ gave a mixture of regioisomers that are hard to separate by HPLC.[161] Instead, the reaction mixture containing **7** from the condensation of **3** and **6** was washed with water and cold methanol and used directly for the RFK-catalyzed phosphorylation, thereby preventing a substantial loss of material during repeated washings, extractions, and recrystallization. Incubation of crude **7** with ATP and RFK gave 5'-FMN in > 95% yield.

The reactions shown in Scheme 3.2 were used to synthesize **7** with $^{15}N$ at positions N1/N3 and N5, $^{13}C$ at C4a, and $^{13}C/^{15}N$ at C4a/N5. [N1,N3-$^{15}N_2$]- and [C4a-

$^{13}$C]**7** were synthesized from labeled barbituric acid as outlined in Scheme 3.1. [1,3-$^{15}N_2$]- and [5-$^{13}$C]Barbituric acids were prepared from [1,3-$^{15}N_2$]urea and diethyl [3-$^{13}$C]malonate, respectively[162,163]. Condensation of the labeled barbiturates with azoribitol **6** gave the corresponding labeled riboflavins. [N5-$^{15}$N]- and [C4a-$^{13}$C, C5-$^{15}$N]Riboflavin were prepared as shown in Scheme 3.3. [N5-$^{15}$N]**7** was prepared by treatment of ribityl amine **5** with Na$^{15}NO_2$/HCl followed by coupling of the labeled diazonium intermediate with aniline to give $^{15}$N-azoribitol **6**. Condensation of labeled **6** with barbituric acid gave [5-$^{15}$N]**7** and with [5-$^{13}$C]barbituric acid gave [C4a-$^{13}$C, C5-$^{15}$N]**7**.

The overall yields of labeled riboflavins for the three steps from barbituric acid ranged from 29-43%. The poorest yields were for the final conversion of **6** to **7** (43-64%). We experienced additional losses at this step during attempts to purify **7** from the reaction mixture. Riboflavin is poorly soluble in water and common organic solvents, which severely limits its purification by chromatography, and we encountered substantial losses during recrystallization. As a result, *homo sapiens* riboflavin kinase (*hs*RFK) was used to phosphorylate unpurified **7** with ATP. The labeled riboflavins were dissolved in a minimal volume of DMSO and added to *hs*RFK to give a reaction buffer that contained ~1% DMSO. The enzyme-catalyzed phosphorylation was regioselective for synthesis of 5-FMN. Impurities in the labeled riboflavin samples did not interfere with the reaction, giving excellent conversions of **7** to FMN, which was purified by HPLC (Scheme 3.4, Table 3.1). The same procedure was used to phosphorylate 5-deazariboflavin **8** to give 5-deazaFMN **9**, an analogue frequently used in mechanistic studies of flavin-dependent enzymes.[164]

*Dissociation constants.* The dissociation constants ($K_D$) for apo wild type *sp*IDI-2 and monomeric *sp*IDI-2 for FMN were determined with an ultrafiltration assay and data were fit to the Hill Equation shown below. The data and best-fit lines are shown in Figure 3.4. $K_D^{FMN} = 3.07 \pm 0.43$ μM and $n = 1.9 \pm 0.18$ for wild type tetramer, $K_D^{FMN} = 98 \pm 3.5$ μM and $n = 2.72 \pm 0.21$ for monomeric *sp*IDI-2 where $n$ represents the number of $FMNH_2$ molecules bound per molecule of apo-*sp*IDI-2. There are no reports suggesting that IDI-2 binds more than one molecule of FMN, however, these results yielded an $n$ value significantly greater than 1, with data fitting $n$ for FMN ~ 2. Dissociation constants were determined in order to carry out NMR studies with unlabeled wild type and monomeric *sp*IDI-2 by reconstituting the apo enzymes with $^{15}$N- and $^{13}$C-labeled FMN isotopologues that were previously synthesized and discussed earlier in this chapter. Identifying dissociation constants for FMN in both proteins will help to accurately reconstitute both enzymes with FMN in the completely enzyme-bound form to detect its NMR signals. The NMR studies are aimed to gain insights in to the structure of enzyme bound flavin zwitter-ion as well as the pKa of the labeled centers in FMN as outlined in the following section.

*$^{15}$N-$^{1}$H HMBC NMR studies.* We performed HMBC NMR experiments in an attempt to study the reduced flavin zwitter-ionic structure in the active site of the enzyme as shown in Figure 1.14 (Chapter 1). By utilizing the [5-$^{15}$N] FMN and incorporating into both wild-type and monomeric apo IDI-2, the goal is to observe the [5-$^{15}$N] multiplicity of FMN in the oxidized, reduced and zwitter-ionic states including the catalytically active complex IDI-2•$FMN_{red}$•IPP/DMAPP in which we predict $FMN_{red}$ exists in zwitter-ionic tautomer. Additionally, we aimed to study the change in $^{15}$N chemical shift (δ) as a

function of pH to identify the pKa of N(5) in the active site of the enzyme. This similar pH-pKa titration study could be extended to study the pKa of the other labeled centers in the FMN isotopologues that we synthesized. Towards these goals, we have collected the $^{15}$N-$^{1}$H HMBC spectrum of [5-$^{15}$N] FMN and observed the $^{3}$J $^{15}$N-$^{1}$H correlation of C(6)-H and N(5) (Figure 3.5 and 3.6A) in the free form but when the flavin binds either the wild type *sp*IDI-2 tetramer or monomer, the $^{3}$J $^{15}$N-$^{1}$H HMBC signal disappeared indicating an exchange mechanism and the corresponding HMBC signal could not be detected (Figure 3.6B and 3.6C).

Similarly, $^{1}$H-NMR study utilizing unlabeled FMN by monitoring the C7 and C8 methyl groups of FMN indicated that at lower concentrations of FMN (up to 1:4 Protein:FMN for wild type and 1:8 for monomer) $^{1}$H signals were absent but the $^{1}$H signals appeared at higher FMN concentrations indicating that the observed $^{1}$H signals are indicative of free unbound FMN but not enzyme bound FMN (Figure 3.7). Therefore, both the $^{15}$N-$^{1}$H HMBC and $^{1}$H-NMR studies revealed that NMR signals for the FMN in the enzyme-bound state could not be observed by NMR due to rapid exchange mechanisms between bound and unbound forms.

As an alternative strategy, we are utilizing Raman spectroscopy to study the proposed enzyme-bound flavin zwitter-ionic structure in IDI-2. Raman spectroscopy is an important tool to study flavins and flavoproteins since the Raman bands of flavins are sensitive to redox, protonation states of flavin isoalloxazine ring, hydrogen bonding, steric interactions, and planarity of the isoalloxazine ring.[165,166] Isotopically labeled flavins have been applied to study the flavins in oxidized and semiquinone states along with computational approaches such as DFT calculations.[167-170] Therefore, we are

currently utilizing resonance Raman spectroscopy to study the differences of Raman bands of FMN in oxidized, reduced, and zwitter-ionic states in the active site of IDI-2.

In summary, we describe an efficient five-step synthesis of $^{13}C$ and $^{15}N$ FMN isotopologues labeled at positions C1, C3, C4a, and N5 of pyrazine and pyrimidine rings in the isoalloxazine nucleus in yields ranging from 29% to 43% from commercially available labeled precursors (Figure 3.8). Our synthesis can be also adapted to label other carbon, nitrogen, hydrogen, and oxygen atoms in the isoalloxazine ring system by starting with the suitable $^{15}N$ or $^{13}C$ enriched precursors. Although the final step involves a RFK-catalyzed phosphorylation requiring ATP to synthesize the labeled riboflavins to the corresponding FMN derivatives, an expression plasmid for RFK is available and ATP regeneration protocols can be used for larger scale syntheses.[171]

Furthermore, we have measured the dissociation constants ($K_d$) for FMN in both wild type tetrameric and monomeric *sp*IDI-2 and performed $^{15}N$-$^{1}H$ HMBC and $^{1}H$-NMR studies by reconstituting the wild type and monomeric apo *sp*IDI-2 with [5-$^{15}N$]FMN and unlabeled FMN. These studies were performed to identify the pKa of N(5) and other nuclei such as C(4a), N(1) in FMN as well as the multiplicity of N(5) NMR signal in IDI-2•$FMN_{red,}$ IDI-2•$FMN_{red}$•IPP/DMAPP complexes to gain insights about the protonation states and the pKa's of the labeled positions in FMN responsible for IDI-2 catalysis. We found that NMR is not a suitable technique to study the enzyme-bound FMN pKa's and the zwitter-ionic structure since the FMN signals could not be detected due to exchange mechanism between bound and unbound states. Therefore, we are currently utilizing resonance Raman spectroscopy to identify the differences in the Raman spectra of flavin in oxidized, reduced and zwitter-ionic states along with computational approaches. The

$^{15}$N- and $^{13}$C-FMN isotopologues will be utilized to collect the Raman spectra of FMN-bound IDI-2. Resonance Raman studies are currently in progress.

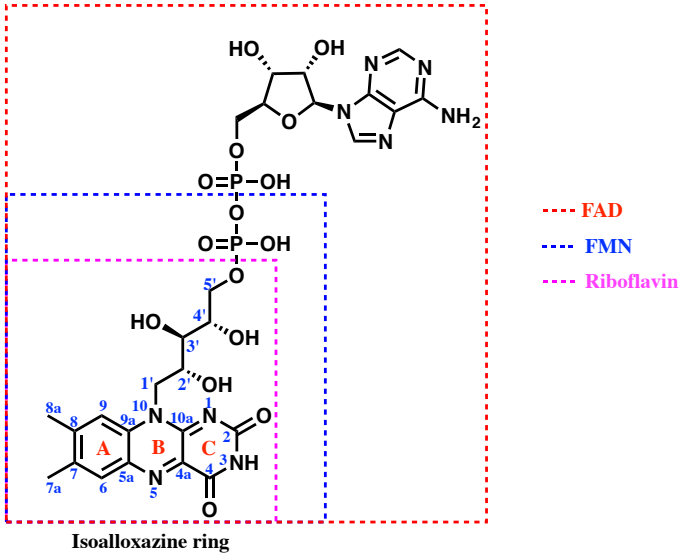


**Figure 3.1.** Structures of riboflavin, FMN, and FAD.

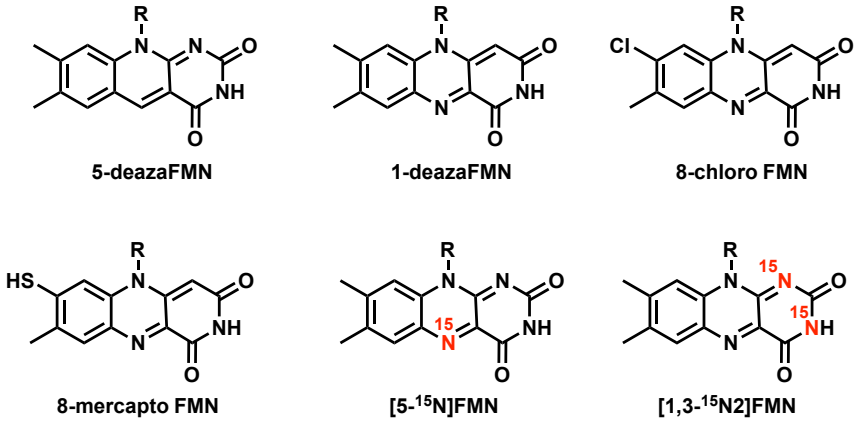


**Figure 3.2.** Some flavin analogs used as probes for enzyme-catalyzed reactions.

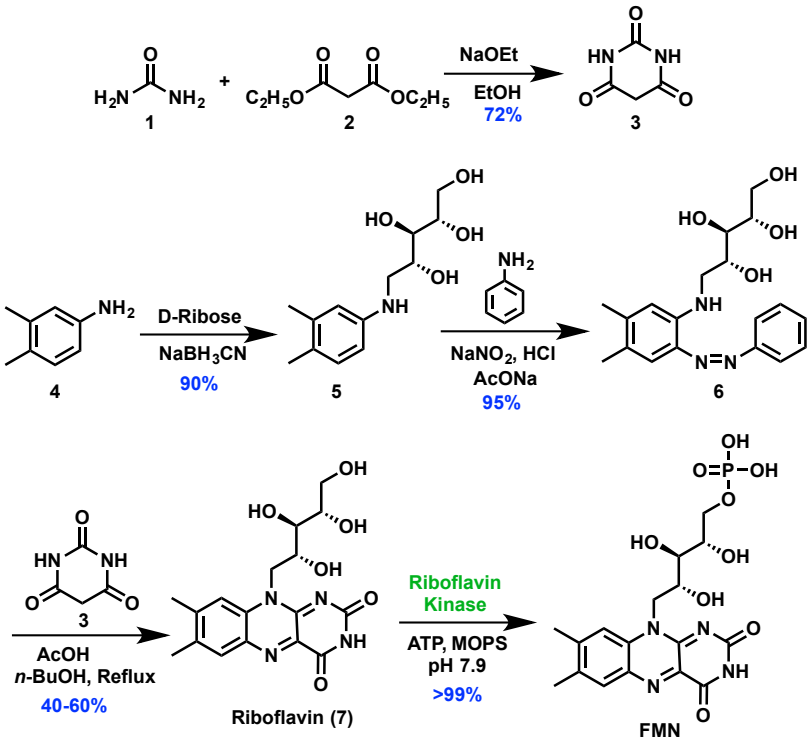


**Scheme 3.1.** Synthesis of $^{13}C$ and $^{15}N$ labeled FMN.

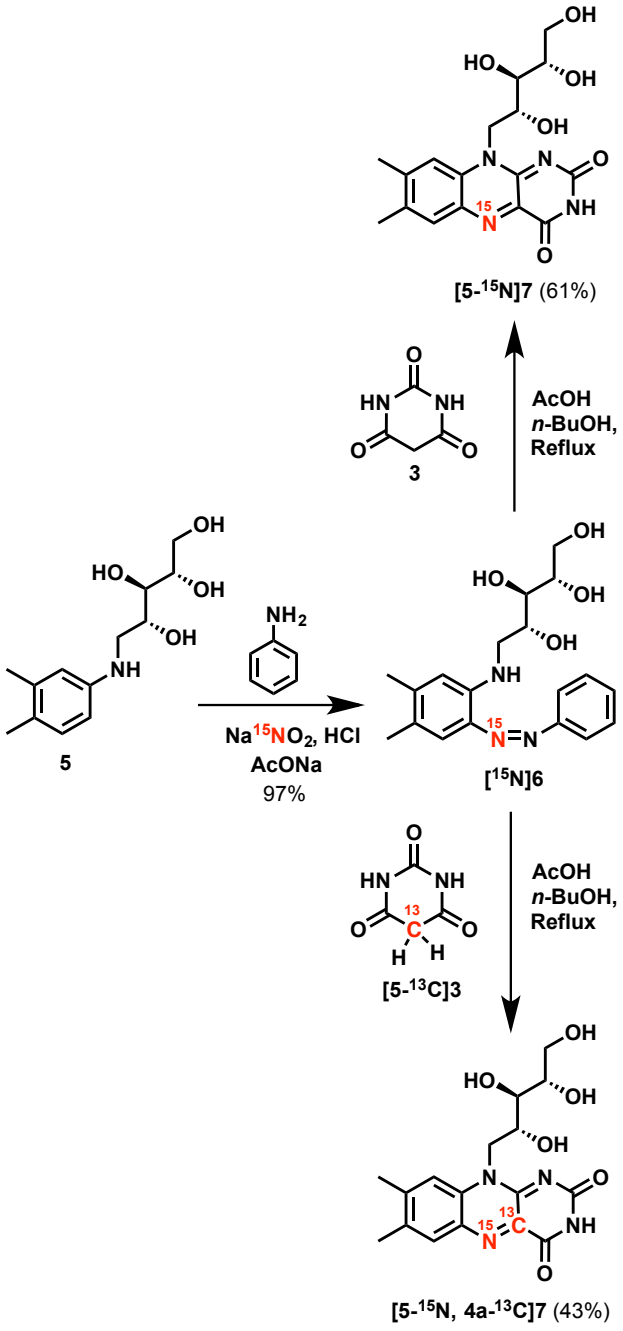


**Scheme 3.2.** Synthesis of [5-$^{15}$N]**7** and [5-$^{15}$N, 4a-$^{13}$C]**7.**

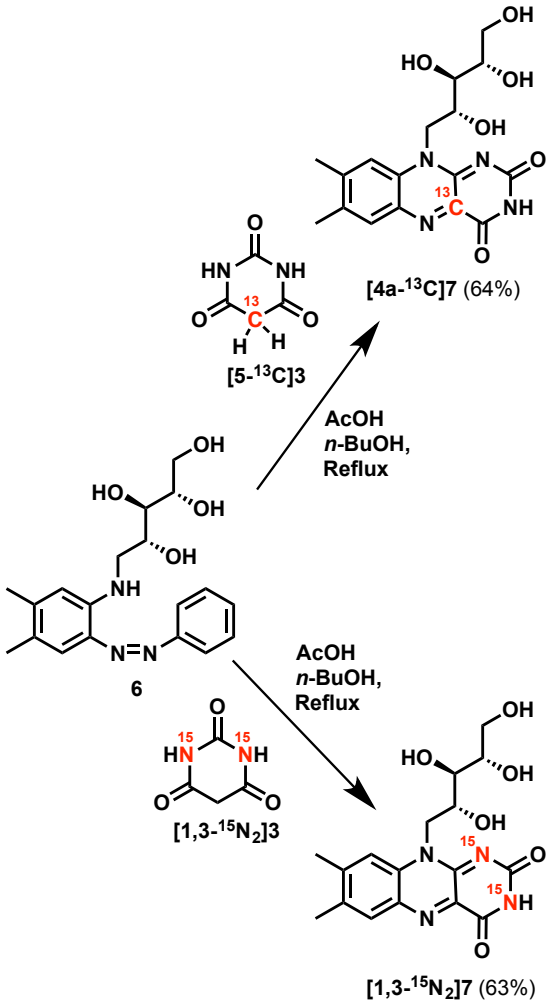


**Scheme 3.3.** Synthesis of [4a-$^{13}$C]**7** and [1,3-$^{15}N_2$]**7.**

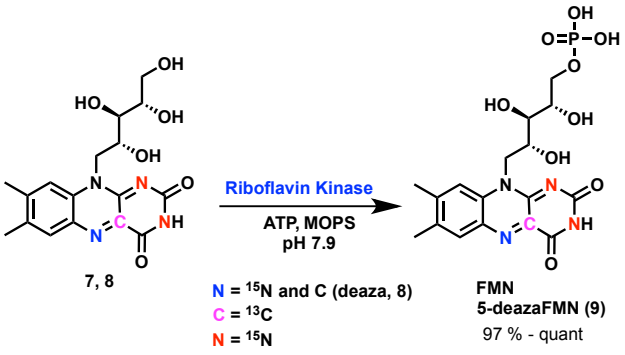


**Scheme 3.4.** RFK phosphorylation of labeled riboflavin precursors and 5-deazariboflavin (**8**).

**Table 3.1**. RFK-catalyzed phosphorylation of $^{15}N$- and $^{13}C$-enriched riboflavins.

| Substrate | Purity* (%) | Product | Yield (%) |
|---|---|---|---|
| $^{15}N(5)$-Riboflavin 7a (10 mg) | 75 | $^{15}N(5)$-FMN (8.94 mg) | 98 |
| $^{13}C(4a)$-Riboflavin 7b (10 mg) | 80 | $^{13}C(4a)$-FMN (9.38 mg) | 97 |
| $^{15}N(5)^{13}C(4a)$-Riboflavin 7c (10 mg) | 59 | $^{15}N(5)^{13}C(4a)$-FMN (7.19 mg) | >98 |
| $^{15}N(1)^{15}N(3)$-Riboflavin 7d (10 mg) | 86 | $^{15}N(1)^{15}N(3)$-FMN (10.66 mg) | >98 |
| 5-deazaRiboflavin 7e (12 mg) | 88 | 5-deaza-FMN (12.52 mg) | 98 |

***** Evaluated by RP $C_{18}$-HPLC by integrating area of the peak (Figure 3.3).

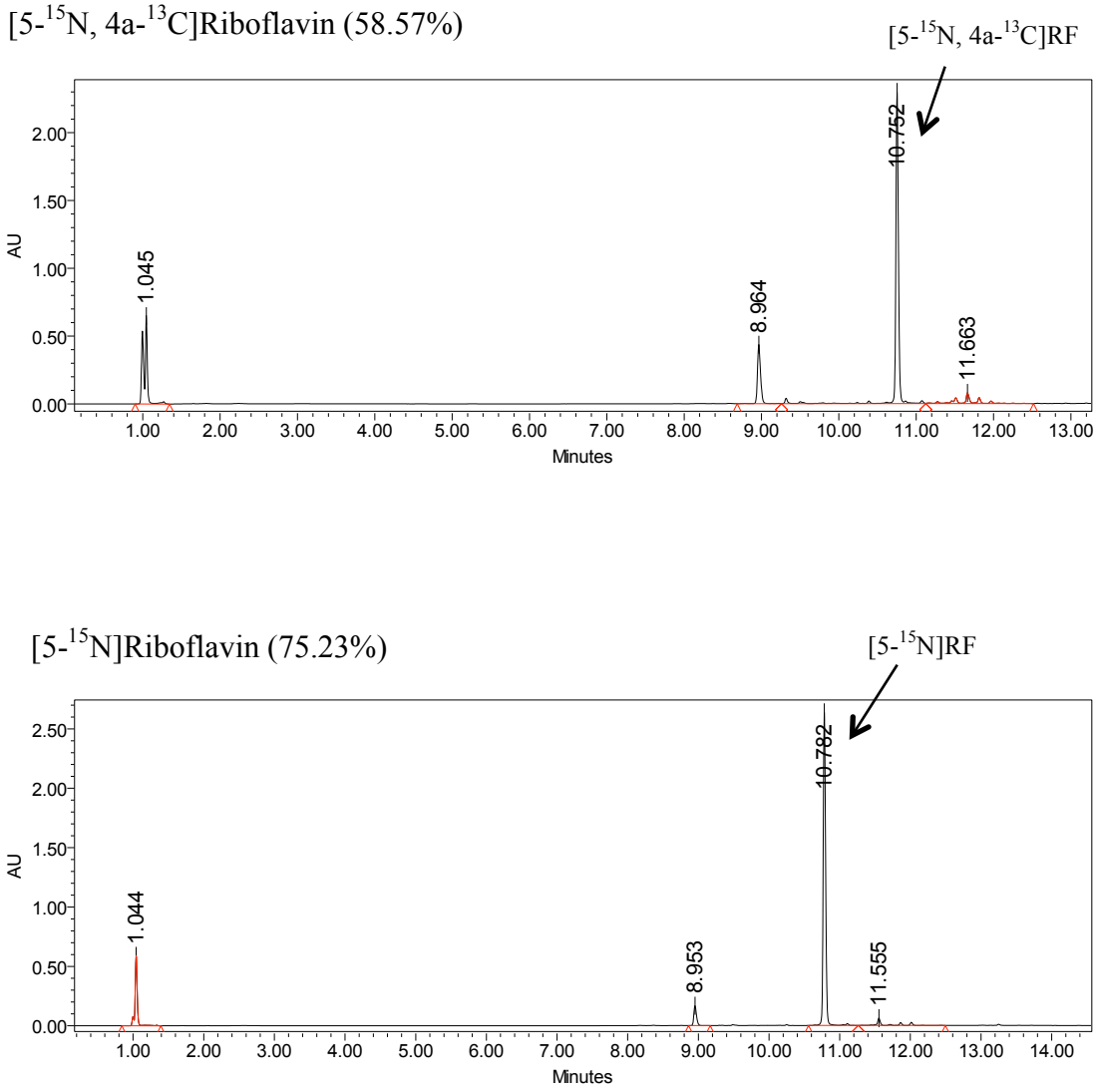


**Figure 3.3.** C18 analytical HPLC chromatograms of $^{15}N$ and $^{13}C$-labeled crude riboflavins (RF).

[1,3-$^{15}N_2$]Riboflavin (85.58%)

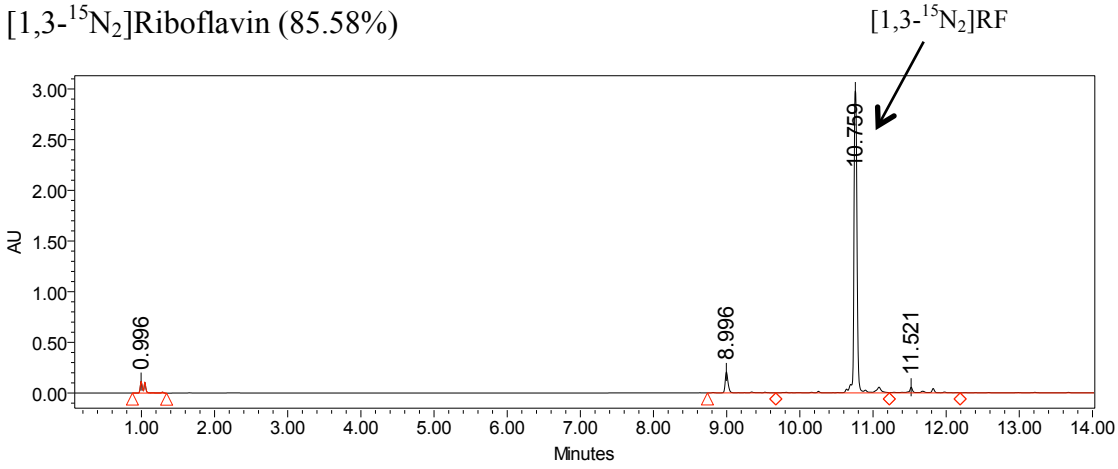


[4a-$^{13}$C]Riboflavin (80.09%)

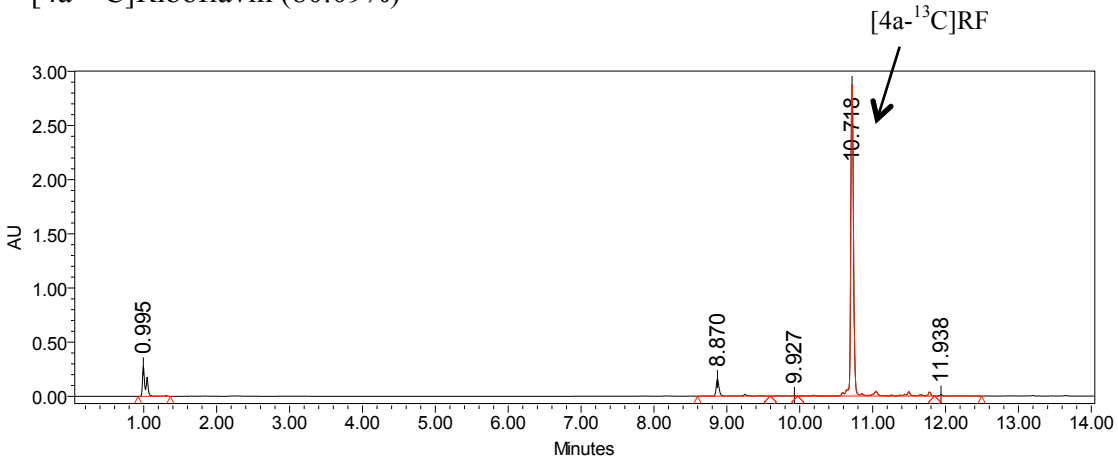


5-deazaRiboflavin (87.81%)

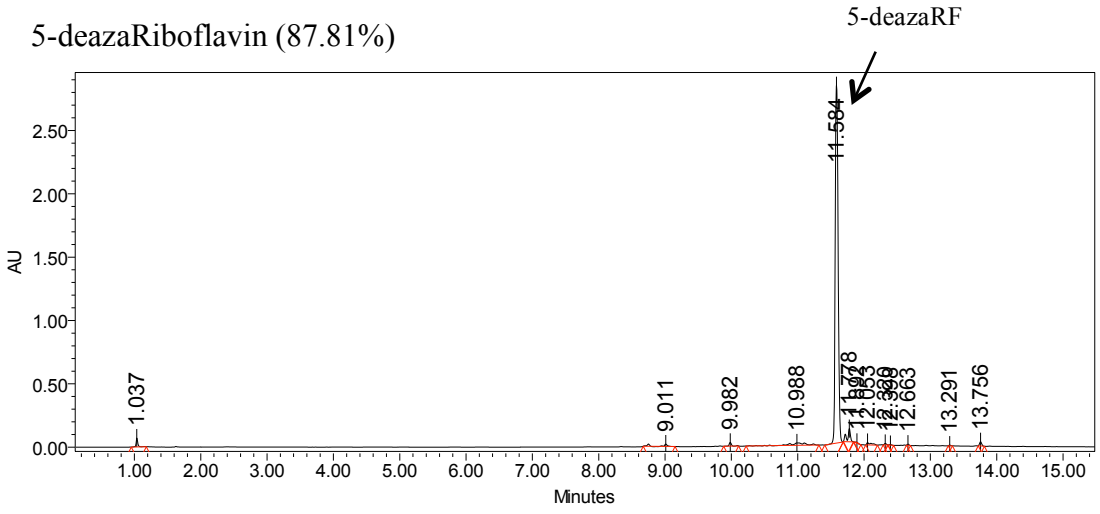


**Figure 3.3 continued**

$$\frac{[\mathrm{E^*FMN}]}{\mathrm{E}_{total}} = \frac{n}{1+\left(\frac{K_d}{[\mathrm{FMN}_{free}]}\right)^n} = \frac{y_{max}}{1+\left(\frac{K_d}{[\mathrm{FMN}_{free}]}\right)^n}$$

**A**

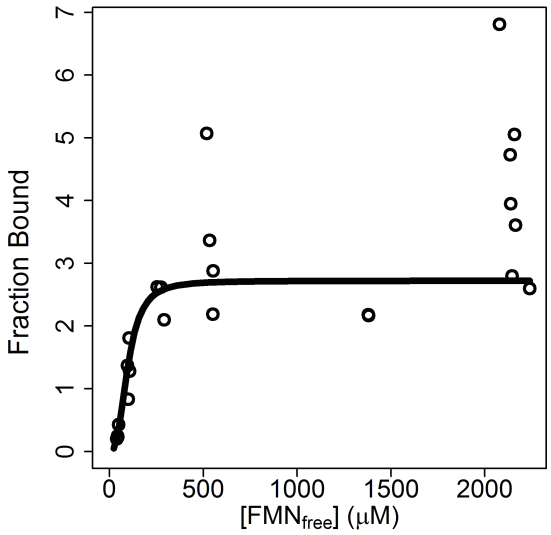


**B**

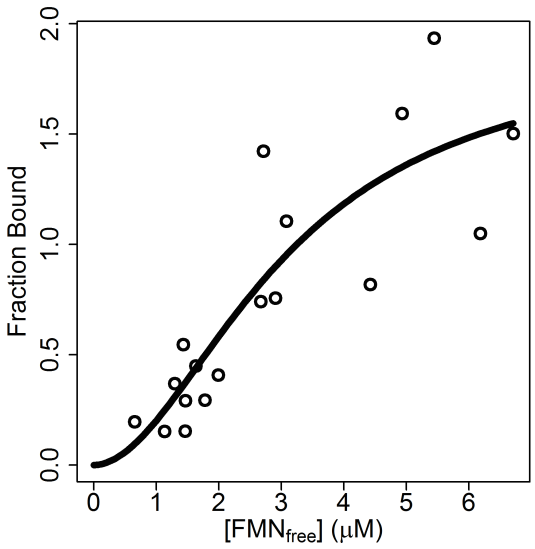


**Figure 3.4.** $K_D$ for FMN in A) Monomeric *sp*IDI-2 B) wt *sp*IDI-2.

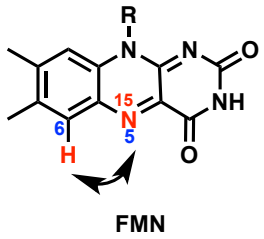


**Figure 3.5.** $^{3}J$ (5-$^{15}$N) - (C6-$^{1}$H) correlation of FMN.

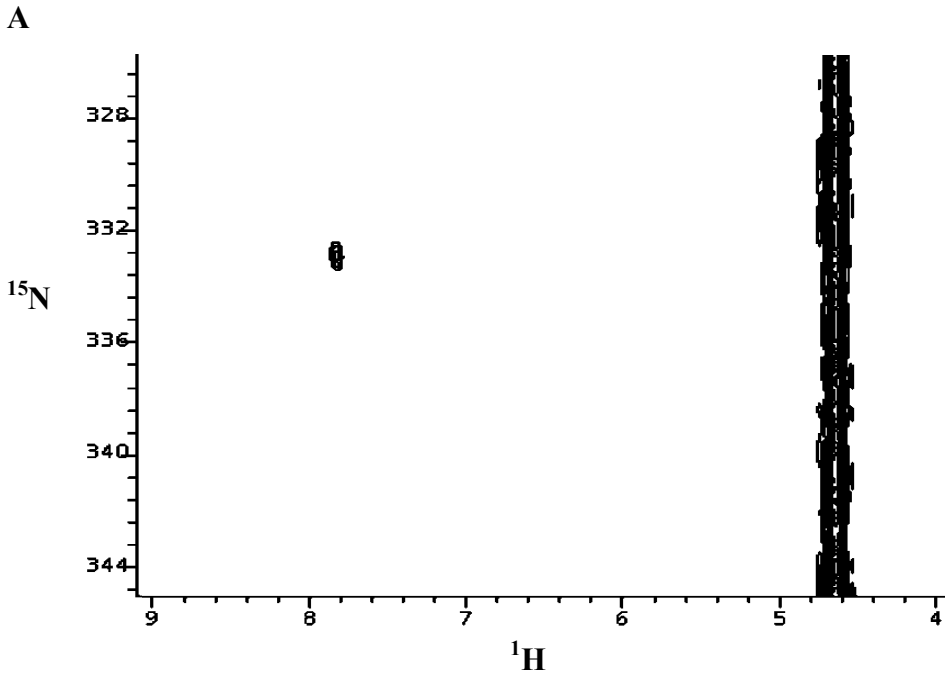


**Figure 3.6.** $^{15}$N-$^{1}$H HMBC of A) [5-$^{15}$N]FMN B) [5-$^{15}$N]FMN + monomeric *sp*IDI-2 C) [5-$^{15}$N]FMN + wild type *sp*IDI-2.

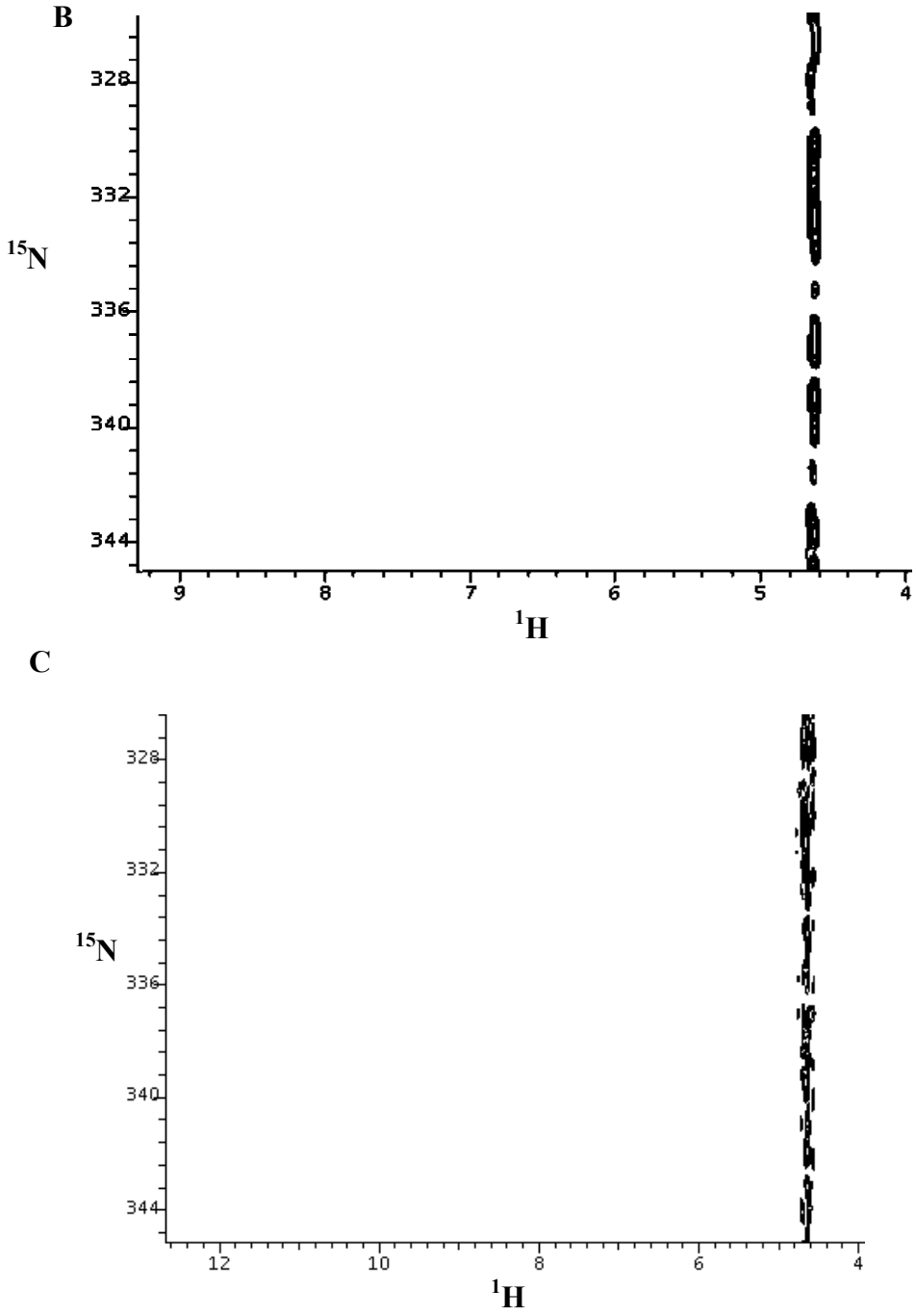


**Figure 3.6 continued.**

A

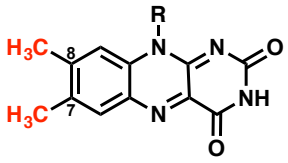


**Wild-type IDI2 ($^1$H NMR of –Me groups of the FMN)**

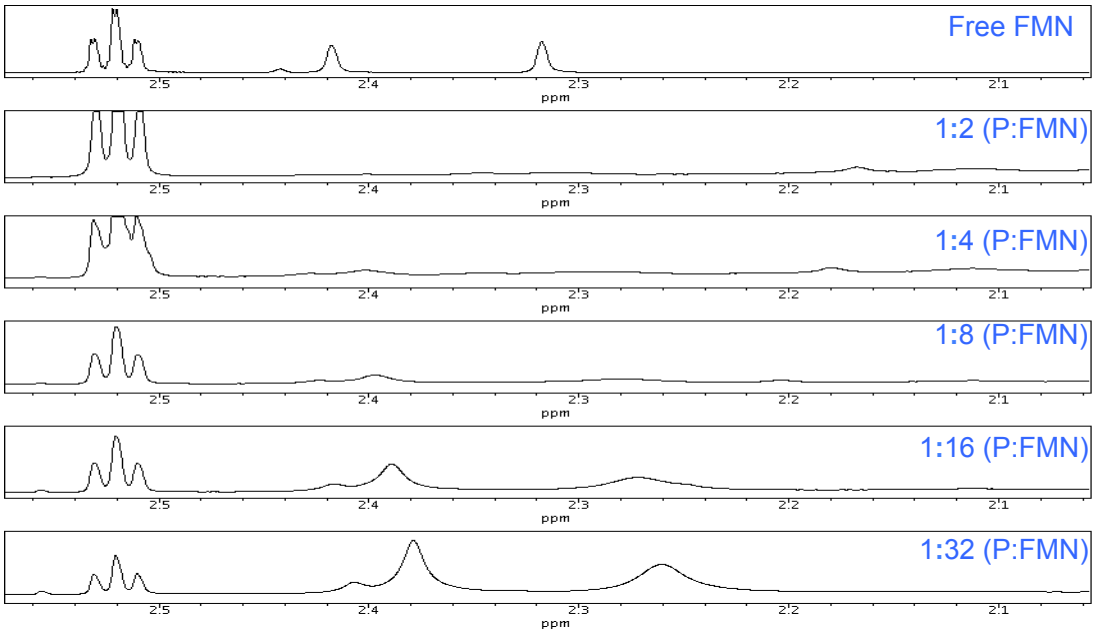


**Figure 3.7.** $^1$H-NMR of increasing concentrations of FMN at constant concentration of protein A) FMN + wild type *sp*IDI-2 B) FMN + monomeric *sp*IDI-2 (P indicates protein). Flavin structure with methyl groups is also shown.

**B**

**Monomeric IDI2**

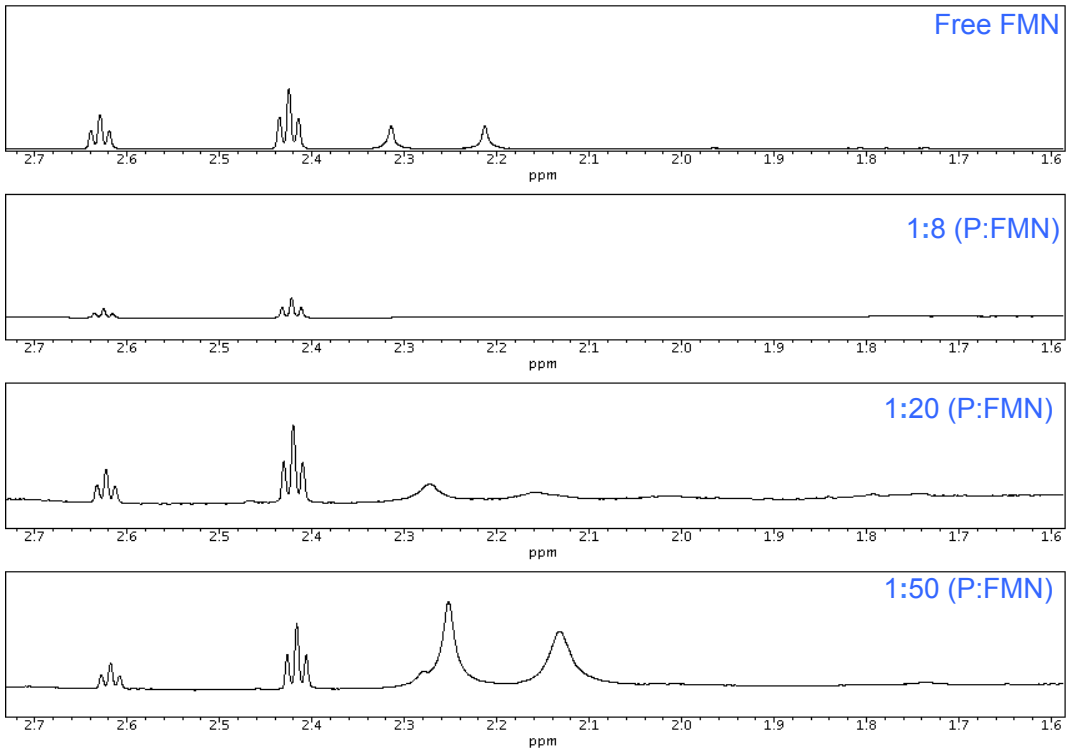


**Figure 3.7. continued.**

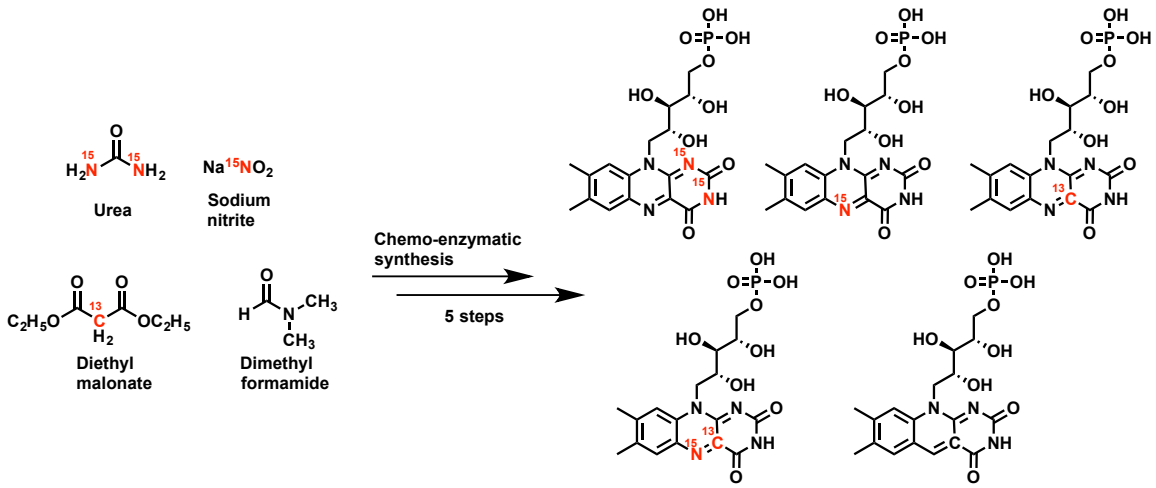


**Figure 3.8.** Chemo-enzymatic synthesis of flavin isotopologues.

CHAPTER 4

# MECHANISTIC STUDIES OF TYPE 1 AND TYPE 2 ISOPENTENYL DIPHOSPHATE ISOMERASE

## Introduction

Several lines of evidence, including active-site-directed inhibition, site-directed mutagenesis, and studies with substrate analogues and transition state inhibitors, suggest that IDI-1 and IDI-2 catalyze isomerization via a protonation-deprotonation mechanism.[50,52,82,85,88,90-92,98,104b,172] IDI-1 and IDI-2 differ not only by their amino acid sequences, their tertiary and quaternary structures, and the catalytic residues in their active sites, but also by their facial selectivity during protonation-deprotonation. IDI-1 catalyzes an antarafacial isomerization[57] during which the active site glutamate acts as an acid by protonating the *si*-face of the double bond and cysteine acts as a base to stereospecifically abstract the pro-*R* proton from C2. In contrast, IDI-2 catalyzes a suprafacial isomerization[91] where the flavin cofactor acts as an acid-base catalyst to protonate the *re*- face of the double bond of IPP and abstract the pro-*R* proton from C2 (Scheme 4.1).[76] The isomerization of IPP to DMAPP catalyzed by IDI-1 or IDI-2 could proceed via tertiary ($3^o$) carbocationic intermediate or a structurally related transition state (Figure 4.1). Two groups (Abeles and Poulter) independently obtained support for the carbocationic intermediate for the reaction catalyze by IDI-1 in their studies with

IPP analogs for IDI-1, including a positively charged ammonium mimic of the putative carbocation (NIPP).[58,59,80,89] Formation of the carbocationic intermediate requires a step-wise mechanism. Poulter and coworkers obtained additional support for the carbocationic intermediate for IDI-2 using a thiomethyl analog of IPP and with other electrophilic IPP analogs. Collectively, the studies suggested that both IDI-1 and IDI-2 behave similarly by generating a $3^o$ carbocationic intermediate via a step-wise mechanism for IPP/DMAPP isomerization. Richard and coworkers suggested a concerted mechanism from model studies based on linear free energy (LFE) correlations of the nonenzymatic acid catalyzed isomerization of 4-(4-methoxyphenyl)-2-methyl-1-butene to 4-(4-methoxyphenyl)-2-methyl-2-butene in mixtures of trifluoroethanol (TFE)/water (Figure 4.2A).[68] The results suggest that the kinetic barrier for deprotonation of the tertiary carbocation is significantly less than that for protonation of enolates by water. Due to the low-energy kinetic barrier for deprotonation, they proposed a concerted mechanism. Comparison of a carbocationic intermediate to an ‘‘enolate’’ intermediate in enzymatic reactions suggests that “enolate” intermediates have ‘‘low barrier’’ hydrogen bonds to hydrogen bond donors in the active site residues of the enzymes. However, this type of hydrogen bonding, which requires that the p*Ka*’s of the hydrogen bond donor and acceptor be closely matched, does not seem plausible for an enzyme-bound $3^o$ carbocationic intermediate where its estimated p*Ka* of ~ -12 is much more negative than those of hydrogen bond donors in amino acid side chains.

Richard and coworkers also undertook model studies with 1-(4-methoxyphenyl)-3-methyl-3-butyl-X derivatives in aqueous solvents both in the presence and absence of the strong nucleophile azide ($N_3^-$) (Figure 4.2B).[69] Addition of azide did not affect the

yields of the resulting alkene products which further supports a concerted mechanism that operates via a carbocationic-like transition state.

Although these reports favor a concerted mechanism, they are based on nonenzymatic model reactions in aqueous solvents rather than the active sites of IDI-1 and IDI-2. Thus, we undertook a different approach by studying deuterium incorporation into IPP and DMAPP during isomerizations catalyze by IDI-1 and IDI-2 reactions in $D_2O$. We now present compelling evidence that the protonation-deprotonation steps in IPP and DMAPP in both IDI-1 and IDI-2 proceed via a $3^o$ carbocationic intermediate in a step-wise manner.

## Experimental Procedures

*Reagents and chemicals*. Cell culture growth media, salts, and chemicals were purchased from Fisher Scientific, B&D, and Sigma-Aldrich. HRMS-ESI data were recorded on LC-TOF and LTQ-FTMS mass spectrometers. Samples from incubation of IPP with IDI-1 and IDI-2 were analyzed by RP-HPLC on a Phenyl column (Waters, 19 × 100 mm) that had been equilibrated with $H_2O$. Products were eluted with a $H_2O$-ACN gradient (0-100% $H_2O$/ACN) with a run time of 15 min at a flow rate of 1 mL/min. Under these conditions, the retention time (rt) for dimethylallyltryptophan (DMAT) was ~ 14 min. IDI-2 assays were performed under oxygen free conditions in an anaerobic chamber (Coy). The purity of the proteins was determined by sodium dodecyl sulphate-polyacrylamide gel electrophoresis (SDS-PAGE). Protein concentration was determined by the BCA assay (Pierce).

*IPP and DMAPP synthesis.* Isopentenyl diphosphate and dimethylallyl diphosphate was synthesized as per the procedure described by Davisson et. al.[173]

*E. coli IDI-1 overexpression and purification.* Plasmid (pAPHIII22) encoding the gene for *E. Coli* IDI-1 and the *E. coli* expression strain JM101 was used as reported[174] with the following modifications. The cell cultures were grown in Luria broth, containing 100 μg/mL of ampicillin, at 37 °C, 230 rpm until $OD_{600}$ ~ 0.6. Overexpression of the protein was induced by the addition of nalidixic acid (final concentration of 0.2 mM) as described previously. The cells were suspended in lysis buffer (50 mM sodium phosphate, pH 8.0, containing 300 mM NaCl and 10 mM imidazole) with the addition of lysozyme (10 mg), one protease inhibitor tablet (Roche), and DNase I (2 mg) on ice for 30 min followed by sonication (6 X 30 s cycles, 1 min cooling intervals on ice). The cell lysate was centrifuged (12000 rpm, 25 min, 4 °C) and the resulting supernatant was mixed with 10 mL of Ni-NTA Agarose resin (Qiagen) and loaded on to a column. Flow-through was collected, and the protein-bound Ni-NTA agarose resin was washed with 50 mM sodium phosphate, pH 8.0, containing 300 mM NaCl and 20 mM imidazole. Protein was eluted with 50 mM sodium phosphate, pH 8.0, containing 300 mM NaCl, and 250 mM imidazole and the fractions containing IDI-1 were pooled, concentrated with a 10 kDa MWCO filter (Centriprep, Millipore) and dialyzed against 10 mM Tris buffer, pH 8.0. The protein was then lyophilized and suspended in 99.9% $D_2O$ and concentrated with a 10 kDa MWCO filter. This process was repeated 4-5 times before the protein was suspended in 10 mM Tris, pD 8.0 $D_2O$ buffer and stored at -80 $^oC$ until use.

*Streptococcus pneumoniae IDI-2 overexpression and purification. sp*IDI-2 overexpression and purification was performed as described previously.[98] After

purification and dialysis, the protein was lyophilized and suspended in 99.9% $D_2O$ buffer and washed 4-5 times with 10 mM Tris, pD 8.0 in a 10 kDa MWCO filter and stored at -80 $^oC$ until use.

*Claviceps purpurea 4-DMATS overexpression and purification. cp*4-DMATS overexpression and purification was performed as described previously.[175] After purification and dialysis, the protein was lyophilized and suspended in 99.9% $D_2O$ buffer and washed 4-5 times with 10 mM Tris, pD 8.0 in a 10 kDa MWCO filter and stored at -80 $^oC$ until use.

*IDI-1, 4-DMATS coupled assay in $D_2O$ buffer.* All the reagents were thoroughly exchanged with $D_2O$ by repeated lyophilization. 4-DMATS (40 μM) was incubated with 10 mM L-Trp, 2 mM IPP, 0.1 mg/mL BSA, 10 mM $MgCl_2$, 1 mM DTT in a total volume of 2.5 mL (pH 7.8). The reaction was initiated by addition of (20 μL) 1 μM IDI-1. Samples (260 μL) were collected at 0.5h, 1h, 1.5h, 2.5h, 4h, 6h, 9h, and 12.5h. The enzyme was removed with a 10 kDa MWCO filter and the resulting filtrate was lyophilized, and fractionated by RP-HPLC (phenyl column, 0-100% $H_2O$-ACN gradient) into samples containing IPP and DMAT. IPP, which eluted in the void volume under these conditions, was further purified by anion-exchange chromatography as described below. The samples of IPP and DMAT were analyzed by ESI-MS to identify the deuterium content in both compounds.

*Anion-exchange chromatography.* The void volume fraction from the reversed phase separation were lyophilized, dissolved in 500 μL of water and loaded on to an anion-exchange column (Strata-Z-AW 33 μm, Phenomenex) that had been washed with methanol equilibrated with water. IPP was eluted ammonium hydroxide ($NH_4OH$) in

MeOH (5:95 v/v). Samples were lyophilized and analyzed by mass spectrometry.

*IDI-2, 4-DMATS coupled assay in $D_2O$ buffer.* The same procedure outlined above was repeated with the following modifications. 10 nM IDI-2 was used and the time point aliquots were collected at 0h, 1h, 4h, 6h, 8h, 12h, and 24h and the enzyme was separated with a 30 kDa MWCO filter.

*Control assays with DMAPP.* Same procedure as above except 2 mM DMAPP was used and the reaction was run for 24h for both IDI-1 and IDI-2.

## Results

*Stepwise versus concerted mechanism of IDI: Design of the experiment.* To distinguish between step-wise and concerted mechanisms for isomerization of IPP to DMAPP, we designed a time-course experiment where isomerization of IPP to DMAPP by IDI was coupled to alkylation of tryptophan by DMAPP with dimethylallyltryptophan (4-DMAT) synthase under conditions where newly synthesized DMAPP that had been released from IDI was removed from the system and could not return to IPP. The coupled assay was run in $D_2O$ where a deuterium was added to C4 of IPP during the isomerization (Scheme 4.2).

IPP was incubated with *S. pneumoniae* IDI-2 or *E. Coli* IDI-1 and *Claviceps purpurea* 4-DMAT synthase. The [Trp] was 5-fold greater that the [IPP] and the specific activity of DMAT synthase activity was 40 times greater than that of IDI-1 and 1000 times than IDI-2. All of the buffer reagents, substrates and proteins were thoroughly exchanged with deuterium by repeated lyophilization and the reactions were initiated by the addition of IDI. As the reaction proceeded, samples were removed, the enzymes were

immediately separated from small molecules by ultrafiltration. The reactants and substrates were purified by HPLC and analyzed by positive ion mass spectrometry (MS). For both IDI isozymes, the final product, 4-DMAT, contained one, two, and ultimately three deuterium atoms from DMAPP during the course of the incubation (Figures 4.3 and 4.4). The $^{13}C$ isotope peaks in unlabeled DMAT for M+1 (~20 % of M) and M+2 (2 % of M) agreed with theoretical values. The intensities of the M+1 and M+2 peaks were greater that the $^{13}C$ background and there was no background at M+3, reflecting incorporation of additional deuterium atoms into the DMAPP during isomerization. In control experiments for both isoforms where unlabeled DMAPP replaced IPP, no deuterium was incorporated into DMAT, indicating that DMAPP was efficiently trapped without isomerizing to IPP even under conditions were the initial concentration of DMAPP was substantially higher than DMAPP was formed from IPP (Figures 4.5 and 4.6). In the control assay with DMAPP, the observed M+1 peak was ~20% of M and M+2 is of ~2% of M and are similar to the unlabeled DMAT standard. Time courses for incorporation of IPP into DMAT via DMAPP for IDI-1 and IDI-2 are shown in the Figure 4.7. The ratios of $d_1$, $d_2$, and $d_3$ DMAT at each point in the time course for the isozymes are given in Tables 4.1 – 4.8, respectively.

The relative ratios of $d_2$, $d_3$-DMAPP (or $d_2$, $d_3$-DMAT) in IDI-2 catalyzed reactions are much higher than the IDI-1 catalyzed reactions indicating more deuterium incorporation in to the product DMAPP and eventually into DMAT (Table 4.1 – 4.8). Lower deuterium incorporation in IDI-1 conversion could be due to lower rates of enzymatic release of the product DMAPP as reported by Richard and coworkers.

IPP was also isolated and analyzed by negative ion mass spectrometry at each of

the above time points for IDI-1 and IDI-2. Since IPP elutes in the void volume of the phenyl column used in the LCMS analysis of DMAT (Figures 4.8 – 4.10), the void volumes were collected, lyophilized, and analyzed by LCMS on a phenyl column. Along with unlabeled IPP, the $d_1$, $d_2$, $d_3$ isotopomers of IPP were detected at each point in the time course (Figures 4.8 and 4.9). The relative amounts of $d_1$, $d_2$, $d_3$-IPP increased as the reactions proceeded (Tables 4.9 – 4.15). The presence of deuterium in IPP under conditions where free DMAPP is trapped by DMAT synthase unambiguously demonstrates that a portion of newly bound IPP is protonated (deuterated) and ultimately released as IPP before being released as DMAPP.

The isomerization reactions of IDI-1 and IDI-2 are highly stereoselective for protonation/deprotonation at C2 and C4 of IPP and DMAPP.[65,78] The $d_1$ and $d_2$ isotopomers of IPP can be explained by incorporation of deuterium as C4. However, $d_3$-IPP, especially at the relatively high percentages found in the time course experiments, is predominantly [C2-$^2H_2$, C4-$^2$H]IPP and the $d_2$-isotopomer is a mixture of [C2-$^2H_2$]IPP and [C2-$^2$H, C4-$^2$H]IPP isomers.

## Discussion

The design of the deuterium incorporation experiment prevents DMAPP newly released from the active site of IDI from being isomerized back to IPP. Inspection of the reactions involved in transformation of IPP to DMAPP shown in Scheme 4.3 shows a potential difference in the pattern of deuterium incorporation into unbound IPP during the time course of the reaction depending on whether the mechanism is concerted or step-wise.

In a concerted mechanism, enzyme bound unlabeled IPP is converted into enzyme bound $d_1$-DMAPP labeled at C4, which can be released and trapped as DMAT or isomerized to IPP. If the proton removed from C2 during isomerization protonates C2 in the reverse reaction, $d_1$-IPP will be formed. However, if the proton exchanges with deuterium before protonation, $d_2$-IPP will be generated. In a stepwise mechanism, the initially formed species is the tertiary carbocation labeled at C4. This species can partition to DMAPP by elimination of a proton from C2 or to IPP by elimination of a proton/deuterium from C4. The lifetime of the tertiary carbocation (estimated at ~10 ns)[176] is sufficiently long for the deuterium atom at C4 to scramble with the two hydrogen atoms in the newly formed methyl group by rotation about the C3-C4 bond. The primary isotope effect $k_H/k_D \sim 6$[177] for removing hydrogen versus deuterium from C4 will result in a ~12-fold selectivity for removal of one of the two C4 hydrogens over the deuterium. In this case, $d_1$-IPP is formed directly from the carbocationic intermediate. In addition, enzyme bound $d_1$-DMAPP can revert to IPP to generate $d_1$- or $d_2$-IPP as described for the concerted mechanism. These possibilities are illustrated in Scheme 4.3.

IPP, deuterated IPP, and DMAPP shown above could be formed from either the concerted mechanism (Scheme 4.3A) or the step-wise mechanism through a $3^o$ carbocationic intermediate (Scheme 4.3B) generated upon "$D^+$" addition to IPP as outlined above. There is a possibility that the trace amounts of "$H^+$" leak from the C2 or C4 hydrogens in IPP/DMAPP during the isomerization to the active site residues in IDI-1 and IDI-2 in the enzyme assays, and therefore increases unlabeled or labeled IPP and DMAPP peak ratios in the time-course of the reactions analyzed by mass spectrometry. Poulter and coworkers reported that *Saccharomyces cerevisiae* IDI-1 catalyzes the

IPP/DMAPP isomerization in a less stereoselective manner.[65] Upon extended periods of incubation of IDI-1 isomerization of IPP in $D_2O$ all the hydrogens in IPP are exchanged with deuterium except those at C1. Two percent of the time IPP undergoes deuteration from solvent $D_2O$ at *Z*-methyl group (C5 methyl hydrogens in IPP) and one half percent of the time it undergoes deuteration at pro-*R* C2-hydrogen of IPP. Similar behavior was not observed for *E. Coli* IDI-1 even upon extended periods of incubation of IPP. The rate constants in Scheme 4.4 accounts for a statistical factor associated with the number of hydrogens and deuteriums that are present at C4 position in the $3^o$ carbocationic intermediate.

Unlike IDI-1, the mechanism of IDI-2 catalyzed IPP and DMAPP is highly stereoselective. Barkley et. al. observed that only the C-4 methylene hydrogens and the pro-*R* C2-hydrogen were exchanged when IDI-2 reaction catalyzed IPP isomerization was incubated in $D_2O$.[78] Even upon extended incubations of IDI-2 in $D_2O$, there was no deuterium at any other locations other than C2 and C4 of IPP and DMAPP. Similar to IDI-1, IDI-2 also generated $d_1, d_2, d_3$-IPP, and $d_1, d_2, d_3$-DMAPP although the ratios of $d_2,d_3$-DMAPP in IDI-2 are much higher than IDI-1.

Identification of $d_1$, $d_2$, and $d_3$-DMAPP (which are converted into $d_1$, $d_2$, $d_3$-DMAT using a 4-DMATS coupling enzyme) along with IPP, $d_1$, $d_2$, and $d_3$-IPP in the reaction time-courses for both IDI-1 and IDI-2 strongly suggests that both enzymes catalyze the reaction via a step-wise mechanism shown in Scheme 4.3B through the formation of $3^o$ carbocationic intermediate. As predicted for the step-wise mechanism, all the hydrogens on the C4 of IPP and DMAPP are completely exchanged with deuterium. Moreover, IDI-1 and IDI-2 differ significantly in terms of the $d_1$:$d_2$-IPP ratios in the time-

course analysis of IPP isomerization that we developed (Table 4.16). At the early stages of the IDI-1 reaction (0.5 hours) the $d_1$:$d_2$-IPP ratio was found to be ~ 0.48:52. The $d_1$ and $d_2$-IPP ratios will be governed by the 3$^o$ carbocation that is created by the addition of "$D^+$" to C4 of IPP [C4-$^2$H]IPP that has preferential selectivity towards eliminating a proton than a deuterium on $CH_2D$ methyl group of C4 and the KIE estimated for this process to be < 5. On the other hand, the $d_1$:$d_2$-IPP ratio was found to be ~ 0.12:0.88 for the IDI-2 reaction at 1 h and has the estimated KIE of ~ 5 for the similar 3$^o$ carbocation. The $d_1$:$d_2$-IPP ratios were almost identical (1:1) in IDI-1 and significantly different (1:8) in IDI-2 at the early stages of the reaction. $d_1$-IPP is unlikely to be formed by a concerted process (Scheme 4.3A) since it requires the deuterium on C4 to be eliminated when the addition of "$D^+$" to $d_1$-DMAPP that generates $d_1$-IPP. The significant amounts of $d_1$-IPP at the early stages of IDI-1 and IDI-2 reactions indicate a step-wise mechanism for both enzymes. Additionally, if the mechanism is concerted, the $d_1$:$d_2$-IPP ratios for both IDI-1 and IDI-2 should be relatively constant during the time-course of the assays although the individual concentrations of $d_1$:$d_2$-IPP differ. We did not observe constant ratios of $d_1$:$d_2$-IPP in our time-course analysis of IPP isomerization by IDI-1 and IDI-2 further suggesting concerted mechanism is not likely.

Richard and coworkers undertook NMR studies of IDI-1 catalyzed IPP isomerization in $D_2O$ and found that the product after the first catalytic cycle ($d_1$-DMAPP) is not released but rather undergoes additional rounds of catalysis to generate $d_1$-IPP and $d_2$-DMAPP before being released from the active site of the enzyme.[70] Support for this observation came from that both $d_1$-IPP (the product after two catalytic cycles) and $d_1$-DMAPP (the product after first catalytic cycle) forms with the same

reaction velocity and the ratios of these products are constant at the early stages of the reaction. This result indicates that the release of $d_1$-DMAPP is slower than its conversion to $d_1$-IPP and based on these results they propose that the product release is the rate-determining step of the IDI-1 catalysis. We also observed similar trend that the product after first catalytic cycle ($d_1$-DMAPP) undergoes multiple catalytic turnovers to produce $d_2$-DMAPP and $d_3$-DMAPP simultaneously before finally being released from the enzyme for both IDI-1 and IDI-2.

Altogether, the data presented above strongly supports the step-wise mechanism going through a $3^o$ carbocationic intermediate of the IPP and DMAPP isomerization catalyzed by both IDI-1 and IDI-2.

## Conclusions

In summary, we obtained the evidence for the tertiary ($3^o$) carbocationic intermediate for the IPP and DMAPP isomerization catalyzed by both IDI-1 and IDI-2 and the reaction proceed through step-wise mechanism. Both enzymes IDI-1 and IDI-2 are identical in terms of number of deuteriums incorporation into the substrate and product except that the relative deuterium content of $d_2$, $d_3$-IPP and DMAPP is higher for IDI-2. We did not observe reverse reaction of DMAPP isomerization into IPP in our control assays with DMAPP at the mentioned reaction conditions. IDI-1 from *Saccharomyces cerevisiae* reported to incorporate solvent deuterium into all the carbons in IPP except C1,[65] we did not see similar trend with *E. coli* IDI-1 indicating *E. coli* IDI-1 is much more stereoselective in catalysis. The rate constants for the formation of $d_1$, $d_2$, $d_3$-IPP and DMAPP from unlabeled IPP (Schemes 4.3B) as shown for step-wise mechanism

could be obtained by fitting the above experimental data in Tables 4.1 – 4.15 to the kinetic modeling software (KinTek) and this study is currently is in progress. Taken together, IDI preferentially catalyze IPP/DMAPP isomerization through the generation of a $3^{o}$ carbocationic intermediate. The preference for the carbocation probably derives from the large net stabilization energy gained through electrostatic and other noncovalent interactions between the carbocation and the enzyme active site residues.

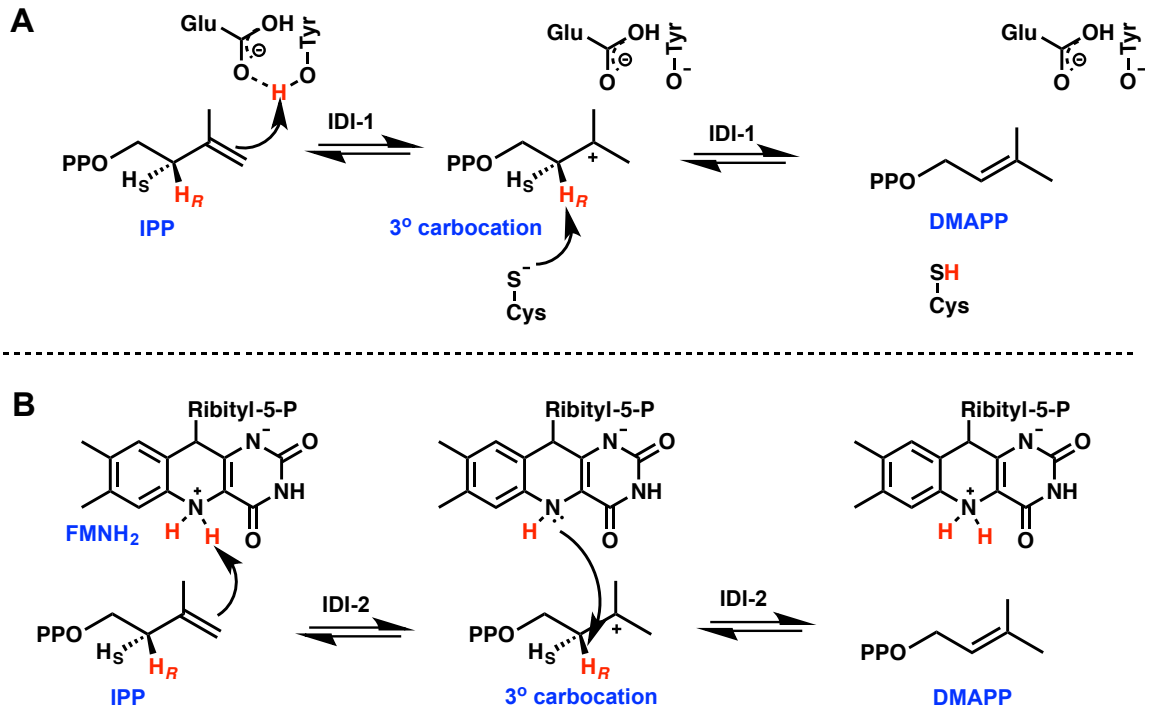


**Scheme 4.1.** IPP/DMAPP isomerization catalyzed by A) IDI-1 in an antarafacial B) IDI-2 in a suprafacial manner.

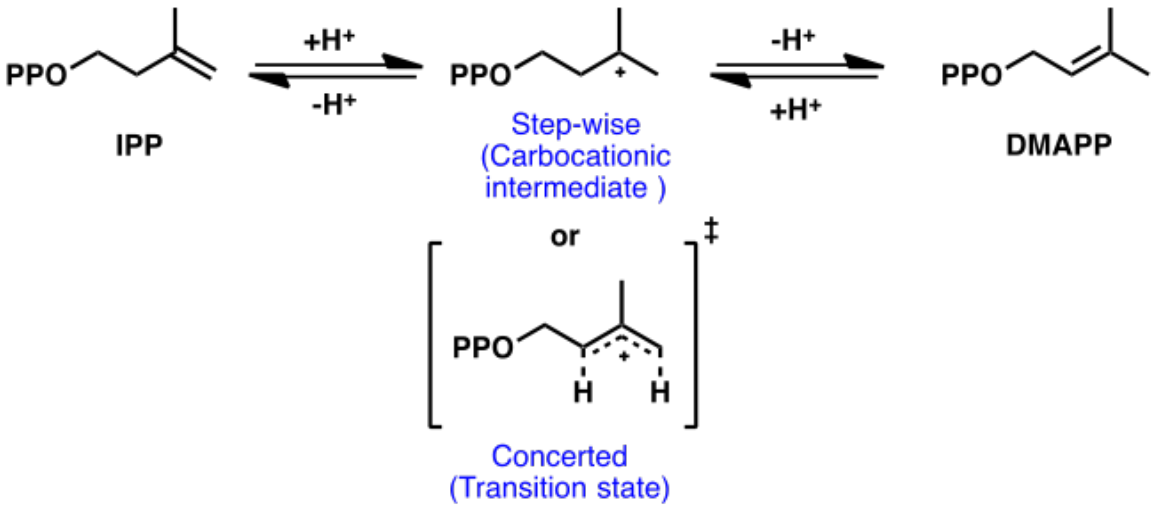


**Figure 4.1.** Step-wise versus concerted mechanisms of IDI-1 and IDI-2.

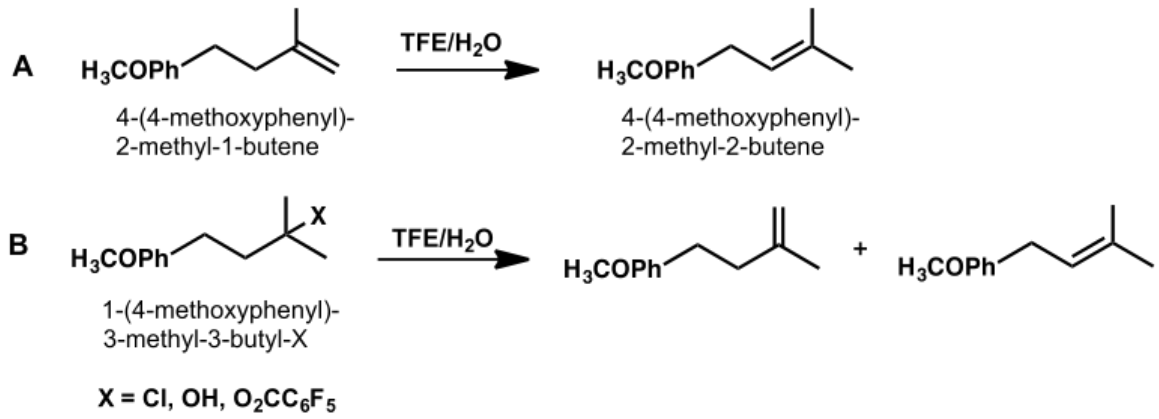


**Figure 4.2.** Nonenzymatic model studies of (A) isomerization and (B) elimination reactions.

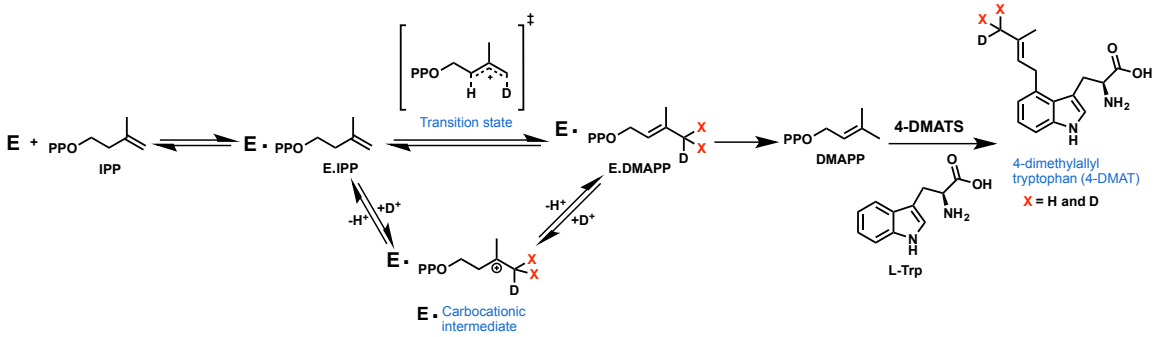


**Scheme 4.2.** IDI – 4-DMATS coupled assay.

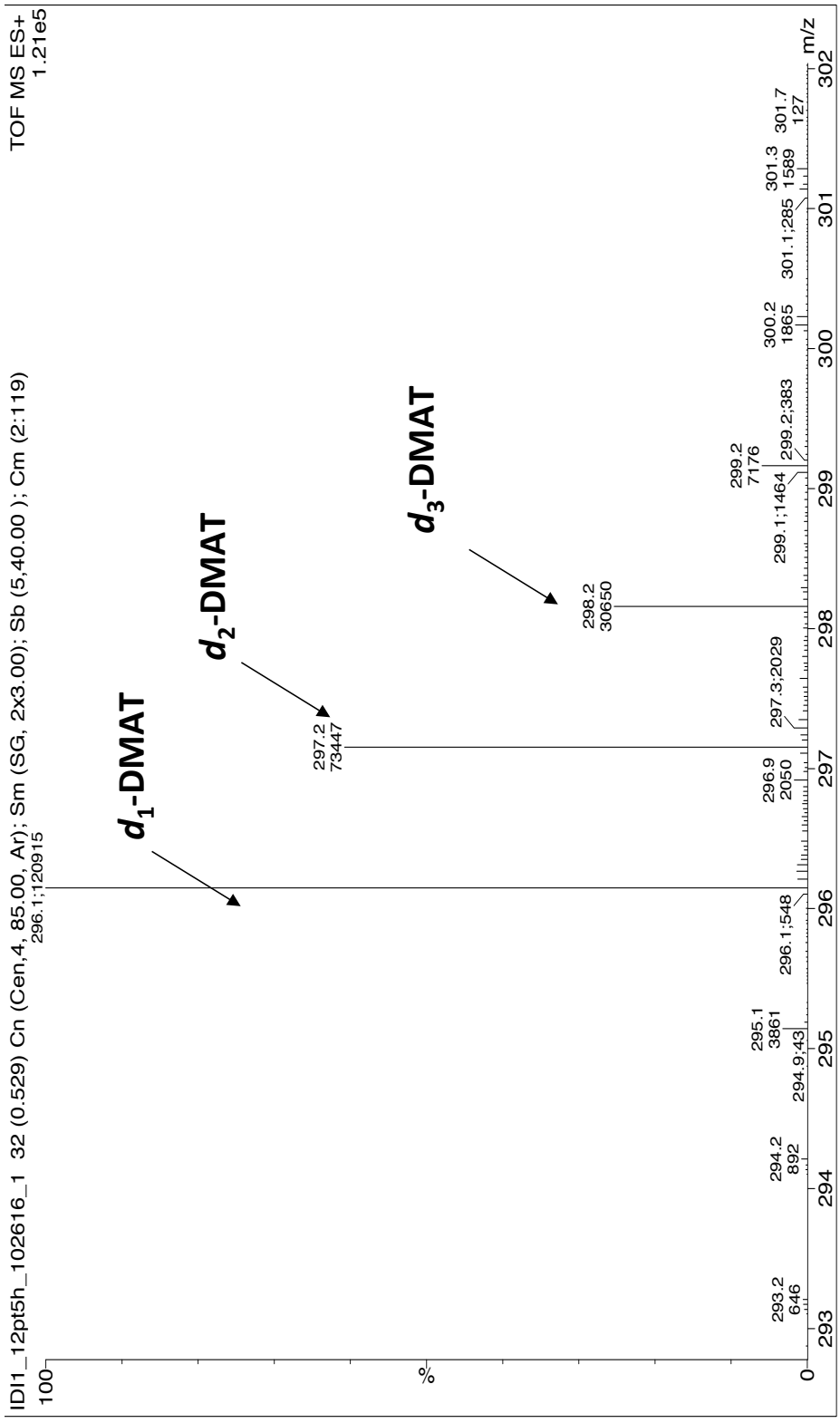


**Figure 4.3.** ESI$^+$-MS of *d*-DMAT products from IDI-1-4-DMATS coupled enzyme reaction.

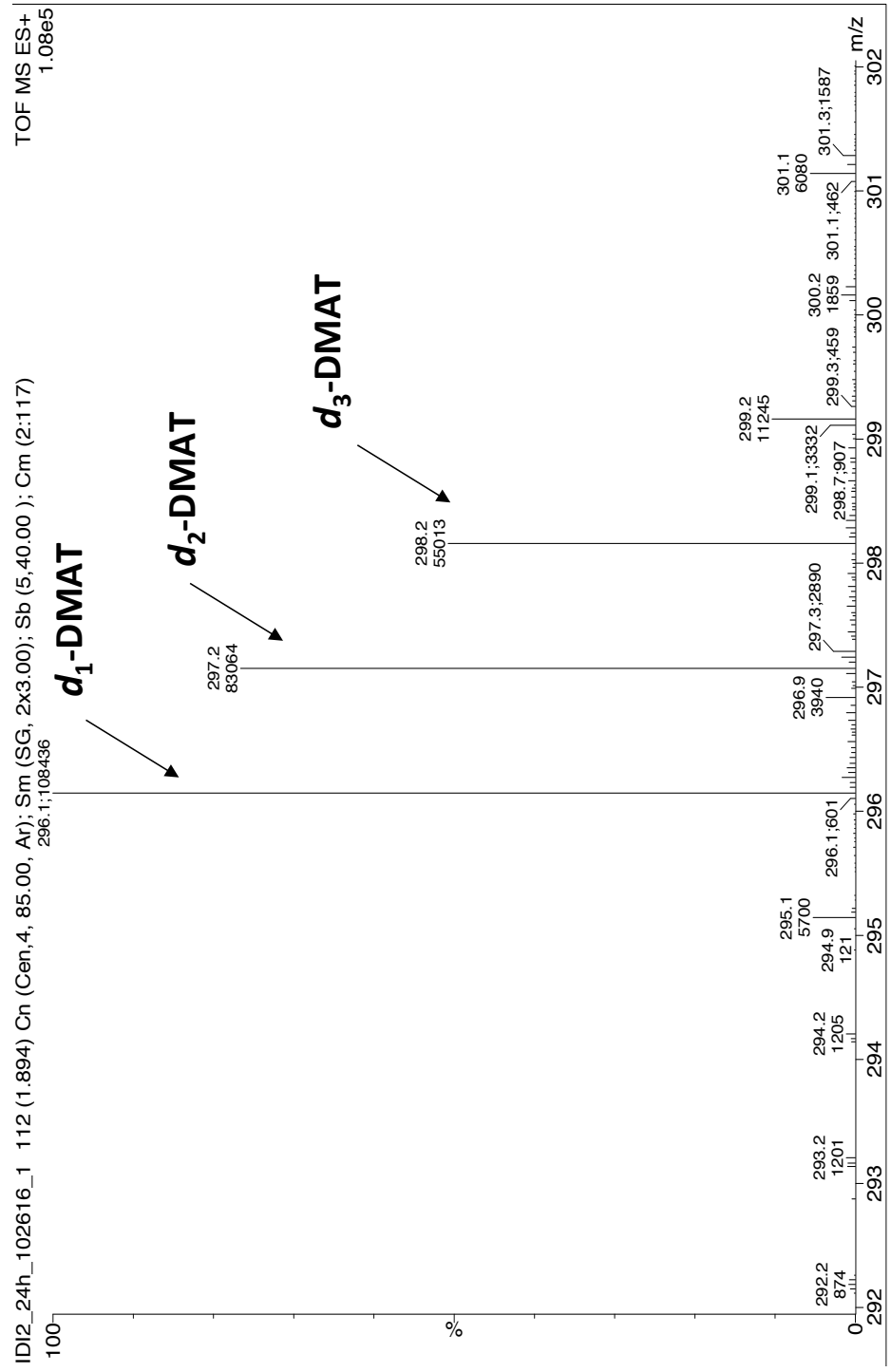


**Figure 4.4.** ESI$^+$-MS of *d*-DMAT products from IDI-1-4-DMATS coupled enzyme reaction.

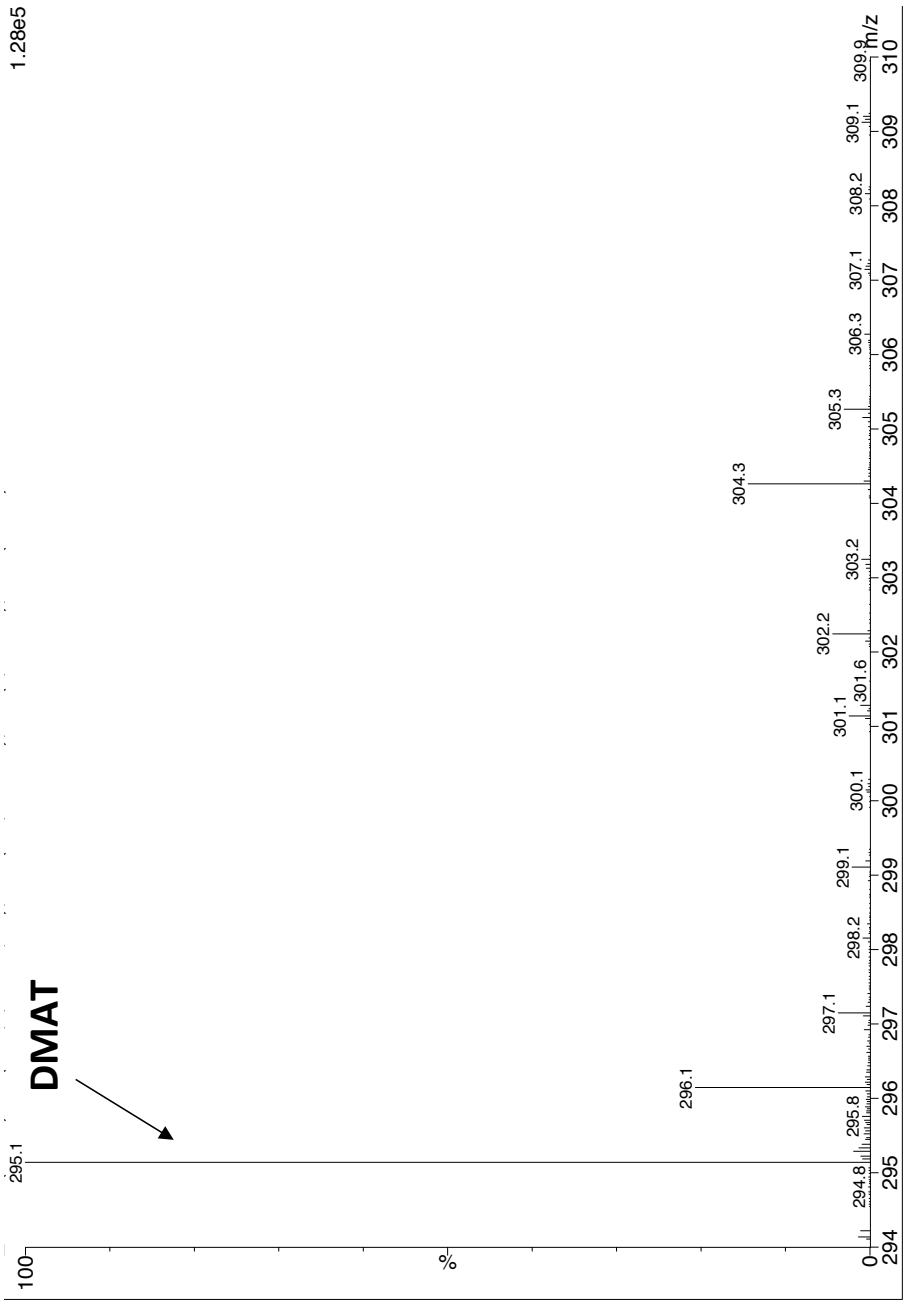


**Figure 4.5.** ESI$^+$-MS of *d*-DMAT products from IDI-1-4-DMATS coupled enzyme reaction.

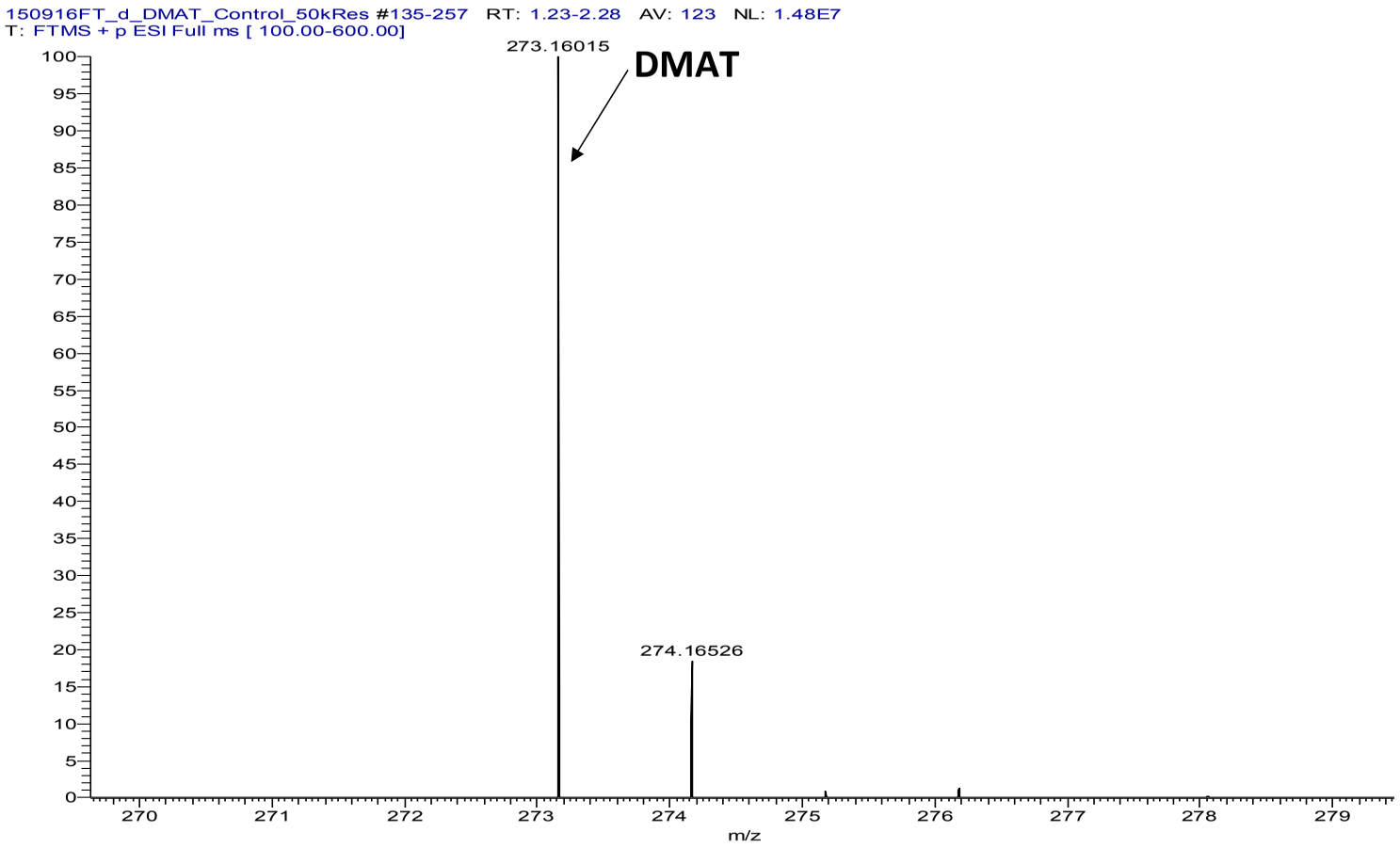


**Figure 4.6.** $ESI^{+}$-MS of *d*-DMAT products from IDI-2-4-DMATS coupled enzyme reaction.

A

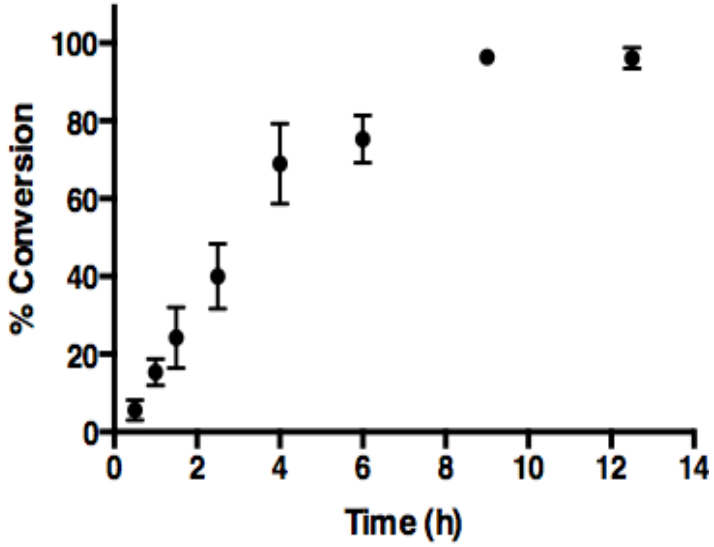


B

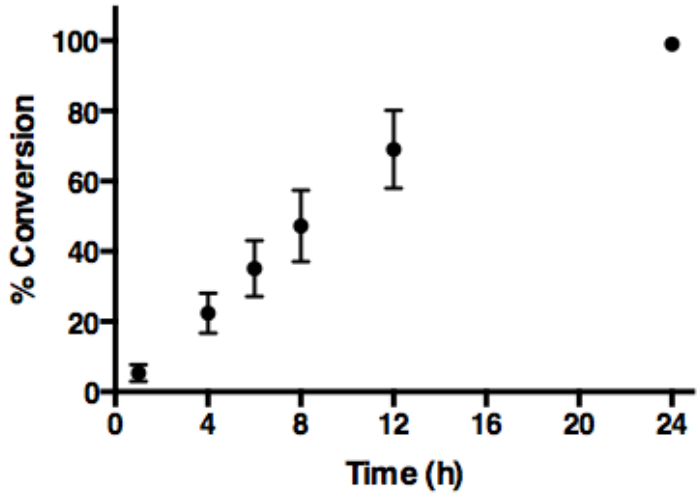


**Figure 4.7.** Time versus percent IPP conversion of A) IDI-1 B) IDI-2.

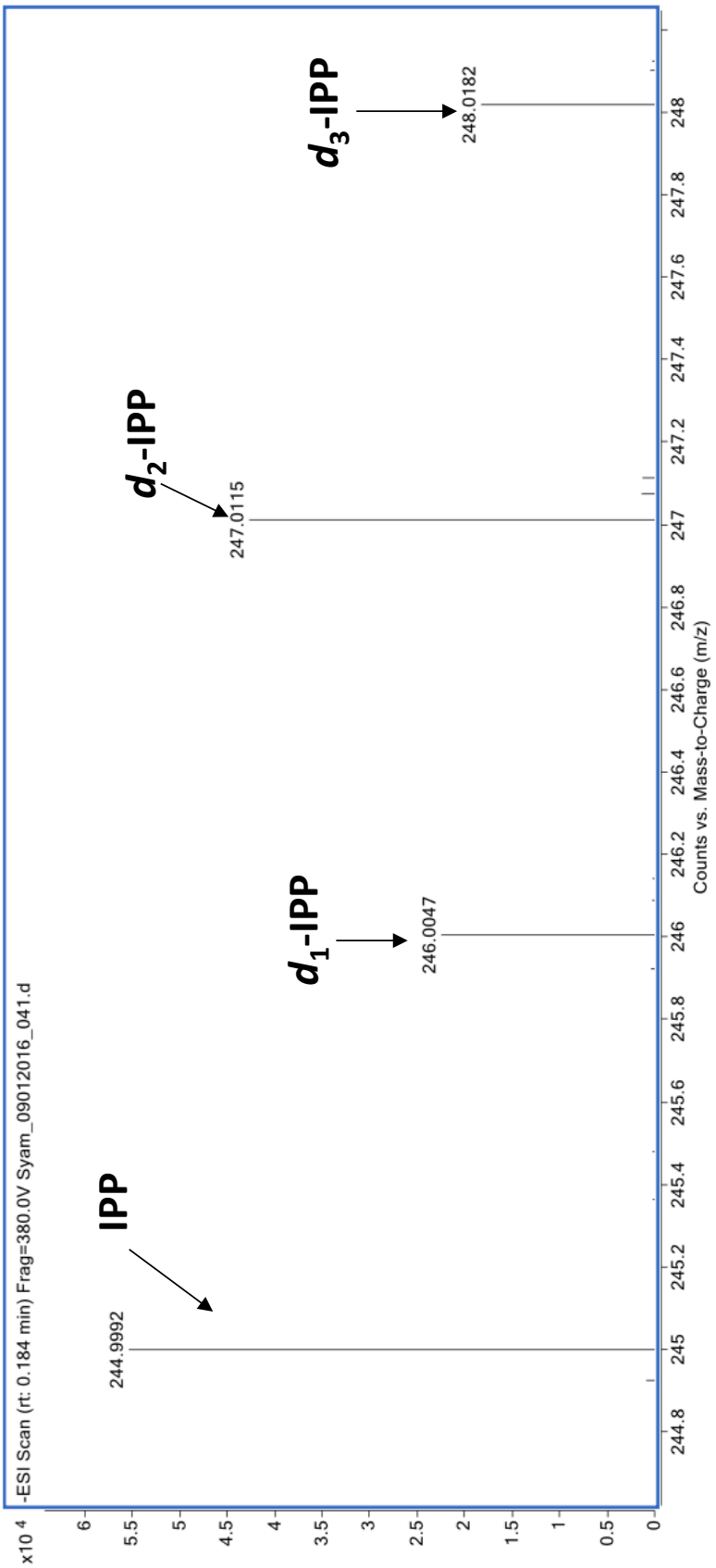


**Figure 4.8.** ESI-MS of *d*-IPP products from IDI-1-4-DMATS coupled enzyme reaction.

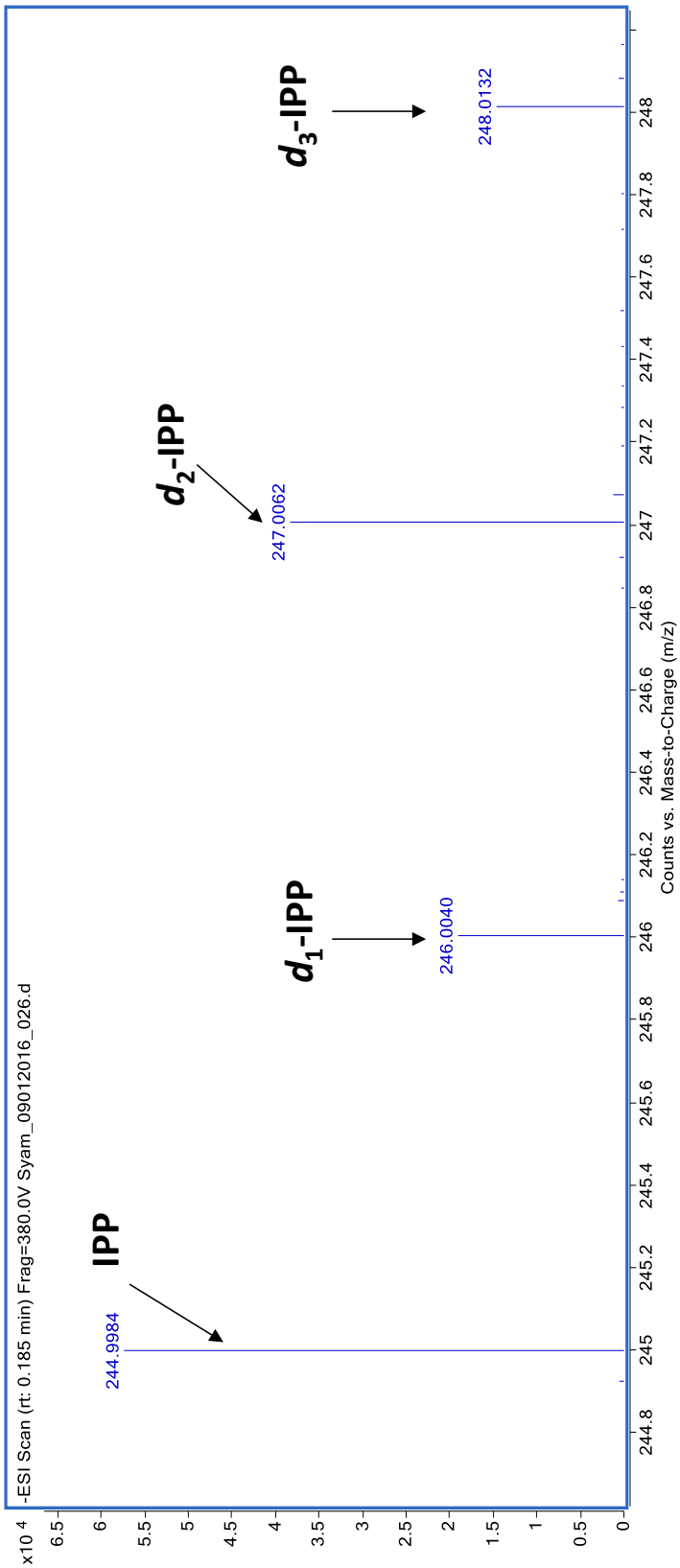


**Figure 4.9.** ESI$^-$-MS of *d*-IPP products from IDI-2-4-DMATS coupled enzyme reaction.

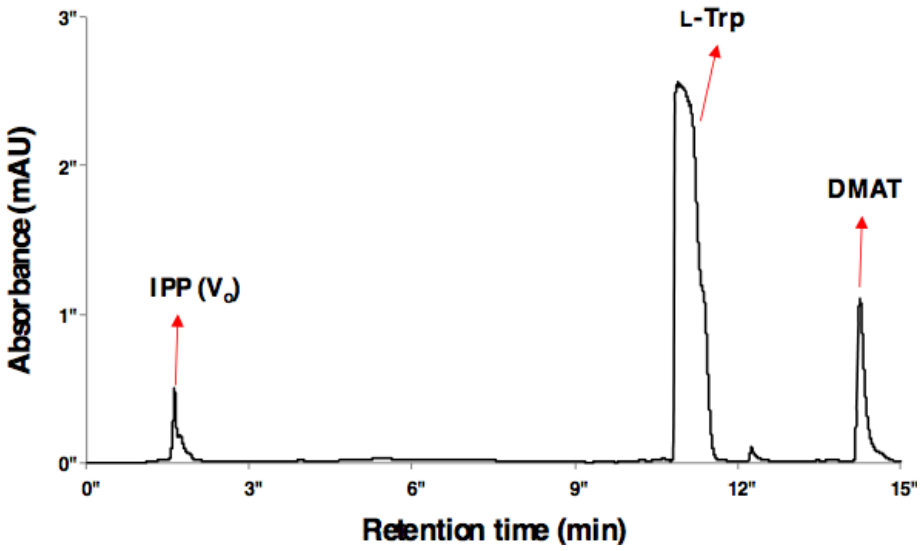


**Figure 4.10.** HPLC chromatogram of retention times (rt) of IPP ($V_o$), L-Trp and DMAT at $\lambda_{210}$ on a RP-Phenyl column. Unreacted L-Trp peak is also shown.

**Table 4.1.** Time-course analysis of DMAT by IDI-1 at 30 $^{o}$C (1$^{st}$ set).

| **Time (h)** | **Conversion (%)*** | **DMAT +Na$^{+}$ (Mole fraction)** | | |
|---|---|---|---|---|
| | | 296.1 ($d_1$) | 297.2 ($d_2$) | 298.2 ($d_3$) |
| 0.5 | 3 | 0.75 | 0.21 | 0.04 |
| 1.5 | 18 | 0.8 | 0.18 | 0.02 |
| 2.5 | 33 | 0.79 | 0.19 | 0.02 |
| 4 | 81 | 0.74 | 0.22 | 0.04 |
| 6 | 79 | 0.73 | 0.23 | 0.04 |
| 12.5 | 96 | 0.68 | 0.26 | 0.06 |

**Table 4.2.** Time-course analysis of DMAT by IDI-1 at 30 $^{o}$C (2$^{nd}$ set).

| Time (h) | Conversion (%)* | DMAT +$Na^+$ (Mole fraction) | | |
|---|---|---|---|---|
| | | 296.1 ($d_1$) | 297.2 ($d_2$) | 298.2 ($d_3$) |
| 0.5 | 9 | 0.74 | 0.22 | 0.04 |
| 1 | 18 | 0.78 | 0.2 | 0.03 |
| 1.5 | 33 | 0.75 | 0.21 | 0.04 |
| 2.5 | 49 | 0.76 | 0.21 | 0.03 |
| 4 | 66 | 0.74 | 0.22 | 0.04 |
| 6 | 68 | 0.7 | 0.25 | 0.05 |
| 12.5 | 94 | 0.64 | 0.27 | 0.09 |

**Table 4.3.** Time-course analysis of DMAT by IDI-1 at 30 $^{o}$C (3$^{rd}$ set).

| Time (h) | Conversion (%)* | DMAT +$Na^+$ (Mole fraction) | | |
|---|---|---|---|---|
| | | 296.1 ($d_1$) | 297.2 ($d_2$) | 298.2 ($d_3$) |
| 0.5 | 5 | 0.75 | 0.21 | 0.04 |
| 1 | 11 | 0.77 | 0.2 | 0.03 |
| 1.5 | 21 | 0.78 | 0.2 | 0.02 |
| 2.5 | 38 | 0.77 | 0.2 | 0.03 |
| 4 | 61 | 0.75 | 0.22 | 0.03 |
| 6 | 79 | 0.68 | 0.27 | 0.05 |
| 9 | 96 | 0.66 | 0.27 | 0.07 |
| 12.5 | 100 | 0.64 | 0.28 | 0.08 |

**Table 4.4.** Time-course analysis of DMAT by IDI-1 at 30 $^{o}$C (Average of 3 data sets).

| Time (h) | Conversion (%)* ± S. D | DMAT +$Na^+$ (Mole fraction) | | |
|---|---|---|---|---|
| | | 296.1 ($d_1$) | 297.2 ($d_2$) | 298.2 ($d_3$) |
| 0.5 | 6 ± 3 | 0.75 ± 0.01 | 0.21 ± 0.01 | 0.04 ± 0 |
| 1 | 15 ± 4 | 0.77 ± 0 | 0.2 ± 0 | 0.03 ± 0 |
| 1.5 | 24 ± 8 | 0.78 ± 0.02 | 0.19 ± 0.01 | 0.03 ± 0.01 |
| 2.5 | 40 ± 8 | 0.77 ± 0.01 | 0.2 ± 0.01 | 0.03 ± 0.01 |
| 4 | 69 ± 10 | 0.74 ± 0.01 | 0.22 ± 0 | 0.04 ± 0.01 |
| 6 | 75 ± 6 | 0.71 ± 0.03 | 0.25 ± 0.02 | 0.04 ± 0.01 |
| 9 | 96 ± 0 | 0.66 ± 0 | 0.27 ± 0 | 0.07 ± 0 |
| 12.5 | 96 ± 3 | 0.65 ± 0.02 | 0.27 ± 0.01 | 0.08 ± 0.02 |

**Assay conditions:** 2 mM IPP, 12 mM L-Trp, 0.1 mg/mL BSA, 10 mM $MgCl_2$, 1 μM IDI-1, 40 μM 4-DMATS pD 7.8, 30 $^{o}$C, reaction volume 2.5 mL. *Conversions were quantified by RP-HPLC on a phenyl column. 9h is not average. S.D Standard Deviation.

**Table 4.5.** Time-course analysis of DMAT by IDI-2 at 30 $^{o}$C (1$^{st}$ set).

| Time (h) | Conversion (%)* | DMAT +$Na^+$ (Mole fraction) | | |
|---|---|---|---|---|
| | | 296.1 ($d_1$) | 297.2 ($d_2$) | 298.2 ($d_3$) |
| 1 | 6 | 0.68 | 0.24 | 0.08 |
| 4 | 25 | 0.67 | 0.25 | 0.08 |
| 8 | 51 | 0.63 | 0.28 | 0.09 |
| 12 | 70 | 0.59 | 0.29 | 0.12 |
| 24 | 100 | 0.49 | 0.3 | 0.21 |

**Table 4.6.** Time-course analysis of DMAT by IDI-2 at 30 °C (2nd set).

| Time (h) | Conversion (%)* | DMAT +Na+ (Mole fraction) | | |
|---|---|---|---|---|
| | | 296.1 ($d_1$) | 297.2 ($d_2$) | 298.2 ($d_3$) |
| 1 | 3 | 0.66 | 0.28 | 0.06 |
| 4 | 16 | 0.66 | 0.26 | 0.08 |
| 6 | 26 | 0.65 | 0.27 | 0.08 |
| 8 | 36 | 0.63 | 0.27 | 0.1 |
| 12 | 53 | 0.6 | 0.29 | 0.1 |
| 24 | 100 | 0.51 | 0.3 | 0.19 |

**Table 4.7.** Time-course analysis of DMAT by IDI-2 at 30 °C (3rd set).

| Time (h) | Conversion (%)* | DMAT +Na+ (Mole fraction) | | |
|---|---|---|---|---|
| | | 296.1 ($d_1$) | 297.2 ($d_2$) | 298.2 ($d_3$) |
| 1 | 7 | 0.69 | 0.25 | 0.06 |
| 4 | 27 | 0.67 | 0.26 | 0.07 |
| 6 | 37 | 0.65 | 0.27 | 0.08 |
| 6 | 42 | 0.65 | 0.27 | 0.08 |
| 8 | 55 | 0.63 | 0.27 | 0.1 |
| 12 | 76 | 0.59 | 0.29 | 0.12 |
| 12 | 77 | 0.59 | 0.29 | 0.12 |
| 24 | 100 | 0.51 | 0.31 | 0.18 |

**Table 4.8.** Time-course analysis of DMAT by IDI-2 at 30 $^{o}$C (Average of 3 data sets).

| Time (h) | Conversion (%)* ± S. D | DMAT +$Na^+$ (Mole fraction) | | |
|---|---|---|---|---|
| | | 296.1 ($d_1$) | 297.2 ($d_2$) | 298.2 ($d_3$) |
| 1 | 5 ± 2 | 0.68 ± 0.02 | 0.26 ± 0.02 | 0.06 ± 0.02 |
| 4 | 22 ± 6 | 0.67 ± 0 | 0.26 ± 0 | 0.07 ± 0 |
| 6 | 35 ±8 | 0.65 ± 0 | 0.27 ± 0 | 0.08 ± 0 |
| 8 | 47 ± 10 | 0.63 ± 0 | 0.28 ± 0 | 0.09 ± 0 |
| 12 | 69 ± 11 | 0.59 ± 0.01 | 0.29 ± 0 | 0.12 ± 0 |
| 24 | 100 ± 0 | 0.5 ± 0.05 | 0.31 ± 0.01 | 0.19 ± 0.05 |

**Assay conditions:** 2 mM IPP, 10 mM L-Trp, 0.5 mM FMN, 5 mM $Na_2S_2O_4$, 0.1 mg/mL BSA, 10 mM $MgCl_2$, 10 nM *sp*IDI-2, 10 µM 4-DMATS pD 7.8, 30 $^{o}$C, reaction volume 5.2 mL. *Conversions were quantified by RP-HPLC on a phenyl column. S.D Standard Deviation.

**Table 4.9.** Time-course analysis of IPP by IDI-1 at 30 $^{o}$C (1$^{st}$ set).

| Time (h) | Conversion (%)* | IPP-$H^-$ (Mole fraction) | | | |
|---|---|---|---|---|---|
| | | 245 ($d_0$) | 246 ($d_1$) | 247 ($d_2$) | 248 ($d_3$) |
| 0.5 | 9 | 0.91 | 0.04 (0.44) | 0.04 (0.44) | 0.01 (0.12) |
| 1 | 18 | 0.9 | 0.03 (0.26) | 0.06 (0.56) | 0.01 (0.18) |
| 1.5 | 33 | 0.85 | 0.05 (0.32) | 0.08 (0.52) | 0.02 (0.16) |
| 2.5 | 49 | 0.8 | 0.07 (0.36) | 0.11 (0.53) | 0.02 (0.11) |
| 4 | 66 | 0.65 | 0.1 (0.3) | 0.2 (0.56) | 0.05 (0.14) |
| 6 | 68 | 0.41 | 0.14 (0.25) | 0.31 (0.53) | 0.14 (0.22) |
| 12.5 | 94 | 0.47 | 0 | 0.44 (0.84) | 0.09 (0.16) |

**Table 4.10.** Time-course analysis of IPP by IDI-1 at 30 $^{o}$C (2$^{nd}$ set).

| **Time (h)** | **Conversion (%)*** | **IPP-H$^-$ (Mole fraction)** | | | |
|---|---|---|---|---|---|
| | | 245 ($d_0$) | 246 ($d_1$) | 247 ($d_2$) | 248 ($d_3$) |
| 0.5 | 5 | 0.96 | 0.01 (0.25) | 0.02 (0.5) | 0.01 (0.25) |
| 1 | 11 | 0.94 | 0.03 (0.5) | 0.02 (0.33) | 0.01 (.17) |
| 1.5 | 21 | 0.91 | 0.03 (0.33) | 0.05 (0.55) | 0.01 (0.12) |
| 2.5 | 38 | 0.81 | 0.07 (0.37) | 0.11(0.58) | 0.01 (0.05) |
| 4 | 61 | 0.66 | 0.09 (0.26) | 0.2 (0.59) | 0.05 (0.15) |
| 6 | 79 | 0.41 | 0.14 (0.23) | 0.31 (0.54) | 0.14 (0.23) |
| 9 | 96 | 0.23 | 0.12 (0.15) | 0.4 (0.52) | 0.25 (0.32) |
| 12.5 | 100 | 0.31 | 0.09 (0.13) | 0.35 (0.5) | 0.25 (0.36) |

**Table 4.11.** Time-course analysis of IPP by IDI-1 at 30 $^{o}$C (Average of 2 data sets).

| **Time (h)** | **Conversion (%)*** ± S. D | **IPP-H$^-$ (Mole fraction)** | | | |
|---|---|---|---|---|---|
| | | 245 ($d_0$) | 246 ($d_1$) | 247 ($d_2$) | 248 ($d_3$) |
| 0.5 | 7 ± 2 | 0.93 ± 0.03 | 0.03 ± 0.03 (0.42 ± 0.21) | 0.03 ± 0.01 (0.42 ± 0.1) | 0.01 ± 0 (0.16 ± 0.11) |
| 1 | 15 ± 4 | 0.92 ± 0.03 | 0.03 ± 0 (0.4 ± 0.2) | 0.04 ± 0.03 (0.45 ± 0.15) | 0.01 ± 0.01 (0.15 ± 0.05) |
| 1.5 | 27 ± 8 | 0.88 ± 0.04 | 0.04 ± 0.01 (0.33 ± 0.02) | 0.07 ± 0.02 (0.55 ± 0.03) | 0.01 ± 0.01 (0.12 ± 0.06) |
| 2.5 | 44 ± 8 | 0.8 ± 0.01 | 0.07 ± 0 (0.36 ± 0) | 0.11 ± 0 (0.54 ± 0.02) | 0.02 ± 0.01 (0.1 ± 0.02) |
| 4 | 64 ± 3 | 0.66 ± 0.01 | 0.11 ± 0.01 (0.28 ± 0.03) | 0.2 ± 0 (0.57 ± 0.02) | 0.05 ± 0 (0.15 ± 0.01) |
| 6 | 74 ± 7 | 0.41 ± 0 | 0.14 ± 0.01 (0.24 ± 0.01) | 0.31 ± 0 (0.54 ± 0) | 0.14 ± 0 (0.23 ± 0) |
| 9 | 96 ± 0 | 0.23 ± 0 | 0.12 ± 0 (0.16 ± 0) | 0.4 ± 0 (0.52 ± 0) | 0.25 ± 0 (0.32 ± 0) |
| 12.5 | 97 ± 5 | 0.39 ± 0.12 | 0.09 ± 0 (0.07 ± 0) | 0.39 ± 0.07 (0.67 ± 0.24) | 0.17 ± 0.12 (0.27 ± 0.14) |

**Assay conditions:** 2 mM IPP, 12 mM L-Trp, 0.1 mg/mL BSA, 10 mM $MgCl_2$, 1 μM IDI-1, 40 μM 4-DMATS pD 7.8, 30 $^{o}$C, reaction volume 2.5 mL. 9h is not average. *Conversions of IPP were quantified by RP-HPLC on a phenyl column. Data in parentheses indicates mole fraction of 246, 247, and 248 peaks only. S.D Standard Deviation.

**Table 4.12.** Time-course analysis of IPP by IDI-2 at 30 °C (1st set).

| Time (h) | Conversion (%)* | IPP-H⁻ (Mole fraction) | | | |
|---|---|---|---|---|---|
| | | 245 ($d_0$) | 246 ($d_1$) | 247 ($d_2$) | 248 ($d_3$) |
| 1 | 6 | 0.71 | 0.01 (0.04) | 0.27 (0.93) | 0.01 (0.03) |
| 4 | 25 | 0.35 | 0.02 (0.03) | 0.59 (0.9) | 0.05 (0.07) |
| 8 | 51 | 0.11 | 0.02 (0.02) | 0.76 (0.85) | 0.11 (0.13) |
| 12 | 70 | 0.45 | 0.14 (0.24) | 0.31 (0.56) | 0.11 (0.19) |
| 24 | 100 | 0.32 | 0.04 (0.05) | 0.59 (0.86) | 0.06 (0.09) |

**Table 4.13.** Time-course analysis of IPP by IDI-2 at 30 °C (2nd set).

| Time (h) | Conversion (%)* | IPP-H⁻ (Mole fraction) | | | |
|---|---|---|---|---|---|
| | | 245 ($d_0$) | 246 ($d_1$) | 247 ($d_2$) | 248 ($d_3$) |
| 1 | 3 | 0.88 | 0.03 (0.24) | 0.08 (0.7) | 0.01 (0.05) |
| 4 | 16 | 0.79 | 0.05 (0.22) | 0.15 (0.74) | 0.01 (0.04) |
| 6 | 26 | 0.76 | 0.06 (0.26) | 0.15 (0.62) | 0.03 (0.12) |
| 8 | 36 | 0.66 | 0.09 (0.26) | 0.2 (0.59) | 0.05 (0.16) |
| 12 | 53 | 0.17 | 0.03 (0.03) | 0.7 (0.84) | 0.11 (0.13) |
| 24 | 100 | 0.27 | 0.04 (0.06) | 0.62 (0.85) | 0.07 (0.09) |

**Table 4.14.** Time-course analysis of IPP by IDI-2 at 30 $^{o}$C (3$^{rd}$ set).

| **Time (h)** | **Conversion (%)*** | **IPP-H$^-$ (Mole fraction)** | | | |
|---|---|---|---|---|---|
| | | 245 ($d_0$) | 246 ($d_1$) | 247 ($d_2$) | 248 ($d_3$) |
| 1 | 7 | 0.82 | 0.01 (0.05) | 0.16 (0.9) | 0.01 (0.05) |
| 4 | 27 | 0.68 | 0.04 (0.13) | 0.26 (0.82) | 0.02 (0.06) |
| 6 | 37 | 0.58 | 0.06 (0.14) | 0.33 (0.78) | 0.04 (0.09) |
| 6 | 42 | 0.67 | 0.06 (0.19) | 0.24 (0.7) | 0.04 (0.12) |
| 8 | 55 | 0.4 | 0.05 (0.09) | 0.48 (0.8) | 0.07 (0.11) |
| 12 | 76 | 0.17 | 0.05 (0.07) | 0.64 (0.77) | 0.14 (0.16) |
| 12 | 77 | 0.1 | 0.04 (0.05) | 0.71 (0.77) | 0.16 (0.18) |
| 24 | 100 | 0.19 | 0.06 (0.08) | 0.64 (0.79) | 0.11 (0.13) |

**Table 4.15.** Time-course analysis of IPP by IDI-2 at 30 $^{o}$C (Average of 3 data sets).

| **Time (h)** | **Conversion (%)*** ± S. D | **IPP-H$^-$ (Mole fraction)** | | | |
|---|---|---|---|---|---|
| | | 245 ($d_0$) ± S.D | 246 ($d_1$) ± S.D | 247 ($d_2$) ± S.D | 248 ($d_3$) ± S.D |
| 1 | 5 ± 2 | 0.81 ± 0.09 | 0.02 ± 0.01 (0.11 ± 0.11) | 0.17 ± 0.09 (0.84 ± 12) | 0.01 ± 0 (0.04 ± 0.01) |
| 4 | 22 ± 6 | 0.74 ± 0.08 | 0.04 ± 0.01 (0.17 ± 0.07) | 0. 2 ± 0.08 (0.78 ± 0.06) | 0.01 ± 0.01 (0.05 ± 0.01) |
| 6 | 35 ± 8 | 0.67 ± 0.09 | 0.06 ± 0 (0.2 ± 0.06) | 0.24 ± 0.09 (0.7 ± 0.08) | 0.04 ± 0.01 (0.11 ± 0.02) |
| 8 | 47 ± 10 | 0.53 ± 0.19 | 0.07 ± 0.02 (0.17 ± 0.12) | 0.34 ± 0.2 (0.75 ± 0.14) | 0.06 ± 0.01 (0.13 ± 0.03) |
| 12 | 69 ± 11 | 0.15 ± 0.04 | 0.04 ± 0.01 (0.05 ± 0.02) | 0.68 ± 0.04 (0.79 ± 0.04) | 0.13 ± 0.03 (0.17 ± 0.03) |
| 24 | 100 ± 0 | 0.26 ± 0.07 | 0.05 ± 0.01 (0.06 ± 0.01) | 0.62 ± 0.03 (0.83 ± 0.04) | 0.08 ± 0.02 (0.1 ± 0.02) |

**Assay conditions:** 2 mM IPP, 10 mM L-Trp, 0.5 mM FMN, 5 mM $Na_2S_2O_4$, 0.1 mg/mL BSA, 10 mM $MgCl_2$, 10 nM *sp*IDI-2, 10 µM 4-DMATS pD 7.8, 30 $^{o}$C, reaction volume 5.2 mL. Data highlighted in red were not considered for average analysis. *Conversions of IPP were quantified by RP-HPLC on a phenyl column. Data in parentheses indicates mole fraction of 246, 247, and 248 peaks only. S.D Standard Deviation.

**Table 4.16.** Relative ratios of $d_1$ and $d_2$-IPP in IDI-1 and IDI-2 reactions.

| | **Conversion (%)** | **$d_1$-IPP (M.F)** | **$d_2$-IPP (M.F)** |
|---|---|---|---|
| **IDI-1** | 7 ± 2 | 0.48 | 0.52 |
| | 15 ± 4 | 0.43 | 0.57 |
| | 27 ± 8 | 0.38 | 0.62 |
| | 44 ± 8 | 0.40 | 0.60 |
| | 64 ± 3 | 0.33 | 0.67 |
| | 74 ± 7 | 0.31 | 0.69 |
| | 96 ± 0 | 0.23 | 0.77 |
| | 97 ± 5 | 0.19 | 0.81 |
| **IDI-2** | 5 ± 2 | 0.12 | 0.88 |
| | 22 ± 6 | 0.18 | 0.82 |
| | 35 ± 8 | 0.22 | 0.78 |
| | 47 ± 10 | 0.19 | 0.81 |
| | 69 ± 11 | 0.06 | 0.94 |
| | 100 ± 0 | 0.07 | 0.93 |

M. F. Mole Fraction

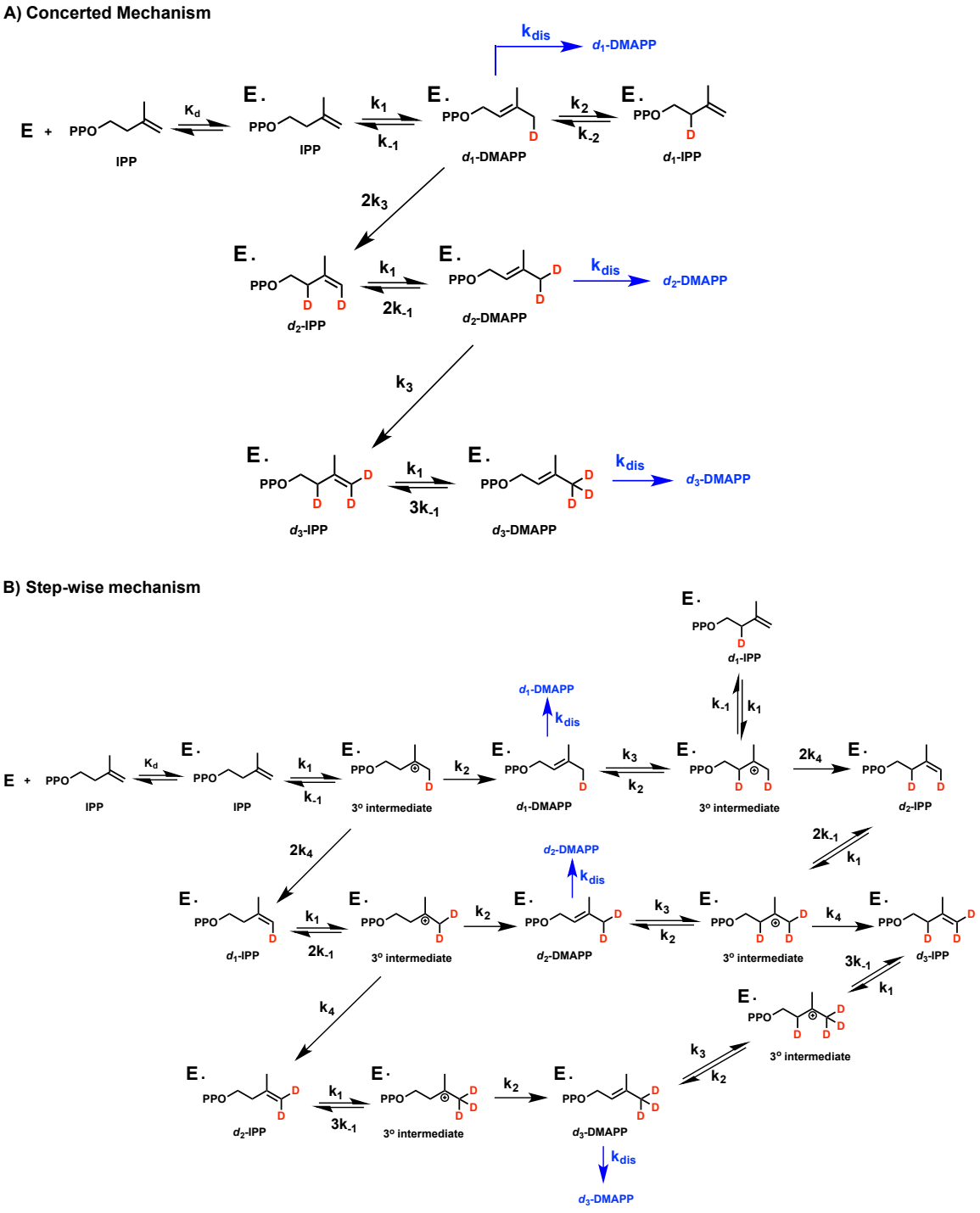


**Scheme 4.3.** Deuterium incorporation and partitioning of substrates and products in A) Concerted mechanism B) Step-wise mechanism of IDI.

# APPENDIX A

## NMR SPECTRAL DATA OF SYNTHETIC INTERMEDIATES AND FMN ISOTOPOLOGUES

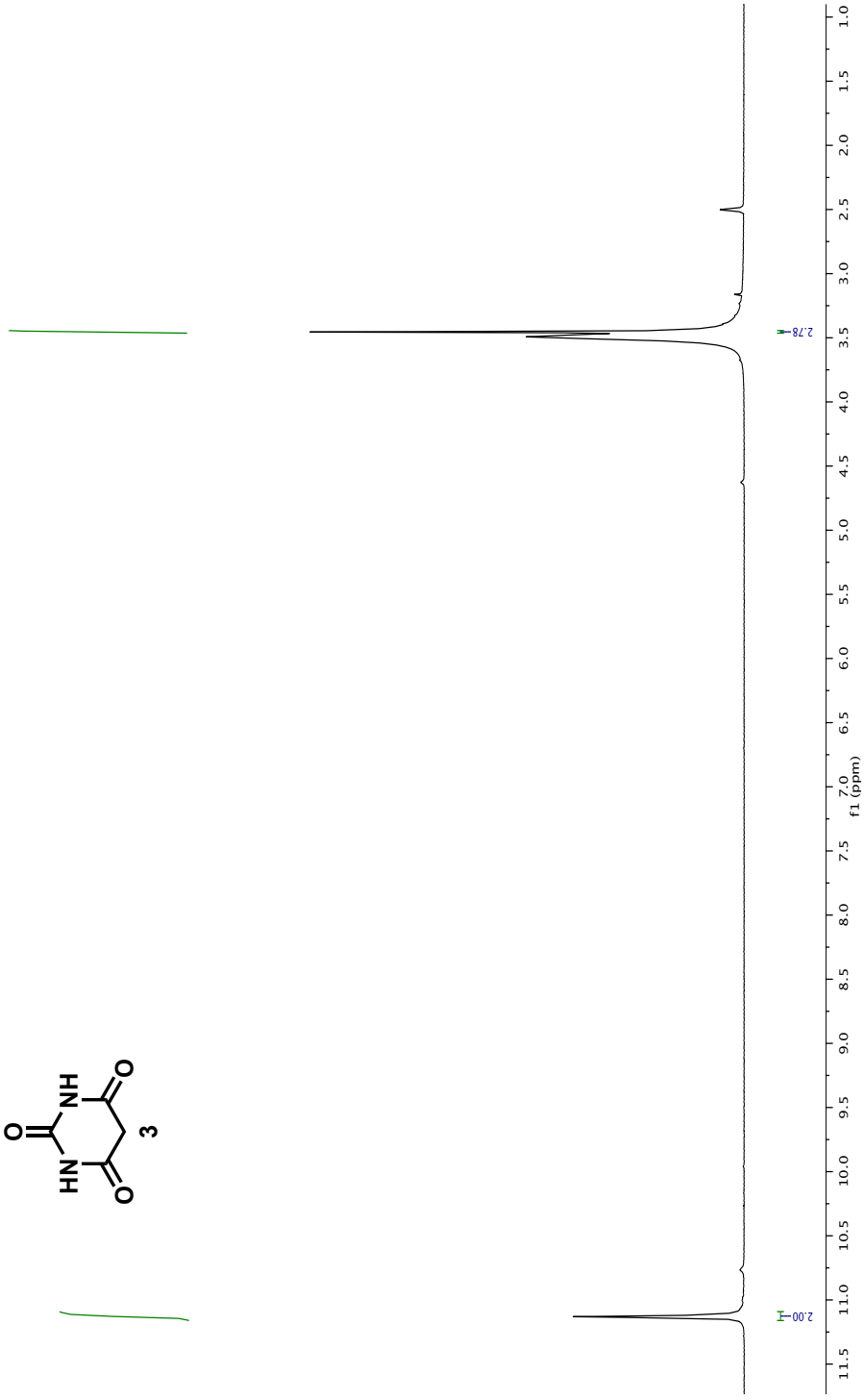


**Figure A.1** 300MHz $^{1}$H-NMR of barbituric acid **3** in $d_6$-DMSO.

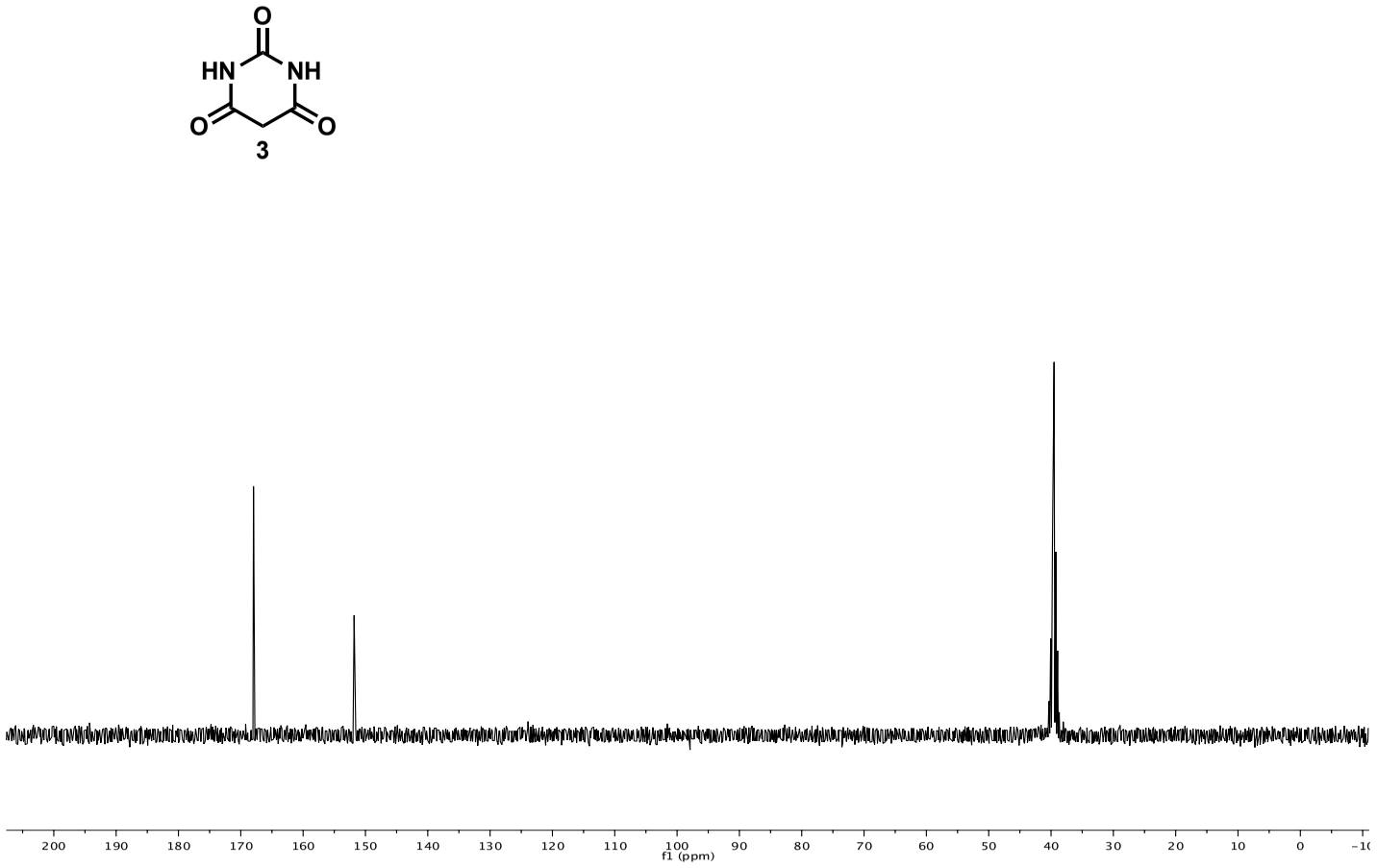


**Figure A.2** 75MHz $^{13}$C-NMR of barbituric acid **3** in $d_6$-DMSO.

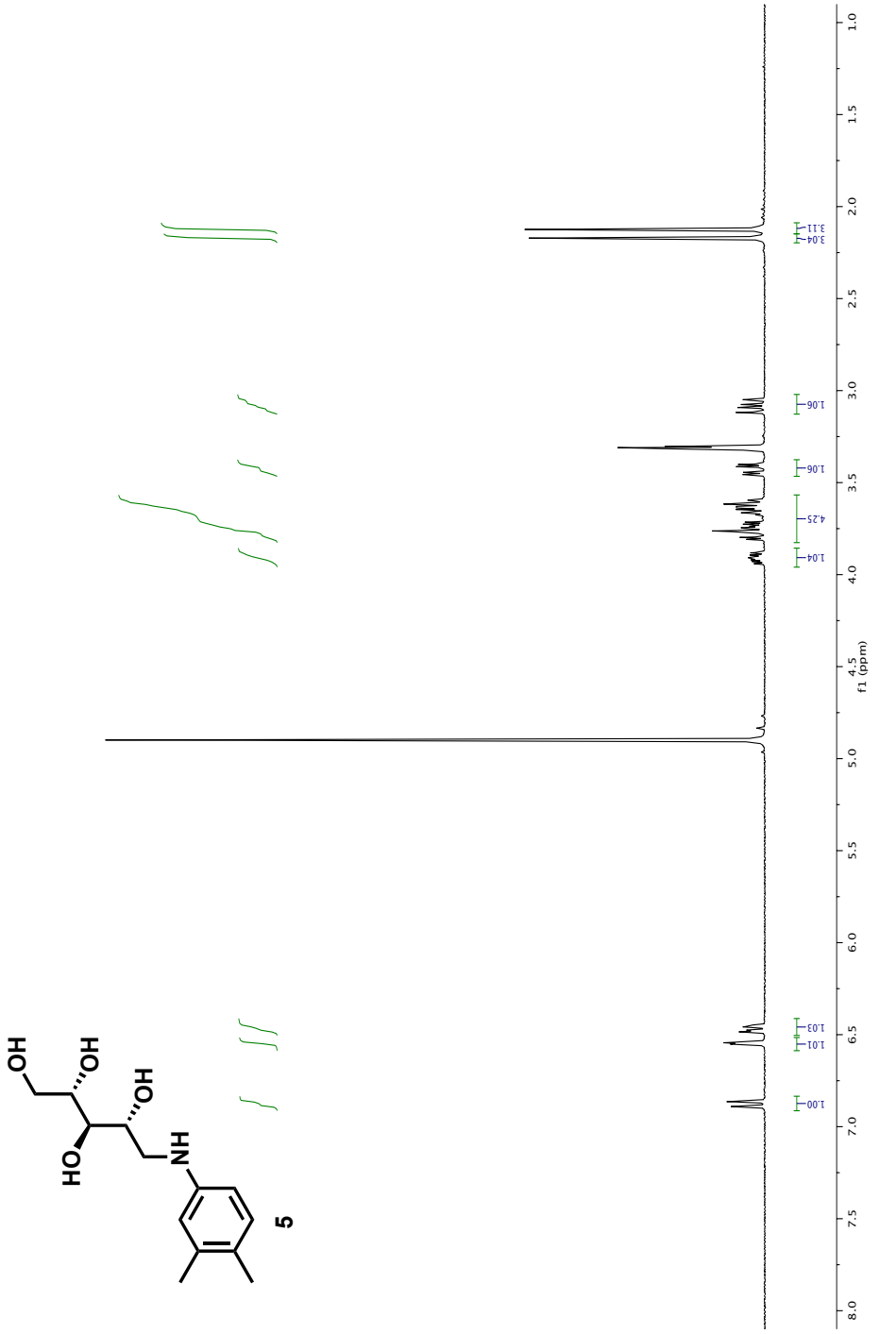


**Figure A.3** 300MHz $^{1}$H-NMR of *N*-ribityl 3,4-dimethyl aniline **5** in $CD_3OD$.

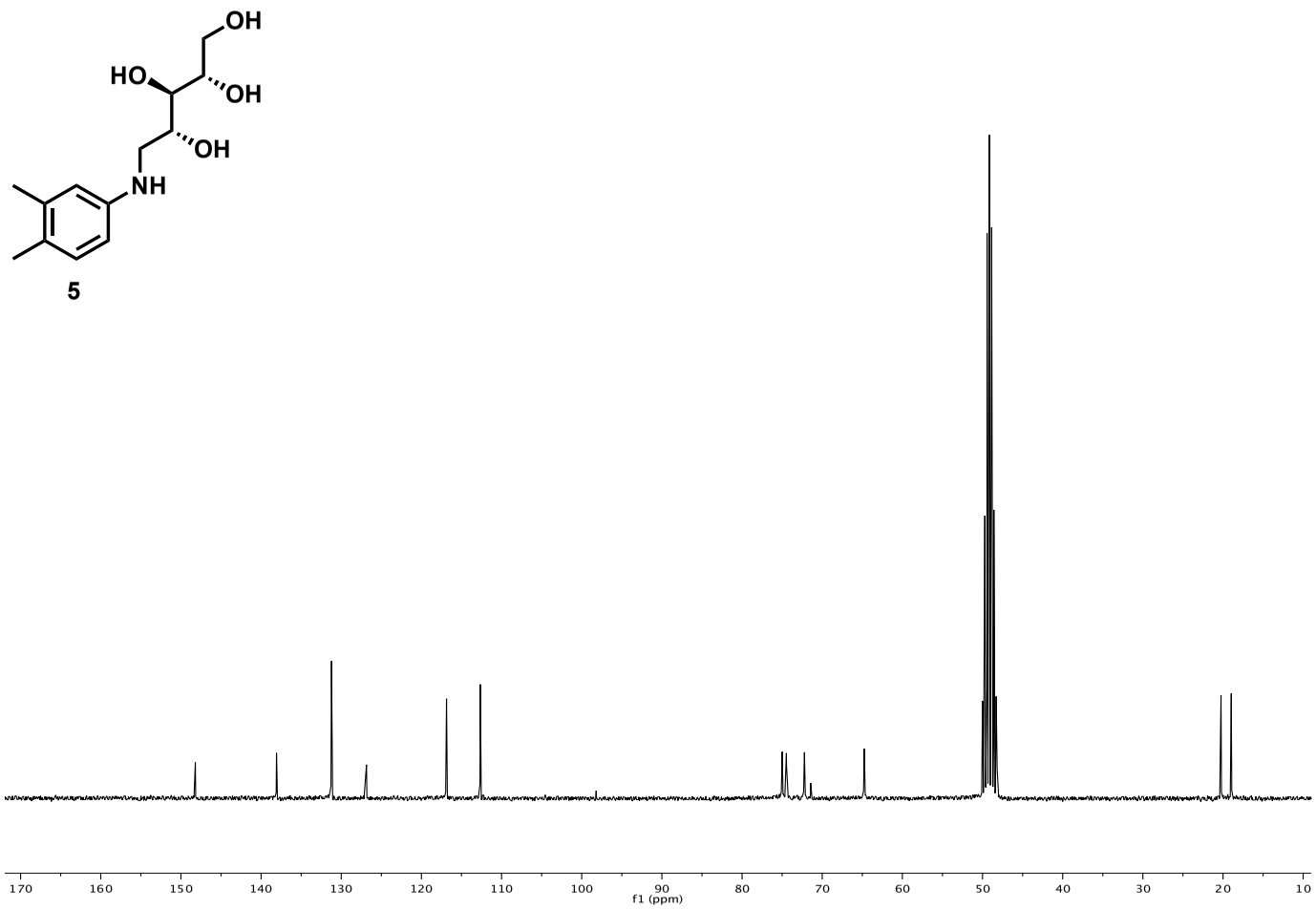


**Figure A.4** 75MHz $^{13}$C-NMR of *N*-ribityl 3,4-dimethyl aniline **5** in $CD_3OD$.

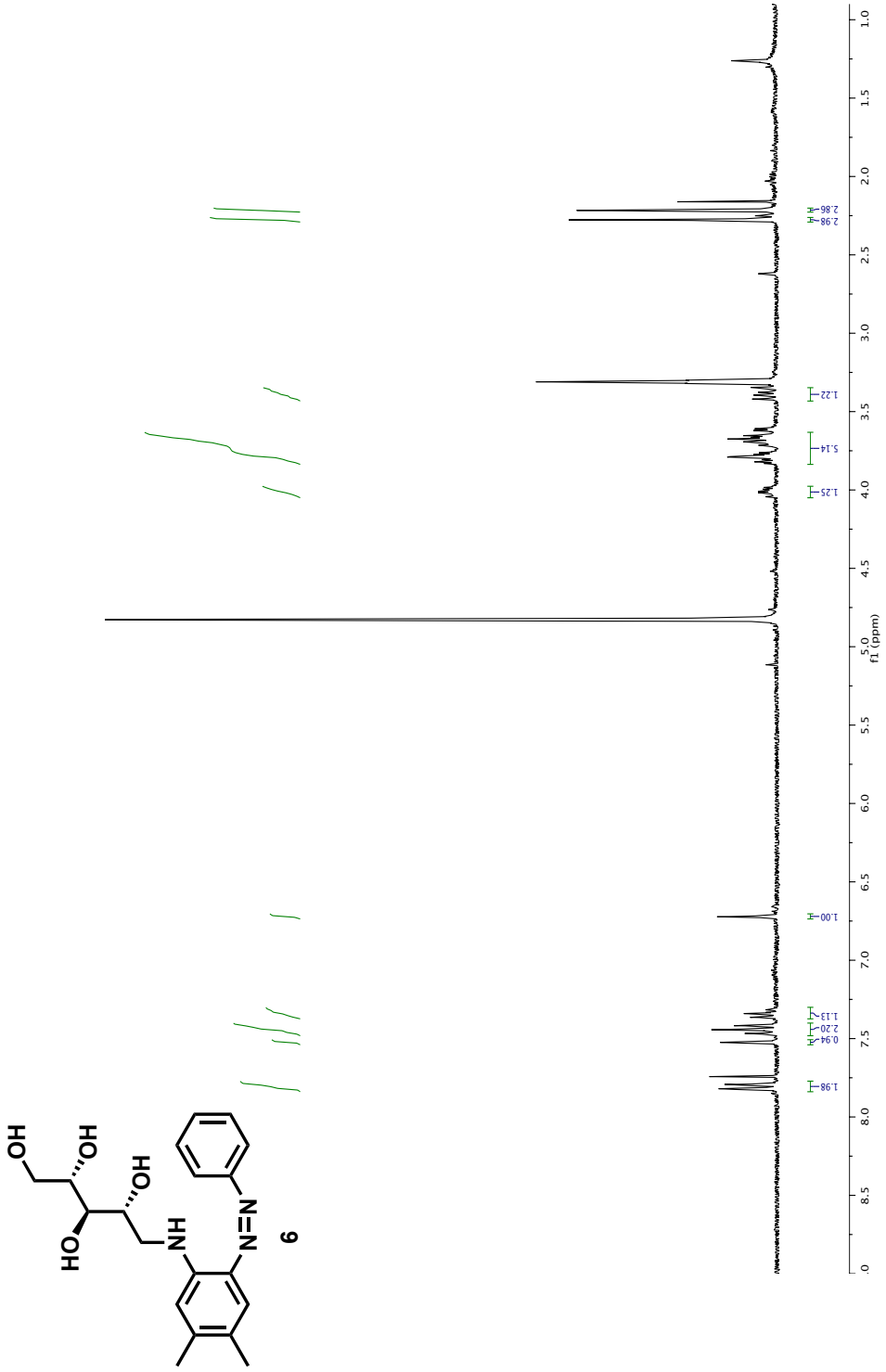


**Figure A.5** 300MHz $^{1}$H-NMR of *N*-ribityl-2-pheylazo-4,5-dimethyl aniline **6** in $CD_3OD$.

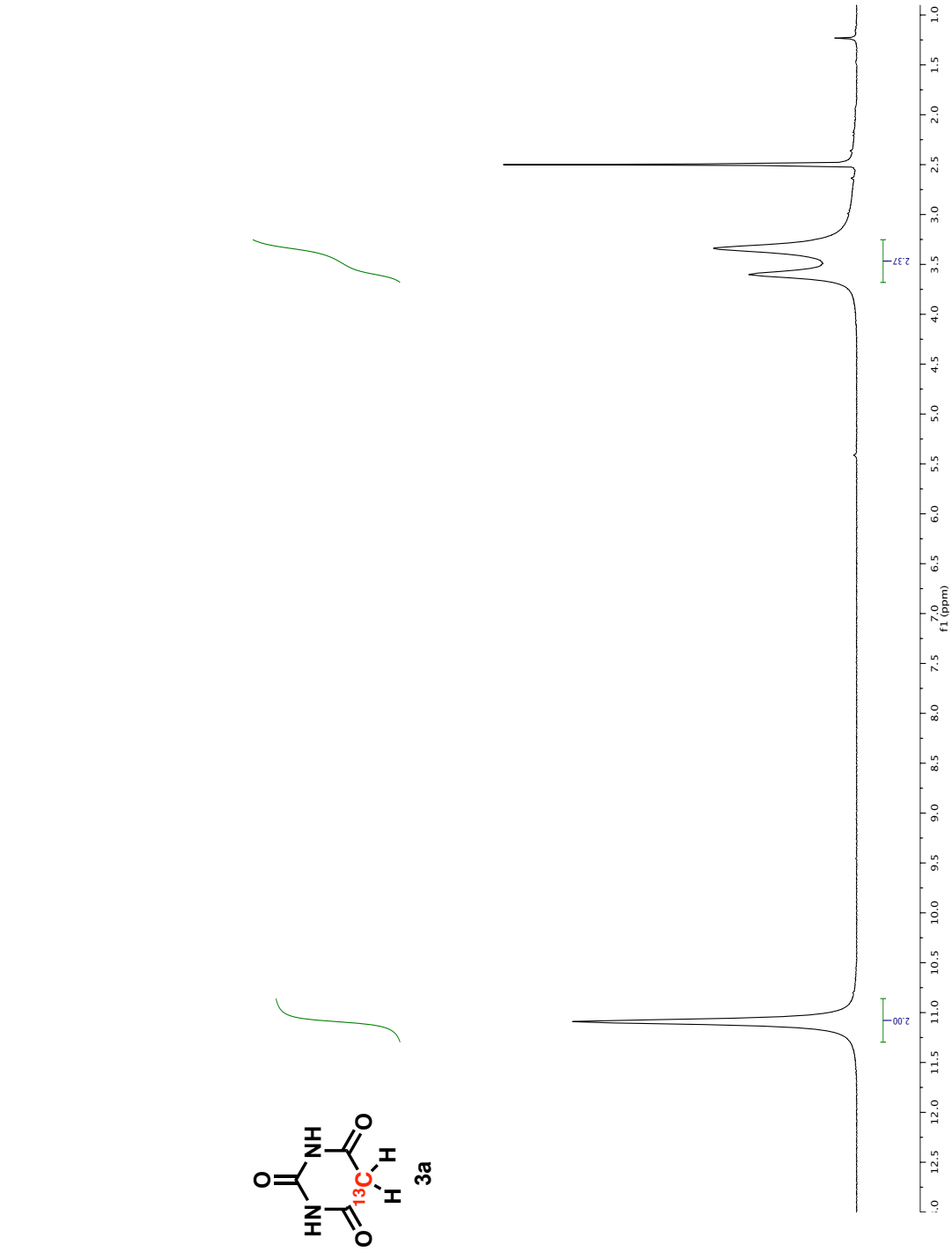


**Figure A.6** 500MHz $^{1}$H-NMR of $^{13}$C-barbituric acid **3a** in $d_6$-DMSO.

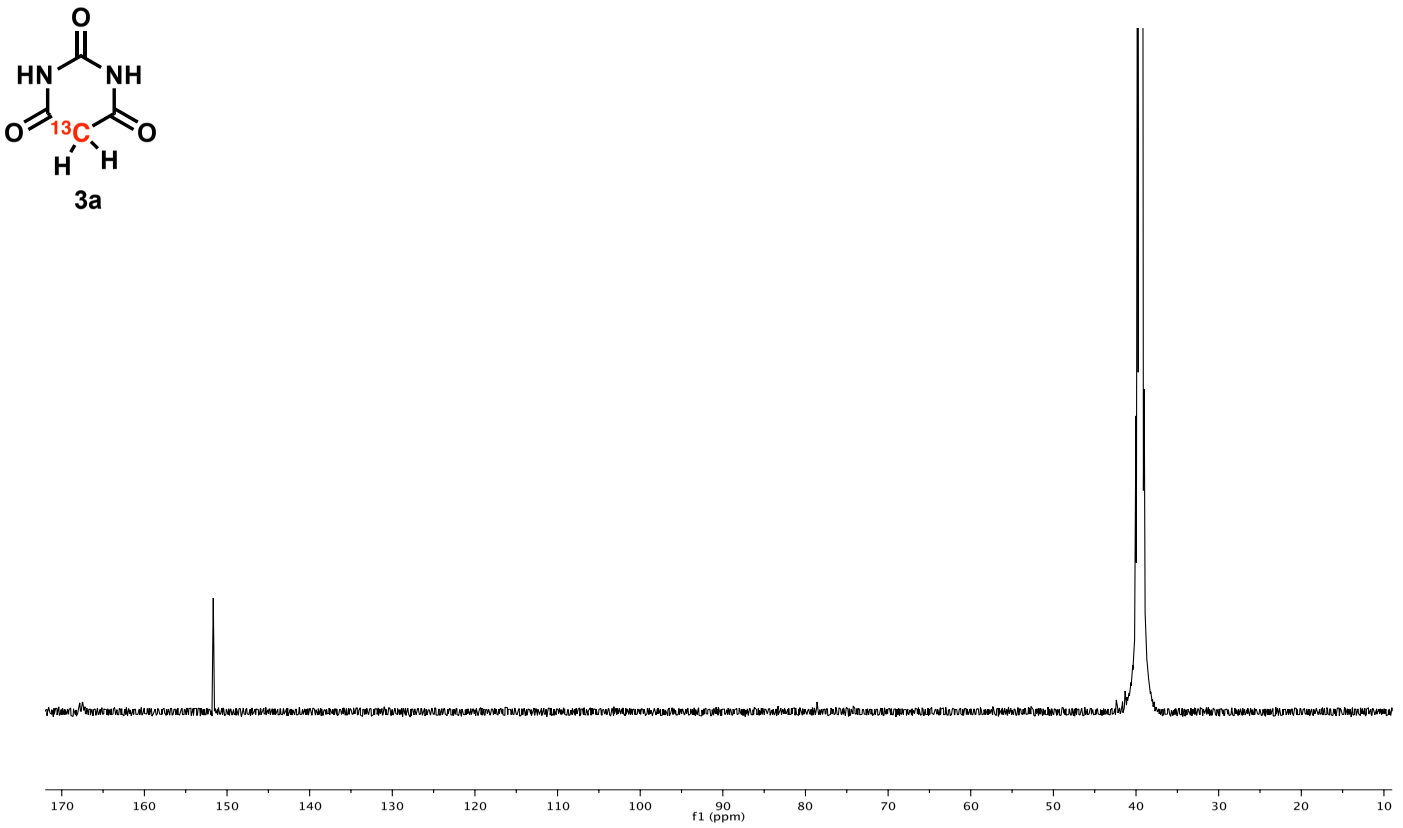


**Figure A.7** 125MHz $^{13}$C-NMR of $^{13}$C-barbituric acid **3a** in $d_6$-DMSO.

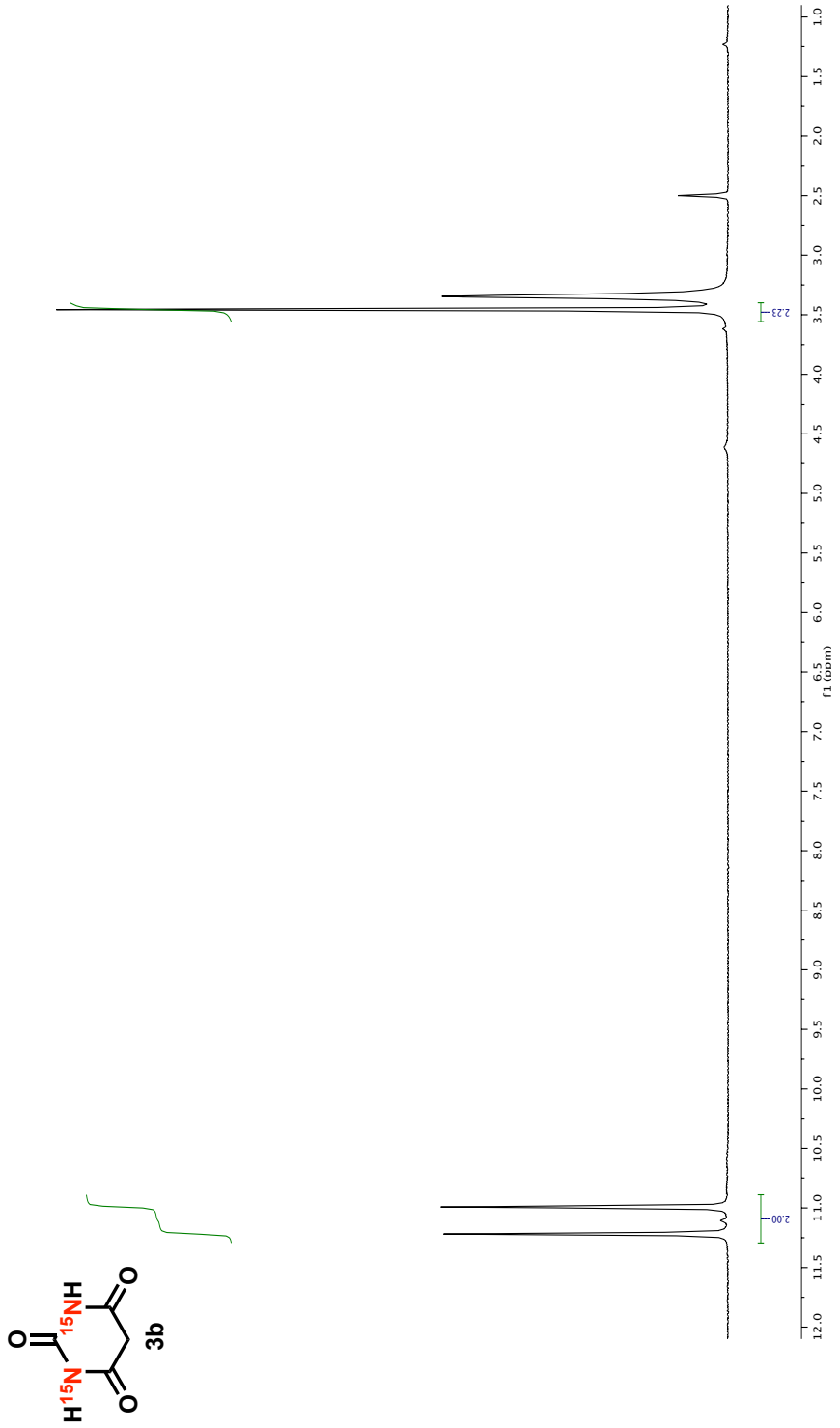


**Figure A.8** 400MHz $^{1}$H-NMR of $^{15}N_2$-barbituric acid **3b** in $d_6$-DMSO.

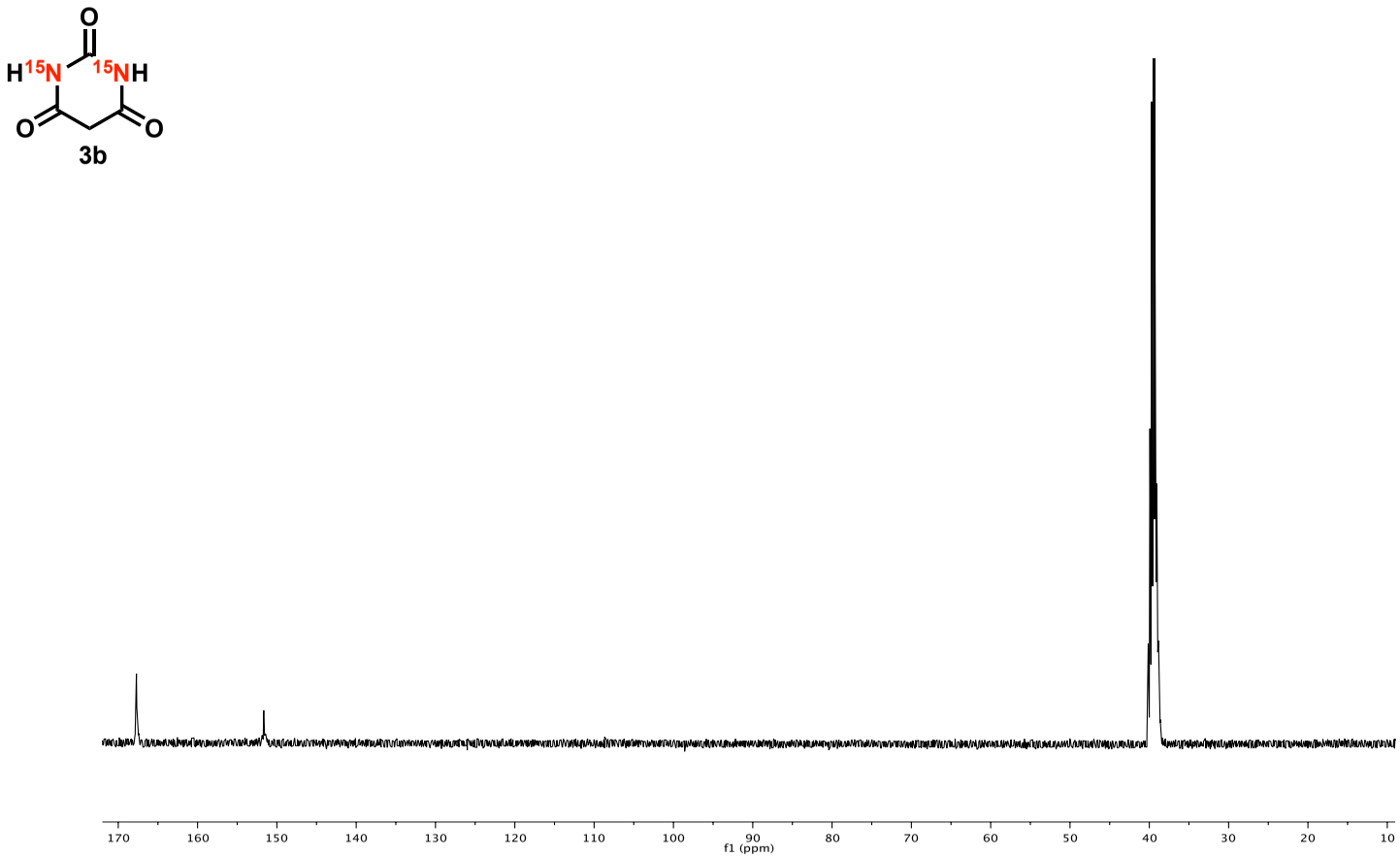


**Figure A.9** 100MHz $^{13}$C-NMR of $^{15}N_2$-barbituric acid **3b** in $d_6$-DMSO.

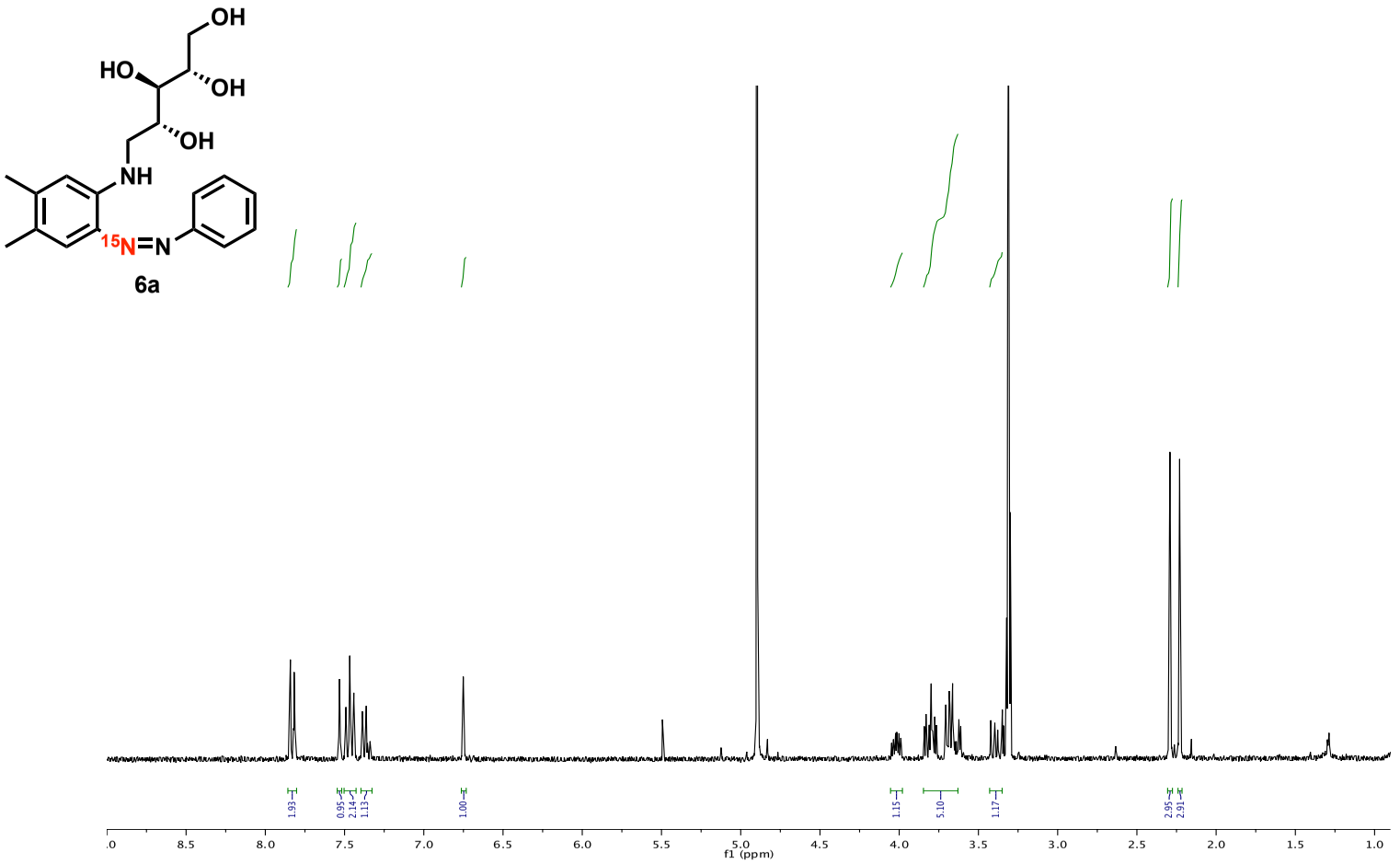


**Figure A.10** 300MHz $^{1}$H-NMR of N-ribityl-2-pheylazo-4,5-dimethyl aniline **6a** in $CD_3OD$.

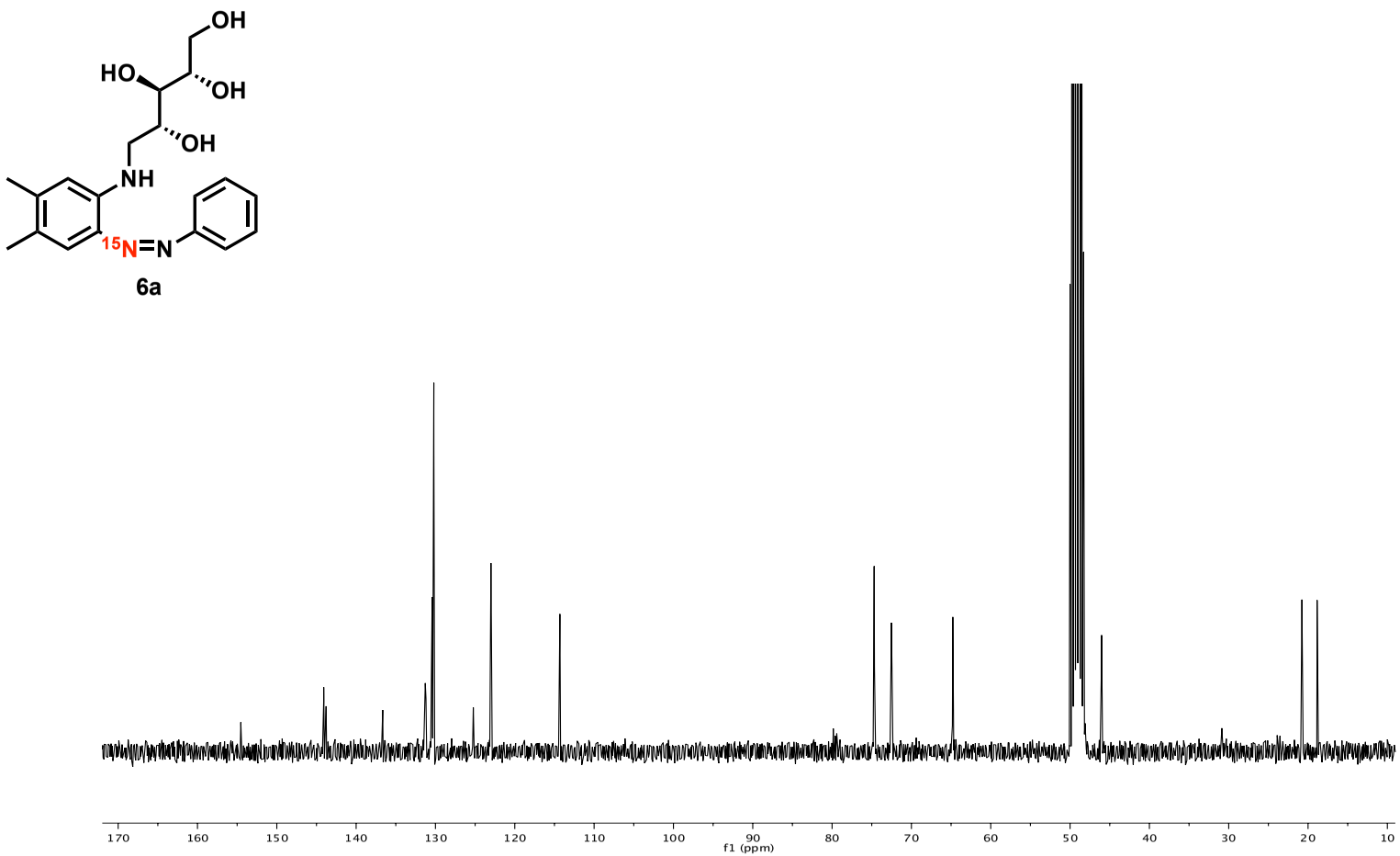


**Figure A.11** 75MHz $^{13}$C-NMR of N-ribityl-2-pheylazo-4,5-dimethyl aniline **6a** in $CD_3OD$.

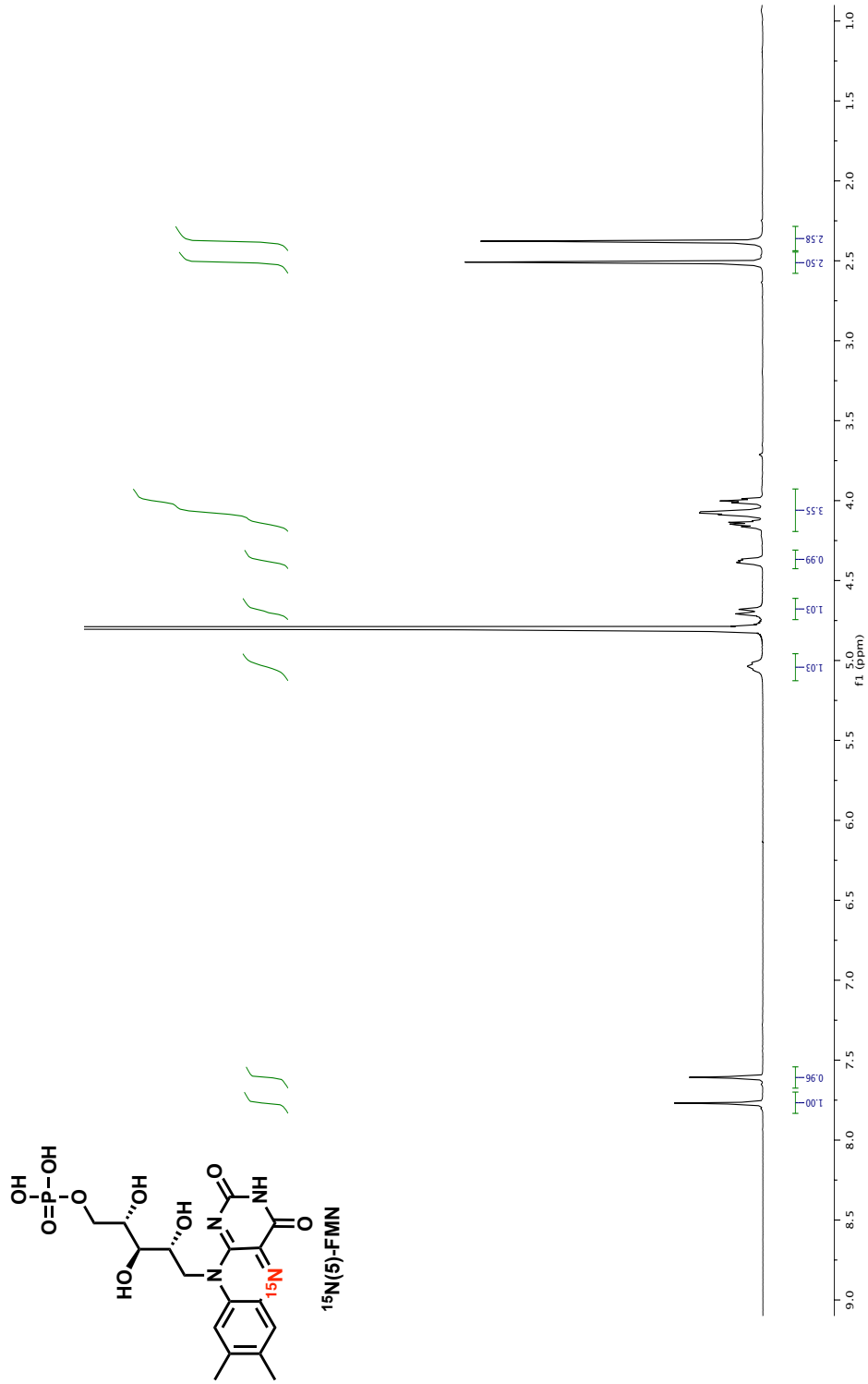


**Figure A.12** 500MHz $^{1}$H-NMR of $^{15}$N(5)-FMN in $D_2O$.

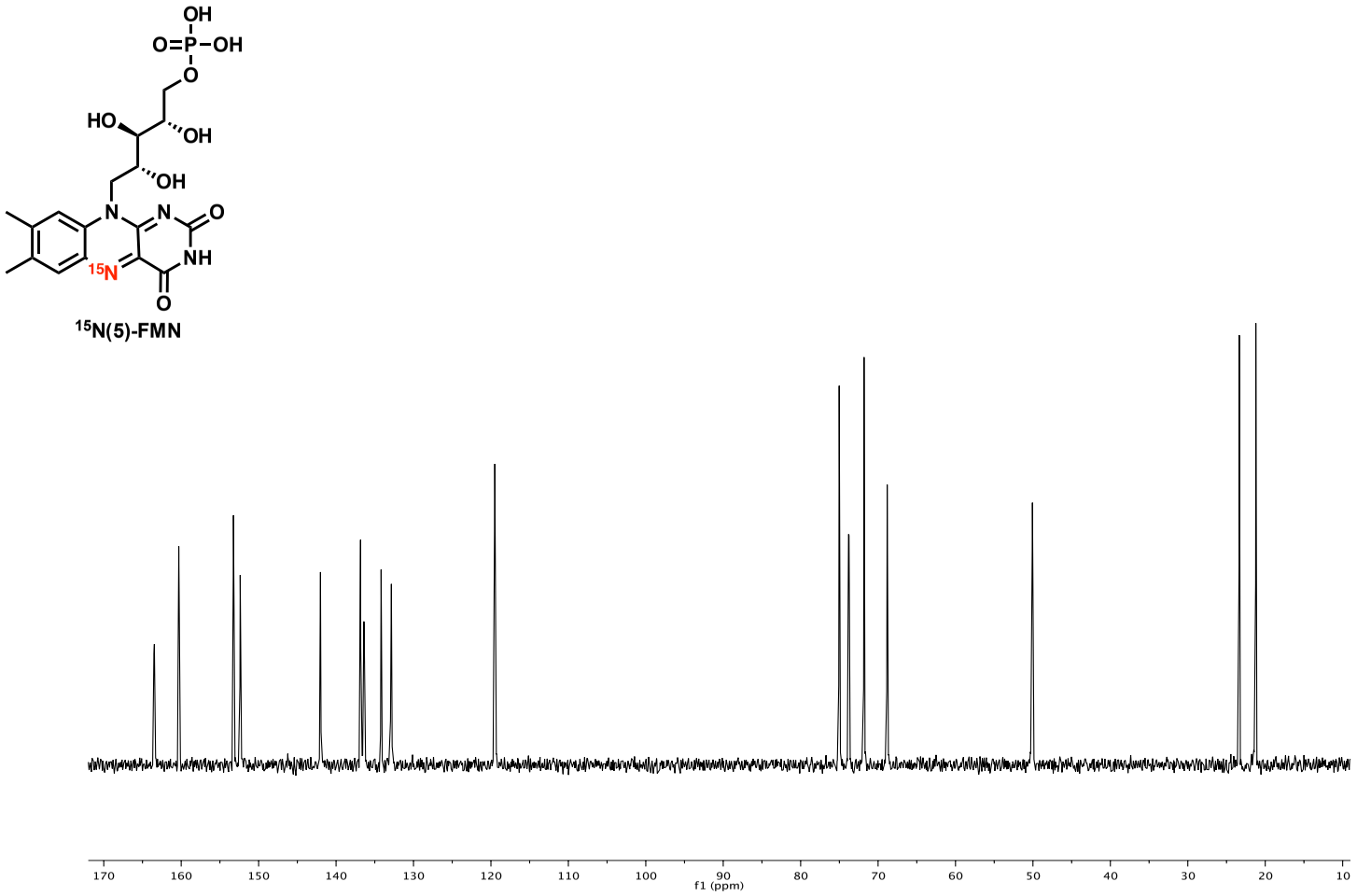


**Figure A.13** 125MHz $^{13}$C-NMR of $^{15}$N(5)-FMN in $D_2O$.

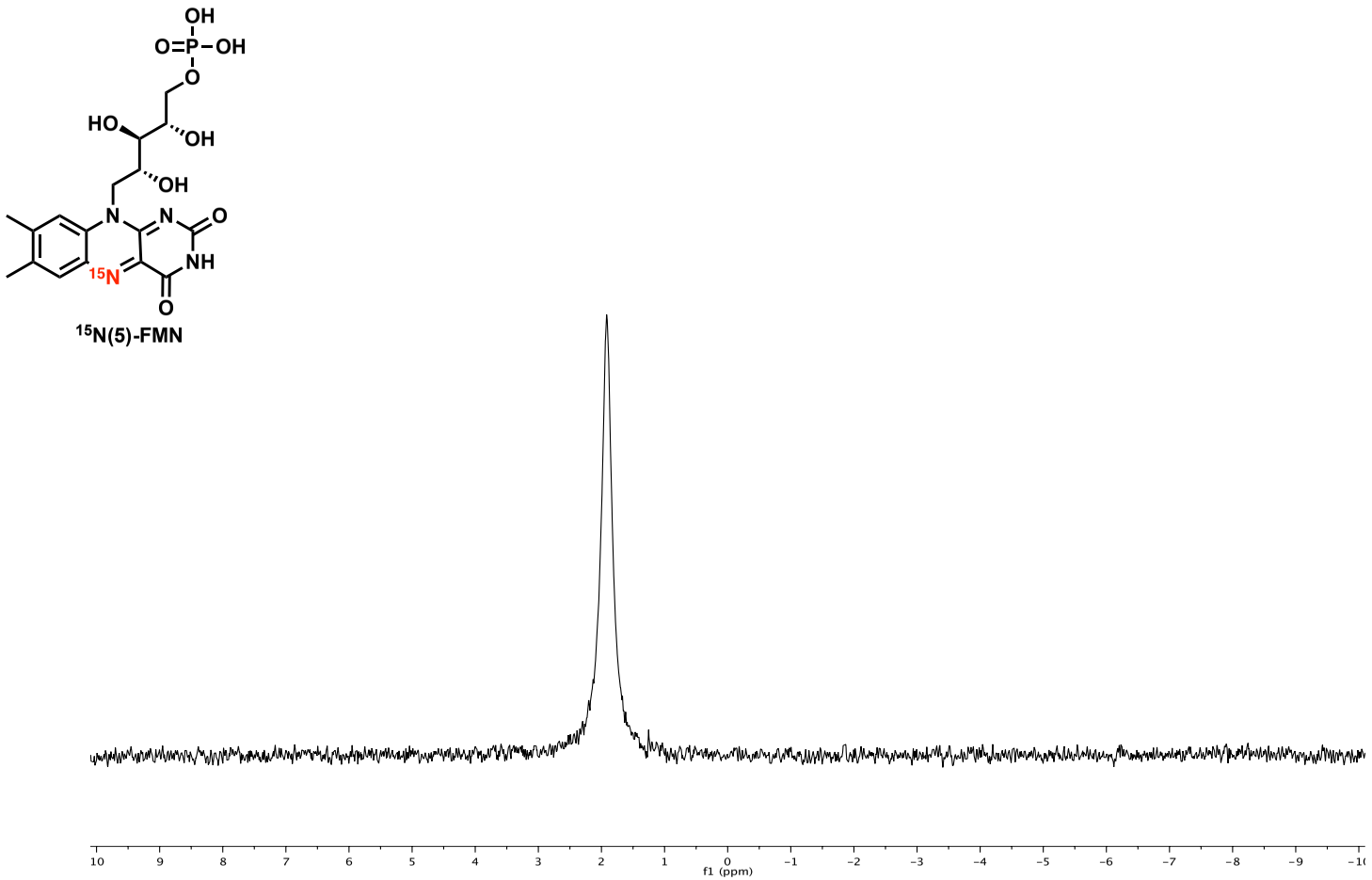


**Figure A.14** 121MHz $^{31}$P-NMR of $^{15}$N(5)-FMN in $D_2O$.

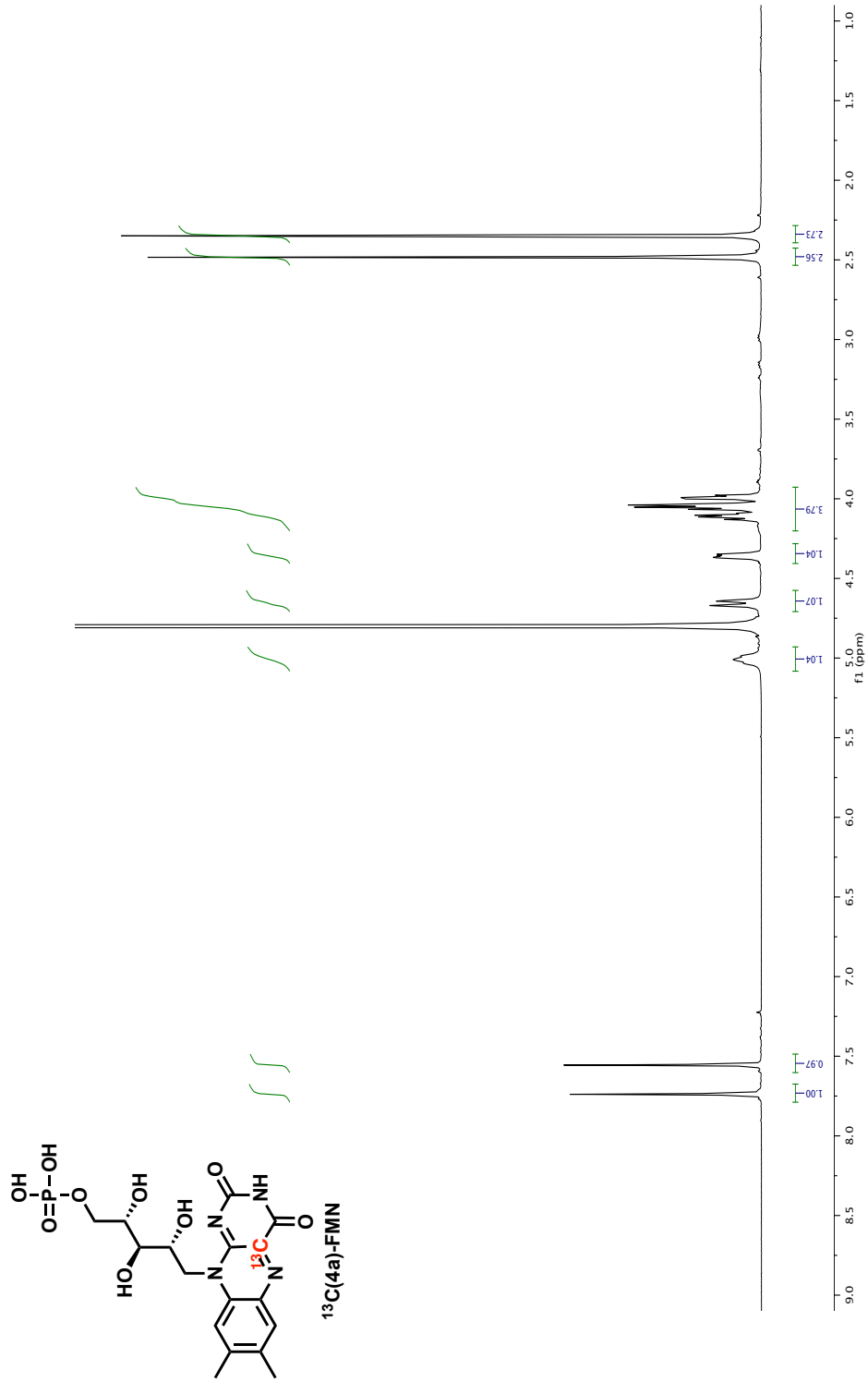


**Figure A.15** 500MHz $^{1}$H-NMR of $^{13}$C(4a)-FMN in $D_2O$.

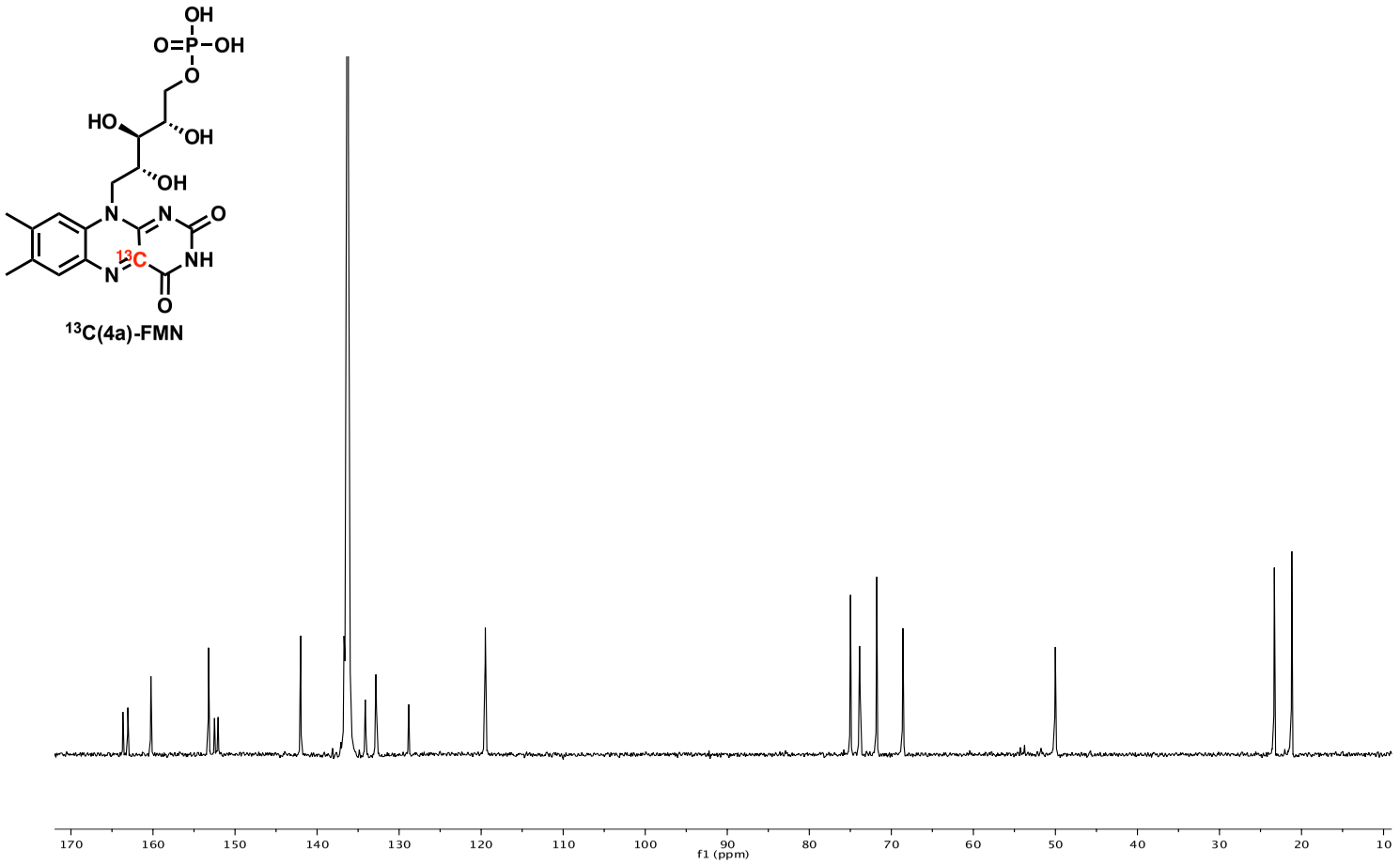


**Figure A.16** 125MHz $^{13}$C-NMR of $^{13}$C(4a)-FMN in $D_2O$.

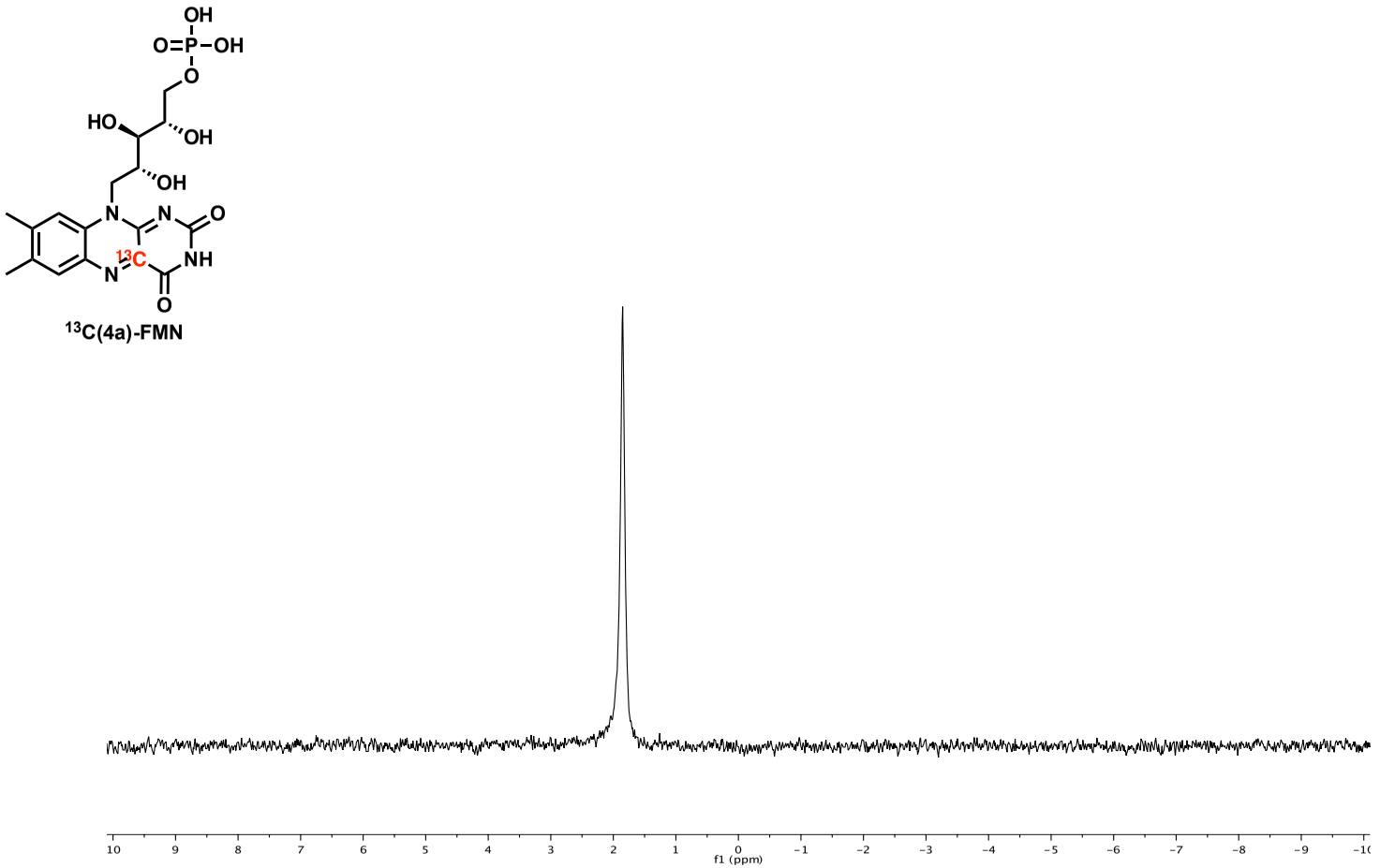


**Figure A.17** 121MHz $^{31}$P-NMR of $^{13}$C(4a)-FMN in $D_2O$.

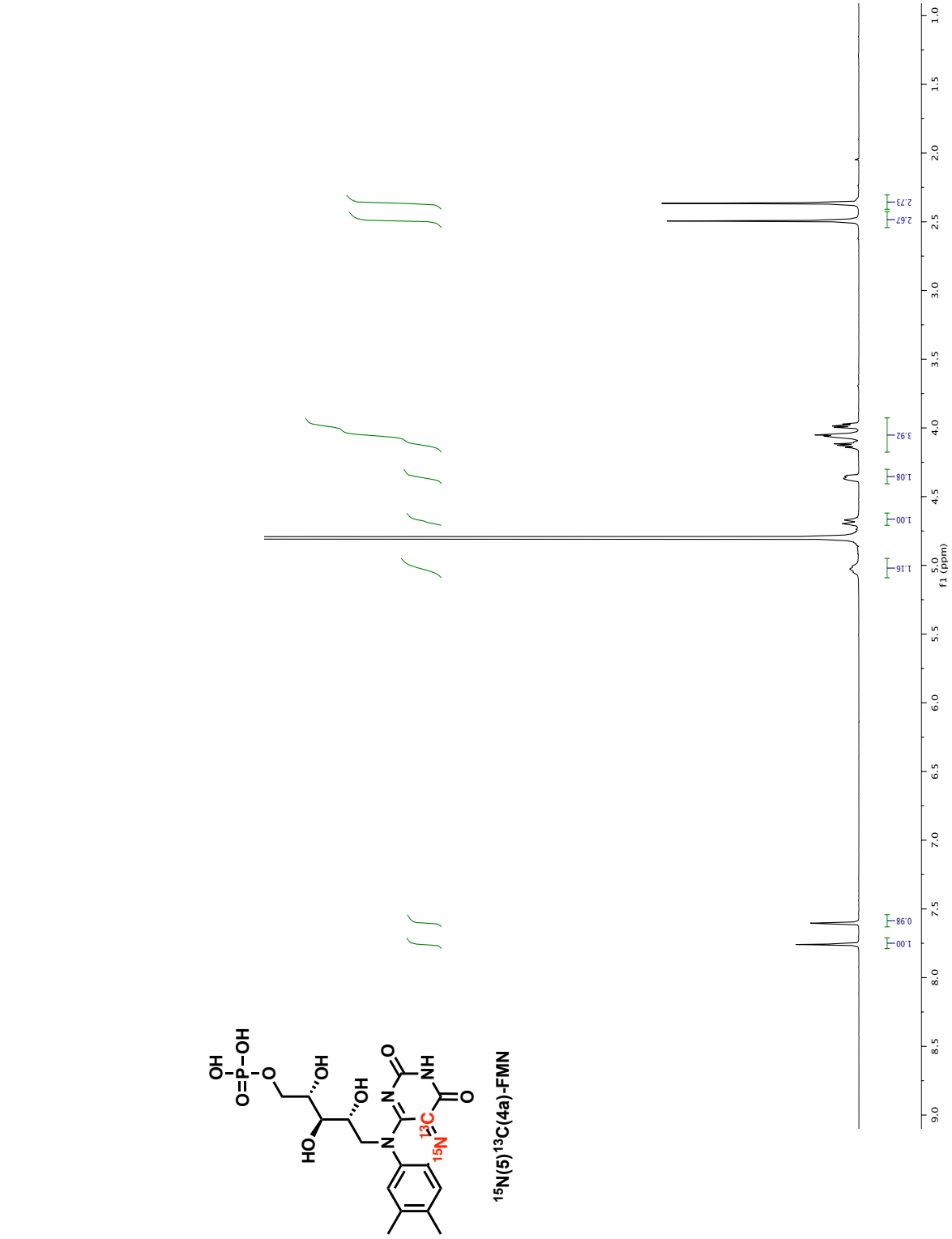


**Figure A.18** 500MHz $^{1}$H-NMR of $^{15}$N(5)$^{13}$C(4a)-FMN in $D_2O$.

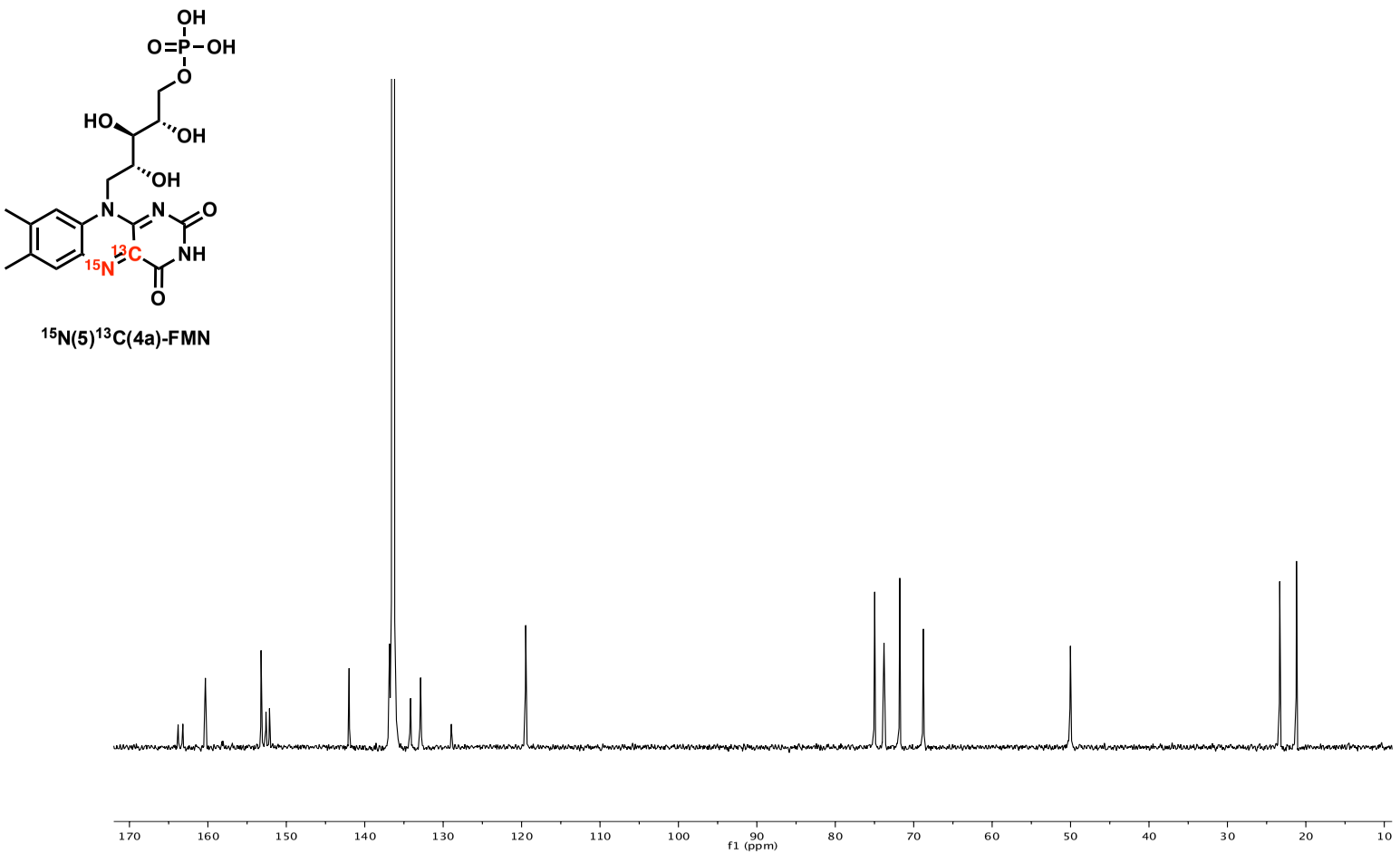


**Figure A.19** 125MHz $^{13}$C-NMR of $^{15}$N(5)$^{13}$C(4a)-FMN in $D_2O$.

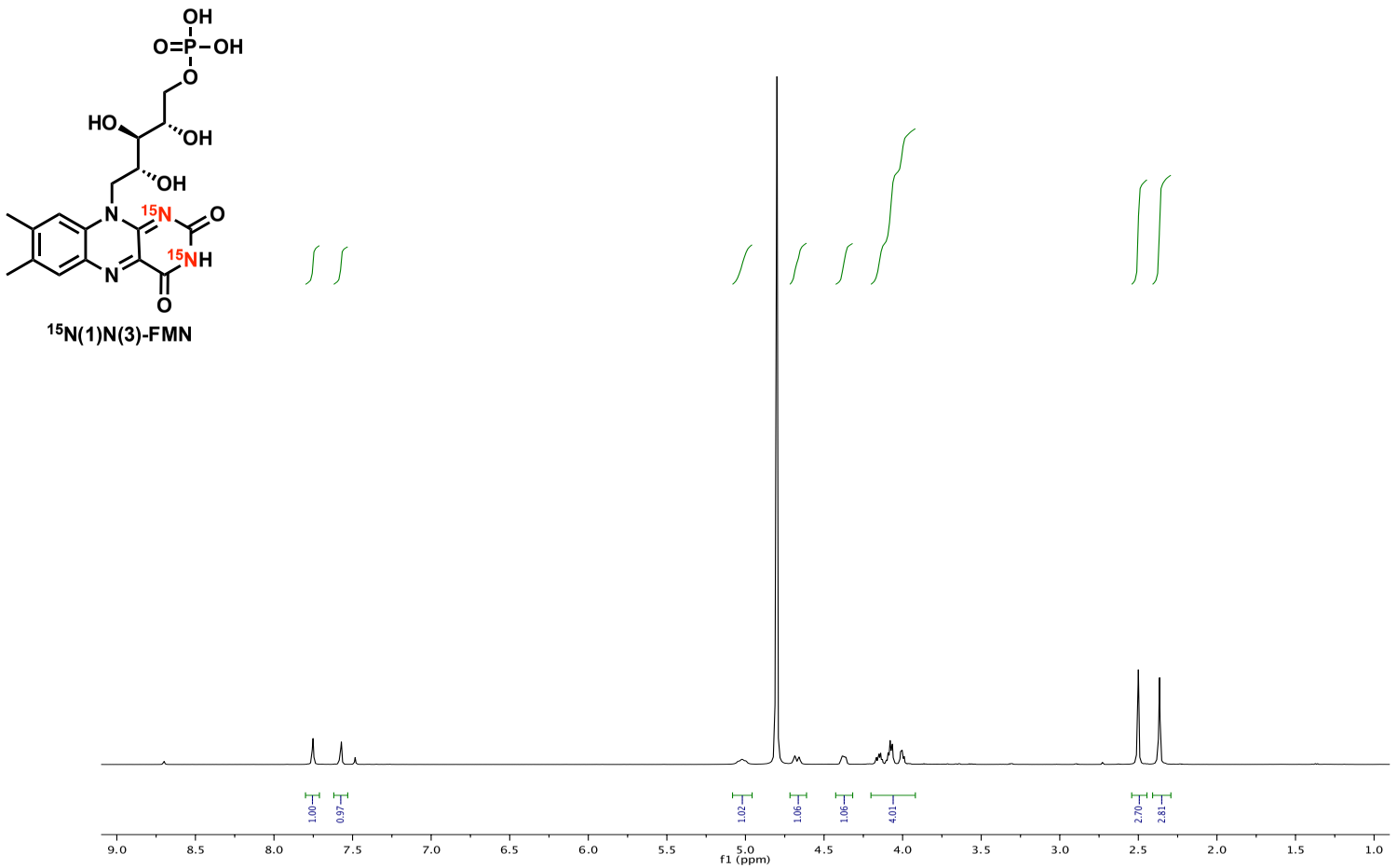


**Figure A.20** 121MHz $^{31}$P-NMR of $^{15}$N(5)$^{13}$C(4a)-FMN in $D_2O$.

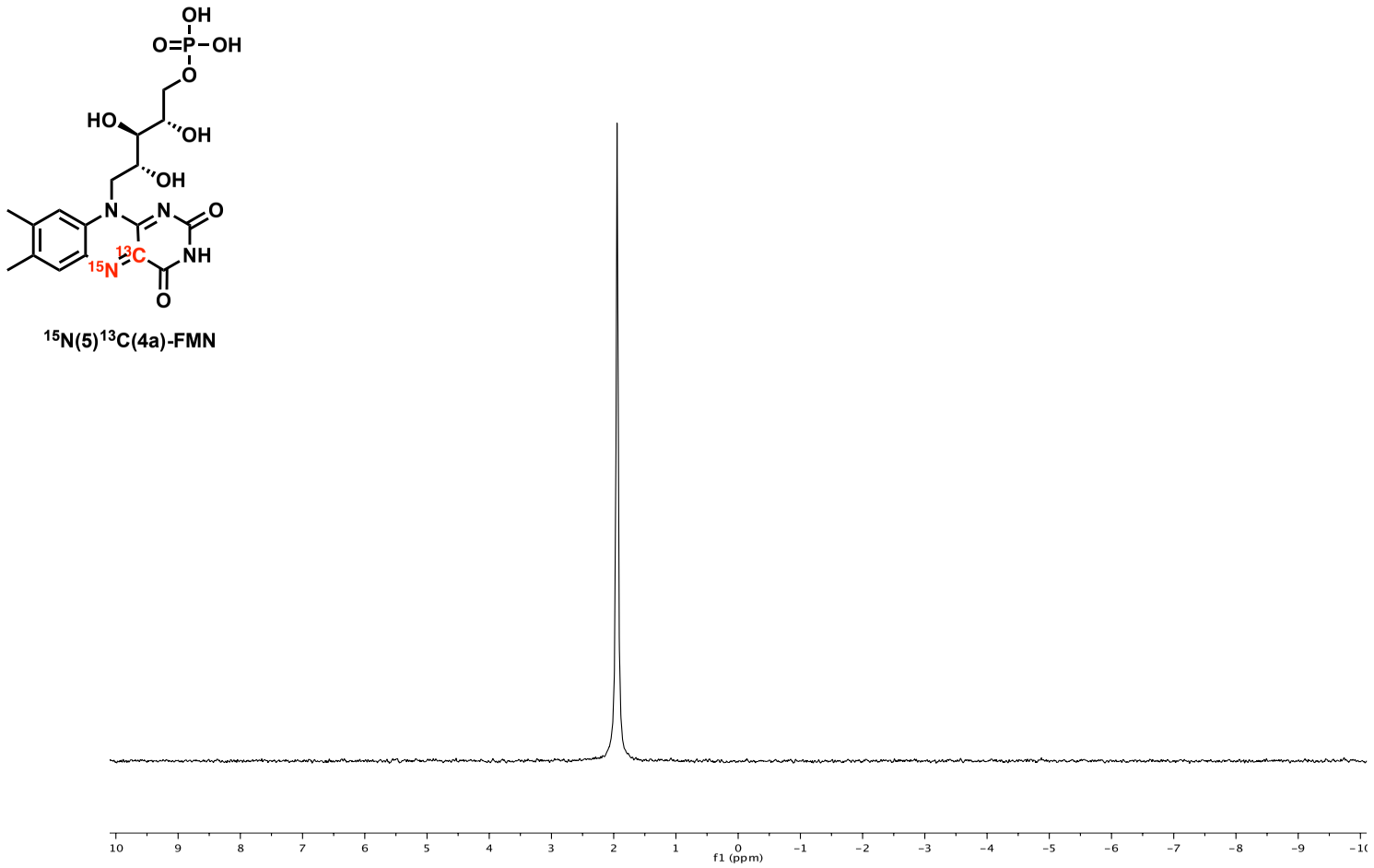


**Figure A.21** 500MHz $^{1}$H-NMR of $^{15}$N(1)$^{15}$N(3)-FMN in $D_2O$.

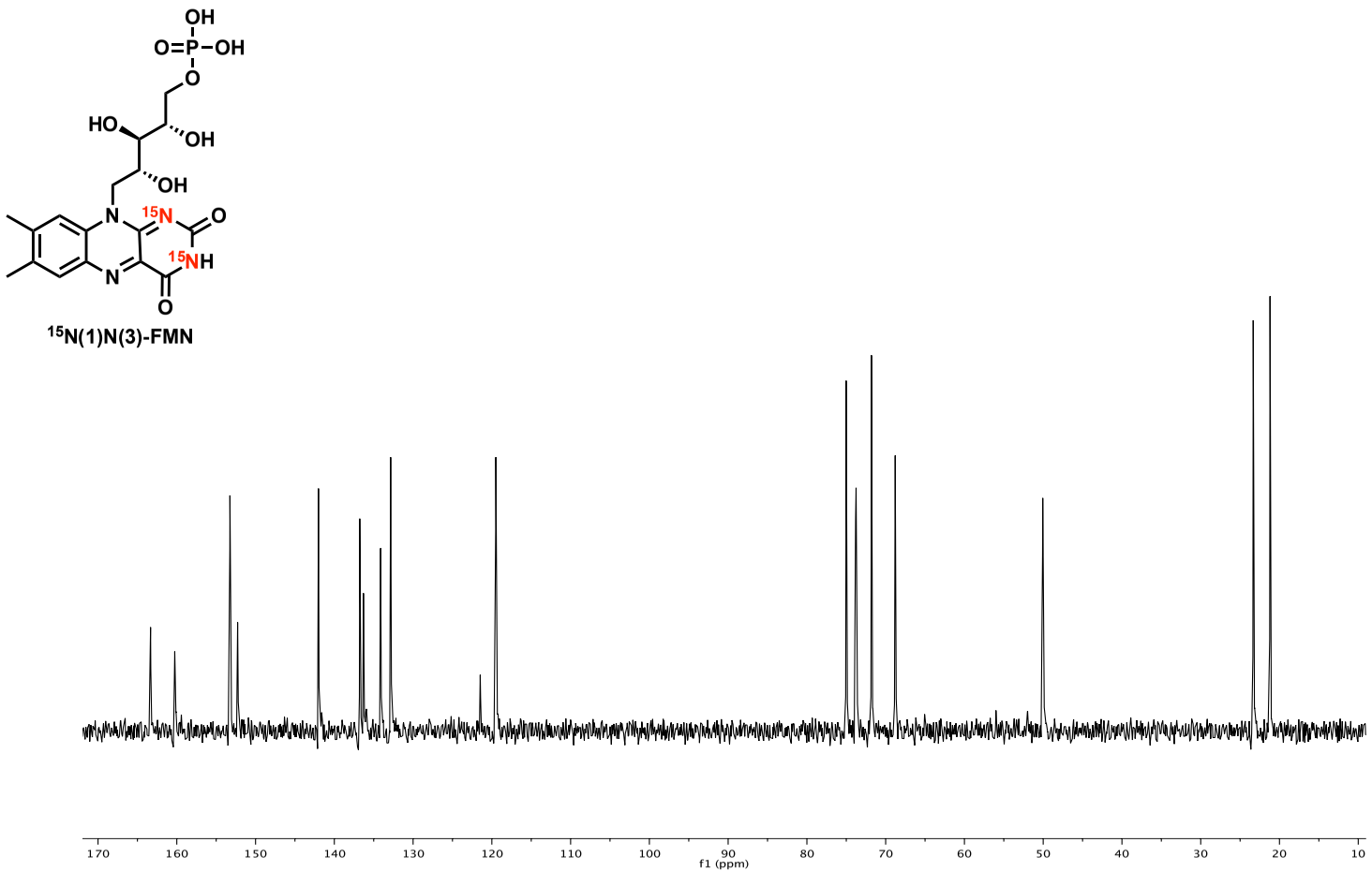


**Figure A.22** 125MHz $^{13}$C-NMR of $^{15}$N(1)$^{15}$N(3)-FMN in $D_2O$.

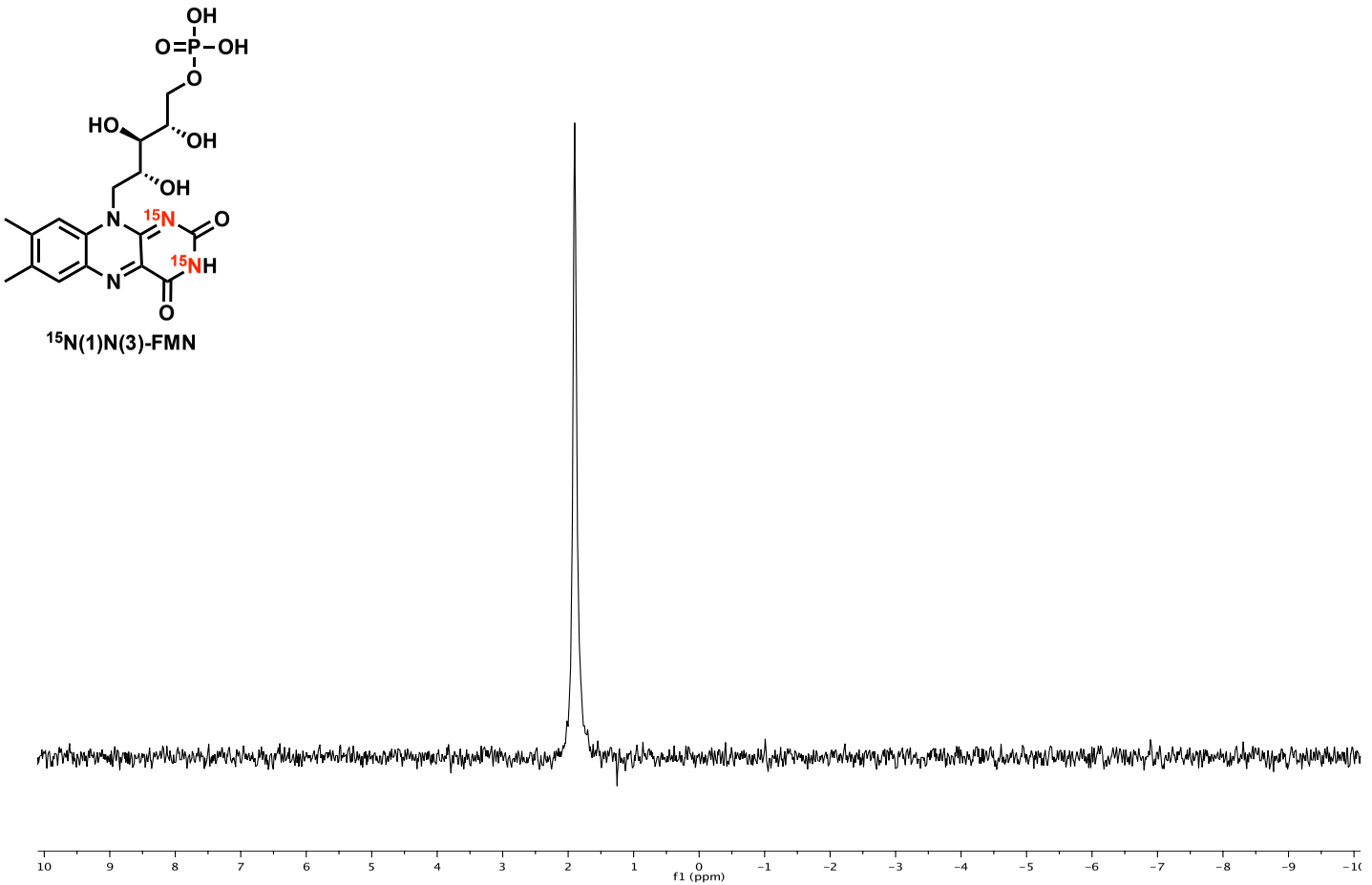


**Figure A.23** 121MHz $^{31}$P-NMR of $^{15}$N(1)$^{15}$N(3)-FMN in $D_2O$.

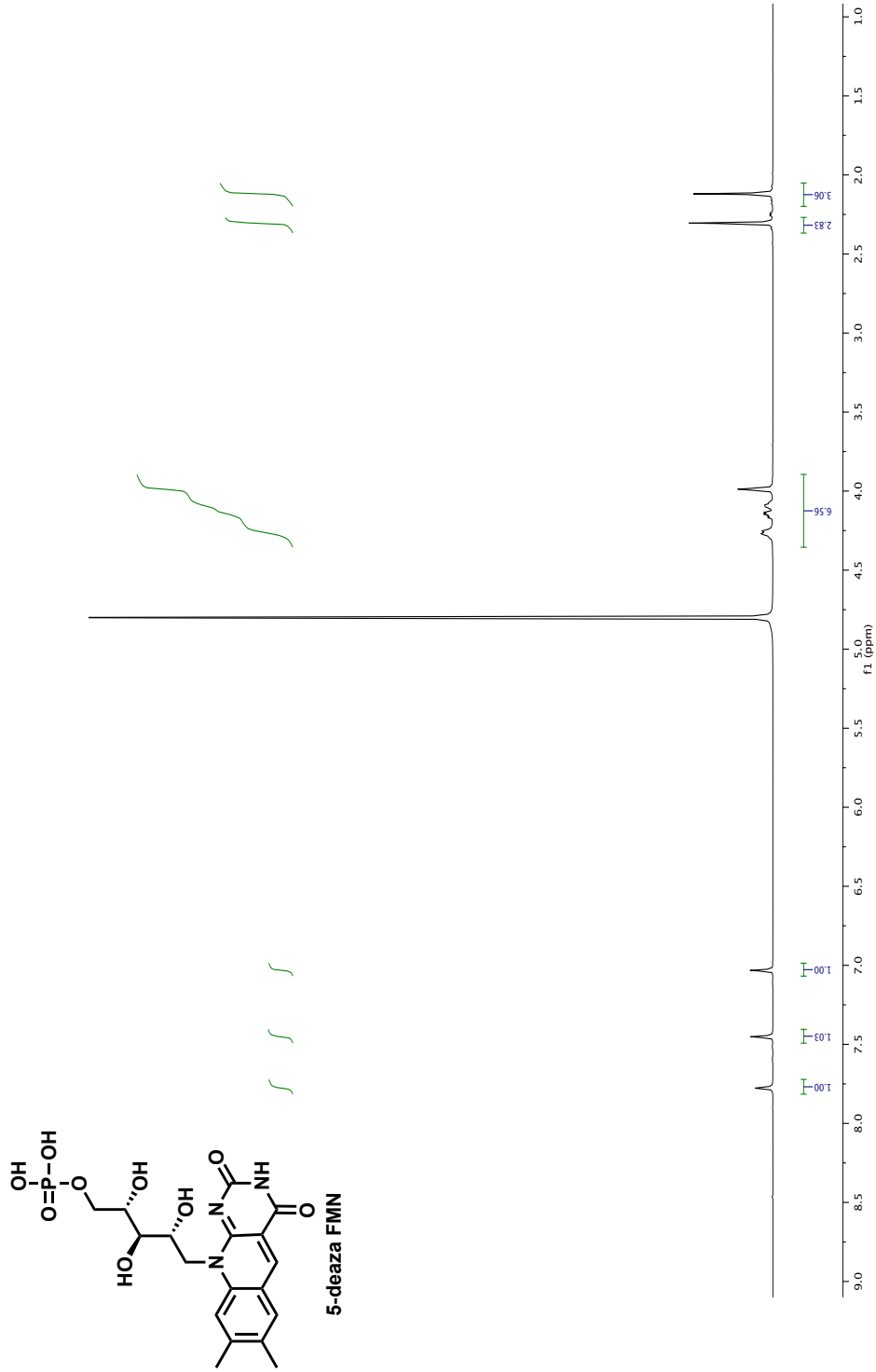


**Figure A.24** 500MHz $^{1}$H-NMR of 5-deaza-FMN in $D_2O$.

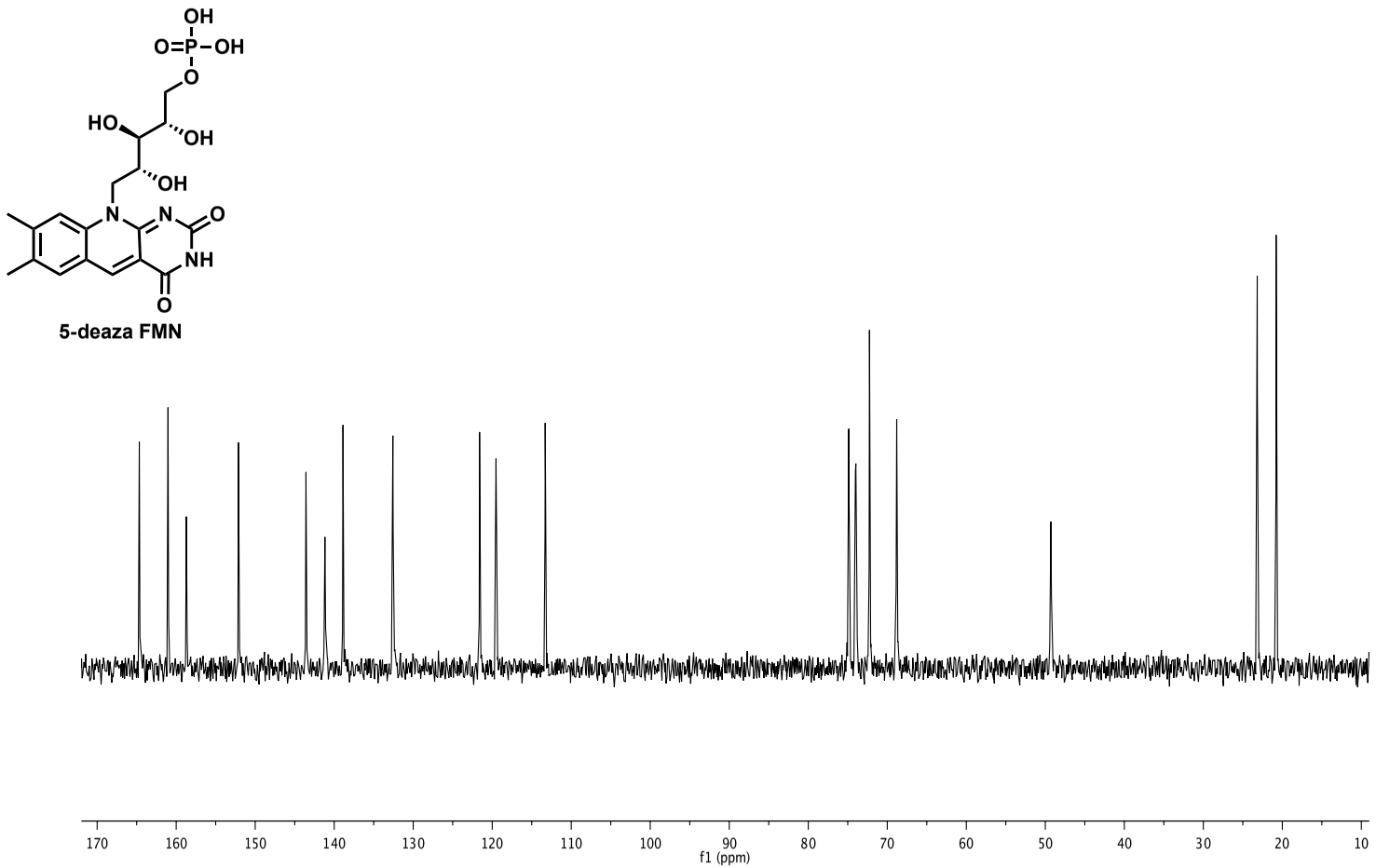


**Figure A.25** 125MHz $^{13}$C-NMR of 5-deaza-FMN in $D_2O$.

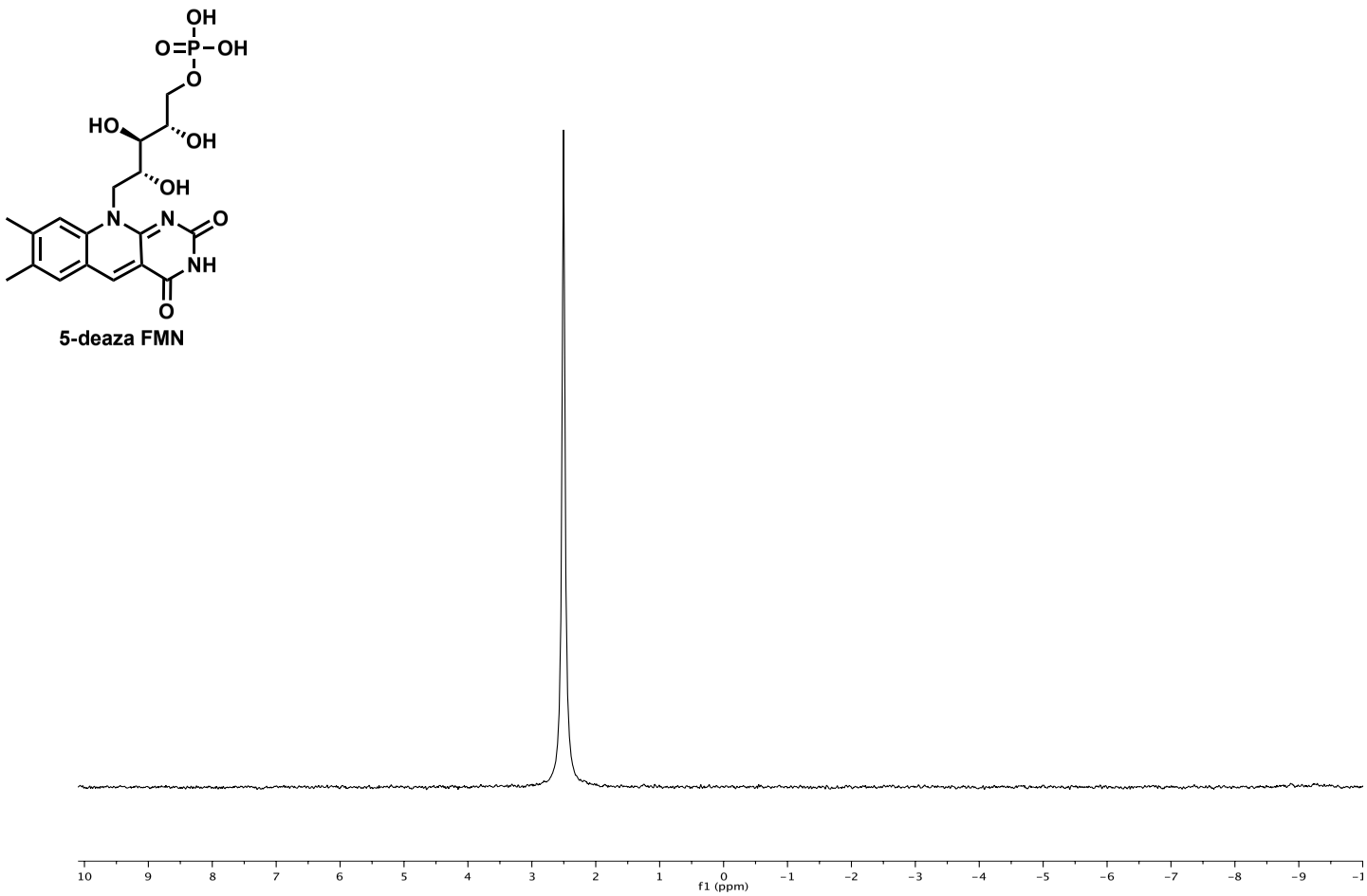


**Figure A.26** 121MHz $^{31}$P-NMR of 5-deaza-FMN in $D_2O$.

# APPENDIX B

## MASS-SPECTRAL CHROMATOGRAMS OF DMAT AND DEUTERATED-DMAT

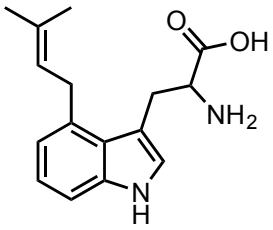

DMAT

Molecular formula = $C_{16}H_{20}N_2O_2$

Exact mass = 295.1417 $[M+Na]^+$

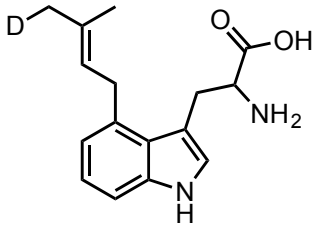

*$d_1$*-DMAT

Molecular formula = $C_{16}H_{19}DN_2O_2$

Exact mass = 296.1480 $[M+Na]^+$

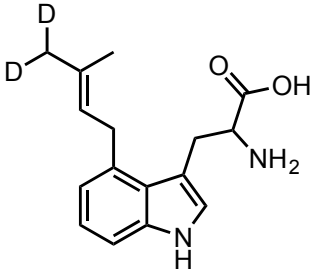

*$d_2$*-DMAT

Molecular formula = $C_{16}H_{18}D_2N_2O_2$

Exact mass = 297.1543 $[M+Na]^+$

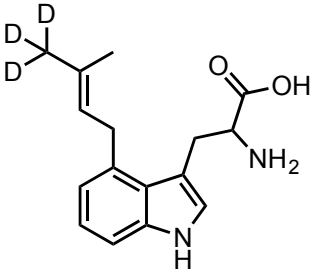

*$d_3$*-DMAT

Molecular formula = $C_{16}H_{17}D_3N_2O_2$

Exact mass = 298.1605 $[M+Na]^+$

**Masses of DMAT and *d*-DMAT**

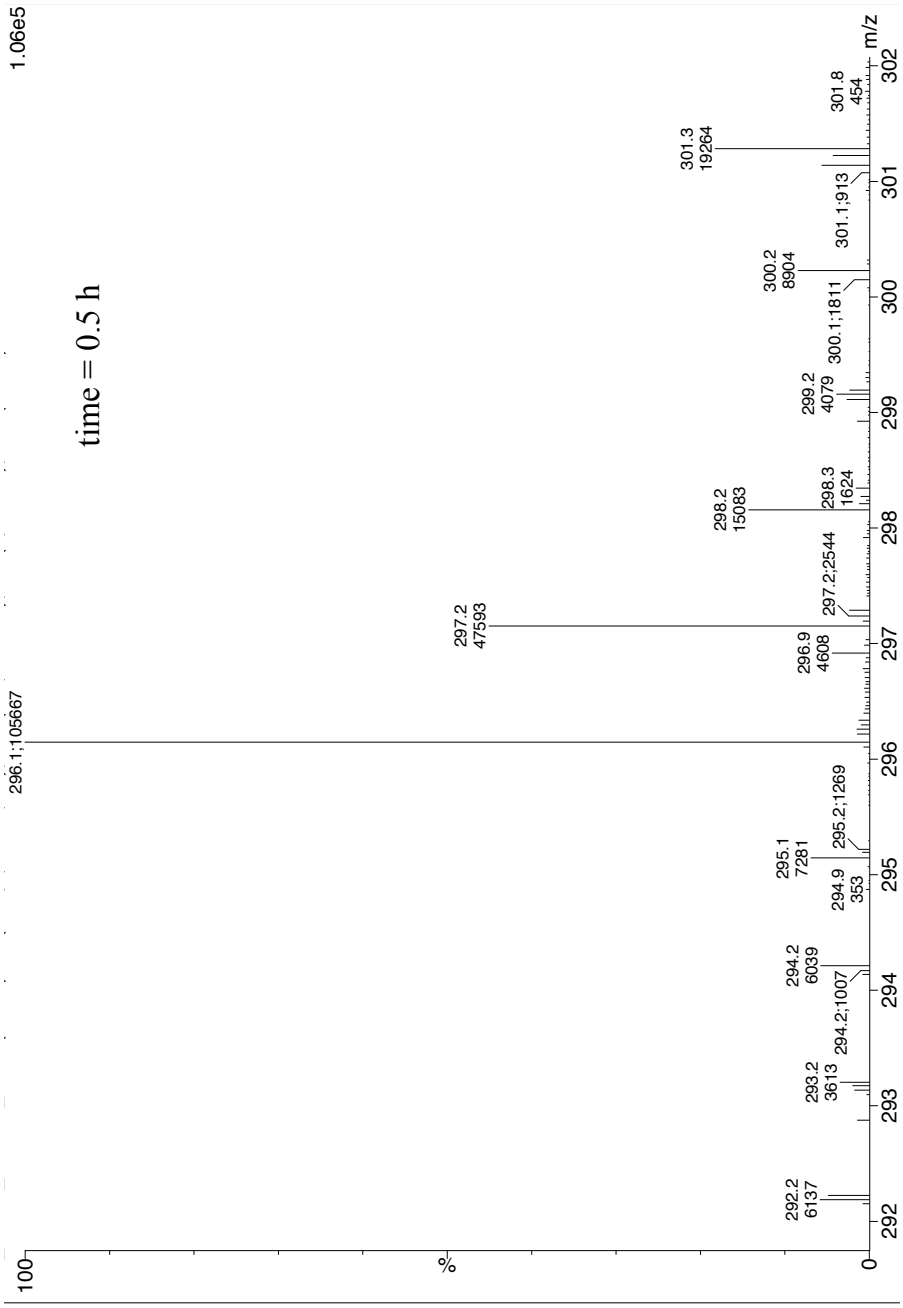


**Figure B.1** ESI$^{+}$-MS of *d*-DMAT products from IDI-1-4-DMATS coupled enzyme reaction.

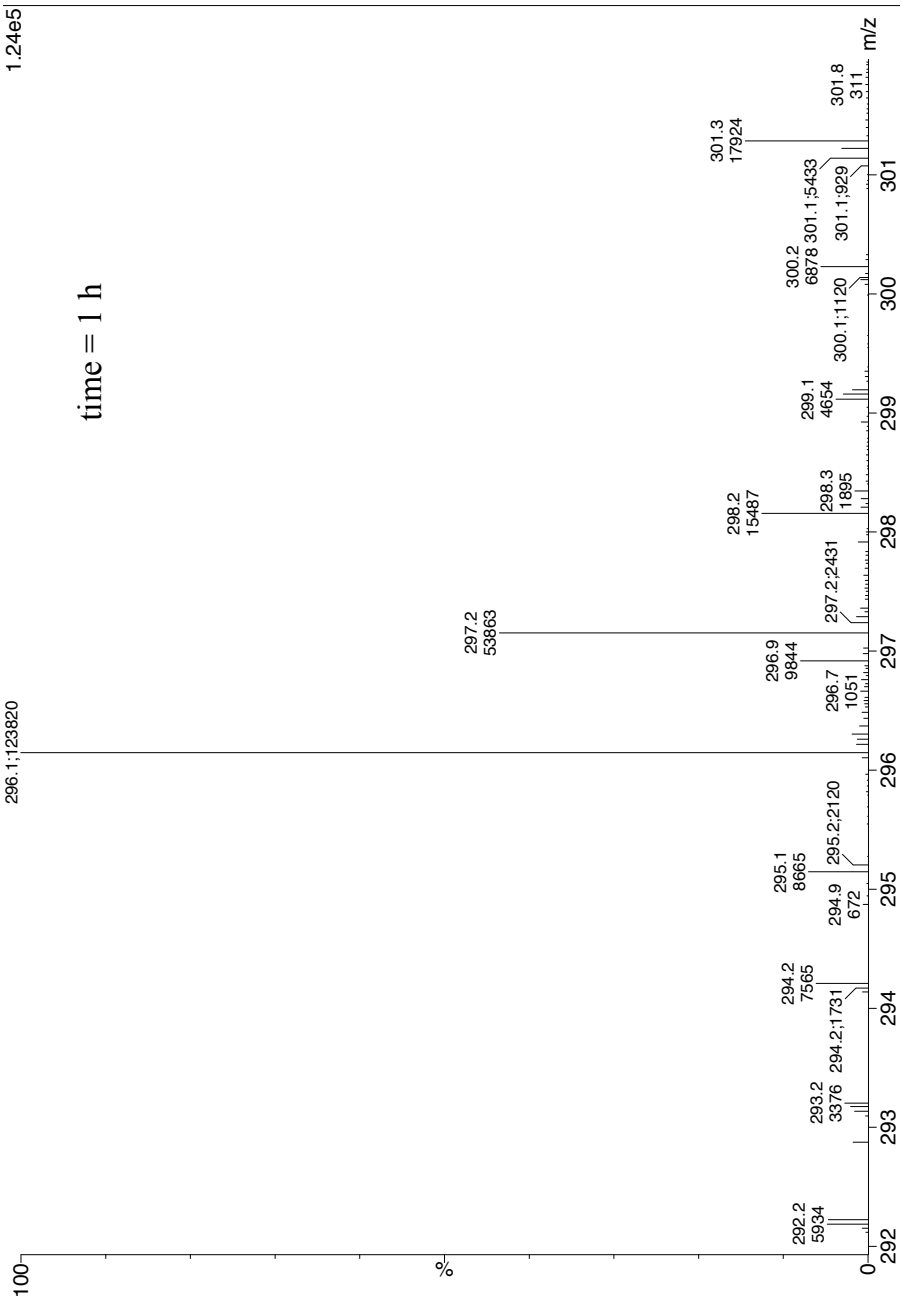


**Figure B.2** ESI$^+$-MS of *d*-DMAT products from IDI-1-4-DMATS coupled enzyme reaction.

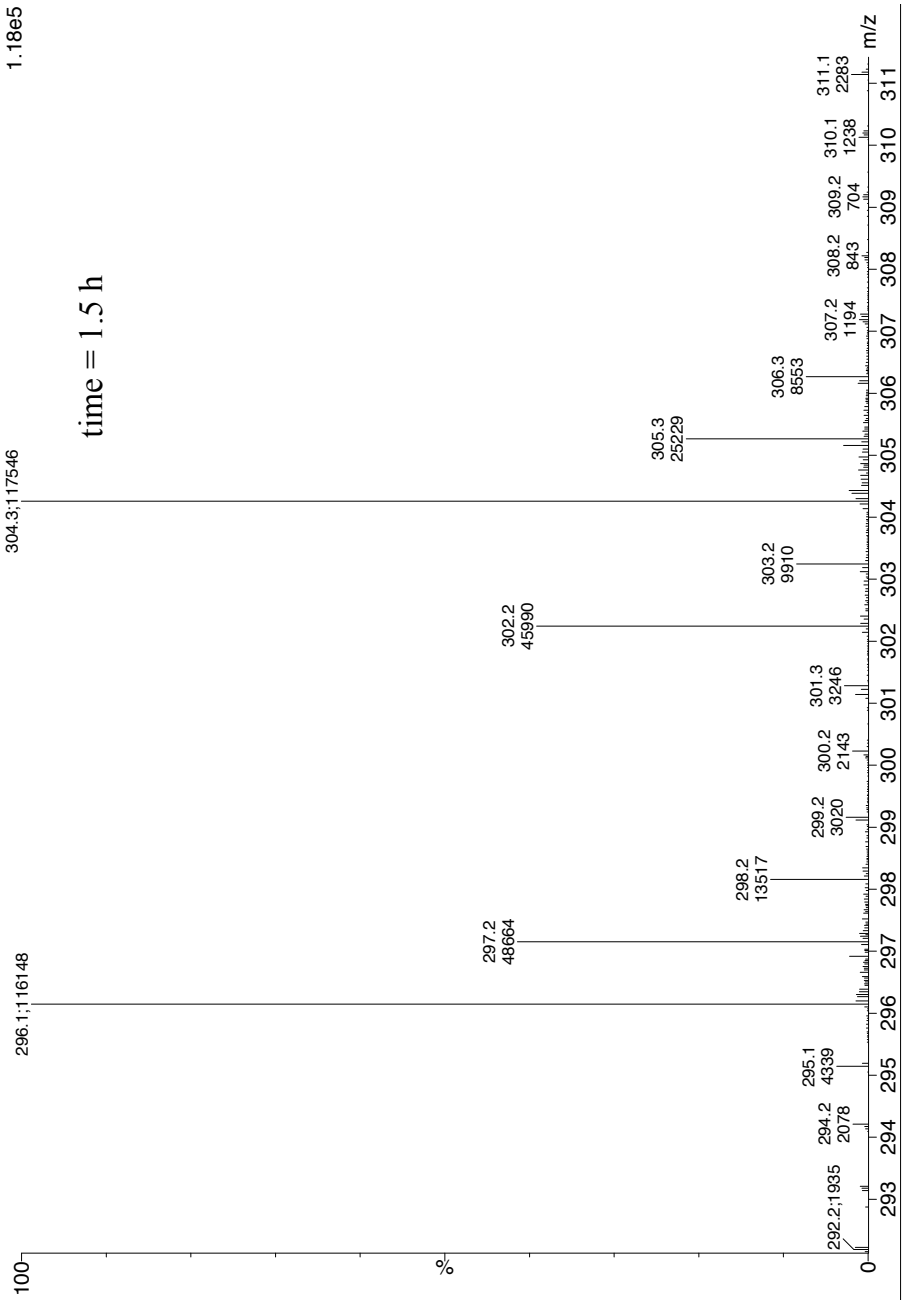


**Figure B.3** ESI$^{+}$-MS of *d*-DMAT products from IDI-1-4-DMATS coupled enzyme reaction.

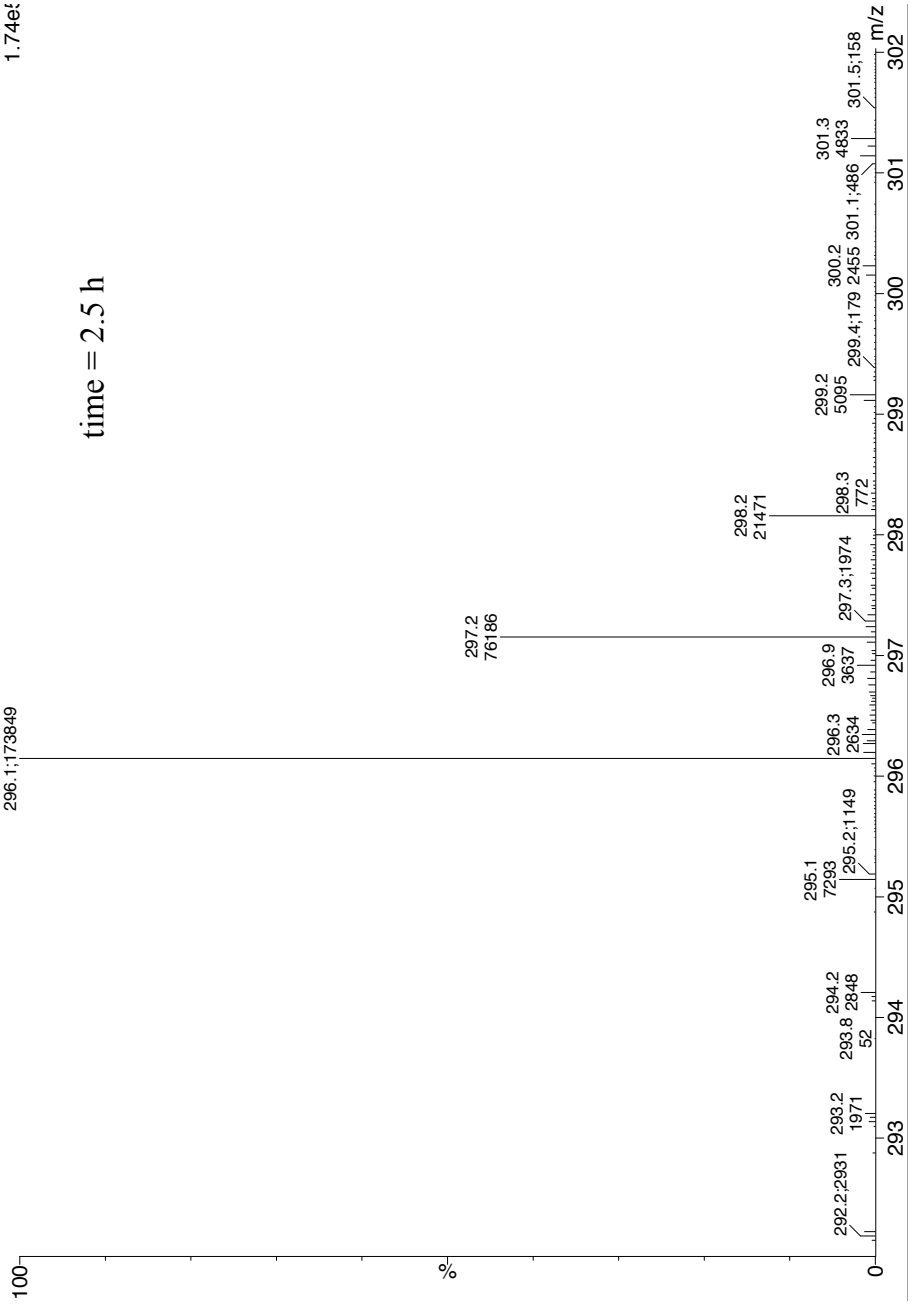


**Figure B.4** ESI$^+$-MS of *d*-DMAT products from IDI-1-4-DMATS coupled enzyme reaction.

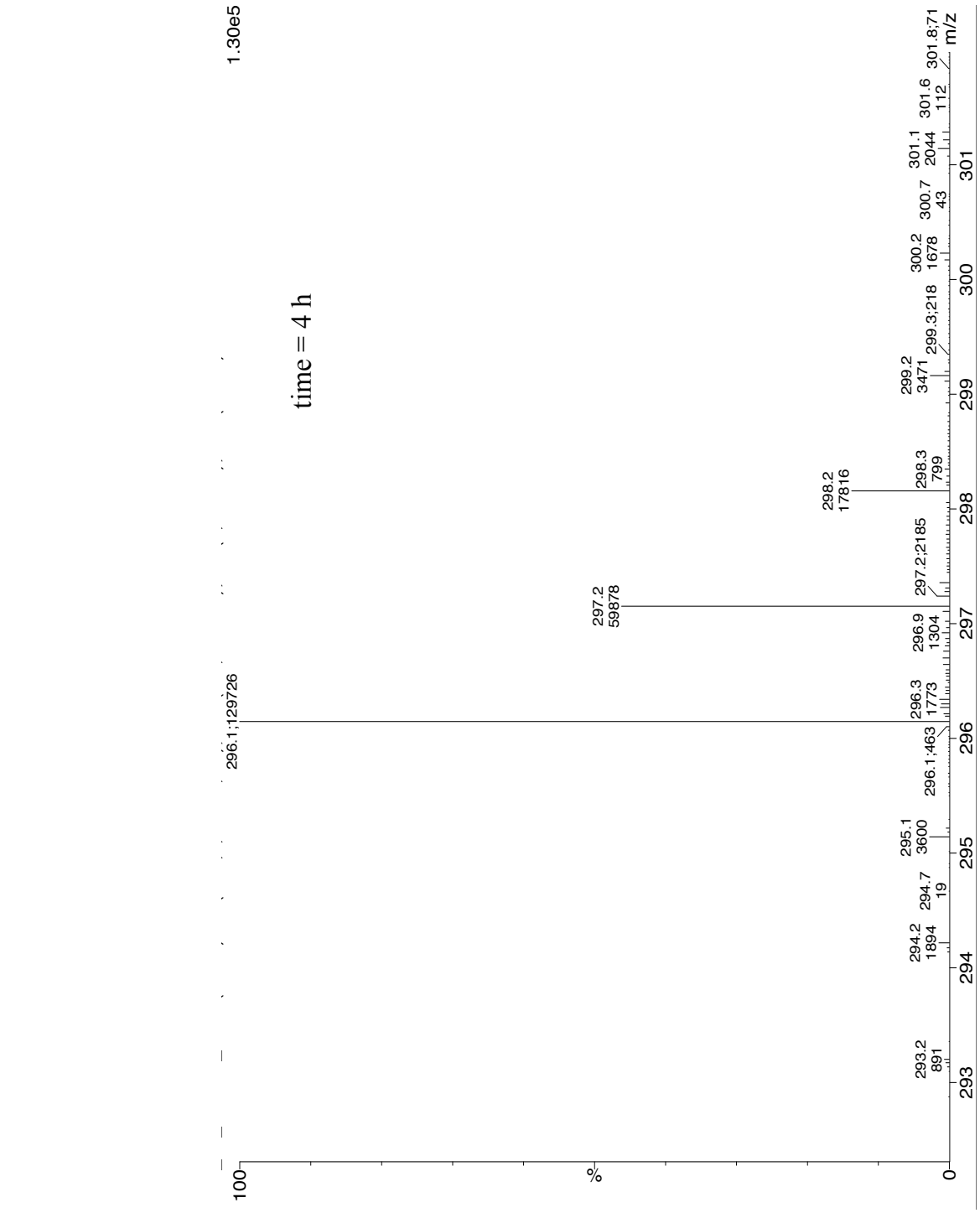


**Figure B.5** ESI$^+$-MS of *d*-DMAT products from IDI-1-4-DMATS coupled enzyme reaction.

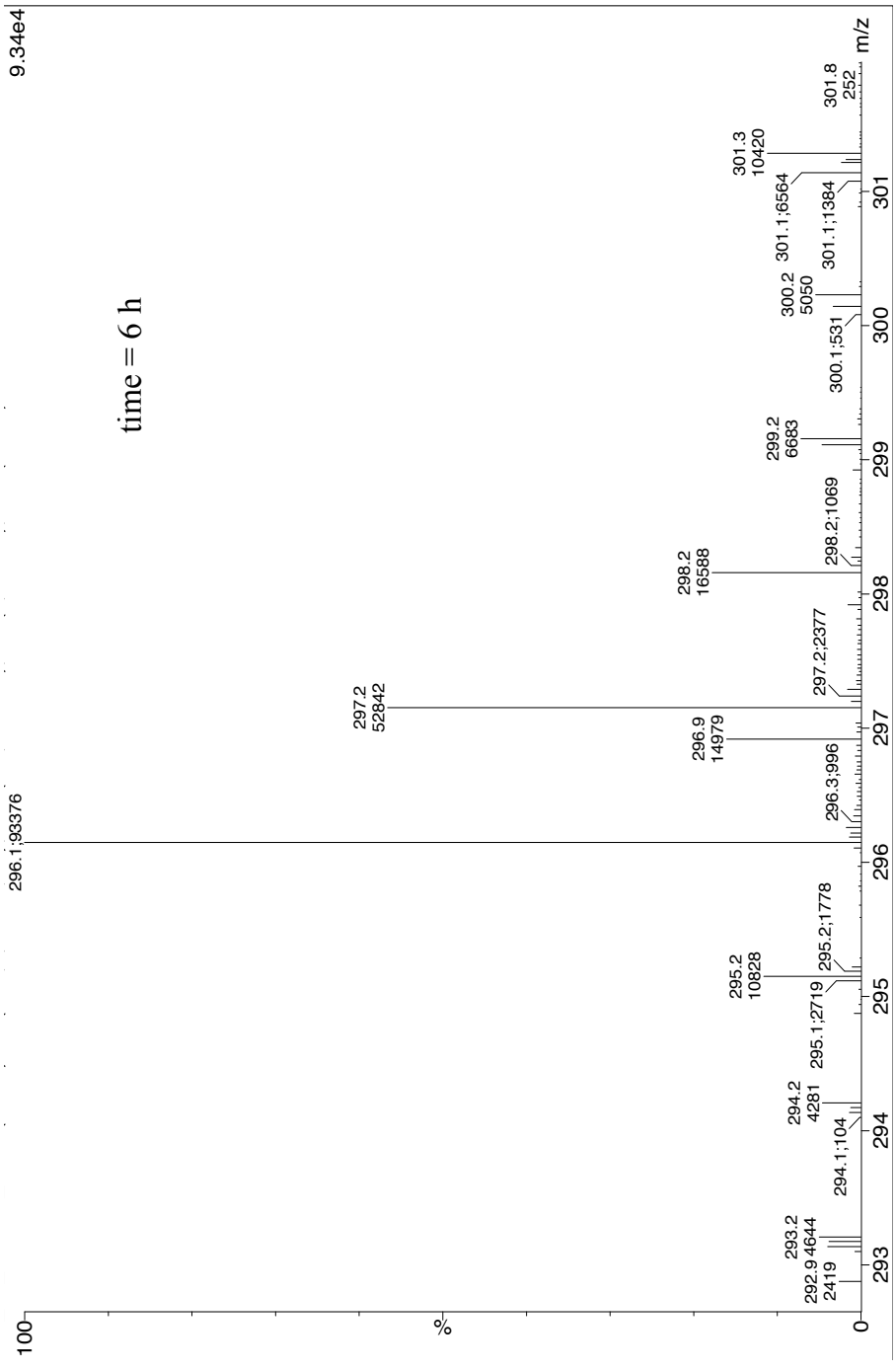


**Figure B.6** ESI$^+$-MS of *d*-DMAT products from IDI-1-4-DMATS coupled enzyme reaction.

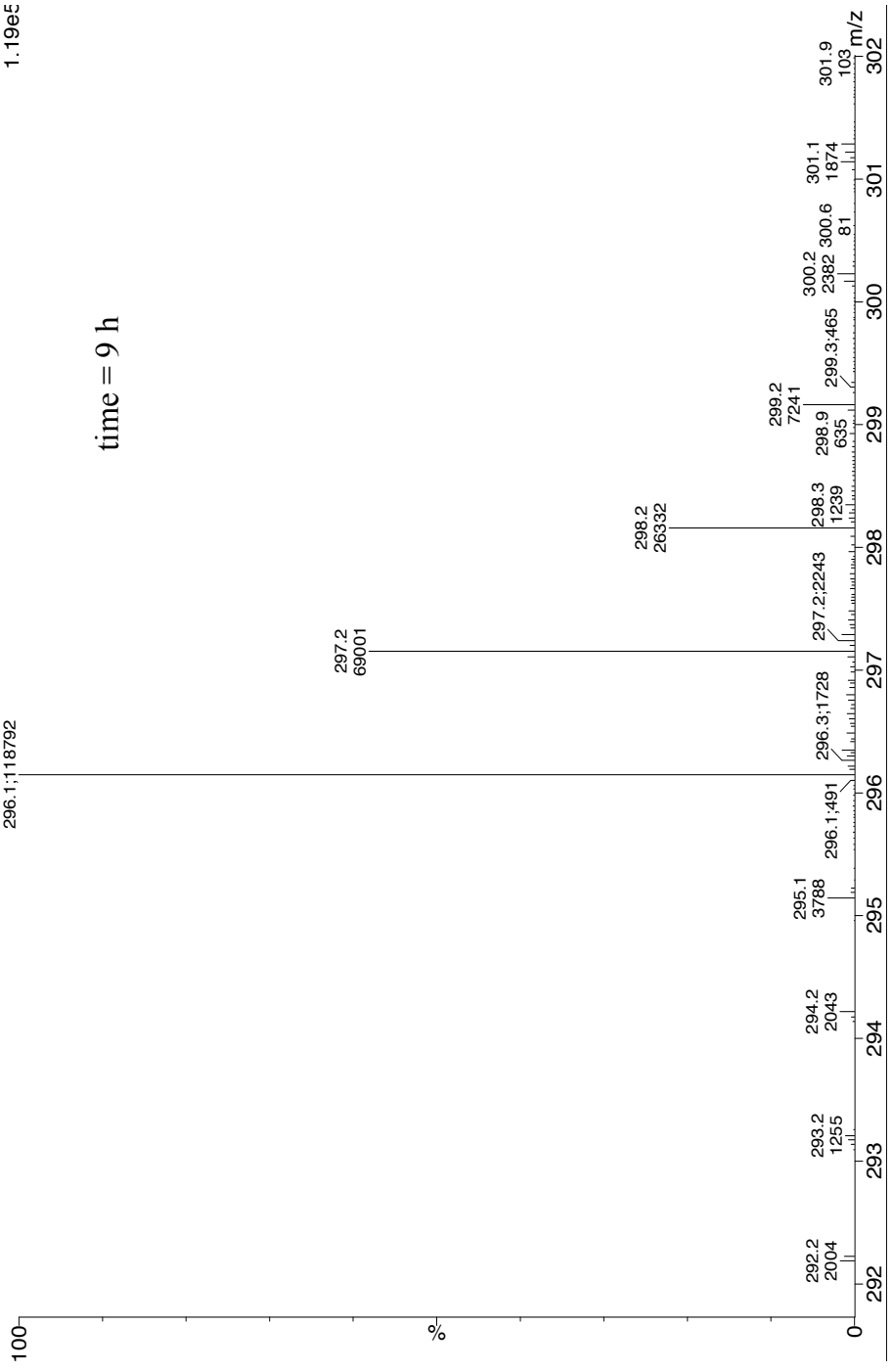


**Figure B.7** ESI$^+$-MS of *d*-DMAT products from IDI-1-4-DMATS coupled enzyme reaction.

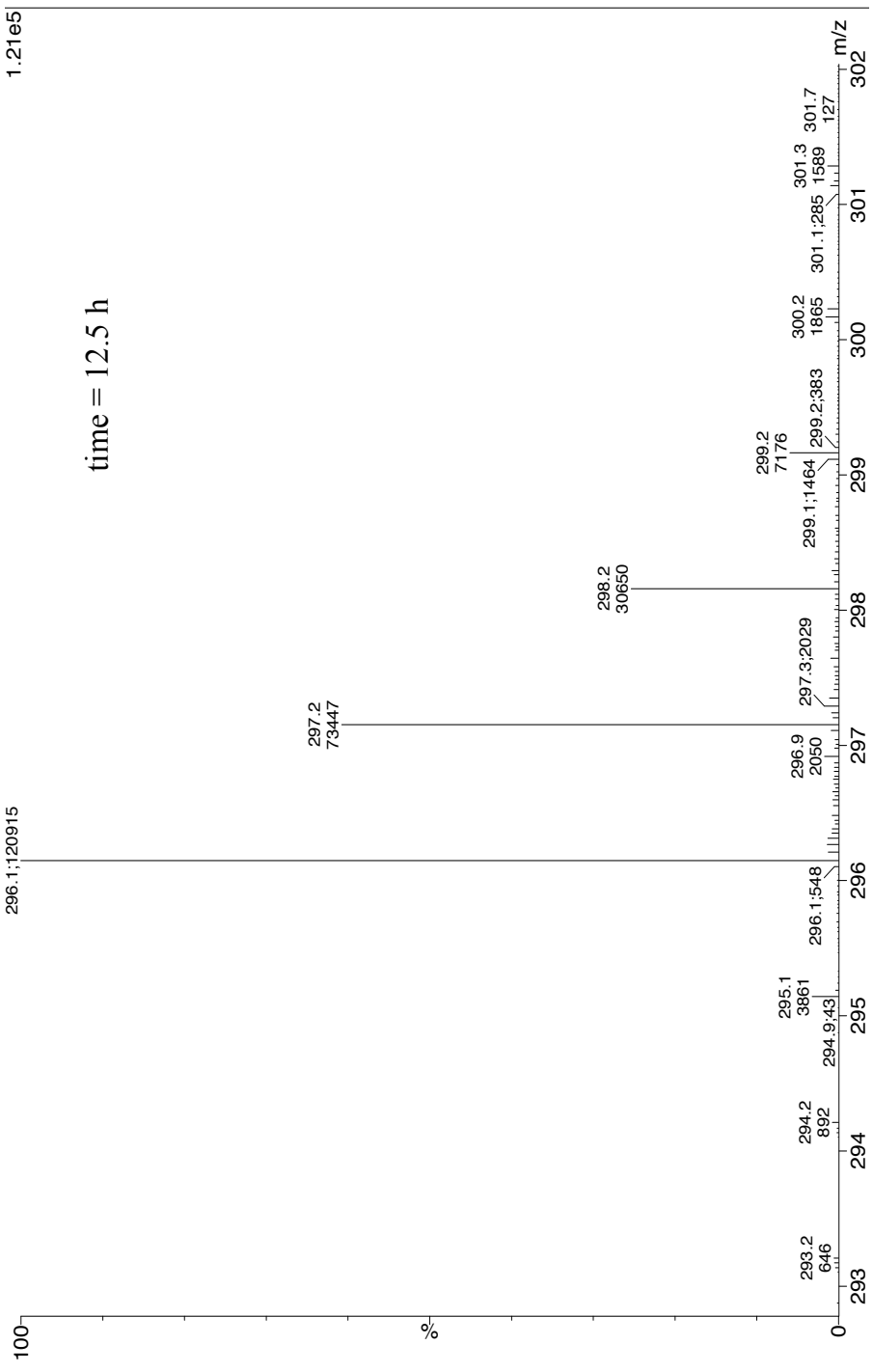


**Figure B.8** ESI$^+$-MS of *d*-DMAT products from IDI-1-4-DMATS coupled enzyme reaction.

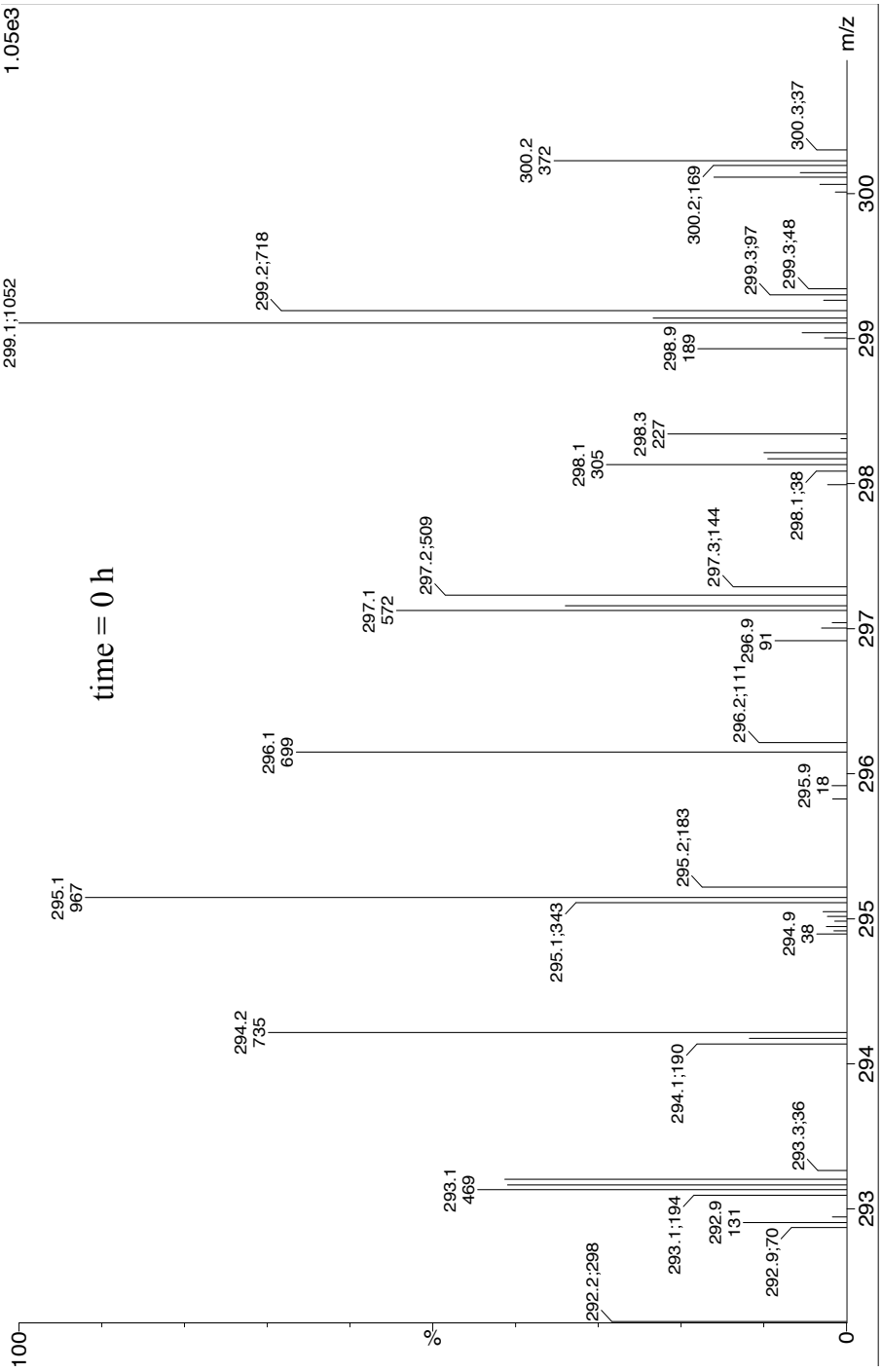


**Figure B.9** ESI$^+$-MS of *d*-DMAT products from IDI-2-4-DMATS coupled enzyme reaction.

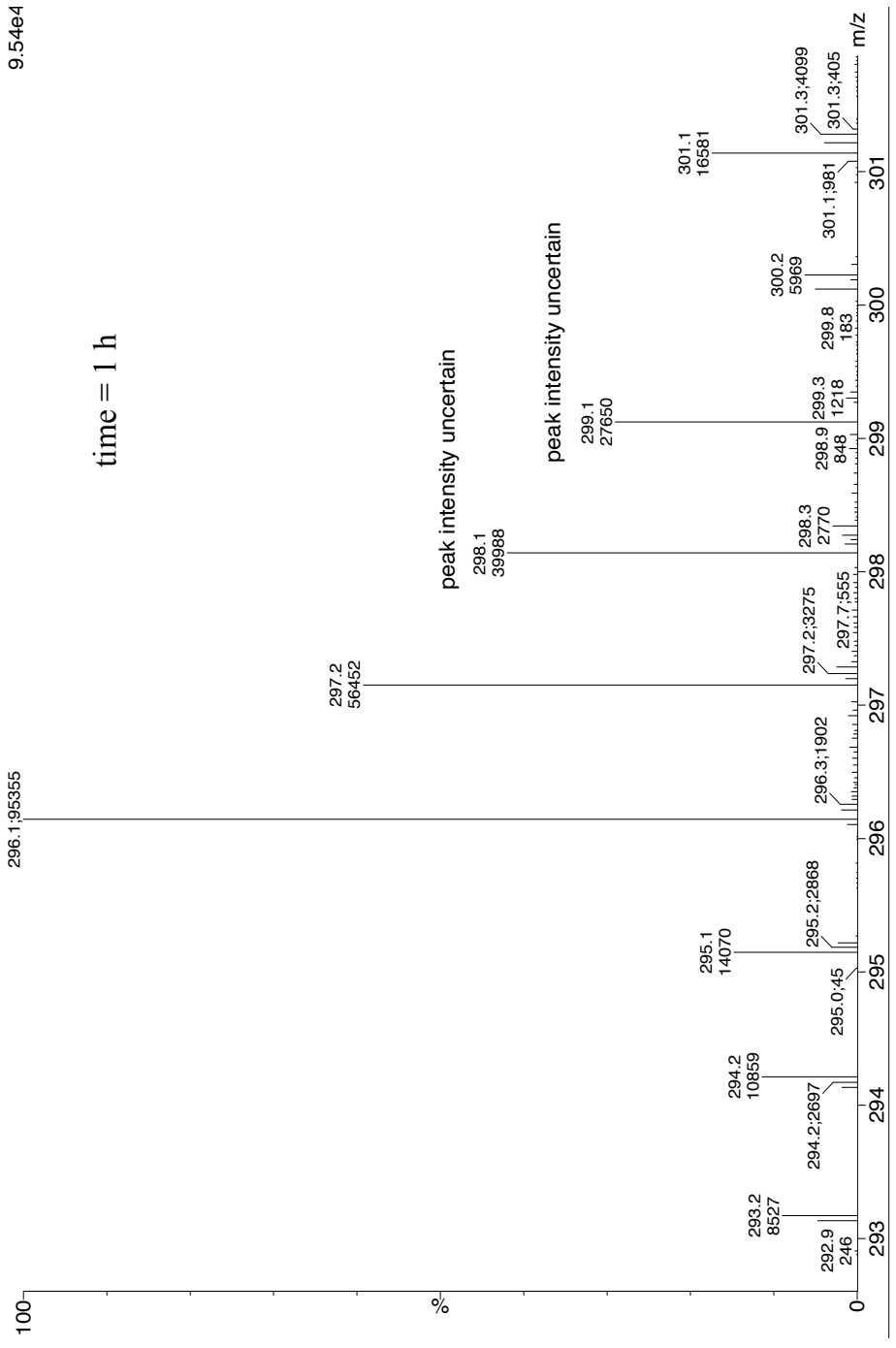


**Figure B.10** ESI$^+$-MS of *d*-DMAT products from IDI-2-4-DMATS coupled enzyme reaction.

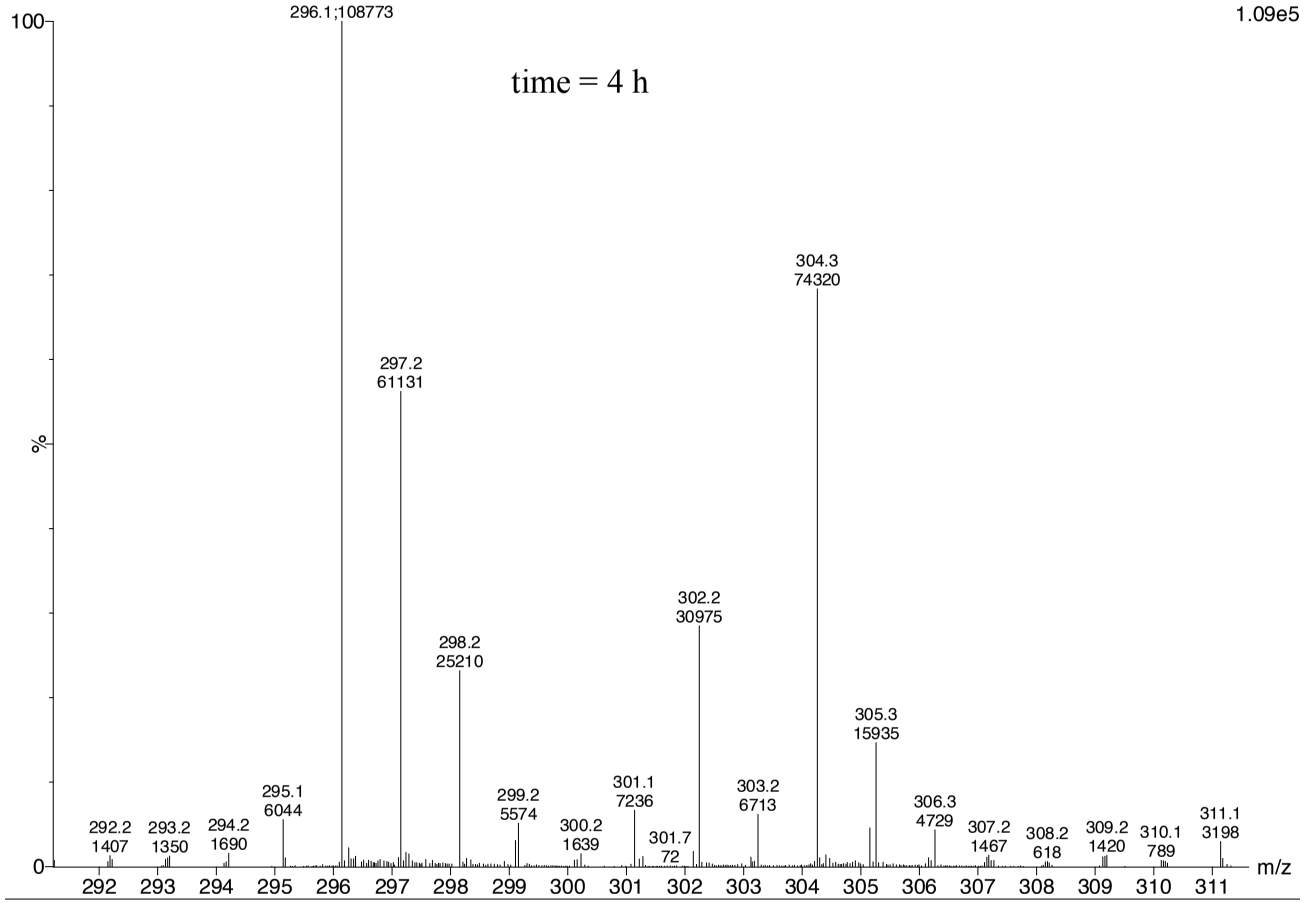


**Figure B.11** ESI$^+$-MS of *d*-DMAT products from IDI-2-4-DMATS coupled enzyme reaction.

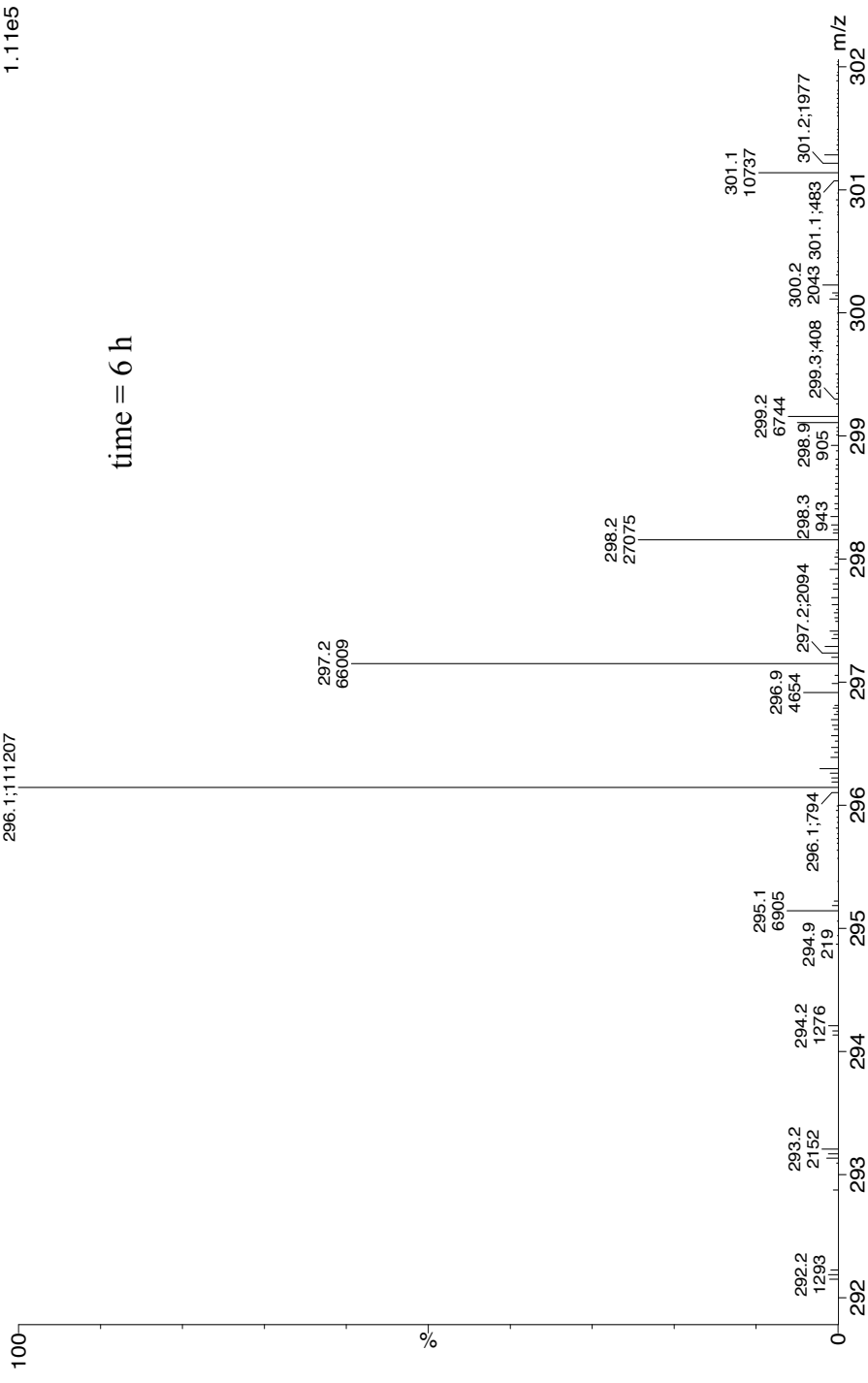


**Figure B.12** ESI$^+$-MS of *d*-DMAT products from IDI-2-4-DMATS coupled enzyme reaction.

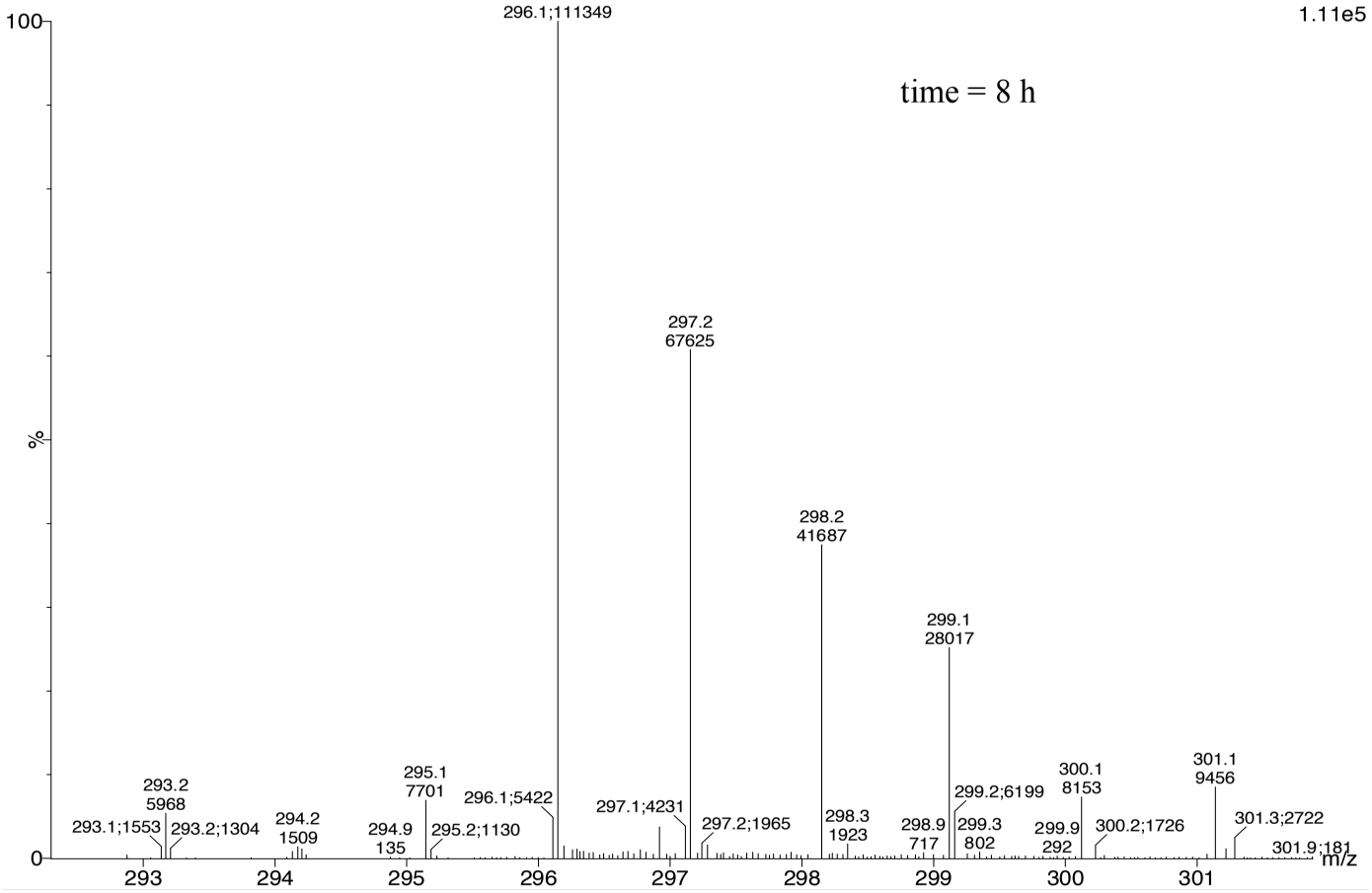


**Figure B.13** ESI$^+$-MS of *d*-DMAT products from IDI-2-4-DMATS coupled enzyme reaction.

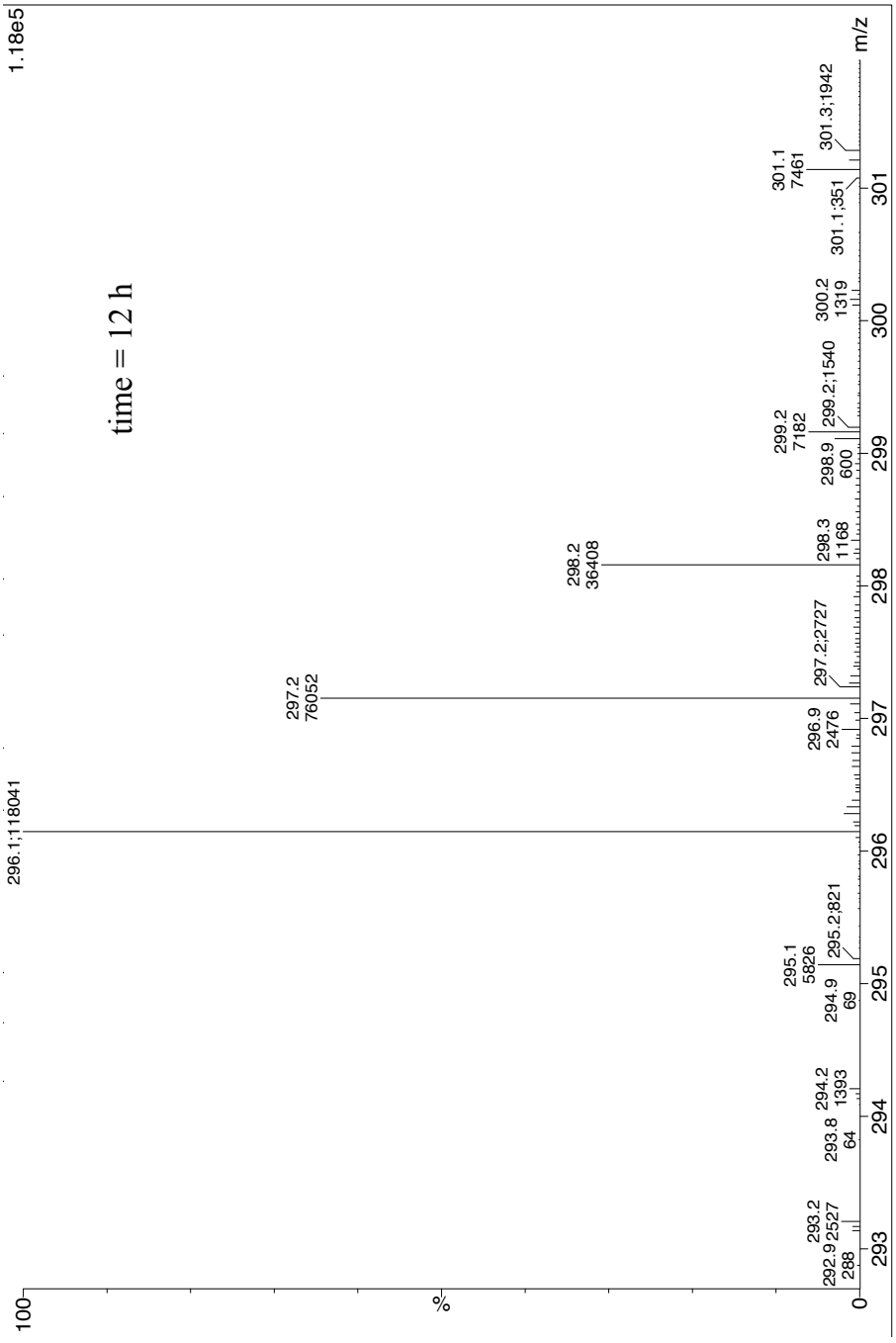


**Figure B.14** EST$^{+}$-MS of *d*-DMAT products from IDI-2-4-DMATS coupled enzyme reaction.

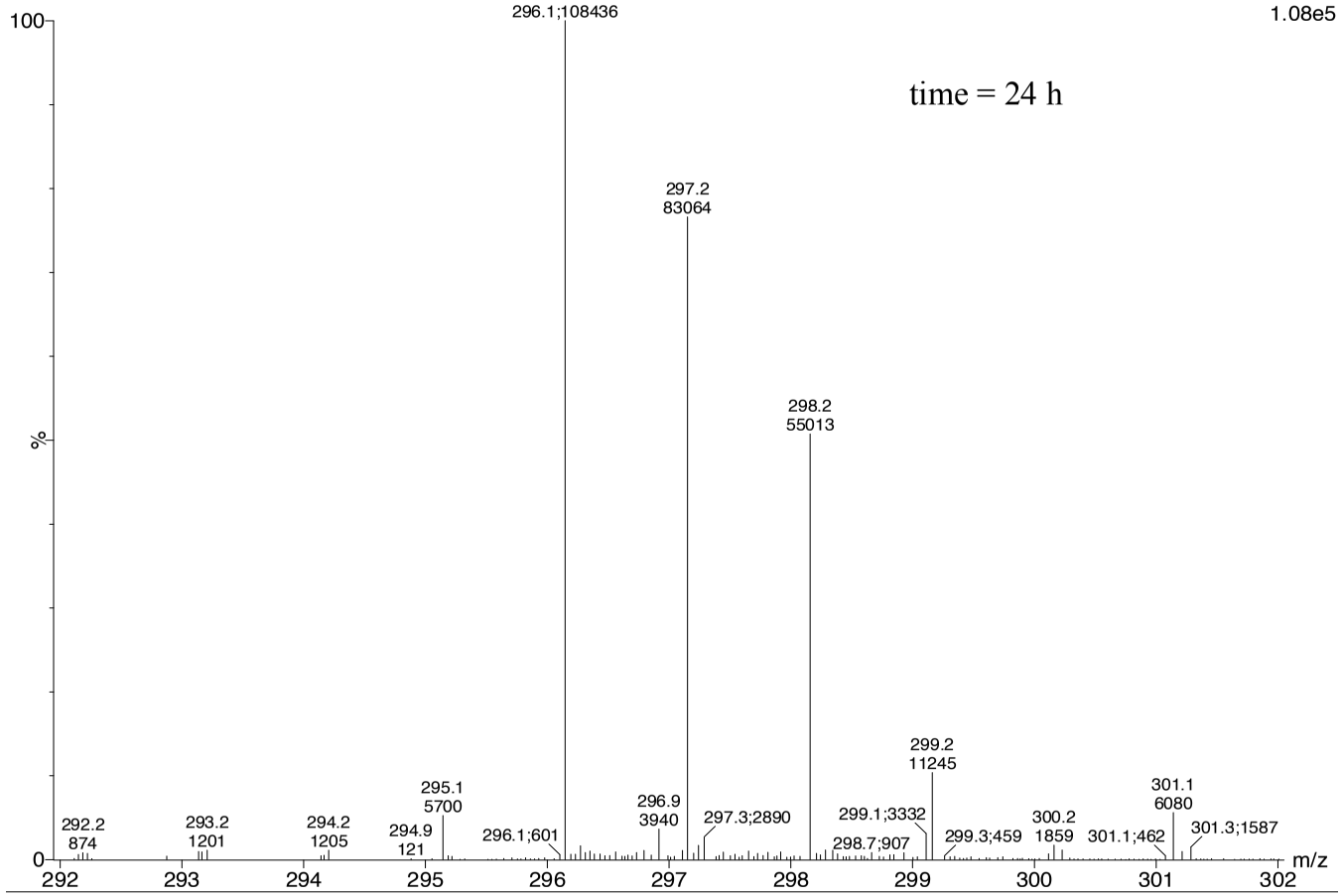


**Figure B.15** ESI$^+$-MS of *d*-DMAT products from IDI-2-4-DMATS coupled enzyme reaction.

# APPENDIX C

## MASS-SPECTRAL CHROMATOGRAMS OF IPP AND DEUTERATED-IPP

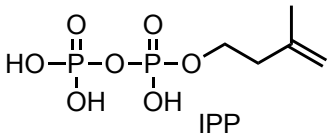

IPP

Molecular formula = $C_5H_{12}O_7P_2$

Exact mass = 244.9985 $[M-H]^-$

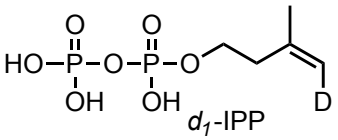

*d*$_1$-IPP

Molecular formula = $C_5H_{11}DO_7P_2$

Exact mass = 246.0048 $[M-H]^-$

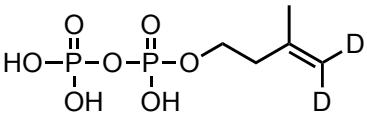

*d*$_2$-IPP

Molecular formula = $C_5H_{11}DO_7P_2$

Exact mass = 247.0111 $[M-H]^-$

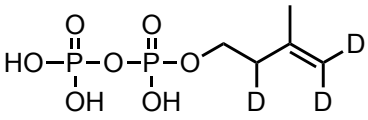

*d*$_3$-IPP

Molecular formula = $C_5H_{11}DO_7P_2$

Exact mass = 248.0174 $[M-H]^-$

**Masses of IPP and *d*-IPP**

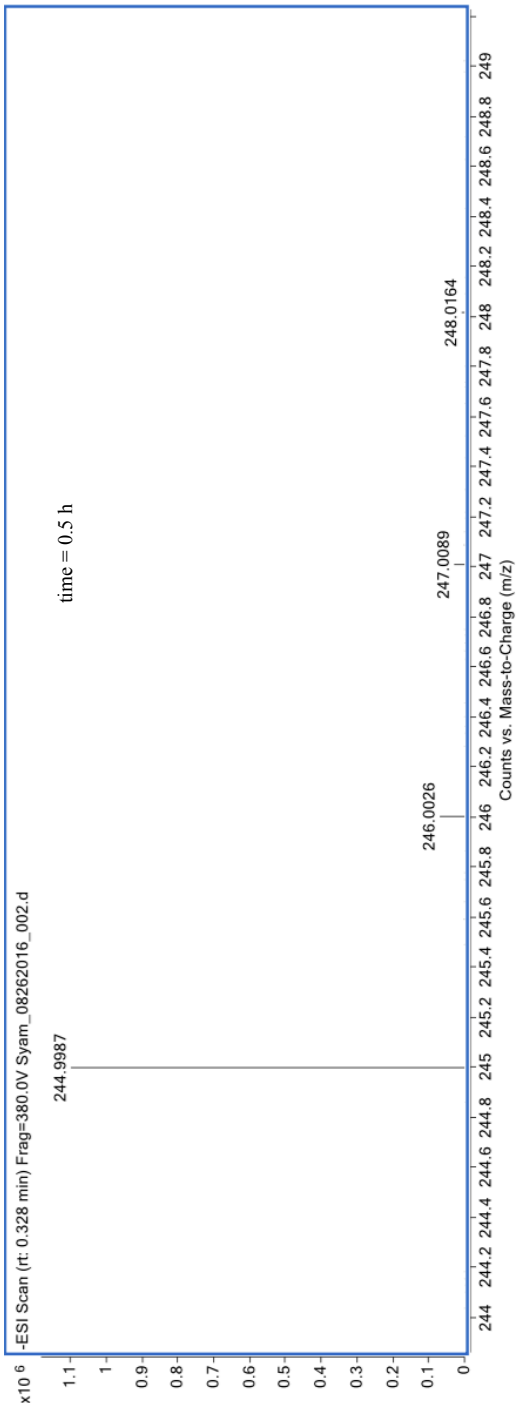


**Figure C.1** ESI-MS of IPP from IDI-1-4-DMATS coupled enzyme reaction.

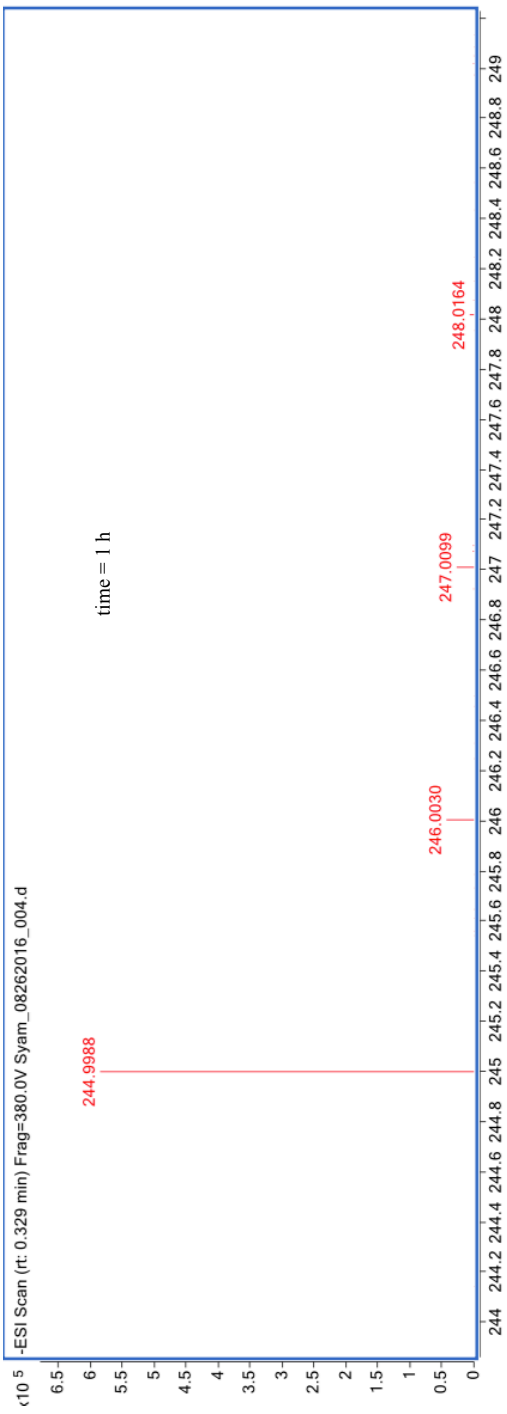


**Figure C.2** ESI-MS of IPP from IDI-1-4-DMATS coupled enzyme reaction.

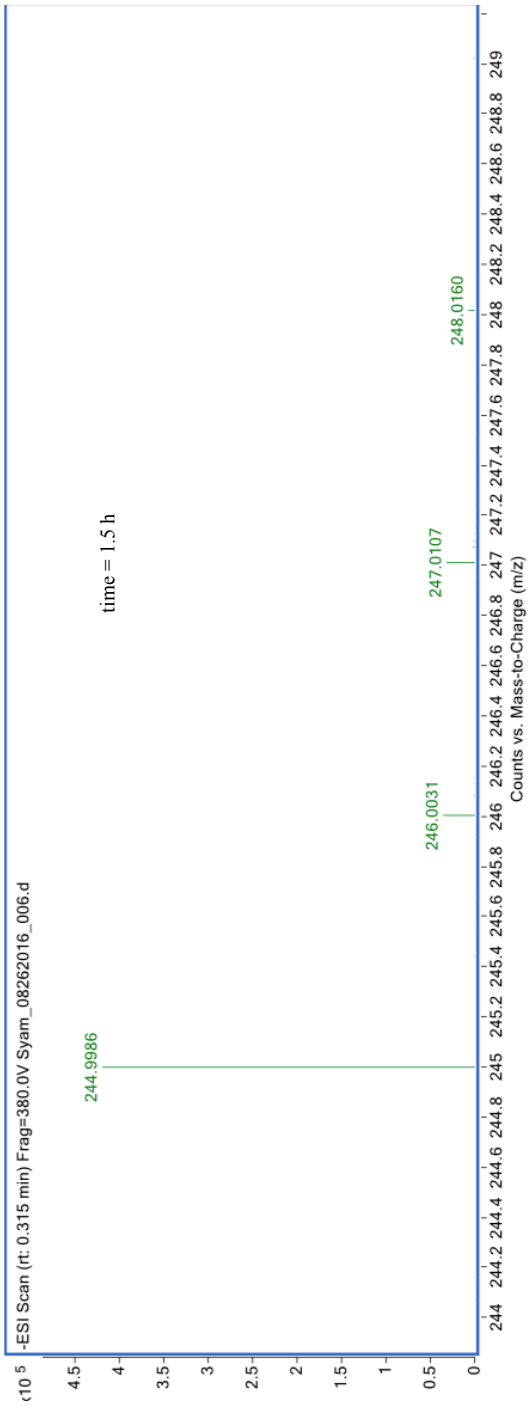


**Figure C.3** ESI-MS of IPP from IDI-1-4-DMATS coupled enzyme reaction.

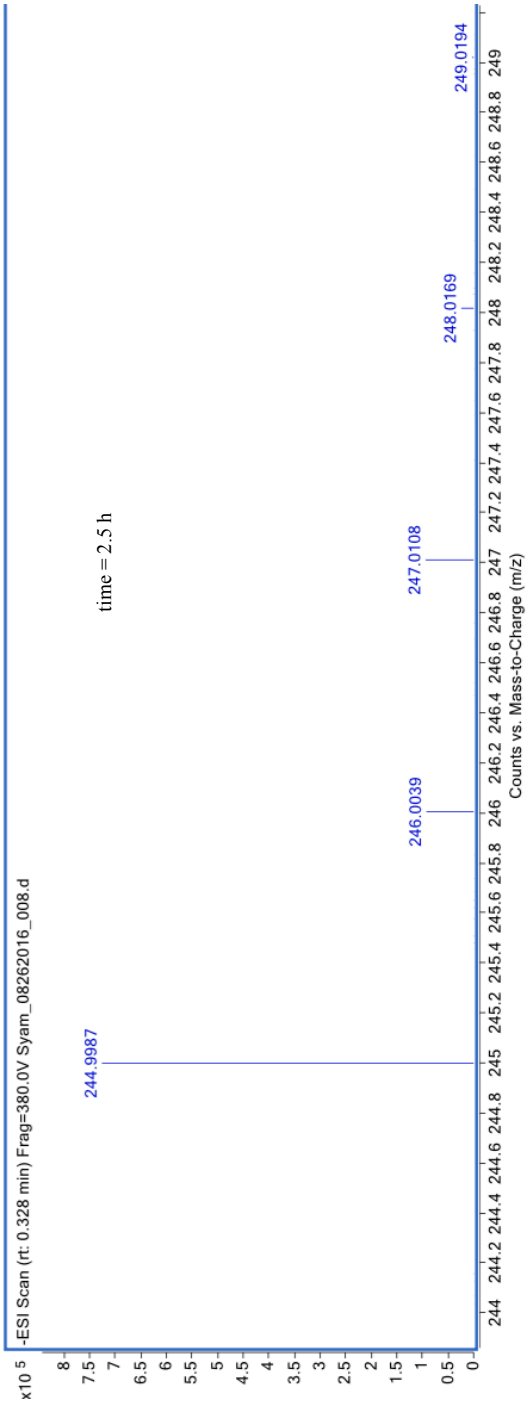


**Figure C.4** ESI-MS of IPP from IDI-1-4-DMATS coupled enzyme reaction.

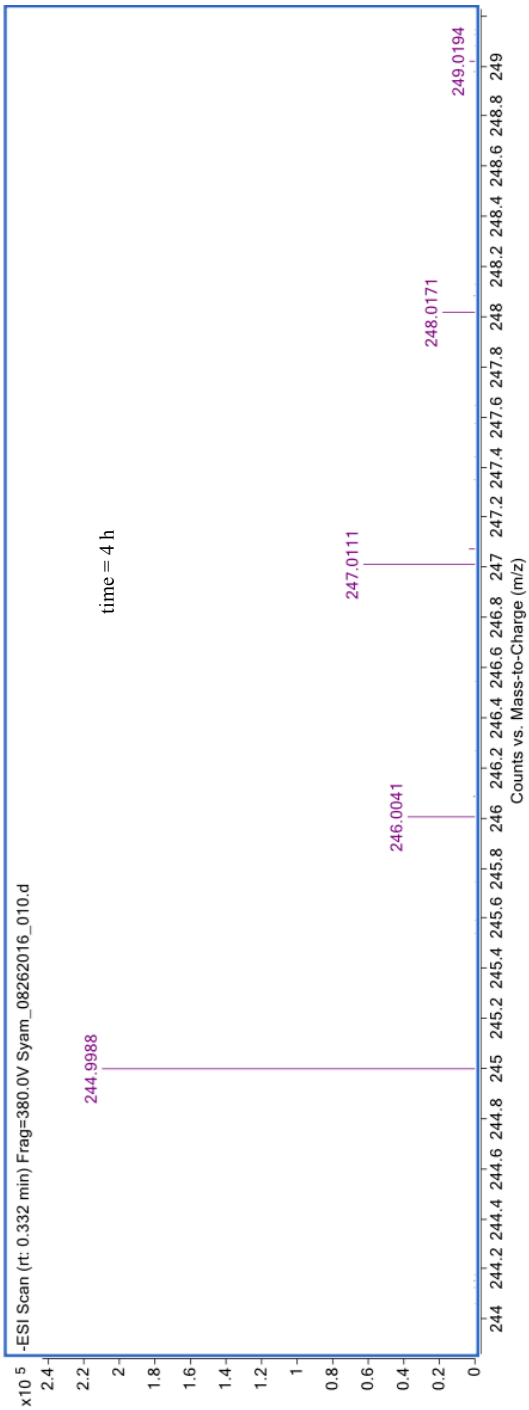


**Figure C.5** ESI$^-$-MS of IPP from IDI-1-4-DMATS coupled enzyme reaction.

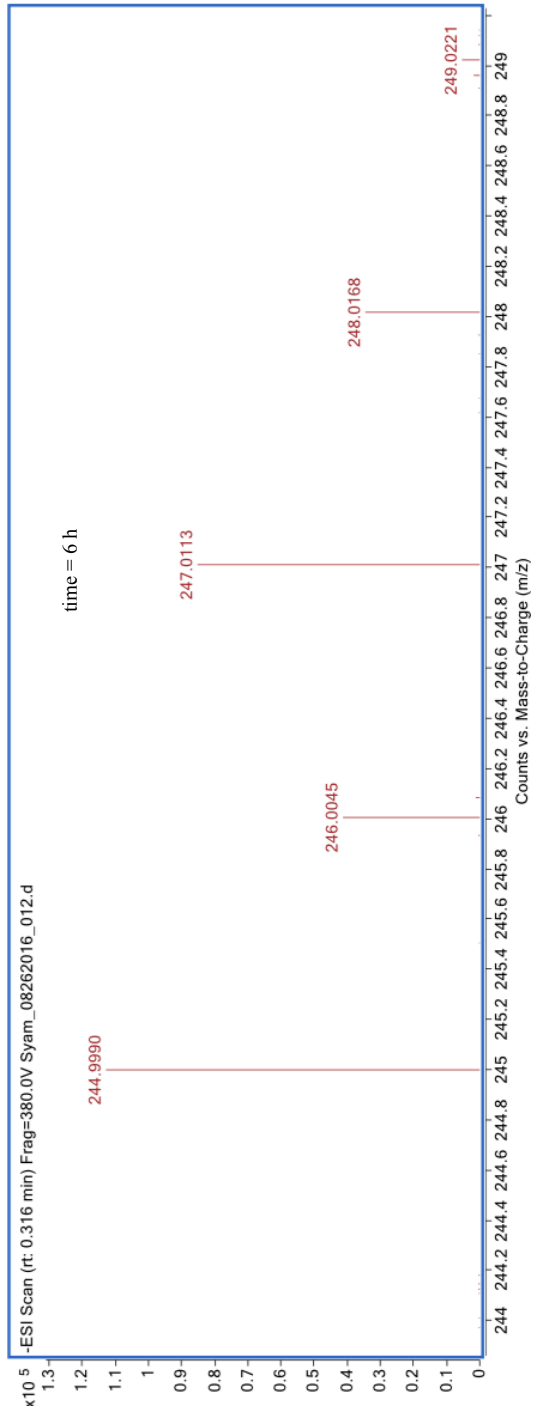


**Figure C.6** ESI-MS of IPP from IDI-1-4-DMATS coupled enzyme reaction.

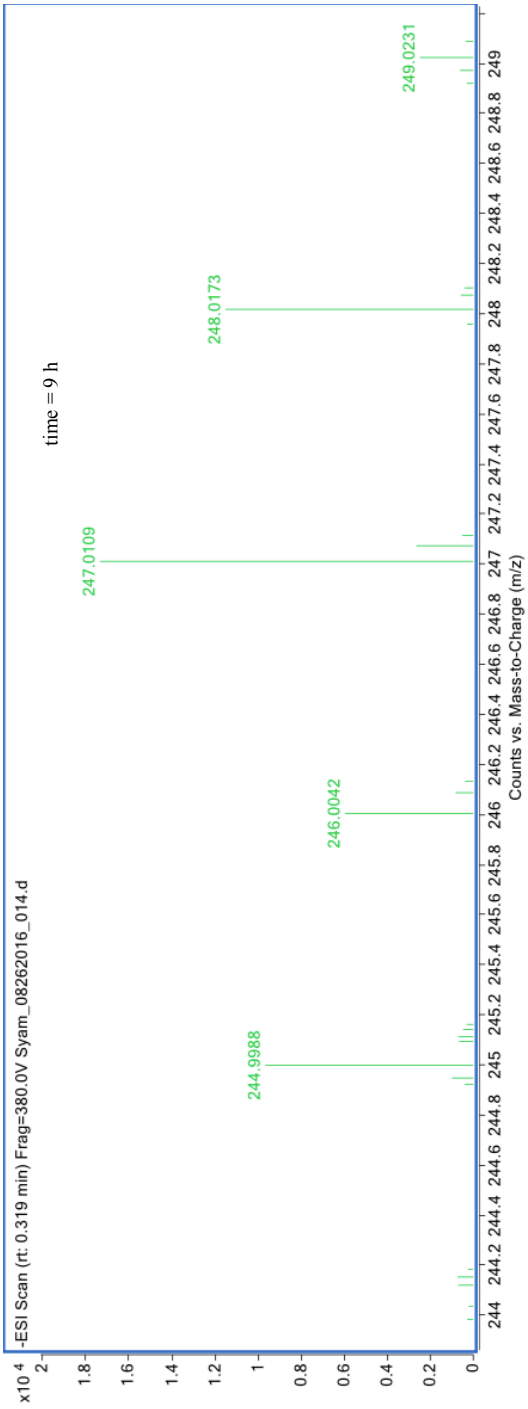


**Figure C.7** ESI-MS of IPP from IDI-1-4-DMATS coupled enzyme reaction.

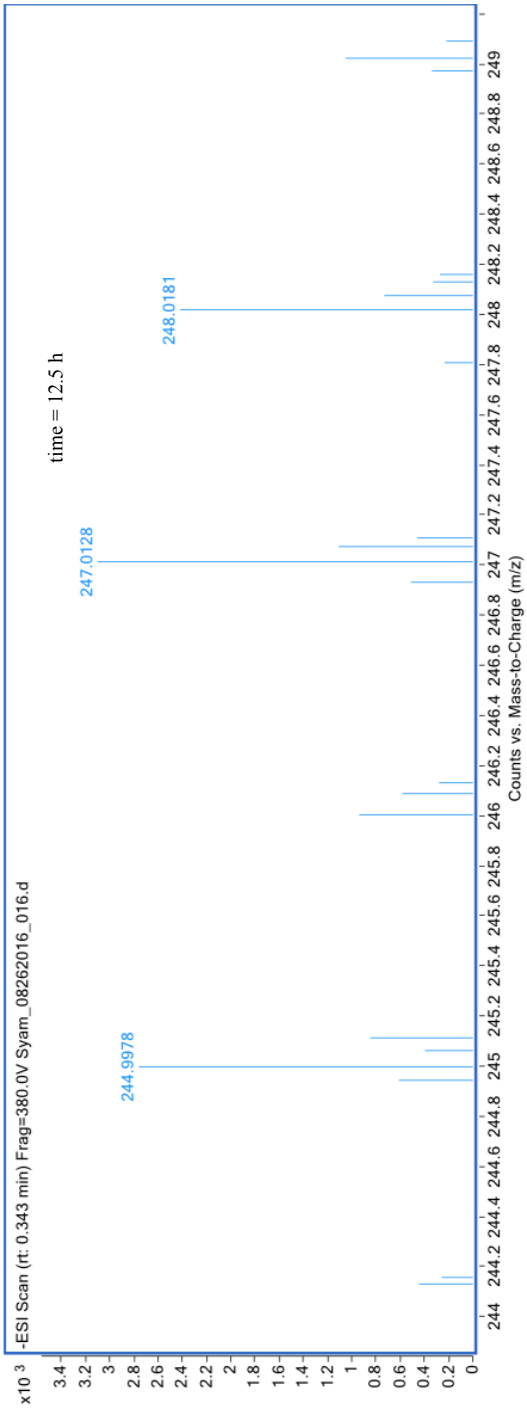


**Figure C.8** ESI-MS of IPP from IDI-1-4-DMATS coupled enzyme reaction.

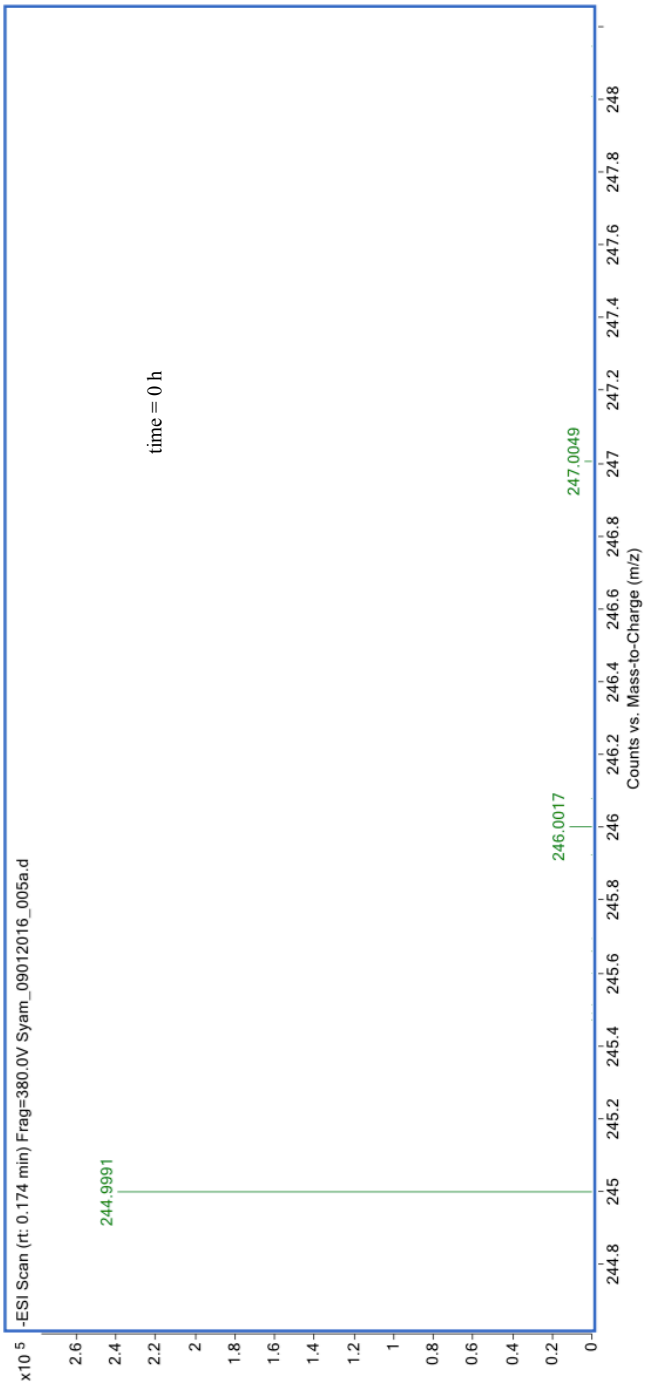


**Figure C.9** ESI-MS of IPP from IDI-2-4-DMATS coupled enzyme reaction.

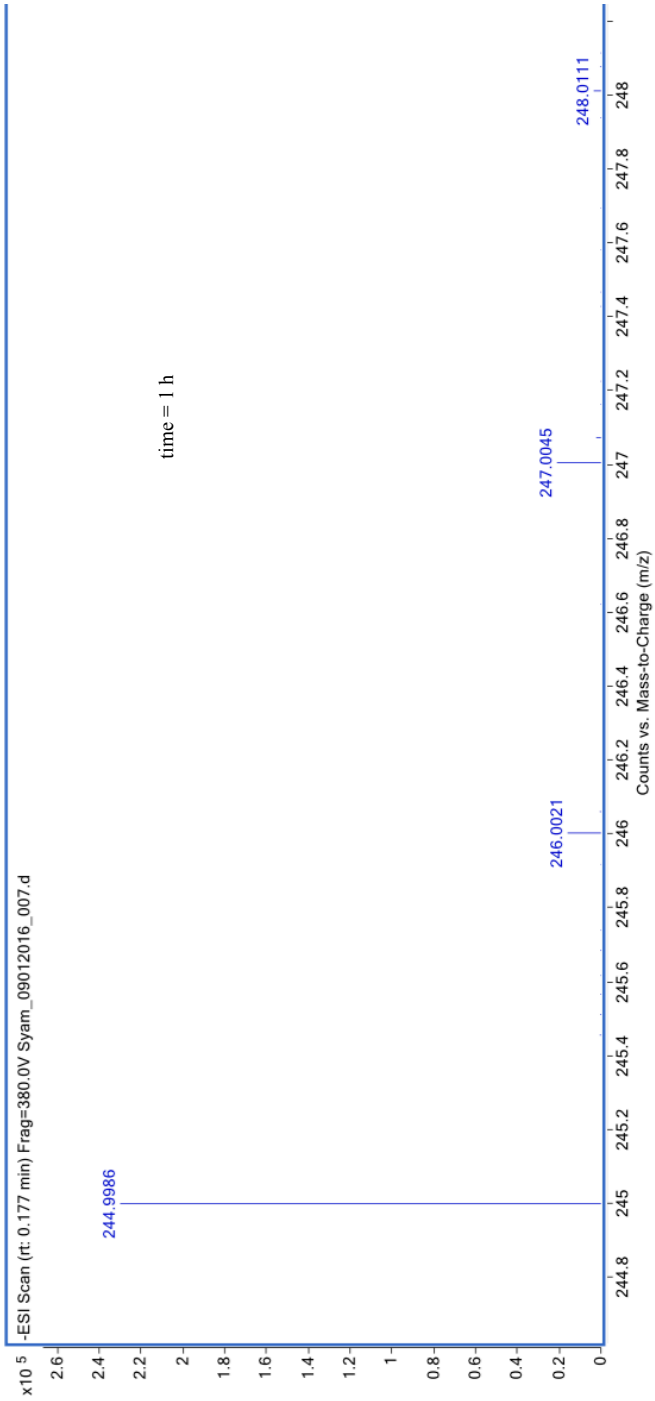


**Figure C.10** ESI-MS of IPP from IDI-2-4-DMATS coupled enzyme reaction.

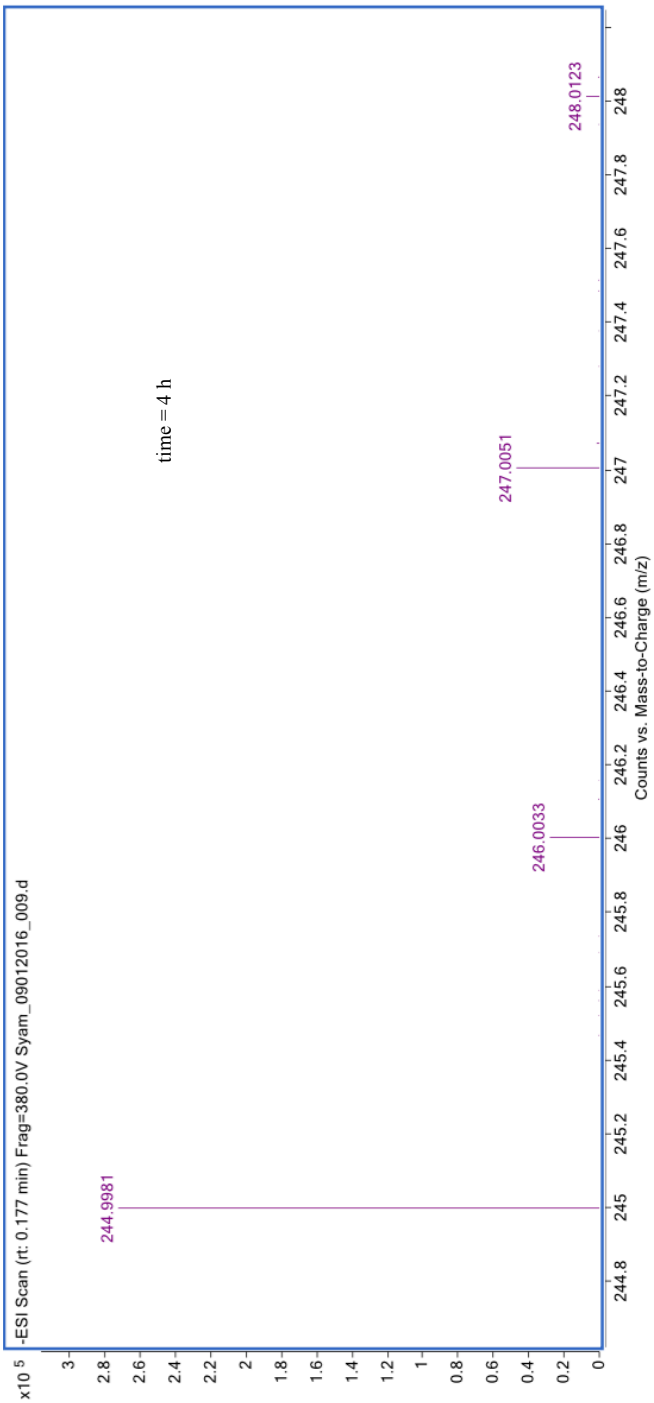


**Figure C.11** ESI-MS of IPP from IDI-2-4-DMATS coupled enzyme reaction.

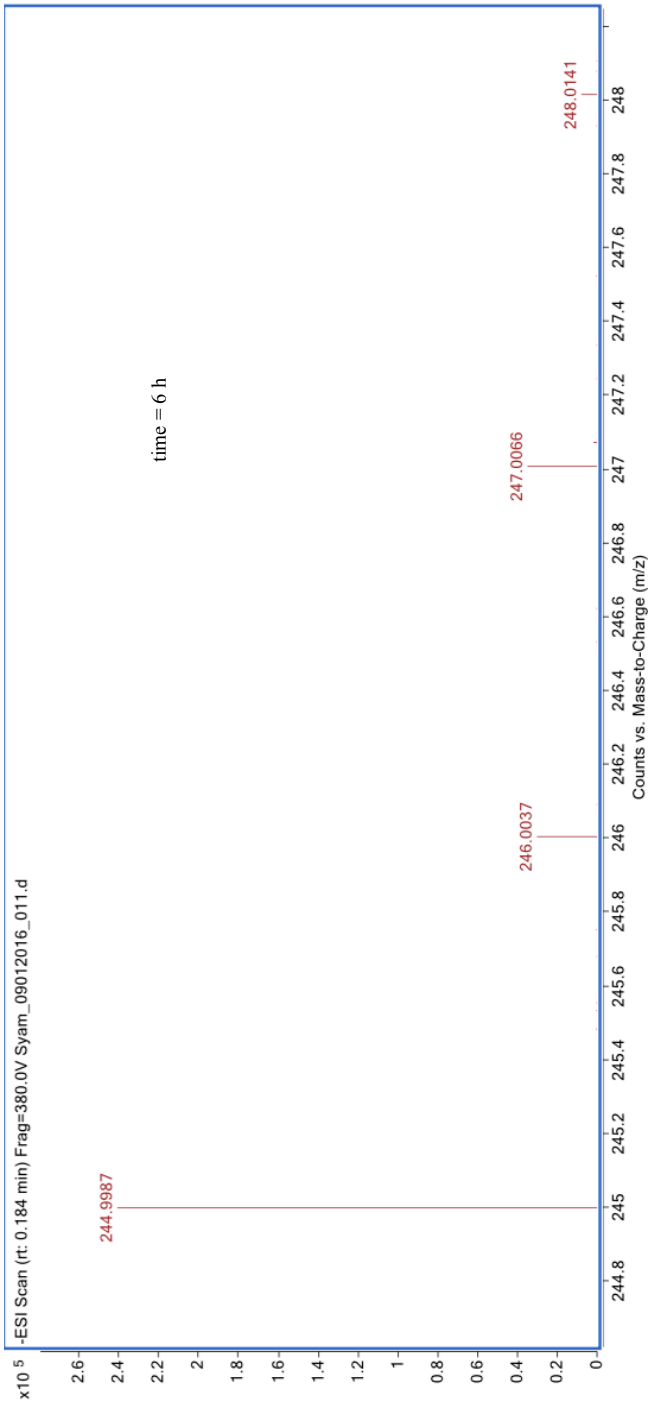


**Figure C.12** ESI-MS of IPP from IDI-2-4-DMATS coupled enzyme reaction.

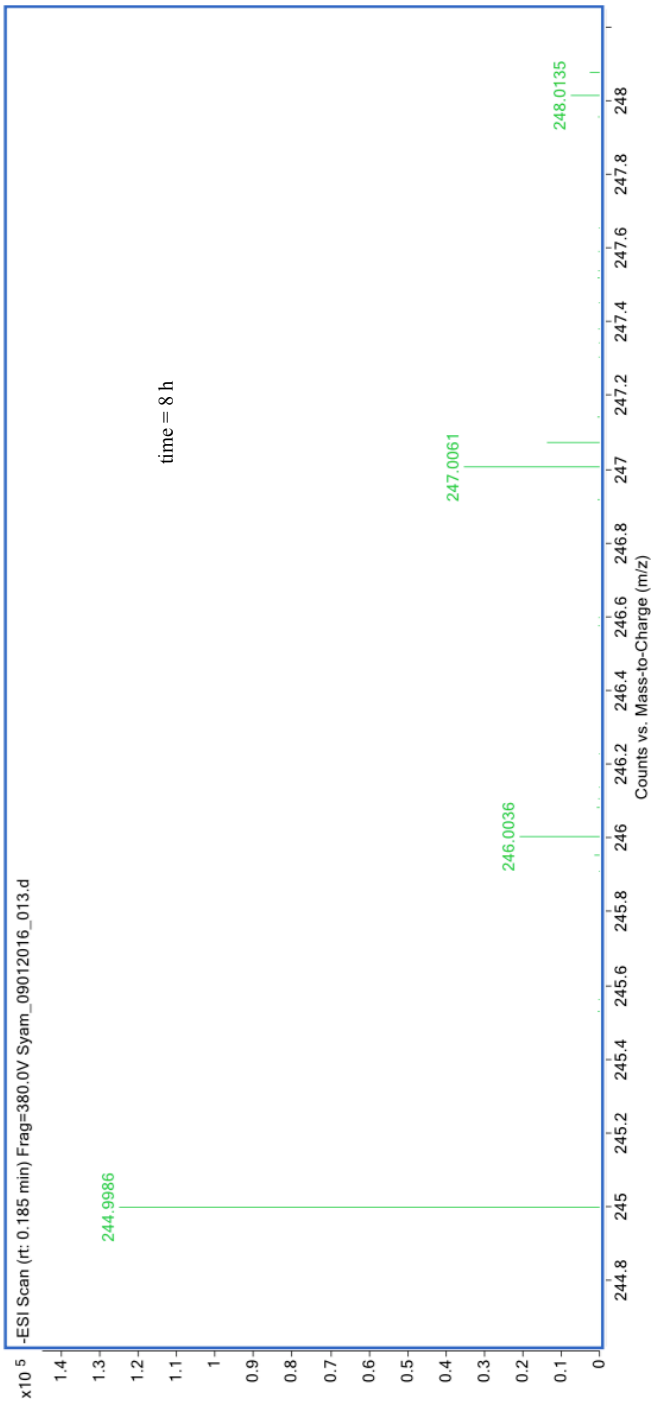


**Figure C.13** ESI-MS of IPP from IDI-2-4-DMATS coupled enzyme reaction.

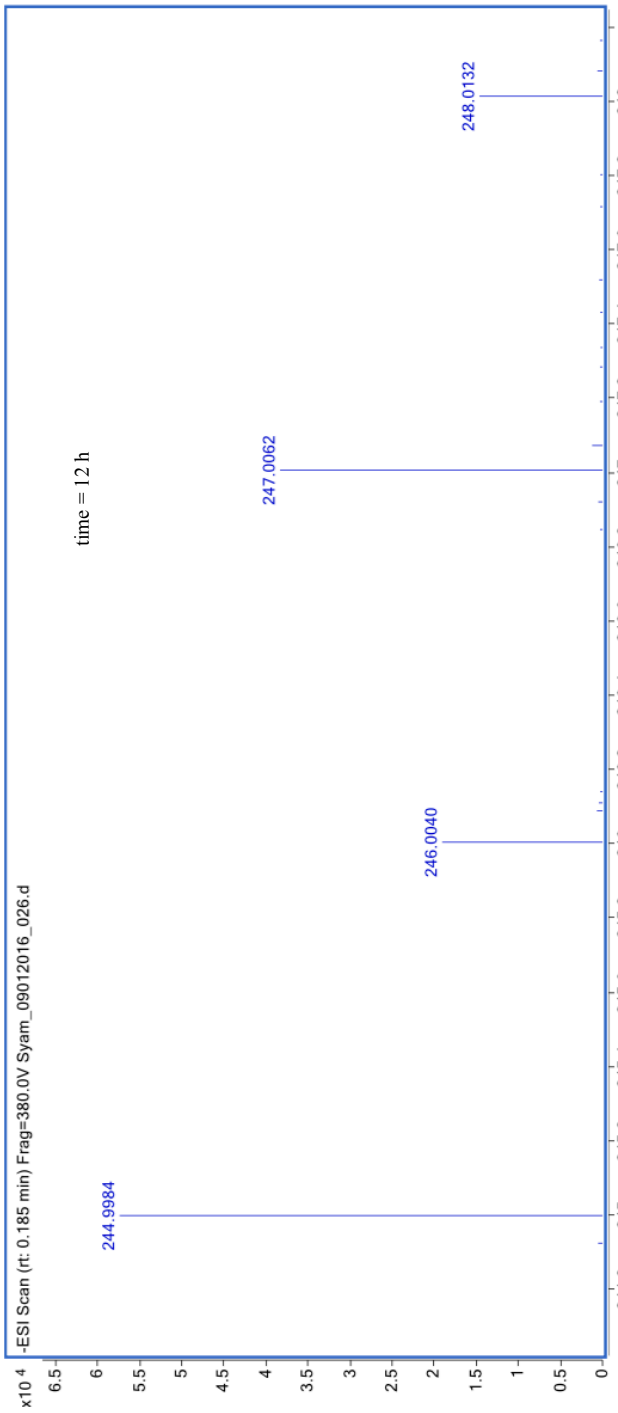


**Figure C.14** ESI-MS of IPP from IDI-2-4-DMATS coupled enzyme reaction.

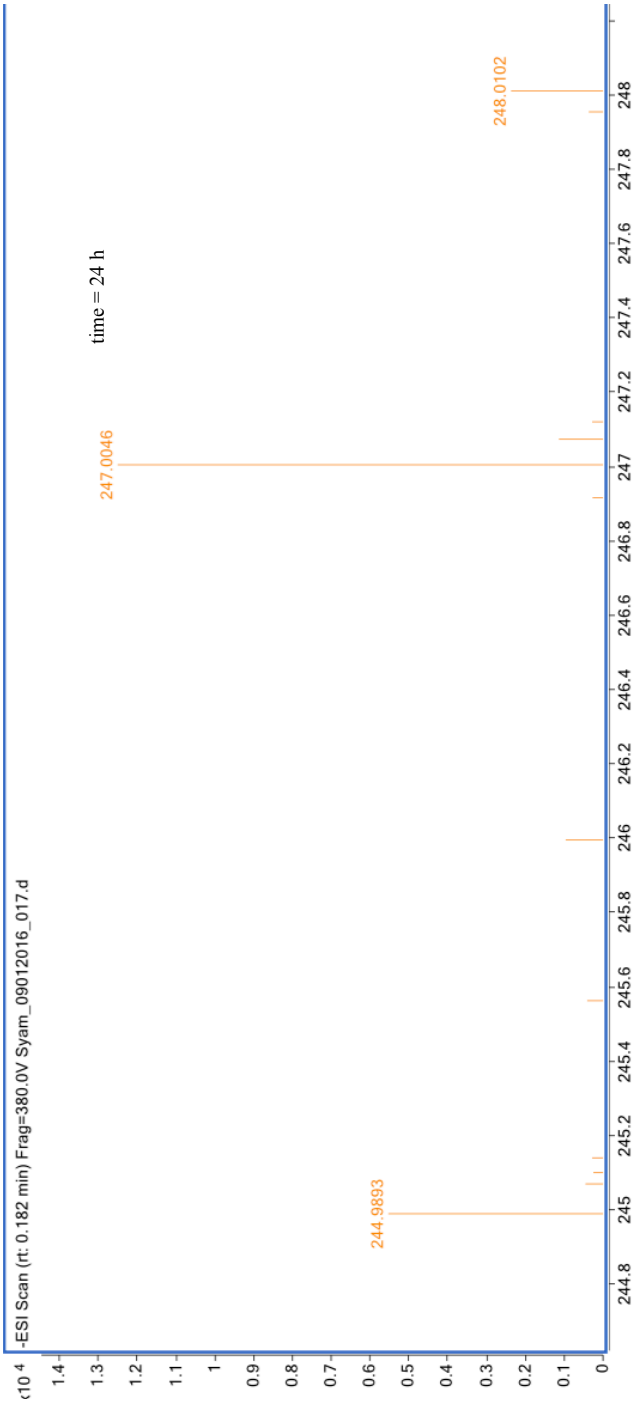


**Figure C.15** ESI-MS of IPP from IDI-2-4-DMATS coupled enzyme reaction.

REFERENCES


1) *Dictionary of Natural Products* [Online]; 25.1. Taylor & Francis Group. http://dnp.chemnetbase.com (accessed July 30, 2016).

2) Porter, J. W.; Spurgeon, S. L. Conversion of Acetyl Coenzyme A to Isopentenyl Pyrophosphate. In *Biosynthesis of Isoprenoid Compounds;* Porter J. W., Spurgeon, S. L. Eds.; John Wiley and Sons, New York, NY, 1981; pp 1-93.

3) Bautista, D. M.; Siemens, J.; Glazer, J. M. Tsuruda, P. R.; Basbaum, A. I.; Stucky, C. L.; Jordt, S.-E.; Julius, D. The Menthol Receptor TRPM8 is the Principal Detector of Environmental Cold. *Nature* **2007**, *448,* 204-208.

4) Rasmann, S.; Kollner, T. G.; Degenhardt, J.; Hiltpold, I.; Toepfer, S.; Kuhlmann, U.; Gerschenzon, J.; Turlings, T. C. J. Recruitment of Entomopathogeni Nematodes by Insect-Damaged Maize Roots. *Nature* **2005**, *434,* 732-737.

5) White N. J. Assessment of the Pharmacodynamic Properties of Antimalarial Drugs *in vivo*. *Antimicrob. Agents Chemother.* **1997**, *41*, 1413–22

6) Springob, K.; Kutchan, T. M. Introduction to the Different Classes of Natural Products. In *Plant-derived Natural Products*; Osbourn, A. E., Lanzotti, V., Eds.; Springer US, New York, NY, 2009; pp 3-50.

7) Nambara, E.; Annie, M-p. Abscisic Acid Biosynthesis and Catabolism. *Annu Rev. Plant. Biol*. **2005**, *56*, 165–85.

8) Pennock, J. F.; Threlfall, D. R. Biosynthesis of Ubiquinone and Related Compounds. In *Biosynthesis of Isoprenoid Compounds*; Porter, J. W., Spurgeon, S. L. Eds.; John Wiley & Sons, New York, NY, 1983; pp 191-303.

9) Burri, B. J. Beta-carotene and Human Health: A Review of Current Research. *Nutr. Res.* **1997**, *17,* 547-580.

10) Krishnani, K. K.; Ravichandran, P.; and Ayyappan, S. Microbially Derived Off-Flavor from Geosmin and 2-Methylisoborneol: Sources and Remediation. In *Reviews of Environmental Contamination and Toxicology*; Whitacre, D. M., Ed.; Springer, New York, NY, 2008; pp 1-27.

11) Van Cleemput, M.; Cattoor, K.; De Bosscher, K.; Haegeman, G.; De Keukeleire, D.;

Heyerick, A. Hop *(Humulus* lupulus)-Derived Bitter Acids as Multipotent Bioactive Compounds. *J. Nat. Prod.* **2009**, *72,* 1220-1230.

12) Ogura, K.; Koyama, T. Enzymatic Aspects of Isoprenoid Chain Elongation. *Chem. Rev.* **1998**, *98*, 1263-1276.

13) Kellogg, B. A.; Poulter, C. D. Chain Elongation in the Isoprenoid Biosynthetic Pathway. *Curr. Opin. Chem. Biol.* **1997**, *1*, 570-578.

14) Poulter, C. D.; Rilling, H. C. The Prenyl Transfer Reaction. Enzymic and Mechanistic Studies of the 1'-4 Coupling Reaction in the Terpene Biosynthetic Pathway. *Acc. Chem. Res.* **1978**, *11*, 307-313.

15) Poulter, C. D.; Rilling, H. C. Prenyl Transferases and Isomerase. In *Biosynthesis of Isoprenoid Compounds*; Porter, J. W., Spurgeon, S. L. Eds.; John Wiley & Sons, New-York, NY, 1981; p. 161.

16) Poulter, C. D. Farnesyl Diphosphate Synthase. A Paradigm for Understanding Structure and Function Relationships in *E*-polyprenyl Diphosphate Synthases. *Phytochem. Rev.* **2006**, *5*, 17-26.

17) Wang, K. C.; Ohnuma, S. Isoprenyl Diphosphate Syntheses. *Biochim. Biophys. Acta* **2000**, 1529, 33-48.

18) Bloch, K. The Biological Synthesis of Cholesterol. *Science* **1965**, *150*, 19-28.

19) Chaykin, S.; Law, J.; Phillips, A. H.; Tchen, T. T.; Bloch, K. Phosphorylated Intermediates in the Synthesis of Squalene. *Proc. Natl. Acad. Sci. USA* **1958**, *44*, 998-1004.

20) Bloch, K.; Chaykin, S.; Phillips, A. H.; de Waard, A. Mevalonicacid Pyrophosphate and Isopentenylpyrophosphate. *J. Biol. Chem.* **1959**, *234*, 2595-2604.

21) Lynen, F.; Eggerer, H.; Henning, U.; Kessel, I. Farnesyl-Pyrophosphat und 3-Methyl-$\Delta^3$-butenyl-1-pyrophosphat, die Biologischen Vorstufen des Squalens. Zur Biosynthese der Terpene, III. *Angew. Chem.* **1958**, *70*, 738- 742.

22) Beytia, E. D.; Porter, J. W. Biochemistry of Polyisoprenoid Biosynthesis. *Annu. Rev. Biochem.* **1976**, *45*, 113-142.

23) Rohmer, M.; Seeman, M.; Horback, S.; Bringer-Meyer, S.; Sahm, H. Glyceraldehyde 3-Phosphate and Pyruvate as Precursors of Isoprenic Units in an Alternative Non-Mevalonate Pathway for Terpenoid Biosynthesis. *J. Am. Chem. Soc.* **1996**, *118*, 2564.

24**)** Rohmer, M. The Discovery of a Mevalonate-Independent Pathway for Isoprenoid Biosynthesis in Bacteria, Algae, and Higher Plants. *Nat. Prod. Rep.* **1999***, 16*, 565-574.

25) Laupitz, R.; Hecht, S.; Amslinger, S.; Zepeck, F.; Kaiser, J.; Richter, G.; Schramek, N.; Steinbacher, S.; Huber, R.; Arigoni, D.; Bacher, A.; Eisenreich, W.; Rohdich, F. Biochemical Characterization of Bacillus Subtilis Type II Isopentenyl Diphosphate Isomerase, and Phylogenetic Distribution of Isoprenoid Biosynthesis Pathways. *Eur. J. Biochem.* **2004**, *271*, 2658-2669.

26) Rodriguez-Concepcion, M. The MEP pathway: A New Target for the Development of Herbicides, Antibiotics and Antimalarial Drugs. *Curr. Pharm. Des.* **2004**, *10*, 2391-2400.

27) Singh, N.; Cheve, G.; Avery, M. A.; McCurdy, C. R. Targeting the Methyl Erythritol Phosphate (MEP) Pathway for Novel Antimalarial, Antibacterial and Herbicidal Drug Discovery: Inhibition of 1-Deoxy-D-Xylulose-5-Phosphate Reductoisomerase (DXR) Enzyme. *Curr. Pharm. Des.* **2007***, 13*, 1161-1177.

28) Rohdich, F.; Bacher, A.; Eisenreich, W. Perspectives in Anti-infective Drug Design. The Late Steps in the Biosynthesis of the Universal Terpenoid Precursors, Isopentenyl Diphosphate and Dimethylallyl Diphosphate. *Bioorg. Chem.* **2004**, *32*, 292-308.

29) Gibson, D. M.; Parker, R. A. Hydroxymethylglutaryl-Coenzyme A Reductase. In *The Enzymes*; Boyer, P. D., Krebs, E. G., Eds.; Academic Press, New York, NY, 1987; pp 179- 215.

30) Istvan, E. S.; Deisenhofer, J. Structural Mechanism for Statin Inhibition of HMG-CoA Reductase. *Science* **2001**, *292*, 1160-1164.

31) Timson, D. J. GHMP Kinases-Structures, Mechanisms, and Potential for Therapeutically Relevant Inhibition. *Curr. Enzy. Inhib.* **2007**, *3*, 77-94.

32) Krepkiy, D.; Miziorko, H. M. Investigation of the Functional Contributions of Invariant Serine Residues in Yeast Mevalonate Diphosphate Decarboxylase. *Biochemistry* **2005**, *44*, 2671-2677.

33) Byres, E.; Alphey, M. S.; Smith, T. K.; Hunter, W. N. Crystal Structures of *Trypanosoma brucei* and *Staphylococcus aureus* Mevalonate Diphosphate Decarboxylase Inform on the Determinants of Specificity and Reactivity. *J. Mol. Biol.* **2007**, *371*, 540-553.

34) Chen, M., and Poulter, C. D. Characterization of Thermophilic Archaeal Isopentenyl Phosphate Kinases. *Biochemistry* **2010**, *49,* 207-217.

35) Agranoff, B. W.; Eggerer, H.; Henning, U.; Lynen, F. Isopentenol Pyrophosphate Isomerase. *J. Am. Chem. Soc.* **1959**, *81*, 1254-1255.

36) Rohdich, F.; Hecht, S.; Bacher, A.; Eisenreich, W. The Deoxyxylulose Phosphate Pathway of Isoprenoid Biosynthesis. Discovery and Function of *ispDEFGH* Genes and their Cognate Enzymes. *Pure Appl. Chem.* **2003**, *75*, 393-405.

37) Rohmer, M. Mevalonate-independent Methylerythritol Phosphate Pathway for Isoprenoid Biosynthesis. Elucidation and Distribution. *Pure Appl. Chem.* **2003**, *75*, 375-387.

38) Kuzuyama, T. Mevalonate and Nonmevalonate Pathways for the Biosynthesis of Isoprene Units. *Biosci. Biotechnol. Biochem.* **2002**, *66*, 1619-1627.

39) Himmeldirk, K.; Kennedy, I. A.; Hill, R. E.; Sayer, B. G.; Spenser, I. D. Biosynthesis of vitamins $B_1$ and $B_6$ in *Escherichia coli*: Concurrent Incorporation of 1-deoxy-D-xylulose into Thiamin ($B_1$) and Pyridoxol ($B_6$). *Chem. Commun*. **1996**, *10*, 1187-1188.

40) Rohdich, F.; Wungsintaweekul, J.; Fellermeier, M.; Sagner, S.; Herz, S.; Kis, K.; Eisenreich, W.; Bacher, A.; and Zenk, M. H. Cytidine 5′-Triphosphate-Dependent Biosynthesis of Isoprenoids: YgbP Protein of *Escherichia coli* Catalyzes the Formation of 4-Diphosphocytidyl-2-*C*-Methylerythritol *Proc. Natl. Acad. Sci. USA* **1999**, 96, 11758–11763.

41) Lüttgen, H.; Rohdich, F.; Herz, S.; Wungsintaweekul, J.; Hecht, S.; Schuhr, C. A.; Fellermeier, M.; Sagner, S.; Zenk, M. H.; Bacher, A.; Eisenreich, W. Biosynthesis of Terpenoids: YchB Protein of *Escherichia coli* Phosphorylates the 2-Hydroxy Group of 4-Diphosphocytidyl-2C-Methyl-d-Erythritol *Proc. Natl. Acad. Sci. USA* **2000**, 97 1062–1067.

42) Herz, S.; Wungsintaweekul, J.; Schuhr, C. A.; Hecht, S.; Lüttgen, H.; Sagner, S.; Fellermeier, M.; Eisenreich, W.; Zenk, M. H.; Bacher, A.; Rohdich, F. Biosynthesis of Terpenoids: YgbB Protein Converts 4-Diphosphocytidyl-2C-Methyl-d-Erythritol 2-Phosphate to 2C-Methyl-d-Erythritol 2,4-Cyclodiphosphate. *Proc. Natl. Acad. Sci. USA* **2000**, *97* 2486–2490.

43) Nyland II, R. L.; Xiao, Y.; Liu, P.; Meyers. C. L. F. IspG Converts an Epoxide Substrate Analogue to (*E*)-4-Hydroxy-3-Methylbut-2-Enyl Diphosphate: Implications for IspG Catalysis in Isoprenoid Biosynthesis. *J. Am. Chem. Soc.* **2009**, *131*, 17734-17735.

44) Graewert, T.; Rohdich, F.; Span, I.; Bacher, A.; Eisenreich, W.; Eppinger, J.; Groll, M. Structure of Active IspH Enzyme from Escherichia coli Provides Mechanistic Insights into Substrate Reduction. *Angew. Chem. Int. Ed.* **2009**, *48*, 5756-5759.

45) Rohmer, M. A mevalonate-independent route to isopentenyl diphosphate. In *Comprehensive Natural Products Chemistry;* Cane, D., Ed.; Pergamon Press, New York, 1999; pp 45−67.

46) Chaykin, S.; Law, J.; Phillips, A. H.; Tchen, T. T.; Bloch, K. Phosphorylated Intermediates in the Synthesis of Squalene. *Proc. Natl. Acad. Sci. U.S.A.* **1958**, 44, 998-1004.

47) Agranoff, B. W.; Eggerer, H.; Henning, U.; Lynen, F. Biosynthesis of terpenes VII.

Isopentenyl Pyrophosphate Isomerase. *J. Biol. Chem.* **1960**, *235*, 326-332.

48) Clifford, K.; Conforth, J. W.; Mallaby, R.; Phillips, G. T. Stereochemistry of isopentenyl pyrophosphate isomerase. *J. Chem. Soc. D*, **1971**, 1599- 1600.

49) Shah, D. H.; Cleland, W. W.; Porter, J. W. The Partial Purification, Properties, and Mechanism of Action of Pig Liver Isopentenyl Pyrophosphate Isomerase. *J. Biol. Chem.* **1965**, *240*, 1946-1956.

50) Lee, S.; Poulter, C. D. *Escherichia coli* Type I Isopentenyl Diphosphate Isomerase: Structural and Catalytic Roles for Divalent Metals. *J. Am. Chem. Soc.* **2006**, *128*, 11545-11550.

51) Carrigan, C. N.; Poulter, C. D. Zinc Is an Essential Cofactor for Type I Isopentenyl Diphosphate:Dimethylallyl Diphosphate Isomerase. *J. Am. Chem. Soc.* **2003**, *125*, 9008-9009.

52) Wouters, J.; Oudjama, Y.; Barkley, S. J.; Tricot, C.; Stalon, V.; Droogmans, L.; Poulter, C. D. Catalytic Mechanism of *Escherichia coli* Isopentenyl Diphosphate Isomerase Involves Cys-67, Glu-116, and Tyr-104 as Suggested by Crystal Structures of Complexes with Transition State Analogues and Irreversible Inhibitors. *J. Biol. Chem.* **2003**, *278,* 11903-11908.

53) Zhang, C.; Liu, L.; Xu, H.; Wei, Z.; Wang, Y.; Lin, Y.; Gong, W. Crystal Structures of Human IPP Isomerase: New Insights into the Catalytic Mechanism. *J. Mol. Biol.* **2007**, *366*, 1437-1446.

54) Street, I. P.; Poulter, C. D. Isopentenyl Diphosphate:Dimethylallyl Diphosphate Isomerase: Construction of a High-level Heterologous Expression System for the Gene from *Saccharomyces cerevisiae* and Identification of an Active-site Nucleophile. *Biochemistry* **1990**, *29*, 7531- 7538.

55) Street, I. P.; Coffman, H. R.; Baker, J. A.; Poulter, C. D. Identification of Cys139 and Glu207 As Catalytically Important Groups in the Active Site of Isopentenyl Diphosphate:Dimethylallyl Diphosphate Isomerase. *Biochemistry* **1994**, *33*, 4212-4217.

56) Durbecq, V.; Sainz, G.; Oudjama, Y.; Clantin, B.; Bompard-Gilles, C.; Tricot, C.; Caillet, J.; Stalon, V.; Droogmans, L.; Villeret, V. Crystal Structure of Isopentenyl Diphosphate:Dimethylallyl Diphosphate Isomerase. *EMBO J.* **2001**, *20*, 1530- 1537.

57) Poulter, C. D.; Rilling, H. C. Prenyl Transferases and Isomerase. In *Biosynthesis of Isoprenoid Compounds;* Porter, J. W., Spurgeon, S. L., Eds.; John Wiley & Sons, New York, NY, 1981; pp 161-224.

58) Reardon, J. E.; Abeles, R. H. Mechanism of Action of Isopentenyl Pyrophosphate Isomerase: Evidence for a Carbonium Ion Intermediate. *Biochemistry* **1986**, *25,* 5609-5616.

59) Muehlbacher, M.; Poulter, C. D. Isopentenyl Diphosphate Isomerase: Inactivation of the Enzyme with Active-site-directed Irreversible Inhibitors and Transition State Analogues. *Biochemistry* **1988**, *27,* 7315-7328.

60) De Ruyck, J.; Durisotti, V.; Oudjama, Y.; Wouters, J. Structural role for Tyr-104 in *Escherichia coli* Isopentenyl-diphosphate Isomerase: Site-directed Mutagenesis, Enzymology, and Protein Crystallography. *J. Biol. Chem.* **2006**, *281,* 17864 17869.

61) Wouters, J.; Oudjama, Y.; Stalon, V.; Droogmans, L.; Poulter, C. D. Crystal Structure of the C67A Mutant of Isopentenyl Diphosphate Isomerase Complexed With a Mechanism-Based Irreversible Inhibitor *PROTEINS: Structure, Function, and Bioinformatics* **2004**, *54*, 216–221.

62) Poulter, C. D.; Satterwhite, D. M. Mechanism of the Prenyl Transfer Reaction. Studies with (*E*)-and (*Z*)-3-Trifluoromethyl-2-buten-1-yl Pyrophosphate. *Biochemistry* **1977**, *16*, 5470-5478.

64) Popjak, G.; Conforth, J. W. Substrate Stereochemistry in Squalene Biosynthesis. *Biochem. J.* **1966**, *101*, 553-568.

65) Street, I. P.; Christensen, D. J.; Poulter, C. D. Hydrogen Exchange During the Enzyme-catalyzed Isomerization of Isopentenyl Diphosphate and Dimethylallyl Diphosphate. *J. Am. Chem. Soc.* **1990**, *112*, 8577-8578.

66) Kellogg, B. A.; Poulter, C. D. Chain Elongation in the Isoprenoid Biosynthetic Pathway. *Curr. Opin. Chem. Biol.* **1997**, *1*, 570-578.

67) Christianson, D. W. Structural Biology and Chemistry of the Terpernoid Cyclases. *Chem. Rev.* **2006**, *106*, 3412-3442.

68) Toteva, M. M.; Richard, J. P. Mechanistic Imperatives for the Reaction Catalyzed by Isopentenyl Pyrophosphate Isomerase: Free Energy Profile for Stepwise Isomerization in Water Through a Tertiary Carbocation Intermediate. *Bioorg. Chem.* **1997**, *25*, 239-245.

69) Toteva, M. M.; Richard, J. P. Mechanism for Nucleophilic Substitution and Elimination Reactions at Tertiary Carbon in Largely Aqueous Solutions: Lifetime of a Simple Tertiary Carbocation. *J. Am. Chem. Soc.* **1996**, *118*, 11434-11445.

70) Jonnalagadda, V.; Toth, K.; Richard J. P. Isopentenyl Diphosphate Isomerase Catalyzed Reactions in $D_2O$: Product Release Limits the Rate of This Sluggish Enzyme-Catalyzed Reaction *J. Am. Chem. Soc.* **2012**, *134*, 6568−6570.

71) Smit, A.; Mushegian, A. Biosynthesis of Isoprenoids via Mevalonate in Archaea: The Lost Pathway *Genome Res.* **2000**, *10*, 1468-1484.

72) Kaneda, K.; Kuzuyama, T.; Takagi, M.; Hayakawa, Y.; Seto, H. An Unusual Isopentenyl Diphosphate Isomerase in the Mevalonate Pathway Gene Cluster from *Streptomyces* sp. Strain CL190. *Proc. Natl. Acad. Sci. U.S.A.* **2001**, *98*, 932-937.

73) Bornemann, S. Flavoenzymes that Catalyse Reactions with No Net Redox Change. *Nat. Prod. Rep*. **2002**, *19*, 761–772.

74) Kittleman, W.; Thibodeaux, C. J.; Zhang, H.; Liu, Y.-n.; Liu, H.-w. Characterization and Mechanistic Studies of Type II Isopentenyl Diphosphate:Dimethylallyl Diphosphate Isomerase from *Staphylococcus aureus*. *Biochemistry* **2007**, *46*, 8401-8413.

75) Yamashita, S.; Hemmi, H.; Ikeda, Y.; Nakayama, T.; Nishino, T. Type 2 Isopentenyl Diphosphate Isomerase From a Thermoacidophilic Archaeon *Sulfolobus shibatae*. *Eur. J. Biochem.* **2004**, *271*, 1087-1093.

76) Rothman, S. C.; Helm, T. R.; Poulter, C. D. Kinetic and Spectroscopic Characterization of Type II Isopentenyl Diphosphate Isomerase from *Thermus thermophilus:* Evidence for Formation of Substrate-induced Flavin Species. *Biochemistry* **2007**, *46,* 5437-5445.

77) Kao, C.-l.; Kittleman, W.; Zhang, H.; Seto, H.; Liu, H.-w. Stereochemical Analysis of Isopentenyl Diphosphate Isomerase Type II from *Staphylococcus aureus* Using Chemically Synthesized (*S*)- and (*R*)-[2-$^{2}$H]Isopentenyl Diphosphates. *Org. Lett.* **2005**, *7*, 5677-5680.

78) Barkley, S. J.; Desai, S. B.; Poulter, C. D. Proton Exchange in Type II Isopentenyl Diphosphate Isomerase. *Org. Lett.* **2004**, *6*, 5019-5021.

79) Steinbacher, S.; Kaiser, J.; Gerhardt, S.; Eisenreich, W.; Huber, R.; Bacher, A.; Rohdich, F. Crystal Structure of the Type II Isopentenyl Diphosphate:Dimethylallyl Diphosphate Isomerase from *Bacillus subtilis*. *J. Mol. Biol.* **2003**, *329*, 973-982.

80) Nagai, T.; Unno, H.; Janczak, M. W.; Yoshimura, T.; Poulter, C. D.; Hemmi, H. Covalent Modification of Reduced Flavin Mononucleotide in Type-2 Isopentenyl Diphosphate Isomerase by Active-site-directed Inhibitors. *Proc. Natl. Acad. Sci. U.S.A.* **2011**, *108,* 20461-20466.

81) Mayhew, S. G. The Effects of pH and Semiquinone Formation on the Oxidation-Reduction Potentials of Flavin Mononucleotide. A Reappraisal. *Eur. J. Biochem.* **1999**, *265,* 698-702.

82) Thibodeaux, C. J.; Mansoorabadi, S. O.; Kittleman, W.; Chang, W.; Liu, H. Evidence for the Involvement of Acid/Base Chemistry in the Reaction Catalyzed by the Type II Isopentenyl Diphosphate/Dimethylallyl Diphosphate Isomerase from *Staphylococcus aureus*. *Biochemistry* **2008**, *47,* 2547-2558.

83) Engel, P. S.; He, S.-L.; Banks, J. T.; Ingold, K. U.; Lusztyk, J. Clocking Tertiary Cyclopropylcarbinyl Radical Rearrangements. *J. Org. Chem.* **1997**, *62,* 5656-5656.

84) Krishnamurthy, V.; Rawal, V. H. Kinetics of the Oxiranylcarbinyl Radical Rearrangement. *J. Org. Chem.* **1997**, *62,* 1572-1573.

85) Johnston, J. B.; Walker, J. R.; Rothman, S. C.; Poulter, C. D. Type-2 Isopentenyl Diphosphate Isomerase. Mechanistic Studies with Cyclopropyl and Epoxy Analogues. *J. Am. Chem. Soc.* **2007**, *129,* 7740-7741.

86) Hoshino, T.; Tamegai, H.; Kakinuma, K.; Eguchi, T. Inhibition of Type 2 Isopentenyl Diphosphate Isomerase From *Methanocaldococcus jannaschii* by a Mechanism-based Inhibitor of Type 1 Isopentenyl Diphosphate Isomerase. *Bioorg. Med. Chem.* **2006**, *14*, 6555- 6559.

87) Rothman, S. C.; Johnston, J. B.; Lee, S.; Walker, J. R.; Poulter, C. D. Type II Isopentenyl Diphosphate Isomerase: Irreversible Inactivation by Covalent Modification of Flavin. *J. Am. Chem. Soc.* **2008**, *130,* 4906-4913.

88) Sharma, N. K.; Pan, J.-J.; Poulter, C. D. Type II Isopentenyl Diphosphate Isomerase: Probing the Mechanism with Alkyne/Allene Diphosphate Substrate Analogues. *Biochemistry* **2010**, *49,* 6228-6233.

89) Heaps, N. A; Poulter, C. D. Type-2 Isopentenyl Diphosphate Isomerase: Evidence for a Stepwise Mechanism. *J. Am. Chem. Soc.* **2011**, *133*, 19017–19019.

90) Thibodeaux, C. J.; Chang, W.; Liu, H. Linear Free Energy Relationships Demonstrate a Catalytic Role for the Flavin Mononucleotide Coenzyme of the Type II Isopentenyl Diphosphate:Dimethylallyl Diphosphate Isomerase. *J. Am. Chem. Soc.* **2010**, *132,* 9994-9996.

91) Calveras, J.; Thibodeaux, C. J.; Mansoorabadi, S. O.; Liu, H. Stereochemical Studies of the Type II Isopentenyl Diphosphate-Dimethylallyl Diphosphate Isomerase Implicate the FMN Coenzyme in Substrate Protonation. *ChemBioChem.* **2012**, *13,* 42 46.

92) Unno, H.; Yamashita, S.; Ikeda, Y.; Sekiguchi, S.-Y.; Yoshida, N.; Yoshimura, T.; Kusunoki, M.; Nakayama, T.; Nishino, T.; Hemmi, H. New Role of Flavin as a General Acid-Base Catalyst With No Redox Function in Type 2 Isopentenyl-Diphosphate Isomerase. *J. Biol. Chem.* **2009**, *284,* 9160-9167.

93) Hemmi, H.; Ikeda, Y.; Yamashita, S.; Nakayama, T.; Nishino, T. Catalytic Mechanism of Type 2 Isopentenyl Diphosphate:Dimethylallyl Diphosphate Isomerase: Verification of a Redox Role of the Flavin Cofactor in a Reaction With No Net Redox Change. *Biochem. Biophys. Res. Commun.* **2004**, *322*, 905–910.

94) Macheroux, P.; Ghisla, S.; Sanner, C.; Ruterjans, H.; Muller, F. Reduced Flavin: NMR Investigation of N5-H Exchange Mechanism, Estimation of Ionisation Constants and Assessment of Properties as Biological Catalyst. *BMC Biochem.* **2005**, *6,* 26.

95) Cavelier, G. Amzel, L. M. Mechanism of NAD(P)H:Quinone Reductase: Ab Initio Studies of Reduced Flavin. *Proteins Struct. Funct. Genet.* **2001**, *43,* 420-432.

96) Yu Q. J.; Ghisla S.; Hirschberg, J.; Mann, V.; Beyer, P. Plant Carotene Cis-Trans Isomerase CRTISO: A New Member of the $FAD_{red}$-Dependent Flavoproteins Catalyzing

Non-Redox Reactions. *J. Biol. Chem.* **2011**, 286, 8666–8676.

97) Yu, Q. J. et. al. The Lycopene Cyclase CrtY from *Pantoeaananatis* (formerly *Erwinia uredovora*) Catalyzes an $FAD_{red}$-Dependent Non-Redox Reaction. *J. Biol. Chem.* **2010**, *285*, 12109–12120.

98) de Ruyck, J.; Janczak, M. W.; Neti, S. S.; Rothman, S. C.; Schubert, H.; Cornish, R.; Matagne, A.; Wouters, J.; Poulter, C. D. Determination of Kinetics and the Crystal Structure of a Novel Type 2 Isopentenyl Diphosphate: Dimethylallyl Diphosphate Isomerase from *Streptococcus pneumoniae*. *ChemBioChem.* **2014**, *15*, 1452−1458.

99) Janczak, M. W.; Poulter, C. D. Kinetic and Binding Studies of Streptococcus pneumoniae Type 2 Isopentenyl Diphosphate:Dimethylallyl Diphosphate Isomerase. *Biochemistry* **2016**, *55*, 2260−2268.

100) Nakatani, H.; Goda, S.; Unno, H.; Nagai, T.; Yoshimura, T.; Hemmi, H. Substrate-Induced Change in the Quaternary Structure of Type 2 Isopentenyl Diphosphate Isomerase from *Sulfolobus shibatae. J. Bacteriol.* **2012**, *194,* 3216-3224.

101) Laupitz, R. et al. Biochemical Characterization of *Bacillus subtilis* Type II Isopentenyl Diphosphate Isomerase, and Phylogenetic Distribution of Isoprenoid Biosynthesis Pathways. *Eur. J. Biochem.* **2004**, *271*, 2658 –2669.

102) Barkley S. J.; Cornish R. M.; Poulter C. D. Identification of an Archaeal Type II Isopentenyl Diphosphate Isomerase in *Methanothermobacter thermautotrophicus*. *J. Bacteriol.* **2004**, *186*, 1811–1817.

103) Barkley S. J.; Desai S. B.; Poulter C. D. Type II Isopentenyl Diphosphate Isomerase From *Synechocystis* sp. Strain PCC 6803. *J. Bacteriol.* **2004**, *186*, 8156 – 8158.

104) a) Neti, S. S; Poulter, C. D. unpublished results b) Neti, S. S; Eckert, D. M.; Poulter C. D. Construction of Functional Monomeric Type 2 Isopentenyl Diphosphate:Dimethylallyl Diphosphate Isomerase. *Biochemistry* **2016**, *55*, 4229-4238.

105) de Ruyck J.; Rothman S. C.; Poulter C. D.; Wouters J. Structure of *Thermus thermophilus* Type 2 Isopentenyl Diphosphate Isomerase Inferred From Crystallography and Molecular Dynamics. *Biochem. Biophys. Res. Commun.* **2005**, *338*, 1515–1518.

106) Hoshino, T.; Nango, E.; Baba, S.; Eguchi, T.; Kumasaka, T. Crystallization and Preliminary X-ray Analysis of Isopentenyl Diphosphate Isomerase from *Methanocaldococcus jannaschii. Acta Cryst*. **2011**, F67, 101–103.

107) Dutoit, R.; de Ruyck, J.; Durisotti, V.; Legrain, C.; Jacobs, E.; Wouters, J. Overexpression, Physicochemical Characterization, and Modeling of a Hyperthermophilic *Pyrococcus furiosus* Type 2 IPP Isomerase. *Proteins: Structure, Function, and Bioinformatics* **2008**, *71*, 1699-1707.

108) Siddiqui M. A. et al. Enzymatic and Structural Characterization of Type II

Isopentenyl Diphosphate Isomerase From Hyperthermophilic Archaeon *Thermococcus kodakaraensis*. *Biochem. Biophys. Res. Commun.* **2005**, *331*, 1127–1136.

109) Ali, M. H.; Imperiali, B. Protein Oligomerization: How and Why. *Bioorg. Med. Chem.* **2005**, *13*, 5013 – 5020.

110) Goodsell, D. S.; Olson, A. J. Structural Symmetry and Protein Function. *Annu. Rev. Biophys. Biomol. Struct.* **2000**, *29*, 105 – 153.

111) Imada, K.; Sato, M.; Tanaka, N.; Katsube, Y.; Matsuura, Y.; Oshima, T. Three-Dimensional Structure of a Highly Thermostable Enzyme, 3-Isopropylmalate Dehydrogenase of *Thermus thermophilus* at 2.2 Å Resolution. *J. Mol. Biol.* **1991**, *222*, 725-738.

112) Wells, S.A.; van der Kamp, M.W.; McGeagh, J.D.; Mulholland, A. J. Structure and Function of Homodimeric Enzymes: Simulation of Cooperative and Independent Functional Motion. *PLoSOne* **2015**, *10*, e0133372.

113) Thoma, R.; Hennig, M.; Sterner, R.; Kirschner, K. Structure and Function of Mutationally Generated Monomers of Dimeric Phosphoribosylanthranilate Isomerase from *Thermotoga maritime. Structure*, **2000**, *8*, 265–276.

114) Buchinger, E.; Aachmann, F. L.; Aranko, A.S.; Valla, S.; Sjåk-Bræk, G.; Iwaï, H.; Wimmer, R. Use of Protein Trans-Splicing to Produce Active and Segmentally $^{2}H$, $^{15}N$ Labeled Mannuronan C5-Epimerase AlgE4. *Prot. Sci.* **2010**, *19,* 1534-1543.

115) Smith, P.K. et al. Measurement of Protein Using Bicinchoninic Acid. *Anal. Biochem.* **1985**, *150, 76–85.*

116) Cole J. L. Analysis of Heterogeneous Interactions. *Methods. Enzymol.* **2004**, *384*, 212–232.

117) Laue, T.; Shah, B.; Ridgeway, T.; Pelletier S. Computer-aided interpretation of analytical sedimentation data for proteins. In *Analytical Ultracentrifugation in Biochemistry and Polymer Science*; Harding, S. E., Rowe, A. J., Horton, J. C. Eds.; Royal Society of Chemistry, Cambridge, UK, 1992.

118) Muchmore, D. C.; McIntosh, L. P.; Russell, C. B.; Anderson, D. E.; Dahlquist, F. W. Expression and Nitrogen-15 Labeling of Proteins for Proton and Nitrogen-15 Nuclear Magnetic Resonance. *Methods Enzymol.* **1989**, *177*, 44-73.

119) Kay, L.; Keifer, P.; Saarinen, T. Pure Absorption Gradient Enhanced Heteronuclear Single Quantum Correlation Spectroscopy With Improved Sensitivity. *J. Am. Chem. Soc.* **1992**, *114*, 10663-10665.

120) Satterwhite, D. M. Isopentenyldiphosphate Delta-Isomerase. *Methods. Enzymol.* **1985**, *110*, 92-99.

121) Nonlinear Regression Analysis Was Performed Using GraphPad Prism Version 6.00, GraphPad Software, La Jolla California USA, www.graphpad.com.

122) Walsh, C. Flavin Coenzymes: At the Crossroads of Biological Redox Chemistry. *Acc. Chem. Res.* **1980**, *13*, 148-155.

123) Edwards, A. M. Structure and General Properties of Flavins. In *Flavins and Flavoproteins: Methods and Protocols, Methods in Molecular Biology*; Weber, S., Schleicher, E., Eds.; Springer Science, New York, 2014; *1146*, pp 3-13.

124) McCormick, D. B. 9-Halo-Derivatives of Flavins. *J. Heterocycl. Chem.* **1967**, *4*, 629.

125) Dudley, K. H.; Hemmerich, P. Flavins. XIII. Rearrangement Reactions of 1,3,10-Trialkylflavinium Salts. *J. Org. Chem.* **1967**, *32*, 3049.

126) Haigney, A.; Lukacs, A.; Zhao, R.-K.; Stelling, A. L.; Brust, R.; Kim, R.-R.; Kondo, M.; Clark, I.; Towrie, M.; Greetham, G. M.; Illarionov, B.; Bacher, A.; Romisch-Margl, W.; Fischer, M.; Meech, S. R.; Tonge, P. J. Ultrafast Infrared Spectroscopy of an Isotope-Labeled Photoactivatable Flavoprotein. *Biochemistry* **2011**, *50*, 1321-1328.

127) Massey, V. The Chemical and Biological Versatility of Riboflavin. *Biochem. Soc. Trans.* **2000**, *28*, 283.

128) Briggs, W. R. FlavinBased Photoreceptors in Plants. In *Flavins: Photochemistry and Photobiology*; Silva, E., Edwards, A. M., Eds.; RSC, Cambridge, 2006; 183-216.

129) Teufel, R.; Miyanaga, A.; Michaudel, Q.; Stull, F.; Louie G.; Noel, J. P.; Baran, P. S.; Palfey, B.; Moore, B. S. Flavin-Mediated Dual Oxidation Controls an Enzymatic Favorskii-Type Rearrangement. *Nature* **2013**, *503*, 552.

130) Moglich, A.; Yang, X.; Ayers, R. A.; Moffat, K. Structure and Function of Plant Photoreceptors. *Annu. Rev. Plant Biol.* **2010**, *61*, 21-47.

131) Makarov, V. et. al. Benzothiazinones Kill Mycobacterium Tuberculosis by Blocking Arabinan Synthesis. *Science* **2009**, *324*, 801-804.

132) Chaiyen, P.; Fraaije, M. W.; Mattevi, A. The Enigmatic Reaction of Flavins With Oxygen. *Trends Biochem. Sci.* **2012**, *37*, 373-380.

133) Rhead, W.; Roettger, V.; Marshall, T.; Amendt, B. Multiple Acyl-Coenzyme A Dehydrogenation Disorder Responsive to Riboflavin: Substrate Oxidation, Flavin Metabolism, and Flavoenzyme Activities in Fibroblasts. *Pediatr. Res*. **1993**, *33*, 129.

134) Ghisla, S.; Massey, V. New Flavins for Old: Artificial Flavins as Active Site Probes of Flavoproteins. *Biochem. J.* **1986**, *239*, 1.

135) Chaiyen, P.; Sucharitakul, J.; Svasti, J.; Entsch, B.; Massey, V.; Ballou, D. P. Use of 8-Substituted-FAD Analogues To Investigate the Hydroxylation Mechanism of the Flavoprotein 2-Methyl-3-hydroxypyridine-5-carboxylic Acid Oxygenase. *Biochemistry* **2004**, *43*, 3933.

136) Ballou, D. P.; Massey, V. Flavin Conformational Changes in the Catalytic Cycle of *p*-Hydroxybenzoate Hydroxylase Substituted with 6-Azido- and 6-Aminoflavin Adenine Dinucleotide. *Biochemistry* **1997**, *36*, 15713.

137) Haines, D. C.; Sevrioukova, I. F.; Peterson, J. A. The FMN-Binding Domain of Cytochrome P450BM-3: Resolution, Reconstitution, and Flavin Analogue Substitution. *Biochemistry* **2000**, *39*, 9419-9429.

138) Mehlhorn, J.; Steinocher, H.; Beck, S.; Kennis, J. T. M.; Hegemann, P.; Mathes, T. A Set of Engineered Escherichia coli Expression Strains for Selective Isotope and Reactivity Labeling of Amino Acid Side Chains and Flavin Cofactors. *PLoS One*, **2013**, *8*, e79006.

139) Muller, F. NMR Spectroscopy on Flavins and Flavoproteins. In *Flavins and Flavoproteins: Methods and Protocols, Methods in Molecular Biology*; Weber, S., Schleicher, E., Eds.; Springer Science, New York, 2014; *1146*, pp 229-306.

140) Haigney, A.; Lukacs, A.; Zhao, R. K.; Stelling, A. L.; Brust, R.; Kim, R. R.; Kondo, M.; Clark, I.; Towrie, M.; Greetham, G. M.; Illarionov, B.; Bacher, A.; Römisch-margl, W.; Fischer, M.; Meech, S. R.; Tonge, P. J. Ultrafast Infrared Spectroscopy of an Isotope-Labeled Photoactivatable Flavoprotein. *Biochemistry* **2011**, *50*, 1321-1328.

141) Lukacs, A.; Haigney, A.; Brust, R.; Zhao, R. K.; Stelling, A. L.; Clark, I. P.; Towrie, M.; Greetham, G. M.; Meech, S. R.; Tonge, P. J. Photoexcitation of the Blue Light Using FAD Photoreceptor AppA Results in Ultrafast Changes to the Protein Matrix. *J. Am. Chem. Soc.* **2012**, *133*, 16893.

142) Fleishmann, G.; Lederer, F.; Muller, F.; Bacher, A.; Rüterjans, H. Flavin–Protein Interactions in Flavocytochrome $b_2$ as Studied by NMR After Reconstitution of the Enzyme with $^{13}$C- and $^{15}$N-Labelled Flavin. *Eur. J. Biochem.* **2000**, *267*, 5156-5167.

143) Ghisla, S.; Massey, V. New Flavins for Old: Artificial Flavins as Active Site Probes of Flavoproteins. *Biochem. J.* **1986**, *239,* 1-12.

144) Massey, V. The Chemical and Biological Versatility of Riboflavin. *Biochem. Soc. Trans.* **2000**, *28,* 283-296.

145) Massey, V.; Claiborne, A.; Biemann, M.; Ghisla, S. 4-Thioflavins as Active Site Probes of Flavoproteins. *J. Biol. Chem.* **1984**, *259,* 9667-9678.

146) Neti, S. S.; Poulter C. D. Site-Selective Synthesis of $^{15}$N- and $^{13}$C-Flavin Mononucleotide Coenzyme Isotopologues. *J. Org. Chem.* **2016**, *81*, 5087-5092.

147) Illarionov, B.; Zhu, F.; Eisenreich, W.; Bacher, A.; Weber, S.; Fischer, M. Preparation of Flavocoenzyme Isotopologues by Biotransformation of Purines. *J. Org. Chem.* **2015**, *80*, 2539-2544.

148) Mishanina, T. V.; Kohen, A. Synthesis and Application of Isotopically Labeled Flavin Nucleotides. *J. Label Compd. Radiopharm*. **2015**, *58*, 370–375.

149) Koehn, E. M.; Fleischmann, T.; Conrad, J. A.; Palfey, B. A.; Lesley, S. A.; Mathews, I. I.; Kohen, A. An Unusual Mechanism of Thymidylate Biosynthesis in Organisms Containing the ThyX gene. *Nature* **2009**, *458,* 919-923.

150) Bacher, A.; Illarionov, B.; Eisenreich, W.; Fischer, M. A Roadmap to the Isotopolog Space of Flavocoenzymes. In *Flavins and Flavoproteins: Methods and Protocols, Methods in Molecular Biology*; Weber, S., Schleicher, E., Eds.; Springer Science, New York, 2014; *1146*, 65-78.

151) Tishler, M.; Pfister, K. III.; Babson, R. D.; Ladenburg, K.; Fleming, A. The Reaction between o-Aminoazo Compounds and Barbituric Acid. A New Synthesis of Riboflavin. *J. Am. Chem. Soc.* **1947**, *69*, 1487-1492.

152) Haase, I.; Grawert, T.; Illarionov, B.; Bacher, A.; Fischer, M. Recent Advances in Riboflavin Biosynthesis. In *Flavins and Flavoproteins: Methods and Protocols, Methods in Molecular Biology*; Weber, S., Schleicher, E., Eds.; Springer Science, New York, 2014; *1146*, pp 15-40.

153) Illarionov, B.; Zhu, F.; Eisenreich, W.; Bacher, A.; Weber, S., Fischer, M. Preparation of Flavocoenzyme Isotopologues by Biotransformation of Purines. *J. Org. Chem.* **2015**, *80*, 2539-2544.

154) Mishanina, T. V.; Kohen, A. Synthesis and Application of Isotopically Labeled Flavin Nucleotides. *J. Label Compd. Radiopharm*. **2015**, *58*, 370-375.

155) Dickey, J. B.; Gray, A. R. Preparation of Barbituric Acid. *Org. Syn.* **1943**, *2*, 60.

156) Carlson, E. E.; Kiessling, L. L. Improved Chemical Syntheses of 1- and 5-Deazariboflavin. *J. Org. Chem.* **2004**, *69*, 2614-2617.

157) Heyl, D.; Chase, E. C.; Koniuszy, F.; Folkers, K. Synthesis of Lyxoflavin. *J. Am. Chem. Soc.* **1951**, *73*, 3826-3827.

158) Bertani, G. Studies on lysogenesis I. The Mode of Phage Liberation by Lysogenic Escherichia coli. *J. Bacteriol.* **1952**, *62,* 293–300.

159) Hersh, L. B.; Walsh, C. Preparation, Characterization, and Coenzymic Properties of 5-carba-5-deaza and 1-carba-1-deaza Analogs of Riboflavin, FMN, and FAD. *Methods Enzymol.* **1980**, *66,* 277-287.

160) Kasai, S.; Nakano, H.; Maeda, K.; Matsui, K. Purification, Properties, and Function of Flavokinase from Rat Intestinal Mucosa. *J. Biochem.* **1990**, *107*, 298-303.

161) Nielsen, P.; Rauschenbach, P.; Bacher, A. Preparation, Properties, and Separation by High-Performance Liquid Chromatography of Riboflavin Phosphates. *Methods Enzymol.* **1986**, *122*, 209.

162) Muller, F.; Vervoort, J. J.; Lee, J.; Horowitz, M.; Carreira, L. A. Coherent Anti-Stokes Raman Spectra of Isoalloxazines. *J. Raman Spectrosc.* **1983**, *14*, 106 – 117.

163) Grande, H. J.; Cast, R.; van Schagen, C. G.; van Berkel, W. J. H.; Muller, F. $^{13}$C-NMR. Study on Isoalloxazine and Alloxazine Derivatives. *Helv. Chim. Acta.* **1977**, *60*, 367-379.

164) Fisher, J.; Spencer, R.; Walsh, C. Enzyme-catalyzed Redox Reactions With the Flavin Analogues 5-Deazariboflavin, 5-Deazariboflavin 5'-Phosphate, and 5-Deazariboflavin 5'-Diphosphate, 5'→5'-Adenosine Ester. *Biochemistry* **1976**, *15, 1054-1064.*

165) Clark, R. J.; Hester, R. E. *Spectroscopy of Biological Systems, Advances in Spectroscopy V1B*; John Wiley & Sons: New York, 1986.

166) Tegoni, M.; Gervais, M.; Desbois, A. Resonance Raman Study on the Oxidized and Anionic Semiquinone Forms of Flavocytochrome $b_2$ and l-Lactate Monooxygenase. Influence of the Structure and Environment of the Isoalloxazine Ring on the Flavin Function. *Biochemistry* **1997**, *36*, 8932– 8946.

167) Kitagawa, T.; Nishina, Y.; Kyogoku, Y.; Yamano, T.; Ohishi, N.; Takai-Suzuki, A.; Yagi, K. Resonance Raman spectra of Carbon-13- and Nitrogen-15-Labeled Riboflavin Bound to Egg-white Flavoprotein. *Biochemistry* **1979**, *18*, 1804.

168) Swartz, T. E.; Wenzel, P. J.; Corchnoy, S. B.; Briggs, W. R.; Bogomolni, R. A. Vibration Spectroscopy Reveals Light-Induced Chromophore and Protein Structural Changes in the LOV2 Domain of the Plant Blue-Light Receptor Phototropin 1. *Biochemistry* **2002**, *41*, 7183.

169) Wille, G.; Ritter, M.; Friedemann, R.; Mantele, W.; Hubner, G. Redox-Triggered FTIR Difference Spectra of FAD in Aqueous Solution and Bound to Flavoproteins. *Biochemistry* **2003**, *42*, 14814.

170) Unno, M.; Sano, R.; Masuda, S.; Ono, T.; Yamauchi, S. Light-Induced Structural Changes in the Active Site of the BLUF Domain in AppA by Raman Spectroscopy. *J. Phys. Chem. B*. **2005**, *109*, 12620.

171) Calhoun, K.A.; Swartz, J.R. Energy Systems for ATP Regeneration in Cell-Free Protein Synthesis Reactions. *Meth. Mol. Biol.* **2007**, *375,* 3-17.

172) Walker, J. R.; Rothman, S. C.; Poulter, C. D. Synthesis and Evaluation of Substrate Analogues as Mechanism-based Inhibitors of Type II Isopentenyl Diphosphate Isomerase. *J. Org. Chem.* **2008**, *73*, 726-729.

173) Davisson, V. J.; Woodside, A. B.; Neal, T. R.; Stremler, K. E.; Muehlbacher, M.; Poulter, C. D. Phosphorylation of Isoprenoid alcohols. *J. Org. Chem.* **1986**, *51*, 4768-4779.

174) Hahn, F. M.; Hurlburt, A. P.; Poulter C. D. *Escherichia coli* Open Reading Frame 696 Is *idi*, a Nonessential Gene Encoding Isopentenyl Diphosphate Isomerase. *J. Bacteriol.* **1999**, *181*, 4499-4504.

175) Rudolf, J. D.; Wang, H.; Poulter, C. D. Multisite Prenylation of 4‑Substituted Tryptophans by Dimethylallyltryptophan Synthase. *J. Am. Chem. Soc.* **2013**, *135*, 1895-1902.

176) Jencks, W. P. General Acid-Base Catalysis of Complex Reactions in Water. *Chem. Rev.* **1972**, *72*, 705-718.

177) Pyun, H-J.; Coates, R. M.; Wagschal, K. C.; McGeady, P.; Croteau, R. B. Regiospecificity and Isotope Effects Associated with the Methyl-Methylene Eliminations in the Enzyme-Catalyzed Biosynthesis of (*R*)- and (*S*)-Limonene. *J. Org. Chem.* **1993**, *58*, 3998-4009.